USING A NOVEL SMALL MOLECULE INHIBITOR TO INVESTIGATE THE ROLE OF MPS1 KINASE ACTIVITY

A thesis submitted to the University of Manchester for the degree of Doctor of Philosophy in the Faculty of Life Sciences

2010

Laura Hewitt

Table of Contents

List of Tables

List of Figures

Abbreviations

APC/C	Anaphase promoting complex/cyclosome
APS	Ammonium persulphate
ATCC	American Type Culture Collection
BLM helicase	Bloom's Syndrome helicase
BS cells	Bloom's Syndrome cells
BSA	Bovine Serum Albumin
Bub1-3	Budding uninhibited by benzimidizole 1-3
BubR1	Budding uninhibited by benzimidizole related 1
CCAN	Constitutive centromere-associated network
Cdk	Cyclin-dependent kinase
Cenp-E	Centromeric protein E
Cenp-F	Centromeric protein F
Chk2	Checkpoint kinase 2
CIN	Chromosomal instability
CO2	Carbon dioxide
D-box	Destruction box
DMEM	Dulbecco's modified Eagle medium
DMP	Dimethyl pimelimidate
DMSO	Dimethyl sulfoxide
dNTP	Deoxyribonucleotide triphosphate
DTT	Dithiothreitol
EDTA	Ethylenediaminetetraacetic acid
EGTA	Ethylene glycol tetraacetic acid
FCS	Foetal calf serum
FRAP	Fluorescence recovery after photobleaching
FRET	Förster resonance energy transfer
FRT	Flippase Recognition Target
g	Acceleration due to gravity
G1	Gap phase 1
G2	Gap phase 2
GFP	Green fluorescent protein
GTPase	Guanosine triphosphate hydrolase
hTERT	Human telomerase reverse transcriptase
IgG	Immunoglobulin G
IP	Immunoprecipitation
IPTG	Isopropyl β-D-1-thiogalactopyranoside
KB	Kinetochore buffer
KC-MT	Kinetochore-microtubule
kDa	Kilodalton
Mad1-3	Mitotic arrest deficient 1-3
MAPK	Mitogen-activated protein kinase
MBP	Myelin basic protein
MCC	Mitotic checkpoint protein
MEF	Mouse embryonic fibroblast
MEN	Mitotic exit network
ml	Millilitre
mM	Millimolar
Mps1	Monopolar spindle 1
MUGs	Mitosis with unreplicated genomes
MVA	Mosaic variegated aneuploidy
NaCl	Sodium chloride
NEBD	Nuclear envelope breakdown
Nt	Nucleotide
ORF	Open reading frame
PBS	Phosphate buffered saline
PBS-T	Phosphate buffered saline + Triton X-100
PBST	Phosphate buffered saline + Tween 20
PCR	Polymerase chain reaction
Plk1	Polo-like kinase 1
PMSF	Phenylmethylsulfonyl fluoride
PP1-2	Protein phosphatase 1-2
Ptk1	*Potoroo tridactylis* kidney 1
PVDF	Polyvinylidene fluoride
Rcf	Relative centrifugal force
RNAi	RNA interference
RPE	Retinal pigmented epithelium
Rpm	Revolutions per minute
RZZ	Rod-ZW10-Zwilch complex
S phase	Synthesis phase
SDS-PAGE	Sodium dodecyl sulphate - polyacrylamide gel electrophoresis
SPB	Spindle pole body
TBST	Tris buffered saline + Tween 20
TEMED	N,N,N′,N′-Tetramethylethylenediamine
Tet	Tetracycline

Abstract

During mitosis, accurate chromosome segregation is essential: gain or loss of genetic information can be detrimental to cell viability, or promote tumourigenesis. The mitotic checkpoint (also known as the spindle assembly checkpoint or SAC) ensures accurate chromosome segregation by delaying cell cycle progression until accuracy can be guaranteed. Mps1 is a protein kinase that is crucial for mitotic checkpoint signalling and also for proper chromosome alignment at metaphase. However, the precise role of Mps1's catalytic activity is still unclear. Here, I present AZ3146, a novel small molecule inhibitor of Mps1. AZ3146 inhibits recombinant Mps1 in vitro with an IC_{50} of ~35 nM, and has low activity against a panel of 50 kinases, suggesting a good degree of selectivity. As predicted for an Mps1 inhibitor, AZ1346 treatment led to spindle checkpoint malfunction in cells, accelerated mitotic timing, and perturbed the kinetochore localisation of the checkpoint effector Mad2. AZ3146 has a negative effect on cell viability, suggesting it leads to detrimental missegregations. Thus, the cellular effects of AZ3146 are consistent with Mps1 inhibition, and I was able to use the compound confidently as a tool to further probe the role of Mps1 activity in cells.

Strikingly, levels of Mps1 increased at unattached kinetochores following inhibition of its kinase activity, suggesting Mps1's kinetochore localisation is regulated by its own activity. A kinase-dead GFP-Mps1 fusion protein only accumulated at kinetochores in the absence of endogenous, active Mps1, implicating intra-molecular interactions in regulation of Mps1's kinetochore localisation. I confirm a role for Mps1 in the mechanism of chromosome alignment, but in contrast to previous reports I did not detect a decrease in Aurora B activity following Mps1 inhibition. On the contrary, both Mps1's phosphorylation status and its kinetochore localisation were affected by treatment with the Aurora B inhibitor ZM447439, placing Mps1 downstream of Aurora B. As an alternative explanation for the alignment defect in cells with reduced Mps1 activity, I found that levels of the plus-end directed kinesin Cenp-E were markedly decreased at unaligned kinetochores. I propose a model in which catalytically active Mps1's auto-release from kinetochores simultaneously promotes both mitotic checkpoint signalling and chromosome alignment by facilitating Mad2 dimerisation and Cenp-E binding at unattached kinetochores.

Declaration

No portion of the work referred to in this thesis has been submitted in support of an application for another degree or qualification of this or any other university or other institute of learning.

Copyright statement

Acknowledgements

My sincere thanks go my supervisor, Stephen Taylor, for generously taking on a lab-less postgraduate student and for his valuable help and support. Thanks also to other members of the Taylor laboratory, especially fellow Team-Mps1 member and co-author Anthony Tighe, who has not only been incredibly helpful and a real pleasure to work with, but has also done a lot of great science with AZ3146.

I also thank Pat Eyers, along with other former members of the Eyers lab, especially Beki Tyler, and also Matthew Chu who kindly provided me with recombinant Mps1.

The BBSRC, University of Manchester Alumni Fund and AstraZeneca are gratefully acknowledged, the former two for funding and the latter for providing AZ3146.

I thank my family for their love and support before and during the PhD years. Finally, special thanks go to Benedict Cross, for his unfaltering love, encouragement, and invaluable advice.

1 | Introduction

Successful progression through the cell cycle requires control mechanisms. Protein phosphorylation controls many aspects of cell biology, and some 518 protein kinases are present in the human kinome (Manning et al., 2002). Many of these are implicated in control of cell cycle progression. This thesis focuses one of these kinases: Mps1 (Monopolar Spindle 1) (Weiss and Winey, 1996). Mps1 is involved in regulation of the mitotic checkpoint (otherwise known as the spindle assembly checkpoint or SAC), a critical control mechanism that ensures the genome is partitioned equally between the two new daughter cells during cell division. This introduction will firstly place Mps1's role in context by describing mitosis and its control, focusing on the mitotic checkpoint (otherwise known as the spindle assembly checkpoint), which controls anaphase onset, and the relationship between the mitotic checkpoint, aneuploidy and cancer. I will also outline the mechanism of chromosome alignment, the roles that kinases play in regulating all of these processes, and our current understanding of Mps1's role in mitosis.

1.1 | Mitosis – a brief synopsis

Mitosis, during which the cell divides to produce two new, genetically identical daughter cells, is the final stage of the mammalian cell cycle (see Figure 1.1), and could be called the most visually spectacular. Perhaps partly for this reason, it has been a source of intense fascination for scientists since the advent of microscopy allowed it to be observed. The term mitosis was coined by Walther Flemming (Flemming, 1882), an important figure in the newly emerging field of cell biology (reviewed in Paweletz, 2001). Flemming made detailed drawings and classified cells as they progressed through mitosis, identified the 'chromatin' by its propensity to take up dyes, and noted the formation of 'thread-like' structures which were divided between the two daughter cells; these were later individually called 'chromosomes' by Heinrich Waldeyer in 1888. These observations eclipsed the theory of *de novo* 'free cell formation' that had previously found favour among his contemporaries, and formed the basis for the study of mitosis as we know it today.

Thanks to more than 120 years of research, we now have a much fuller understanding of the process of mitosis. However, mitosis is still commonly split into six distinct phases based largely on cell morphology visible to the early cell biologists

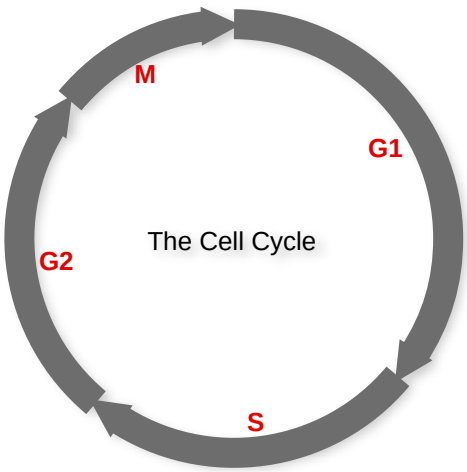

Figure 1.1 The eukaryotic cell cycle
In somatic cells, the cell cycle comprises 4 distinct stages: Gap phase 1 (G1), DNA synthesis phase (S) during which the genome is replicated, Gap phase 2 (G2) and mitosis (M), when the cell divides and the genome is partitioned between two daughter cells. Phases G1, S and G2 are also collectively known as interphase.

(reviewed in Pines and Rieder, 2001; Scholey et al., 2003), which are illustrated in Figure 1.2. After duplicating that genetic material and centrosomes (microtubule organising centres that will become the poles of the mitotic spindle; called spindle pole bodies [SPBs] in yeast) in the preceding DNA synthesis phase (S phase), a cell proceeds through Gap Phase 2 (G2) and, if the DNA is properly replicated, enters the first stage of mitosis, prophase. In prophase, the chromosomes (consisting of two identical chromatids) condense, the centrosomes begin to separate and move towards opposite ends of the cell, and the nuclear envelope fragments. It is during mid-prophase that the cell becomes irreversibly committed to mitosis (Pines and Rieder, 2001). Higher eukaryotes undergo an open mitosis, in which the nuclear envelope disintegrates early in mitosis, whereas in fungi the nuclear envelope remains intact throughout (De Souza and Osmani, 2007). In higher eukaryotes, nuclear envelope breakdown signals the beginning of prometaphase. The bipolar spindle forms, and chromosomes can now make contact with its microtubules. Stable attachments form between the microtubules and the kinetochore, a specialised proteinaceous structure that forms adjacent to the centromeric DNA on each paired chromatid. When all chromosomes have become stably attached, via the kinetochore, to microtubules emanating from both spindle poles (biorientation), and aligned at the cell equator forming a so-called 'plate' of DNA, metaphase is reached. After a brief delay, anaphase is initiated, and the sister chromatids are pulled apart towards opposite spindle poles, which also move further apart. In telophase, the nuclear envelope reforms around the decondensing segregated chromatids, and the cleavage furrow begins to ingress, constricting the spindle midzone. After telophase, as mitosis ends, cytokinesis occurs. This process enables partitioning of the cytoplasm into two daughters and their subsequent physical separation.

1.2 | Regulation of mitosis: Cdk1 as the master regulator

Progression through the cell cycle must be controlled to ensure the correct event sequence. To achieve this, eukaryotic cells have evolved molecular control mechanisms involving posttranslational modification and targeted degradation. The master regulators of the eukaryotic cell cycle are the cyclin-dependent kinases (Cdks), whose activity oscillates during the cell cycle due to a dependence upon association with their regulatory subunits, cyclins. Cyclin levels are regulated by transcription and proteasome-dependent degradation throughout the cell cycle, so that different cyclin/Cdk pairings are active at specific points. Phosphorylation of cyclin/Cdk substrates regulates the major events in, and passage through, mitosis and interphase (Vermeulen et al., 2003). In budding yeast, only one Cdk binds to all types of cyclin, whereas in vertebrate cells, there are 4 Cdks involved in cell cycle regulation.

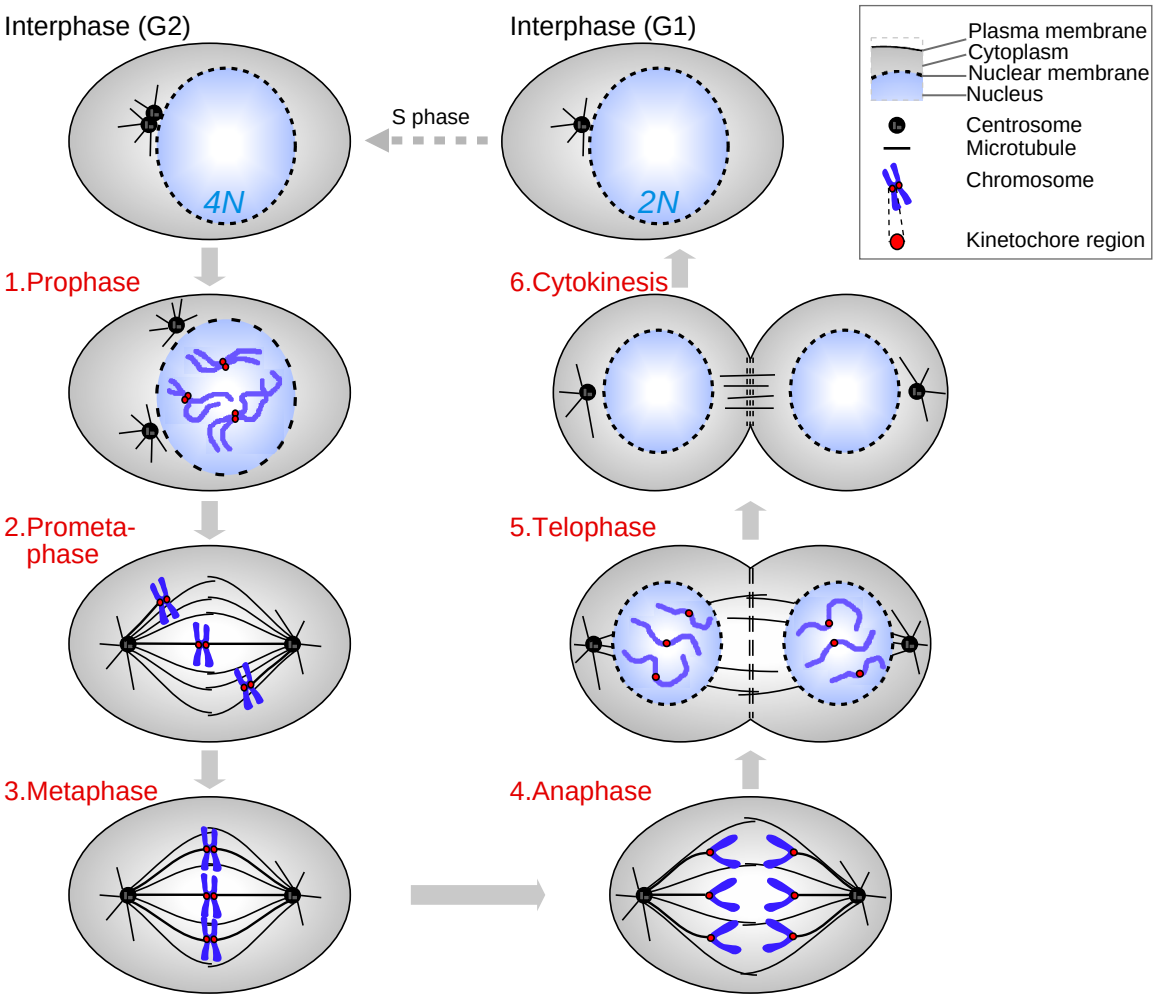

Figure 1.2 Mitosis in a higher eukaryotic cell
This schematic depicts the phases of mitosis in the context of the metazoan cell cycle. The 6 phases of mitosis, as determined by cell morphology, are labelled in red. A G2 cell enters mitosis having replicated its genome (giving it a 4N complement of chromosomes) and its centrosome. In **prophase**, the first phase of mitosis, the chromatin condenses, the kinetochores mature adjacent to the centromeres, the nuclear envelope begins to break down, and the two centrosomes, which will become the poles of the mitotic spindle, move apart. **Prometaphase** begins after nuclear envelope breakdown (NEB). The bipolar mitotic spindle forms, and its dynamic microtubules capture the chromosomes through a stochastic process. **Metaphase** is reached when all chromosomes are attached, via the kinetochores, to microtubules emanating from both poles of the spindle (biorientation). Chromosomes form a metaphase plate at the cell equator. After a brief metaphase delay, **anaphase** is initiated. Sister chromatids are separated by the action of the mitotic spindle and move toward opposite spindle poles. The spindle poles themselves also move further apart. In **telophase**, the nuclear envelope reforms around the decondensing segregated chromatin. The cleavage furrow begins to ingress through contraction of the actomyosin contractile ring, constricting the spindle mid-zone. In **cytokinesis**, the cytoplasm is partitioned into the two new daughter cells, which then separate completely. After mitosis, cells enter G1 phase of the next cell cycle. Cycling cells will then replicate their DNA and re-enter G2, before dividing again.

In vertebrate cells, the initiation of mitosis is thought to be triggered by Cdk2/cyclin A activity (De Boer et al., 2008; Furuno et al., 1999). Cdk2/cyclin A activity declines as cyclin A is degraded after nuclear envelope breakdown (NEBD) (den Elzen and Pines, 2001; Wolthuis et al., 2008). During late G2/early mitosis, Cdk2/cyclin A promotes the accumulation and activity of Cdk1/cyclin B, the major mitotic cyclin/Cdk pairing (Lindqvist et al., 2009). The activity of Cdk1/cyclin B is essential for mitotic progression: a substantial increase in its activity represents a point-of-no-return for the cell (Pines and Rieder, 2001). Cdk1 is active from prophase until metaphase, at which point the mitotic checkpoint is silenced and cyclin B is targeted for destruction by the proteasome (see Section 1.4). Multiple feedback loops govern Cdk1/cyclin B activity, ensuring its rapid activation in early mitosis, and subsequent deactivation (reviewed in Lindqvist et al., 2009), which is necessary for anaphase onset and mitotic exit. Using a Förster resonance energy transfer (FRET) sensor to monitor the net amount of Cdk1/cyclinB substrate phosphorylation in living cells, Gavet and colleagues (2010b) showed that Cdk1/cyclin B is activated in prophase, and reaches maximal activity shortly after NEBD. Its substrates remain maximally phosphorylated through prometaphase and metaphase until anaphase onset, when they are rapidly dephosphorylated (Gavet and Pines, 2010b). In anaphase, phosphatase activity is critical to remove phosphates from Cdk1/cyclin B's substrates and facilitate mitotic exit: in yeast, this function is carried out by Cdc14 (Amon, 2008), and in human cells, a probable candidate for the job is protein phosphatase 1 (PP1) (Gavet and Pines, 2010b; reviewed in Queralt and Uhlmann, 2008; Wu et al., 2009), which itself is phosphorylated and kept inactive by Cdk1 before anaphase onset (Dohadwala et al., 1994; Kwon et al., 1997; Wu et al., 2009).

Cdk1/cyclin B activity is both temporally and spatially regulated: just prior to nuclear envelope breakdown (NEBD) it is transported from the cytoplasm into the nucleus (Pines and Hunter, 1991). The increase in the rate of Cdk1/cyclin B import into the nucleus is dependent upon its continual activity, which is thought to mediate an increase in the rate of nuclear import, by an as yet undetermined mechanism (Gavet and Pines, 2010a). Cdk1/cyclin B phosphorylates numerous substrates in mitotic cells, both cytoplasmic and nuclear. Some of Cdk1/cyclin B's substrates are involved in orchestrating the massive cellular rearrangements seen in mitosis. For example, in prophase, Cdk1/cyclin B activation triggers cell rounding and centrosome separation, likely by phosphorylation of cytoskeletal components (Gavet and Pines, 2010b). As well as the cytoskeleton, Cdk1/cyclin B is known to phosphorylate components of the Golgi apparatus (e.g. Lowe et al., 1998), the nucleolus (Peter et al., 1990a; Sirri et al., 2002), nuclear lamins (Peter et al.,

1990b; Ward and Kirschner, 1990) caspases (Allan and Clarke, 2007), and amongst many others. Numerous mitotic Cdk1 substrates have been identified on purified mitotic spindles (Nousiainen et al., 2006), in whole cell lysates (Dephoure et al., 2008) or by covalent capture of labelled substrates (Blethrow et al., 2008). Many of these substrates are uncharacterised candidates, and suggest many as-yet unknown roles for Cdk1 phosphorylation in the coordination of mitotic events.

To drive human cells into and through mitosis, Cdk1/cyclin B functions in combination with several other mitotic kinases, including Aurora A and Plk1. Aurora A, a centrosomal serine/threonine kinase, promotes centrosome maturation and timely progression of early mitosis by contributing to Cdk1/cyclin B localisation and its full activity, and also promotes formation of a functional, bipolar mitotic spindle (reviewed in Barr and Gergely, 2007). Polo-like kinase 1 (Plk1), a serine/threonine kinase with multiple mitotic functions, also promotes progression through early mitosis, perhaps by participating in Cdk1/Cyclin B activation feedback loops (Lindqvist et al., 2009), or, as has been recently suggested, by promoting mitotic entry upstream of Cdk1/cyclin B activation (Gavet and Pines, 2010b). Plk1 also has a role in centrosome maturation and participates in cytokinesis, promoting contraction of the actomyosin contractile ring by activating Rho GTPase (reviewed in Archambault and Glover, 2009; Petronczki et al., 2008). The role of Plk1 at the kinetochore is discussed in Section 1.7.

1.3 | Ubiquitin-mediated proteolysis: regulating the regulators

The rapid, targeted proteolysis of mitotic regulators including cyclin A, cyclin B, Aurora A and Plk1 is critical to drive the orderly progression of events from prometaphase to mitotic exit (Pines, 2006). This targeted proteolysis is achieved by the ubiquitin-proteasome system (Hershko and Ciechanover, 1998). Proteins tagged with polyubiquitin chains (covalently linked molecules of a small protein, ubiquitin) are recognised and selectively degraded by the constitutively active 26S proteasome, a multisubunit protease. Ubiquitinylation requires a chain of 3 enzymes: a ubiquitin-activating enzyme (E1); a ubiquitin-conjugating enzyme (E2) and finally a ubiquitin ligase (E3), which is responsible for targeting of specific proteins for degradation. The E3 enzyme active in mitosis is called the anaphase-promoting complex/cyclosome (APC/C). The APC/C is a very large, megadalton multisubunit complex that requires a co-activator to simultaneously activate the enzyme and convey substrate specificity (Peters, 2006). APC/C substrates are recruited to the complex via the co-activator subunit if they contain either a destruction-box (D-box) or a KEN-box motif. In mitosis, the APC/C associates with 2 different co-activators, Cdc20 and Cdh1. Pre-anaphase degradation depends upon APC/C^{Cdc20}, since

Cdk1 phosphorylation stimulates Cdc20 binding to the APC/C (Kraft et al., 2003), and also prevents Cdh1 and APC/C from interacting (Crasta et al., 2008; Zachariae et al., 1998).

Recent advances have explained a previously puzzling paradox concerning pre-anaphase, APC/C^{Cdc20}-mediated degradation of cyclin A. It is well accepted that primary target of the mitotic checkpoint is the APC/C^{Cdc20}. The checkpoint delays anaphase onset by preventing APC/C^{Cdc20}-mediated degradation of securin and cyclin B during prometaphase (for detail of the checkpoint mechanism, see below). The Cdc20-dependent, but not mitotic checkpoint-dependent, degradation of cyclin A from NEBD has now been explained by the discovery of a novel, checkpoint-independent mode of APC/C^{Cdc20} substrate recognition. Cyclin A is degraded through interaction of cyclin A, Cdc20 and a Cdk1/cyclin B accessory unit, Cks, and is recruited to the APC/C before checkpoint activation (Wolthuis et al., 2008). Thus, though the APC/C^{Cdc20} is kept inactive in prometaphase towards specific substrates by the mitotic checkpoint, it is still active towards cyclin A, the degradation of which is necessary for mitotic progression.

1.4 | Control of anaphase onset

1.4.1 | The mitotic checkpoint

Regulation of the APC/C^{Cdc20} is critical to ensure the correct timing of anaphase. In prometaphase, each pair of sister chromatids must become attached, via the kinetochore, to microtubules emanating from both spindle poles. Biorientation ensures that at anaphase, the chromatids are evenly split between the two daughters. The process of kinetochore-microtubule attachment is stochastic: it depends upon random chance encounters between the dynamic microtubules of the mitotic spindle and the kinetochore, and while cells have evolved ways of increasing the likelihood of stable kinetochore-microtubule attachment formation (see Section 1.6), the nature of the process means that the duration of prometaphase can vary from cell to cell (Rieder et al., 1994). In order to prevent chromosome loss or gain due to the premature initiation of anaphase before all chromosomes are properly aligned and bioriented on a metaphase plate, cells employ the mitotic checkpoint. The checkpoint is a surveillance mechanism that is active from prometaphase until the last chromosome is correctly attached and aligned at the metaphase plate (Rieder et al., 1995). The target of checkpoint signalling is widely accepted to be the APC/C^{Cdc20}: more specifically, its ubiquitination of cyclin B and securin (for review, see Musacchio and Salmon, 2007; Zich and Hardwick, 2010). The active mitotic checkpoint prevents the polyubiquitination and subsequent proteasome-dependent degradation of cyclin B and securin (see Figure 1.3).

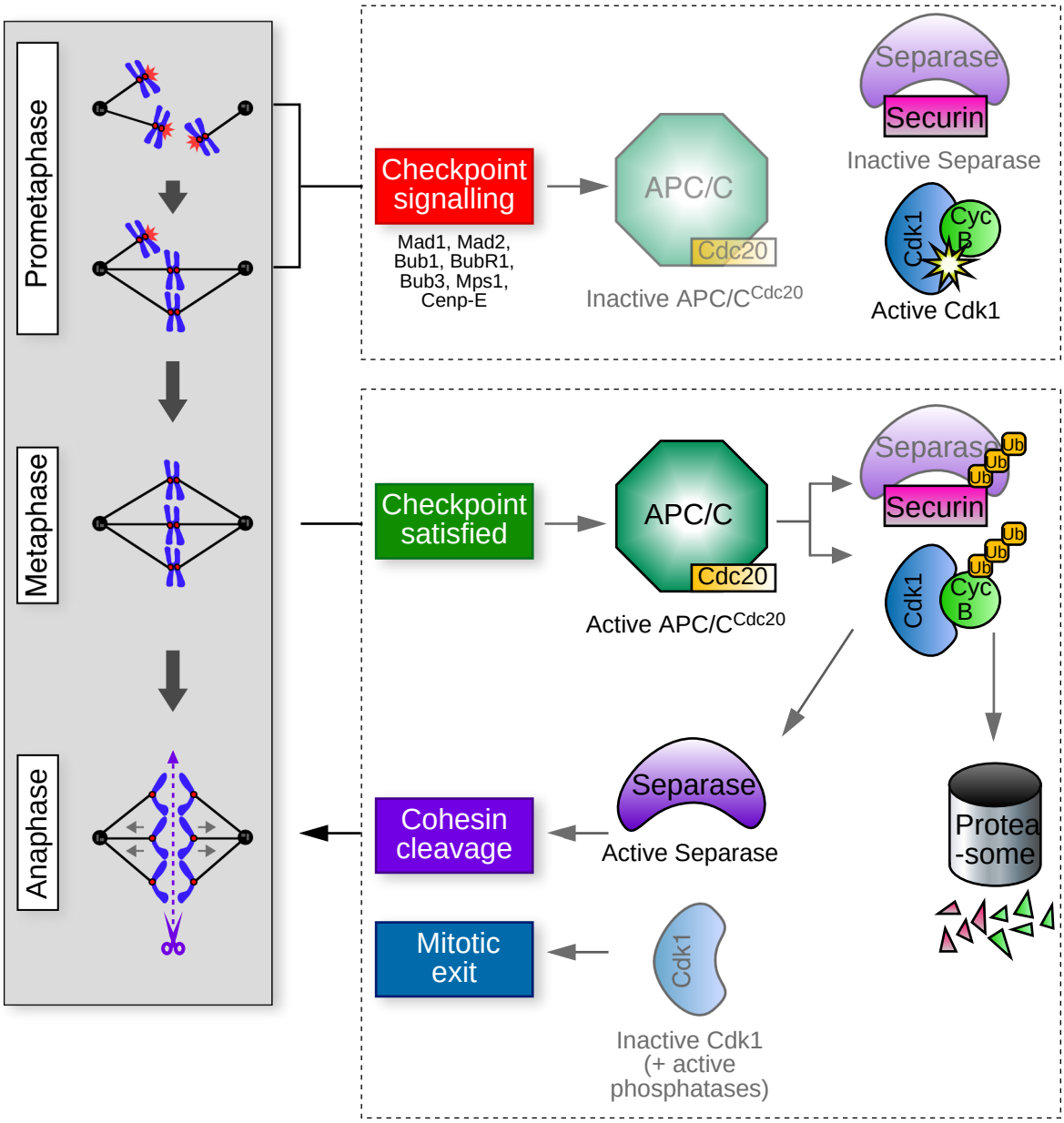

Figure 1.3 The Mitotic Checkpoint
During prometaphase, checkpoint proteins concentrate at the kinetochores (red circles), and unattached kinetochores produce a 'wait anaphase' signal. This results in inhibition of the E3 ubiquitin ligase activity of the APC/C towards cyclin B and securin, and therefore maintains high Cdk1 activity, and inhibits separase's protease activity. Only when all chromosomes are bioriented and aligned at the metaphase plate is the mitotic checkpoint satisfied. The 'wait anaphase' signal is silenced, allowing the APC/C^{Cdc20} to target both cyclin B and securin for proteasome-mediated degradation. Active separase cleaves the cohesins holding sister chromatids together, and Cdk1 is inactivated, triggering anaphase onset and mitotic exit.

1.4.2 | The checkpoint prevents destruction of cyclin B and securin

Cyclin B is the activating partner of Cdk1. High Cdk1 activity facilitates progression through prophase and prometaphase, and its targets must be dephosphorylated to promote anaphase, telophase, cytokinesis and mitotic exit. Seminal work in Xenopus egg extracts pointed to the importance of the fall in cyclin levels in regulating mitotic exit in the embryonic cell cycle (Murray and Kirschner, 1989); moreover, Murray and colleagues showed that a proteolysis-resistant mutant form of cyclin B (CYCΔ90) prevented mitotic exit in cycling egg extracts and intact eggs (Glotzer et al., 1991; Murray et al., 1989). Later, Holloway et al (1993) discovered that non-destructible cyclin B did not prevent the chromatids from separating, though they did not decondense: this, along with the discovery that inhibition of ubiquitin-mediated proteolysis could stop chromatid disjunction, clearly indicated that at least one other protein, in addition to cyclin B, must be degraded to allow chromatids to separate at anaphase. Studies in yeast identified Securin as an inhibitor of a protease called separase, which is required to cleave the mediators of chromatid cohesion, cohesins (reviewed in Nasmyth, 2002). During prophase, cohesion dissolves along the length of the chromosome arms via a mechanism thought to involve phosphorylation by Plk1 (Hauf et al., 2005; Sumara et al., 2002), but centromeric cohesion is resistant to prophase removal. Separase-mediated cohesin cleavage is necessary for resolution of the sister chromatids at anaphase. By targeting both Cyclin B and securin, the checkpoint maintains the early mitotic environment until all chromosomes are aligned, and ensures anaphase spindle behaviour and chromatid disjunction are perfectly synchronised, thereby promoting accurate DNA segregation and the production of viable, genetically identical diploid daughters.

1.4.3 | Components of the checkpoint

Several decades before the molecular targets of the mitotic checkpoint were discovered, microtubule disruption by treatment with drugs such as colcemid (which depolymerises tubulin) was understood to block cells in mitosis through damage to the mitotic spindle (reviewed in Rieder and Palazzo, 1992). Checkpoint mechanisms, which were thought to govern progression through mitosis (e.g. Hartwell and Weinert, 1989), were considered likely to mediate this mitotic block. In the early 1990s, genetic analysis of mutant budding yeast strains that failed to arrest in mitosis after treatment with benzimidizole (another microtubule depolymerising agent) identified three genes, named the budding uninhibited by benzimidizole (BUB1-3) genes (Hoyt et al., 1991; Roberts et al., 1994). A parallel study identified three mitotic arrest deficient (MAD1-3) genes by

similar methods (Li and Murray, 1991). It later became evident that Bub2 was part of the budding yeast mitotic exit network (MEN, Wang et al., 2000), but Bub1, Bub3, Mad1, Mad2 and Mad3 (or BubR1 in humans), along with Mps1 (Weiss and Winey, 1996), are considered core components of the checkpoint (e.g. May and Hardwick, 2006; Taylor et al., 2004). Both Bub1 and Mps1 are protein kinases in lower and higher eukaryotes (Abrieu et al., 2001; Lauze et al., 1995; Mills et al., 1992; Roberts et al., 1994; Taylor et al., 1998; Taylor and McKeon, 1997), whereas Mad1 and Mad2 do not possess enzymatic activity (Li and Murray, 1991). In human cells, Mad3 has no known homologue. However, human cells contain BubR1, a kinase related to both *Saccharomyces cerevisiae* Bub1 and Mad3, which requires binding to non-enzymatic Bub3 to localise it to kinetochores (Taylor et al., 1998).

In addition to these original checkpoint proteins, several new regulators of the checkpoint have been identified. Some of these have no obvious homologues in yeast, pointing to the additional complexity of the mitotic checkpoint in higher eukaryotes. Such proteins include Rod and Zeste-white 10 (ZW-10), part of the Rod-ZW10-Zwilch (RZZ) complex, which was first described in *Drosophila melanogaster* and is conserved in humans (Basto et al., 2000; Chan et al., 2000; reviewed in Karess, 2005; Williams et al., 2003). The RZZ complex is required for Mad1 and Mad2 to localise to kinetochores (Buffin et al., 2005; Kops et al., 2005) and is therefore important for checkpoint function (see below). In addition, the kinetochore microtubule motor Cenp-E may play a role in checkpoint signalling in vertebrates (Mao et al., 2003). Aurora B, a mitotic kinase, may also have a direct role in the mitotic checkpoint in yeast and higher eukaryotes (see Section 1.4.8).

1.4.4 | The kinetochore and checkpoint signalling

Kinetochores are specialised proteinaceous structures which assemble at the beginning of mitosis adjacent to the centromeric DNA. Kinetochores form the point of attachment for microtubules of the mitotic spindle, and their ultrastructure has long been the subject of study (e.g. Jokelainen, 1967). Electron microscopy on samples from cells treated with a microtubule-depolymerising drug showed that unattached kinetochores have a fibrous outer corona region extending away from the outer plate (Dong et al., 2007; McEwen et al., 1998). The outer plate undergoes rearrangement on contact with microtubules, and is directly connected to an inner kinetochore region, which contacts the chromatin (see Figure 1.4).

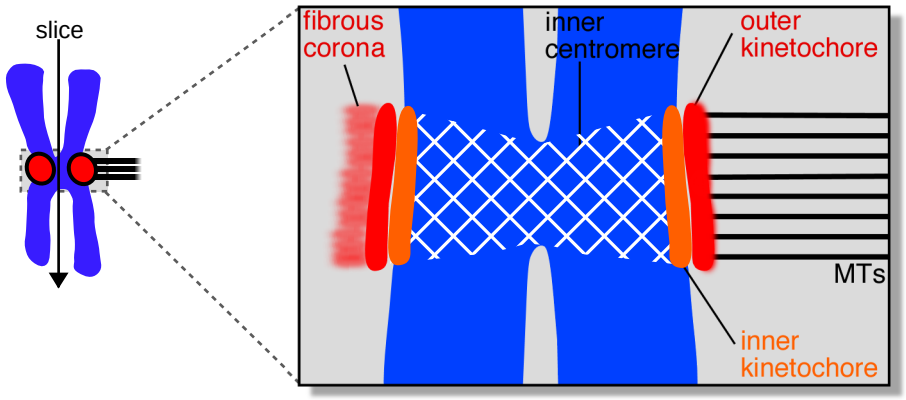

Figure 1.4 The vertebrate centromere and kinetochore region.
On the left is a mitotic chromosome, with one unattached kinetochore (left) and one attached kinetochore (right). When visualised by electron microscopy, the centromere and kinetochore region appears as illustrated in the schematic. The inner centromere is the region of DNA (and associated proteins) between the two kinetochores. The inner kinetochore (orange) contacts the centromeric DNA, and the outer kinetochore (red) forms adjacent to it and provides binding sites for microtubules (MTs). The unattached kinetochore has a clearly visible fibrous corona, where checkpoint proteins and kinetochore-associated motor proteins localise.

The trilaminar ultrastructure of the proteinaceous kinetochore region appears to reflect functionally distinct regions. The inner kinetochore region contains proteins that associate constitutively with the centromeric DNA, such as the histone variant Cenp-A (abbreviated from centromeric protein A), which forms the nucleosomes at centromeres and is critical for kinetochore specification in higher eukaryotes (Foltz et al., 2006). In vertebrates, Cenp-A associates with 13 other proteins (Cenp-H, Cenp-I and Cenp-K to Cenp-U) collectively known as the constitutive centromere-associated network (CCAN) (Cheeseman and Desai, 2008). The proteins of the inner kinetochore region form the platform for outer kinetochore assembly. The outer kinetochore region contains a conserved multisubunit complex known as the KNL network (KNL1-Mis12 complex-Ndc80/Hec1 complex) and Zwint. This region (specifically the Ndc80/Hec1 complex) forms the primary binding site for spindle microtubules (Cheeseman et al., 2006; DeLuca et al., 2006; Guimaraes et al., 2008) and also provides binding sites for constituents of the outermost kinetochore region, the fibrous corona. This is where core checkpoint signalling molecules are enriched, including the Mads, Bubs, and Mps1. It also contains the RZZ complex, Cenp-F, and the kinetochore-based motor proteins Cenp-E and Dynein-dynactin (Musacchio and Salmon, 2007).

The link between the kinetochore and mitotic checkpoint signalling was strengthened by elegant experiments in cultured marsupial *Potoroo tridactylis* kidney cells (Ptk1 cells). Rieder and colleagues filmed cells going through mitosis and noted that cells delayed anaphase until the last chromosome became bioriented and congressed to the metaphase plate (1994). Furthermore, a subsequent report showed that laser ablation of the last remaining unattached kinetochore in a prometaphase cell allowed anaphase to commence in the presence of the laser-ablated unaligned chromosome, leading the authors to conclude that the unattached kinetochore must have been creating a diffusible signal to restrain anaphase (Rieder et al., 1995).

The localisation of all vertebrate checkpoint proteins to the kinetochore in mitosis, and the depletion of these proteins from kinetochores after biorientation further supported a key role for this structure (Chen et al., 1998; Chen et al., 1996; Li and Benezra, 1996; Taylor et al., 1998; Taylor and McKeon, 1997). Furthermore, the vertebrate proteins Bub1, BubR1 and Mps1 are all kinases (Abrieu et al., 2001; Mills et al., 1992; Taylor et al., 1998; Taylor and McKeon, 1997), making these enzymes candidates for production of the diffusible checkpoint signal via a phosphorylation signalling cascade. Kinetochores were already known to contain phosphorylated species: a study using an antibody towards an unknown phosphoepitope (known as 3f3/2) reported kinetochore staining in PtK1 cells

(Gorbsky and Ricketts, 1993). Gorbsky and Ricketts (1993) showed that not only did this antibody stain kinetochores in a phosphorylation-dependent manner, but it preferentially stained the kinetochores of unaligned chromosomes, suggesting these chromosomes were more highly phosphorylated compared to those that had already achieved biorientation. While we now know more about the kinases contributing to kinetochore phosphorylation (e.g. those discussed in Section 1.7), the precise molecular details are far from being fully understood.

1.4.5 | Inhibition of the APC/C by mitotic checkpoint complexes

A great deal of effort has been focused on understanding how the checkpoint prevents anaphase onset by inhibiting APC/C^{Cdc20}. Early observations showed that Mad2 was associated with the APC/C in mitotic HeLa cells, and could inhibit cyclin B ubiquitination in *Xenopus* egg extracts (Li et al., 1997), suggesting Mad2 might mediate the checkpoint's effect by directly inhibiting the activation of APC/C^{Cdc20}. A recombinant tetrameric form of human Mad2 was subsequently shown to bind directly to Cdc20 and inhibit APC/C activity *in vitro* (Fang et al., 1998), giving rise to the idea that Mad2 is a downstream effector of the mitotic checkpoint signalling network. Furthermore, if the interaction between Cdc20 and Mad2 was perturbed in budding or fission yeast, cells lost checkpoint function (Hwang et al., 1998; Kim et al., 1998). A similar role was also described for BubR1: BubR1 and Bub3 co-purified with Cdc20 from mitotic HeLa cell extracts could inhibit APC/C *in vitro* at approximately physiological concentrations independent of its kinase activity, making it a more potent inhibitor than tetrameric Mad2 (Fang, 2002; Tang et al., 2001). The binding of Mad2 and BubR1 to Cdc20, the APC/C coactivator, suggested the checkpoint may function by simply sequestering the coactivator away from APC/C and thereby preventing it from ubiquitinating securin and cyclin B.

An important study by Sudakin and co-workers (2001) identified and named the mitotic checkpoint complex (MCC), which comprised Mad2, Bub3, BubR1 and Cdc20. This complex, which was isolated from mitotic HeLa cells, potently inhibited the APC/C. Biochemical analysis has indicated that the MCC can exist alone or bound to the APC/C itself (Morrow et al., 2005; Sudakin et al., 2001). The structure of the human APC/C in complex with the entire MCC has been reported (Herzog et al., 2009), providing confirmation that the MCC can directly inhibit APC/C, rather than simply sequestering Cdc20. This is in agreement with data from *S. cerevisiae* showing that Mad3 (related to BubR1) is a pseudo-substrate inhibitor of the APC/C (Burton and Solomon, 2007), meaning it is recognised by APC/C^{Cdc20} and binds tightly, precluding the ubiquitination of true substrates.

A recent study by Kulukian and colleagues (Kulukian et al., 2009) also provided evidence against simple sequestration. The authors reconstituted a system of checkpoint-mediated APC/C inhibition by using purified chromosomes as a source of unattached kinetochores, plus purified checkpoint components. This provided a highly manipulable system for analysis of the level of APC/C inhibition produced under different conditions. Kulukian et al found that unattached kinetochores had a catalytic effect on the production of an APC/C inhibitor from purified checkpoint proteins. This inhibitor could be formed by preincubation of Bub3, BubR1, Mad2, and Cdc20 with chromosomes, followed by incubation of this mixture with APC/C. Importantly, it could also equally effectively inhibit APC/C with Cdc20 pre-bound compared to APC/C without Cdc20, demonstrating non-sequestration mediated inhibition, in keeping with previous reports (Morrow et al., 2005; Sudakin et al., 2001). Notably, Kulukian et al (2008) did not find evidence to support the existence of an true MCC consisting of Bub3-BubR1, Mad2 and Cdc20 as others have reported: rather, the authors showed by size-exclusion chromatography of inhibitor-containing complexes that the majority of Cdc20 was bound to BubR1-Bub3, with very little Mad2 present (Kulukian et al., 2009), in keeping with a previous report (Nilsson et al., 2008). The quaternary MCC may exist as a transient intermediate. Importantly however, Mad2 is a critical regulator of first steps of kinetochore mediated checkpoint signalling – see description of the Mad2 template model in Section 1.4.6.

Since a single unattached kinetochore can sustain anaphase arrest, the checkpoint-derived inhibitor has always been thought to be diffusible, at least within the spindle vicinity (Rieder et al., 1997). Kulukian et al (2009) presented evidence that unattached kinetochores can indeed create a soluble, diffusible inhibitor of the APC/C: removal of chromosomes after inhibition with Bub3, BubR1, Mad2 and Cdc20 resulted in the production of an equally effective APC/C inhibitor as when the chromosomes were left in. Taken together with the above data, this implies that the checkpoint is capable of inhibition of APC/C^{Cdc20} directly, and also by production of a soluble inhibitor complex. This soluble inhibitor may function partly by sequestering Cdc20, since APC/C without any bound coactivator has been shown to exist in cells with an active checkpoint (Herzog et al., 2009). However, evidence suggests that an APC/C-bound pseudosubstrate-like inhibitor is an important product of mitotic checkpoint signalling. Interestingly, Cdc20's ubiquitination (via APC/C) and degradation has been shown to be required for checkpoint activity, adding another facet to the function of the Cdc20-containing inhibitory complex (Nilsson et al., 2008).

This section has summarised current ideas regarding the identity of the APC/C inhibitor, the end-point of mitotic checkpoint signalling. As detailed earlier, the

kinetochore, where all checkpoint components localise, is considered important for checkpoint signalling to create this APC/C inhibitor, which is likely to comprise BubR1, Bub3 and Cdc20, with or without Mad2. The following section will address the role of kinetochores as catalytic platforms for checkpoint signal generation.

1.4.6 | The Mad2 template model

A kinetochore-based model for checkpoint signalling has developed, built on several years' worth of biochemical, structural and cell-based data. In this model, the kinetochore provides a catalytic scaffold for production of an APC/C inhibitor. Fixed-cell analysis had shown that Mad2 localised to unattached kinetochores produced by treatment with the microtubule-depolymerising agent nocodazole (Chen et al., 1996; Waters et al., 1998). Subsequently, Howell and colleagues (2000) made a key observation in the development of the kinetochore-based signalling theory: they found that Mad2 is not stable at unattached kinetochores, but dynamic. This important observation helped firmly establish the idea that kinetochores somehow signalled their lack of proper attachment to the cytosol via Mad2. In subsequent studies, Cdc20, BubR1, Bub3 and Mps1 were also found to flux on and off unattached kinetochores, whereas Mad1 and Bub1 were relatively stable components (Howell et al., 2004; Shah et al., 2004). Thus, all components of the MCC (plus Mps1) cycle on and off kinetochores, strengthening the idea that the kinetochore functions as a catalytic platform.

An intriguing observation was made during the analysis of Mad2 dynamics. Mad2 apparently existed in two separate, equally-sized pools: one pool was stably associated with unattached kinetochores, and one rapidly exchanging with the cytosol (Shah et al., 2004). In addition to binding Cdc20 (Fang et al., 1998; Hwang et al., 1998; Kim et al., 1998; Luo et al., 2000), Mad2 binds tightly to Mad1, and this interaction is required for Mad2's kinetochore localisation (Chen et al., 1999; Chen et al., 1998; Chung and Chen, 2002; Sironi et al., 2002). The existence of both free, non-Mad1-associated and also stable, Mad1-bound forms of Mad2 was found to be necessary for checkpoint signalling in Xenopus egg extracts (Chung and Chen, 2002). These data led to the idea that Mad1 recruits Mad2 to kinetochores in order to hand it over to Cdc20, a key step in formation of the MCC or MCC-like APC/C inhibitor complexes.

Structural and biochemical data shed more light on the nature of the Mad1-Mad2 interaction, and how this might mediate checkpoint signalling. Mad2 binds Cdc20 and Mad1 mutually exclusively (Luo et al., 2002; Sironi et al., 2002), and the two ligands share 10-residue Mad2 binding sites despite being otherwise structurally quite dissimilar (Luo et al., 2002). On binding either Mad1 or Cdc20, Mad2 undergoes substantial structural

rearrangement, changing from an inactive, open conformation (O-Mad2), to an active, closed conformation (C-Mad2) through movement of the 'safety belt' domain (Luo et al., 2000; Luo et al., 2002; Luo et al., 2004; Sironi et al., 2002). Thus, Mad1-bound Mad2 exists in the closed conformation at the kinetochore, where it forms a tight tetrameric complex with a second pair of Mad1-C-Mad2 heterodimers (Sironi et al., 2002): this represents the stable, non-dynamic kinetochore pool of Mad2 (Shah et al., 2004). The cytosolic dynamic pool of Mad2 is recruited to kinetochores as unbound O-Mad2 and handed over to Cdc20 (De Antoni et al., 2005b). Since Mad2's conversion from O-Mad2 to active C-Mad2 is not trivial and occurs spontaneously only very slowly (Luo et al., 2004; Simonetta et al., 2009), a pressing question presented itself: how can the kinetochore Mad1-C-Mad2 core complex catalyse the binding of soluble O-Mad2 to Cdc20, so that C-Mad2-Cdc20 could be produced?

This question was elegantly addressed by De Antoni et al (2005a), who proposed the Mad2 template model for initiation of checkpoint signalling (see Figure 1.5). The authors analysed Mad1, Mad2 and Cdc20 binding *in vitro* and were able to show that C-Mad2 bound to Mad1 forms a receptor for soluble O-Mad2. The Mad1-C-Mad2 tetrameric 'template' catalyses the conversion of soluble O-Mad2 to C-Mad2 bound to Cdc20, via dimerisation of C-Mad2 and O-Mad2. This newly formed C-Mad2-Cdc20 is released from kinetochores, allowing the re-recruitment of more soluble O-Mad2, and explaining the dynamics of fluorescently tagged Mad2 at the kinetochore (Shah et al., 2004). After release from the kinetochore, the C-Mad2-Cdc20 dimer could theoretically create an amplification loop in the cytosol, binding more O-Mad2 and catalysing the hand-over to Cdc20, though this remains unproven (De Antoni et al., 2005a; Musacchio and Salmon, 2007).

Aspects of the Mad2 template model have been reinforced by subsequent work. Structural studies and mapping of the C-Mad2-O-Mad2 interface are consistent with a model in which O-Mad2 selectively binds C-Mad2 and undergoes structural rearrangement to enable it to bind Cdc20, probably via an intermediate partially unfolded form (I-Mad2). (Mapelli et al., 2006; Mapelli et al., 2007; Yang et al., 2008). Furthermore, reconstitution of checkpoint signalling with purified chromosomes and checkpoint components reinforced the necessity for direct interaction between kinetochores (with bound Mad1) and Mad2 for subsequent production of an APC/C inhibitor comprising BubR1, Bub3 and Cdc20 (Kulukian et al., 2009). Mad2 homo-dimerisation was also essential for kinetochore-mediated amplification of APC/C inhibition in the reconstituted system (Kulukian et al., 2009), as demonstrated by the double point mutant $Mad2^{RQ}$, which cannot dimerise (De Antoni et al., 2005a; De Antoni et al., 2005b).

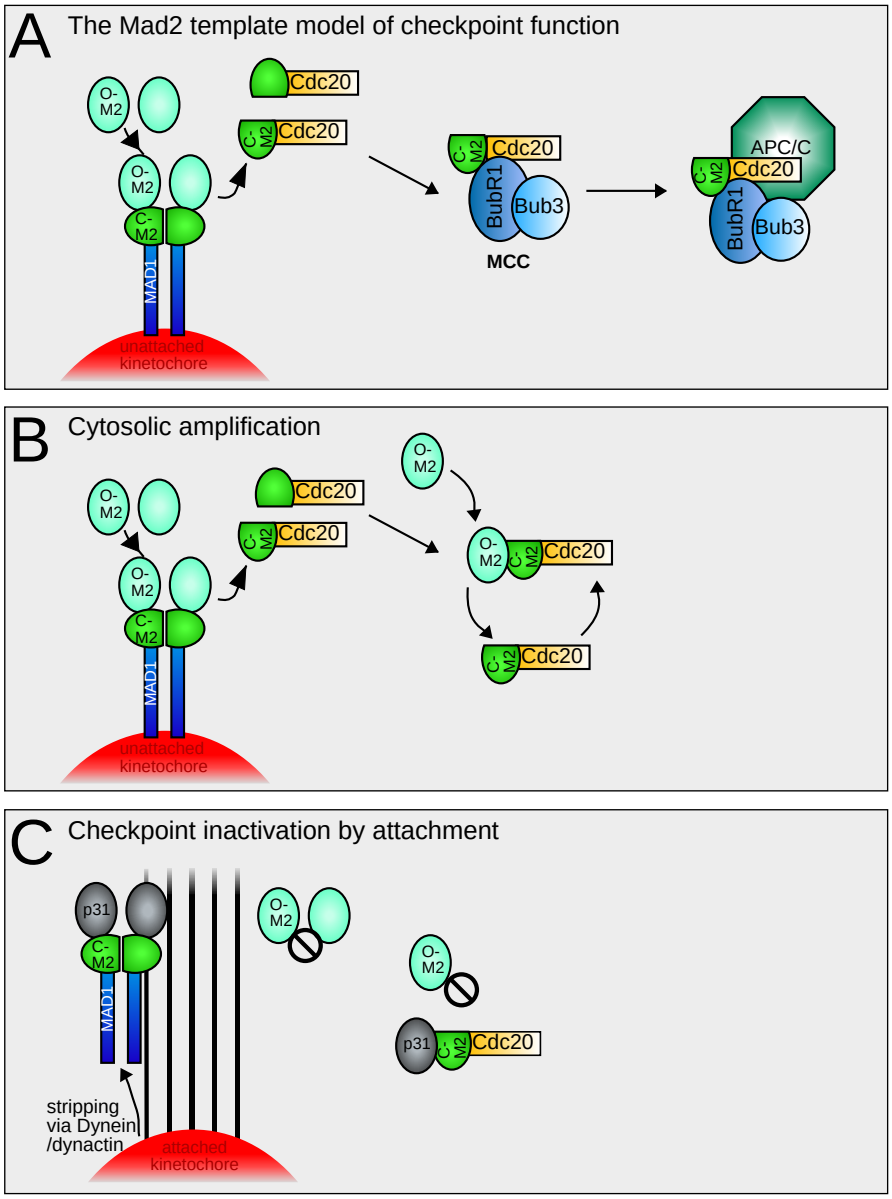

Figure 1.5 The Mad2 template model

(**A**) Stable Mad1-C-Mad2 heterodimers localise to unattached kinetochores, and recruit cytosolic O-Mad2. Conformational dimerisation between O-Mad2 and C-Mad2 facilitates its conversion to C-Mad2 bound to Cdc20. Together with BubR1 and Bub3, C-Mad2-Cdc20 forms the mitotic checkpoint complex (MCC). The MCC may both sequester Cdc20 away from APC/C and also bind directly to the APC/C, preventing it from ubiquitinating cyclin B and securin. Note that the MCC (Cdc20, Mad2, BubR1 and Bub3) may only be transiently formed: Mad2 may be released from the complex (not shown on schematic).

(**B**) Theoretically, cytosolic C-Mad2-Cdc20 can create an positive feedback loop, catalysing the conversion of more O-Mad2 into C-Mad2-Cdc20, and thus amplifying the checkpoint signal.

(**C**) As microtubule occupancy increases, the minus end motor Dynein/dynactin strips Mad1 and Mad2 off kinetochore, contributing to checkpoint silencing. Evidence suggests p31^{comet}, a Mad2 antagonist and structural mimic, may be reactivated at metaphase and bind to C-Mad2, preventing Mad2 conformational dimerisation and inactivating checkpoint signalling.

A putative negative regulator of the Mad2 template model, p31^{comet}, has been described. Originally designated CMT2 (Habu et al., 2002), p31^{comet} is a Mad2-binding protein and negative regulator of the checkpoint: RNAi-mediated knockdown of p31^{comet} leads to a checkpoint-mediated arrest (Habu et al., 2002; Xia et al., 2004). P31^{comet} appears to act as antagonist of Mad2 activation by selectively binding C-Mad2 and competing with O-Mad2 for C-Mad2 binding (Mapelli et al., 2006; Vink et al., 2006; Xia et al., 2004). The crystal structure of the p31^{comet}-Mad2 complex showed that p31^{comet} is structurally very similar to Mad2, and binds C-Mad2 at its dimerisation interface, preventing Mad2 conformational dimerisation by molecular mimicry (Yang et al., 2007a). In this way, p31^{comet} prevents the formation of Mad2-Cdc20 and inactivates the checkpoint (see Figure 1.5).

Whilst the Mad2 template model is now relatively well supported, several questions remain. For example, we do not know how exactly the dramatic Mad2 conformation change is brought about. The O-Mad2 to C-Mad2-Cdc20 transition involves a massive structural alteration, plus the threading of a β-strand of Cdc20's binding site through the β-sheet of Mad2's binding site, making a chain link-like structure (Mapelli et al., 2007; Sironi et al., 2002). Mad2 has been described as 'prion-like' (De Antoni et al., 2005a; Mapelli et al., 2006), and the quite remarkable structural rearrangement it undergoes has led to the suggestion that it may partially unfold and refold during conformational dimerisation and Cdc20 binding (Skinner et al., 2008). The precise mechanisms governing this rate-limiting step in checkpoint signalling are yet to be elucidated.

1.4.7 | Checkpoint satisfaction – tension and attachment

What exactly the mitotic checkpoint senses remains one the most challenging questions in the field. Evidence suggests an important role for kinetochore-microtubule attachment in checkpoint satisfaction: the checkpoint effectors Mad1 and Mad2 enrich at unattached kinetochores, and are depleted from vertebrate kinetochores as microtubule occupancy increases by a mechanism involving Dynein-dynactin-mediated poleward transport (Chen et al., 1996; Howell et al., 2001; Waters et al., 1998). The stripping of Mad1/Mad2 from attached kinetochores is therefore thought to correlate with decreased formation of the APC/C^{Cdc20} inhibitor, and therefore anaphase onset (see Figure 1.5). However, as well as being attached to microtubules emanating from each pole, bioriented kinetochores and the centromeric chromatin between them are also under tension, therefore it seems appropriate for cells to monitor tension as an indicator of correct alignment (McIntosh, 1991). The idea that tension is important for checkpoint silencing was

supported by seminal micromanipulation experiments: Li and Nicklas (1995) showed that preying mantid spermatocytes with a single unaligned chromosome would divide if tension was applied to the chromosome. Furthermore, staining of the 3f3/2 phosphoepitope was reduced at tensionless kinetochores (Nicklas et al., 1995; Waters et al., 1998), and since prevention of dephosphorylation at this site(s) prevented anaphase (Campbell and Gorbsky, 1995), a link between tension and checkpoint silencing was made. Further evidence came from experiments in budding yeast mutants with unreplicated, single chromatids: these cells could not satisfy the checkpoint, leading to the conclusion that tension across the centromere was important for checkpoint satisfaction (Stern and Murray, 2001). In agreement, arresting human cells with a monopolar spindle and normal microtubule dynamics does not prevent attachment, but does prevent tension across the centromere, and causes a checkpoint-mediated arrest (Kapoor et al., 2000).

On the other hand, studies on human cells undergoing mitosis in the presence of an unreplicated genome (MUGs, which have a single centromere and therefore no inter-centromere stretch) indicated that checkpoint satisfaction does not require inter-kinetochore stretch, and supported arguments against a role for tension in checkpoint signalling (O'Connell et al., 2008). However, there is much debate regarding the ability of the checkpoint to sense tension (reviewed in Maresca and Salmon, 2010; Nezi and Musacchio, 2009; Pinsky and Biggins, 2005). At the heart of the debate is the question of whether or not tensionless kinetochores directly influence checkpoint signalling, or have an indirect effect via the destabilisation of low-tension attachments, which produces unattached kinetochores. The role of Aurora B is central to the debate. Aurora B is a serine/threonine kinase that forms a complex with its regulatory subunits INCENP, Survivin and Borealin creating the chromosome passenger complex (CPC), and localises to the centromeric region from prophase to metaphase (Carmena et al., 2009).

1.4.8 | Aurora B – checkpoint signaller or just coincidental?

Aurora B has a well accepted role in error correction (see Section 1.6), but it's role in the checkpoint is subject to some controversy. The budding yeast Aurora B homologue Ipl1 was shown to be required for the checkpoint response to lack of tension (Biggins and Murray, 2001). However, it has been suggested that rather than directly promoting tension-sensitive checkpoint signalling, Aurora B activity may simply destabilise tensionless attachments, leading to reduced microtubule occupancy and attachment-sensitive checkpoint signalling (Hauf et al., 2003; Pinsky et al., 2006; Yang et al., 2009). This would explain why Aurora B inhibition leads to rapid mitotic exit in the presence of Taxol, which stabilises microtubules; but is less effective at inducing checkpoint override

in the presence of nocodazole, which depolymerises microtubules and causes unattached kinetochores (Ditchfield et al., 2003; Hauf et al., 2003).

However, the situation is far from clear cut. There is evidence that Aurora B does contribute directly to checkpoint signalling (Kallio et al., 2002; Morrow et al., 2005; Petersen and Hagan, 2003; Santaguida et al., 2010; Vader et al., 2007). Recent advances have lead to the suggestion that intrakinetochore tension may regulate Aurora B activity, whilst also possibly providing a source of checkpoint signalling independent of microtubule attachment (Maresca and Salmon, 2009; Maresca and Salmon, 2010; Uchida et al., 2009; Wan et al., 2009). These ideas build upon previous work in which inter-kinetochore, centromeric stretching was found to regulate Aurora B's access to substrates and provide an explanation for its ability to sense biorientation (Liu et al., 2009). It is currently unclear whether intrakinetochore stretch contributes to checkpoint activity through Aurora B or some other means, but the evidence is building for a direct role for tension in checkpoint signalling as well as the process of chromosome alignment (reviewed in Maresca and Salmon, 2010; Nezi and Musacchio, 2009).

1.5 | Checkpoint signalling, aneuploidy and cancer

1.5.1 | Aneuploidy and CIN

Aneuploidy, the condition in which cells possess a chromosome number deviating from the normal diploid quota, has been viewed as a likely causal factor in tumourigenesis for almost a century. In his 1914 monograph on the subject, Theodore Boveri proposed that chromosome loss or gain as a result of aberrant cell division could alter the behaviour of a cell and lead to malignancy (reviewed in Manchester, 1995). Cytogenetic analysis indicates that aneuploidy is certainly a common feature of human cancers, in both solid and haematopoietic tumours (Weaver and Cleveland, 2006). In some cases, tumours can be considered stably aneuploid; that is, in possession of an abnormal of chromosome number, but without an elevated frequency of missegregation. In such cases, missegregation will have been induced by a transient event at some point in tumour development, producing a stably inherited aneuploid karyotype (Lingle et al., 2002). A non-tumour related form of stable aneuploidy is found in the cells of humans with trisomy-related syndromes, such as Down's syndrome (Antonarakis et al., 2004). While aneuploidy is not exclusively associated with cancer, chromosomal instability (CIN; an elevated rate of chromosome loss or gain, leading to the state of aneuploidy) is. CIN was first identified as a characteristic of colon cancer cells (Lengauer et al., 1997). Since then, the relationship between aneuploidy, CIN and cancer has been subject to much scrutiny (for recent review, see Holland and Cleveland, 2009; Thompson et al., 2010).

1.5.2 | How is aneuploidy produced?

Aneuploidy (and CIN) has been linked to subnormal mitotic checkpoint function (Cahill et al., 1998). Mitotic checkpoint dysfunction can lead to aneuploidy and CIN, as demonstrated by the cellular phenotype of patients with mosaic variegated aneuploidy (MVA), a rare inherited disorder which is caused by mutations in BUB1B, the gene encoding BubR1 (Hanks et al., 2004; Matsuura et al., 2006). Patients exhibit mosaicism for multiple different chromosome gains and losses throughout different tissues, indicative of CIN. The propensity of MVA individuals to develop childhood cancers provides evidence that aneuploidy can drive the progression of malignancies (Hanks et al., 2004; Matsuura et al., 2006).

Studies using mouse models provide further support for the idea that mitotic checkpoint perturbation can lead to aneuploidy and consequently tumourigenesis. Homozygous deletion of Mad2, Mad1, Bub1, BubR1 or Bub3 is embryonic lethal in mice (Dobles et al., 2000; Iwanaga et al., 2007; Jeganathan et al., 2007; Kalitsis et al., 2000; Perera et al., 2007; Wang et al., 2004), but mice heterozygous for mutations in checkpoint component genes are viable. Such studies have indicated that mice with heterozygous for Mad2 (Michel et al., 2001), Mad1 (Iwanaga et al., 2007), or Bub1 (Jeganathan et al., 2007) had increased rates of spontaneous tumourigenesis. Furthermore, mice heterozygous for a mutant, checkpoint-deficient form of Cdc20 that cannot bind Mad2 (AAA-Cdc20) had a significantly increased tumour formation rate, consistent with the idea that mitotic checkpoint defects (as opposed to unknown, non-checkpoint functions) can promote aneuploidy and tumourigenesis (Li et al., 2009). However, though mutations in mitotic checkpoint genes are occasionally identified in cancer cell lines (e.g. Cahill et al., 1998; Percy et al., 2000) and in tumour samples (e.g. Kan et al., 2010), it has become apparent that mutations in checkpoint genes are too infrequent to account for the amount of aneuploidy and CIN seen in human cancers.

In fact, it is now acknowledged that the original causative link between checkpoint inactivation/weakening and the CIN reported in colon cancer cells (Cahill et al., 1998) might have been misleading. Subsequent studies showed that CIN cells do in fact have robust mitotic checkpoint responses to spindle depolymerisation (Gascoigne and Taylor, 2008; Tighe et al., 2001), and are capable of restraining anaphase until all chromosomes are aligned in an unperturbed mitosis (Thompson and Compton, 2008). It follows that tumour cells often become aneuploid via other mechanisms. Persistent merotelic attachment (see Figure 1.6), leading to lagging chromosomes at anaphase, is a possible alternative cause of aneuploidy in CIN cells (Gascoigne and Taylor, 2008; Thompson and Compton, 2008). Merotelic attachments are not sensed by the mitotic checkpoint since

kinetochores are both attached and under tension, but are usually corrected prior to anaphase (Cimini, 2008). Evidence suggests that aneuploidy can be caused by alterations in microtubule dynamics that prevent effective correction of merotelics: overexpression of two kinetochore/centromeric microtubule-depolymerising kinesins, Kif2b and MCAK, reduced the frequency of missegregation events in a CIN cell line (Bakhoum et al., 2009). Another possible cause of aneuploidy is defective chromatid cohesion: mutations in genes encoding proteins involved in cohesion have been detected in aneuploid colon cancer cells (Barber et al., 2008). Possession of abnormally high numbers of centrosomes has also been linked to the production of aneuploid progeny: while multipolar division can lead to highly aneuploid, inviable daughter cells which are eliminated from the population, cells with more than 2 spindle poles tend to undergo centrosome clustering to simulate a bipolar spindle, allowing relatively normal rates of proliferation (Brinkley, 2001; Ganem et al., 2009). The formation of pseudo-bipolar spindles from a transient multipolar intermediate increases the frequency of erroneous attachments such as merotelics, placing additional stress on the correction machinery and increasing the likelihood that errors will remain uncorrected and lead to missegregation and aneuploidy (Ganem et al., 2009).

However it happens, increased incidence of aneuploidy is clearly able to promote cancer progression (Holland and Cleveland, 2009). This seems logical: CIN allows constant reshuffling of genes in a cell population, meaning cells are more likely to acquire the genetic alterations required to promote tumourigenesis and malignancy. However, it also seems logical that aneuploidy cannot always be beneficial in terms of cell growth and survival: some genetic changes can be detrimental. Indeed, aneuploid yeast strains with extra chromosomes grew slowly compared to those with normal chromosome number (Torres et al., 2007). Moreover, mouse cells engineered to contain extra copies of one of 4 mouse chromosomes grew more slowly than diploid cells (Williams et al., 2008). *In vivo,* tumour-promoting missegregation events are likely to be quite rare compared to detrimental ones, which are presumably eliminated from the cell population. Additionally, further genetic changes are probably required to enable a cell to survive with aneuploidy, since it is frequently detrimental to cell fitness (Torres et al., 2008). In keeping with the idea that aneuploidy does not always promote tumourigenesis, Weaver and co-workers (2007) showed that mice haploinsufficient for Cenp-E exhibited aneuploidy *in vivo*, but developed fewer carcinogen-induced tumours than control mice, and also fewer liver tumours (Weaver et al., 2007). In addition, Cenp-E+/- mice that were genetically predisposed to cancer by deletion of both copies of the tumour suppressor $p19^{ARF}$ developed tumours more slowly then Cenp-E+/+, $p19^{ARF}$-/- mice that were not prone to aneuploidy (Weaver et al., 2007). This indicates that aneuploidy can act as a

tumour suppressor. Remarkably however, in the same Cenp-E+/- animals, the incidence of spontaneous lymphoma and lung cancer was increased, indicating that aneuploidy caused by Cenp-E haploinsufficiency can also act oncogenically (Weaver et al., 2007). Thus, the cellular context has a role in determining the effects of aneuploidy.

1.5.3 | Targeting the mitotic checkpoint as a cancer therapy

It is thought that while relatively minor missegregation events can promote tumourigenesis in some contexts, very severe aneuploidy is incompatible with cell survival (Holland and Cleveland, 2009). In keeping with the embryonic lethality reported in mice with homozygous deletions of checkpoint proteins (Dobles et al., 2000; Iwanaga et al., 2007; Jeganathan et al., 2007; Kalitsis et al., 2000; Perera et al., 2007; Wang et al., 2004), fully ablating the mitotic checkpoint by RNAi leads to apoptosis in cultured cancer cells (Kops et al., 2004; Michel et al., 2004). These observations led to the suggestion that the mitotic checkpoint may be a plausible target for cancer therapeutics (Kops et al., 2004; Michel et al., 2004). However, it remains to be seen whether the mitotic checkpoint can be targeted without affecting normal cells *in vivo,* although there have been encouraging hints that perturbing Mps1 or BubR1 function in combination with low dosage Taxol treatment may be a strategy for selectively targeting cancer cells by raising aneuploidy to intolerable levels (Janssen et al., 2009).

1.6 | The mechanism of chromosome alignment

To prevent errors in segregation, the mitotic checkpoint restrains anaphase until all chromosomes are properly attached to the microtubules mitotic spindle and aligned at the metaphase plate. To get the chromosomes to this point requires the cooperative functioning of kinetochores, spindle microtubules and associated motor proteins (for review, see Walczak and Heald, 2008). As prometaphase progresses, chromosomes are captured by microtubules from each pole, and move towards the spindle equator. In metazoans, chromosomes and microtubules begin to interact after NEBD. The centrosomes nucleate microtubules at the minus ends, allowing the dynamically unstable plus ends to contact chromosomes; following end-on attachment to kinetochores, microtubules become stabilised (Kirschner and Mitchison, 1986). Once stable, end-on attachments have been formed between the kinetochore of each of the paired sister chromatids, biorientation has been achieved. However, since kinetochore-microtubule attachment is stochastic and random, many improper attachments are likely to form before the goal of biorientation is reached. Thus, the correction of errors is crucial to facilitate biorientation. Examples of erroneous attachments between the spindle and kinetochores are depicted in Figure 1.6.

Syntely, the condition in which both sister kinetochores become attached to the same pole of the spindle, is predicted to occur transiently during a normal prometaphase. Syntelic attachments must be corrected, and to do this the microtubule attachments must be destabilised in order to provide a new opportunity for biorientation to occur. Merotelic attachments, where one sister kinetochore forms attachments to both of the spindle poles, must also be corrected before anaphase, or the chromatid will be pulled in both directions creating a lagging chromosome, reminiscent of an anaphase bridge, which may be lost from the daughter cell (Cimini, 2008). Aurora B, as part of the CPC (Carmena et al., 2009) is involved in ensuring syntelic and merotelic attachments are destabilised.

1.6.1 | Aurora B and error correction

In mammalian cells, the Aurora kinase family consists of three members: Aurora A, B and C (for review see Carmena et al., 2009; Vader and Lens, 2008). Yeast only have one Aurora family kinase: Ipl1 in budding yeast and Ark1 in fission yeast. Work in budding yeast showed that Ipl1 activity destabilises kinetochore-microtubule attachments lacking in tension (Tanaka et al., 2002). In keeping with this, inhibiting Aurora B activity in human cells using the small molecule Hesperadin led to an increase in the frequency of syntelic attachments (Hauf et al., 2003). In elegant experiments using successive inhibitor treatments in human cells, Lampson and co-workers were able to demonstrate the importance of Aurora B in correction of syntelic attachments (Lampson et al., 2004). Cells were treated transiently with monastrol, an inhibitor of spindle pole separation (Kapoor et al., 2000; Mayer et al., 1999). Since cells were kept in a monopolar state, they had a high probability of forming syntelic attachments (Kapoor et al., 2000). After monastrol was removed and the spindle allowed to bipolarise, cells with active Aurora B could correct the syntelic attachments, achieving full alignment. Cells lacking Aurora B activity were unable to destabilise the monopolar, syntelic attachments, and persisted with chromosomes attached to only one pole of the bipolar spindle (Lampson et al., 2004). Taken together, these data suggest a role for Aurora B/Ipl1 in correction of erroneous attachments arising during prometaphase.

The molecular mechanisms by which this occurs are becoming clearer. One way Aurora B appears to influence microtubule stability at kinetochores is via the microtubule depolymerase MCAK. Aurora B activity is required to recruit MCAK to the centromere\kinetochore, and phosphorylation leads to a decrease in MCAK activity, and in turn an increase in local microtubule stability (Andrews et al., 2004; Lan et al., 2004).

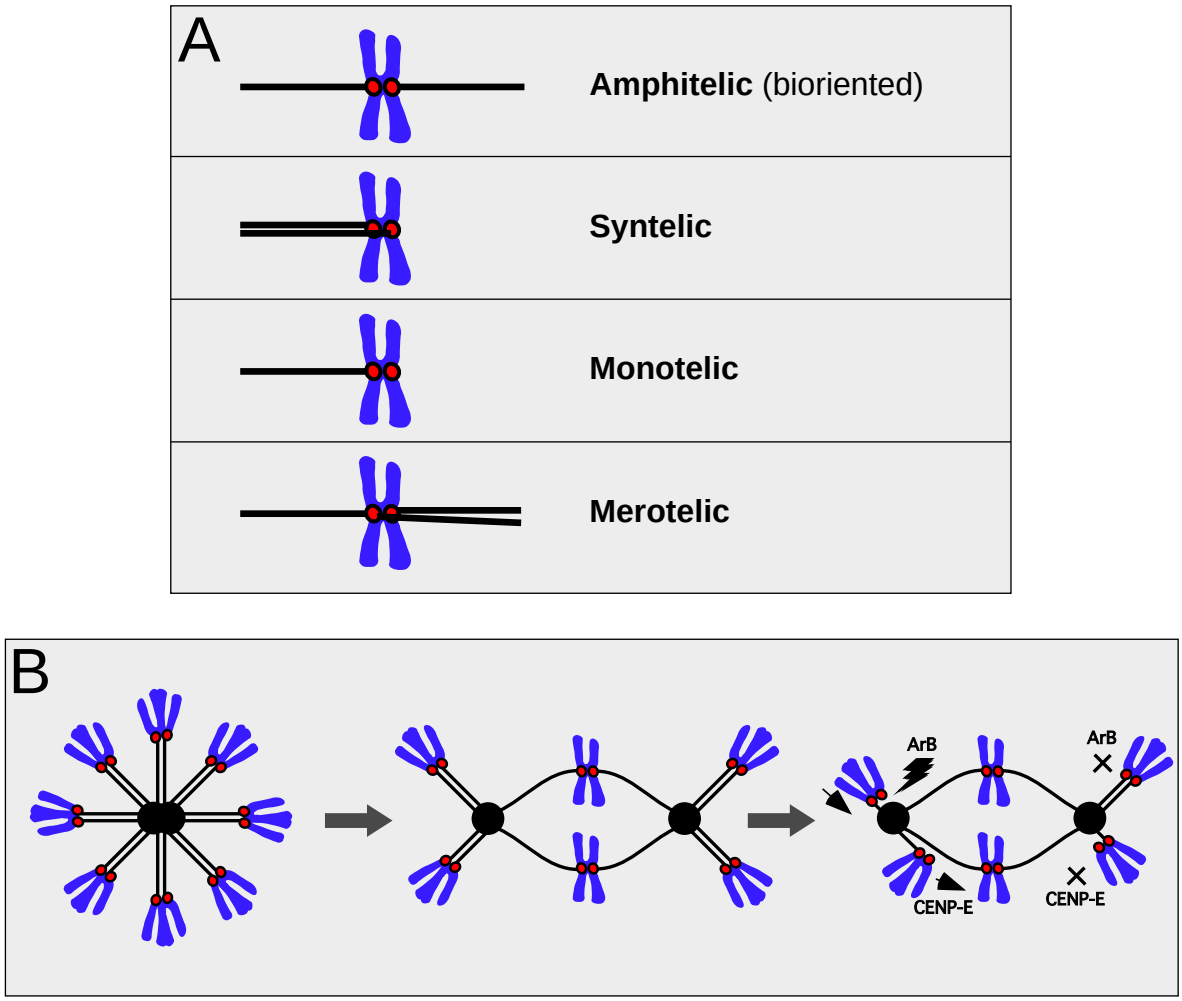

Figure 1.6 Kinetochore-microtubule attachment and alignment
(**A**) Types of correct and incorrect chromosome attachment to the mitotic spindle. Amphitelic attachment: sister kinetochores are correctly attached, via stable end-on microtubule interactions, to opposite spindle poles (bioriented). The kinetochore/centromere region is under tension. When all chromosomes have achieved amphitelic attachment, the checkpoint is satisfied and anaphase commences. Syntelic attachment: a form of incorrect attachment in which both sister kinetochores are attached to one spindle pole. An Aurora B dependent mechanism corrects these attachments. Monotelic attachment: one kinetochore is attached to one spindle pole while its sister remains unattached. Merotelic attachment: One sister kinetochore is attached to both spindle poles. While anaphase is delayed in the presence of monotelic and syntelic attachments, merotelics are not detected by the checkpoint, but are usually corrected prior to anaphase by a mechanism involving Aurora B.
(**B**) Error correction after monastrol wash-out. Monastrol arrests cells with the centrosomes close together, forming a monopolar spindle with a high incidence of syntelic attachments (left-hand diagram). If monastrol is removed from the cells, the spindle poles separate (middle diagram), allowing the syntelic attachments to be effectively corrected and converted to biorientation. In unperturbed cells, Aurora B and Cenp-E cooperate to correct these syntelic attachments: Aurora B activity destabilises syntelic attachments and promotes shortening of microtubules, moving the chromosome toward the pole. At the pole, the mono-oriented chromosome congresses toward the cell equator via lateral association between the unattached sister and a pre-existing K-fibre. Aurora B inhibition or Cenp-E RNAi therefore prevents chromosomes from aligning at the metaphase plate by inhibiting syntelic destabilsation/MT shortening or poleward congression, respectively. (B) is adapted from Kapoor, et al (2006).

Aurora B also phosphorylates Ndc80/Hec1, a component of the Ndc80 complex in the KMN network at the inner kinetochore, and in doing so, destabilises microtubule attachments; this function is conserved from yeast to human (Cheeseman et al., 2002; Cheeseman et al., 2006; Ciferri et al., 2008; DeLuca et al., 2006; Guimaraes et al., 2008). But how might Aurora B distinguish between microtubules that require destabilisation and those that do not? As previously mentioned, spatial separation, governed by tension across the kinetochore and centromere, affects the access of Aurora B to its various substrates and allows error correction to occur only at tensionless kinetochores (Liu et al., 2009). Intrakinetochore stretching may also contribute to this mechanism (Maresca and Salmon, 2010).

1.6.2 | Microtubule motors and chromosome congression

As well as the correction of improper attachments, microtubule motor-mediated movement of chromosomes during mitosis contributes to proper alignment (reviewed in Cheeseman and Desai, 2008; Kops et al., 2010). As well as forming end-on attachment with microtubules, kinetochores can associate laterally with microtubules of the spindle. Evidence suggests these lateral connections facilitate chromosome movement prior to biorientation, thereby helping to position chromosomes in places where end-on attachments are likely to occur. The two motor proteins that are known to localise to kinetochores in mitosis are Cenp-E, a plus-directed kinesin (Kapoor et al., 2006; Schaar et al., 1997; Wood et al., 1997; Yen et al., 1992) and minus-end directed Dynein-dynactin (Pfarr et al., 1990; Yang et al., 2007b).

Early in prometaphase, the Dynein-dynactin complex is thought to promote poleward movement, taking chromosomes to a position where many microtubules are found and thus increasing the chance of end-on kinetochore capture (Yang et al., 2007b). Cenp-E powers congression from the polar region toward the metaphase plate at the cell equator, which, in a normal prometaphase, is necessary for congression of a few chromosomes that become trapped at the poles, though many chromosomes align normally (Kapoor et al., 2006; Weaver et al., 2003; Wood et al., 1997). The role of Cenp-E was elegantly demonstrated by Kapoor and colleagues (2006) who, in an extension of a previous study (Lampson et al., 2004), used monastrol to arrest cells transiently with a monopolar spindle, then washed the drug out, allowing bipolarisation in the presence of numerous syntelic attachments. Using a combination of drug treatments and RNAi, followed by live-cell imaging, immunofluorescence and electron microscopy, the authors showed that Aurora B activity was required for destabilisation of syntelic attachments and shortening of microtubules, bringing the chromosomes towards the pole, but congression of monotelic polar

chromosomes towards the metaphase plate via lateral association with other kinetochore fibres (K-fibres) was not possible without Cenp-E (Kapoor et al., 2006). In other words, Cenp-E takes mono-oriented polar chromosomes towards the equator by 'piggy-backing' on pre-formed K-fibres, promoting contact with microtubules emanating from the opposite pole and, therefore, biorientation. This study demonstrated nicely how cooperation between error correction (via Aurora B) and microtubule motors is required to promote alignment and accurate segregation (see Figure 1.6).

As well as powering chromosome movements to promote biorientation, both Dynein-dynactin and Cenp-E are reported to have other roles at the kinetochore. Dynein-dynactin promotes stable kinetochore-microtubule attachments (Chan et al., 2009; Yang et al., 2008); similarly Cenp-E depleted kinetochores reportedly bind fewer microtubules than those in control cells (McEwen et al., 2001; Putkey et al., 2002). Cenp-E may also contribute to the amplification of checkpoint signalling, via activation of BubR1 kinase activity (Mao et al., 2003; Mao et al., 2005; Weaver et al., 2003), whereas Dynein-dynactin is required for poleward trafficking of checkpoint components away from kinetochores, contributing to checkpoint silencing on bioriented chromosomes (Howell et al., 2001).

1.7 | Mitotic kinases in the checkpoint and chromosome alignment

It is notable that the template model of kinetochore-based checkpoint signalling does not include any kinases. However, the requirement for kinases for full checkpoint function in cells is undisputed, and in addition to their putative role in MCC/MCC-like complex generation, kinetochores may function as a platform to facilitate a phosphorylation cascade (Burke and Stukenberg, 2008). A recent study showed unattached kinetochores were not critical for formation of an APC/C inhibitor from purified MCC components *per se*, but their presence did amplify production of the inhibitor (Kulukian et al., 2009): importantly, a proportion of several kinetochore-bound kinases (Mps1, Aurora B and Bub1) was retained on the purified mitotic chromosomes that provided the unattached kinetochores. This suggests an important function of kinetochore phosphorylation may be signal amplification to enable the checkpoint to sense one unaligned kinetochore. Aurora B is one mitotic kinase with a role in alignment and, arguably, a role in checkpoint signalling too, as has already been outlined in Section 1.4 and 1.6. The role of Mps1 in mitosis will be discussed in Section 1.8. Several other mitotic kinases, some of which have been mentioned above, have been implicated in checkpoint signalling and/or chromosome alignment, including Bub1, BubR1 and Plk1. I will briefly outline the proposed roles of these molecules below.

1.7.1 | Bub1

Bub1 interacts with Bub3 and BubR1 and is recruited to unaligned kinetochores in prophase (Johnson et al., 2004; Taylor et al., 1998). In contrast to Bub3 and BubR1, Bub1 is a relatively stable kinetochore resident (Howell et al., 2004; Shah et al., 2004), and may act as scaffold to facilitate recruitment of other checkpoint proteins (Rischitor et al., 2007; Sharp-Baker and Chen, 2001). Full depletion of Bub1 protein by RNAi (Meraldi and Sorger, 2005) or *BUB1* knock-out (Perera et al., 2007) leads to checkpoint malfunction in human cells and mouse embryonic fibroblasts (MEFs) respectively. Bub1 has been shown to phosphorylate Cdc20, thereby contributing to APC/C inhibition (Kang et al., 2008; Tang et al., 2004). However, the requirement for Bub1 kinase activity in checkpoint signalling is controversial: a recent study found that kinase-dead mutants could rescue checkpoint signalling in *BUB1* null MEFs (Perera and Taylor, 2010). Interestingly, Bub1 is reported to play a role in chromosome alignment (Johnson et al., 2004; Meraldi and Sorger, 2005; Perera et al., 2007); this also appears to be independent of its kinase activity (Perera and Taylor, 2010). So, while Bub1's presence at kinetochores seems to be important for both checkpoint signalling and alignment, the role of its activity is subject to debate.

1.7.2 | BubR1

As discussed above, BubR1 is part of the MCC or MCC-like complex that inhibits the APC/C^{Cdc20}. The analogous protein in budding yeast, Mad3, has no kinase activity (Li and Murray, 1991). In human cells, BubR1 depletion causes spindle checkpoint inactivation and accelerates progression through an unperturbed mitosis (Chan et al., 1999; Meraldi et al., 2004; Morrow et al., 2005); however, there are contrasting reports as to the requirement of its kinase activity for checkpoint signalling in vertebrate cells (Chen, 2002; Malureanu et al., 2009; Mao et al., 2003). BubR1 is also involved in chromosome alignment (Ditchfield et al., 2003; Lampson and Kapoor, 2005), and this function may require its kinase activity (Rahmani et al., 2009). BubR1 is hyperphosphorylated in mitotic cells (Chan et al., 1999; Taylor et al., 2001), and has been shown to be substrate for Aurora B, Plk1 and Mps1 (Ditchfield et al., 2003; Elowe et al., 2007; Hauf et al., 2003; Huang et al., 2008; Matsumura et al., 2007). BubR1's phosphorylation status may be regulated differently by microtubule attachment and tension (Huang et al., 2008), suggesting it may receive and transduce signals from upstream kinases monitoring various aspects of kinetochore-spindle interaction.

1.7.3 | Plk1

Plk1 has multiple roles in mitosis and cytokinesis (reviewed in Archambault and Glover, 2009; Petronczki et al., 2008). Its enrichment at the centromere/kinetochore

region peaks in prometaphase and depends upon its own activity (Arnaud et al., 1998; Lenart et al., 2007). Evidence suggests Plk1 (or the *X. laevis* homologue Plx1) is the kinase responsible for producing the tension-sensitive 3f3/2 phosphoepitope (Ahonen et al., 2005; Wong and Fang, 2005). In *X. laevis* egg extracts, the 3f3/2 epitope is a Plx1-mediated phosphorylation site on BubR1 (Wong and Fang, 2007). Plk1 also phosphorylates Bub1 (Qi et al., 2006), and both Bub1 and BubR1 require prior Cdk1-mediated phosphorylation prime to facilitate Plk1 binding (Qi et al., 2006; Wong and Fang, 2007). There are clearly links between Plk1 and mitotic checkpoint components; however, in human cells devoid of Plk1 activity, cells enter a robust checkpoint-mediated arrest with monopolar spindles and normal levels of kinetochore-bound Mad2 (Lenart et al., 2007), indicating Plk1 kinase activity is dispensable for the mitotic checkpoint. Instead, Plk1 activity appears to promote formation of stable end-on kinetochore-microtubule attachments, perhaps through the aforementioned interaction with BubR1 (Elowe et al., 2007; Lenart et al., 2007; Matsumura et al., 2007).

1.8 | Mps1, a kinase with a dual role in mitosis

1.8.1 | Mps1 family history

The *Monopolar spindle 1* (*MPS1*) gene was discovered in budding yeast in a screen for regulators of spindle pole body (SPB; the yeast equivalent of the centrosome) duplication (Winey et al., 1991). It was later found to encode a dual-specificity protein kinase (Lauze et al., 1995), and to be essential for spindle checkpoint function in budding yeast (Weiss and Winey, 1996). Mps1 is conserved from yeast to humans (Fisk et al., 2004), though *Caernorhabditis elegans* does not possess an obvious homologue; a unique kinase Zyg1 is postulated to play an analogous role (O'Connell et al., 2001). Mps1's human homologue was originally identified as TTK or PYT (Hogg et al., 1994; Lindberg et al., 1993; Mills et al., 1992) a cell cycle-regulated kinase associated with cell proliferation, and is still referred to as TTK in some databases. The human Mps1/TTK gene (NCBI accession number NM_003318) encodes an 857 residue, 97 kDa protein with a 525 amino acid N-terminal domain, followed by the 266 residue catalytic domain and a short C-terminal extension of 66 amino acids (see Figure 1.7).

1.8.2 | Centrosome duplication

Mps1 is required for spindle pole body duplication in budding yeast (Winey et al., 1991), however its role in centrosome duplication in mammals is subject to debate. Several report have suggested that either human or murine Mps1 localises to centrosomes (Fisk et al., 2003; Fisk and Winey, 2001; Tyler et al., 2009) and is required for centrosome

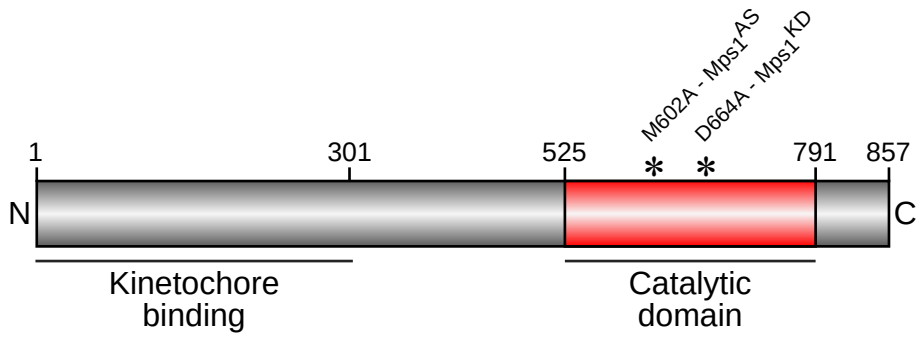

Figure 1.7 Schematic diagram of human Mps1
The domain structure of human Mps1 kinase is shown. The N-terminal region (1-301) is involved in kinetochore binding; the catalytic (kinase) domain is towards the C-terminal of the protein. Catalytic domain point mutants used experimentally are marked with asterisks: the M602A gatekeeper residue mutation renders the kinase sensitive to inhibition with bulky ATP analogues ($Mps1^{AS}$); the D664A mutation renders the kinase catalytically inactive or kinase-dead ($Mps1^{KD}$) because it changes a critical aspartate residue in the highly conserved DFG motif, which is necessary to orient ATP in the active site.

duplication during S phase (Fisk et al., 2003; Fisk and Winey, 2001; Mattison et al., 2007). However, there have also been reports suggesting human Mps1 has no role at the centrosome (Stucke et al., 2004; Stucke et al., 2002). Another very recent report saw no effect on centrosome duplication in cells lacking Mps1 activity (Kwiatkowski et al., 2010). The reason(s) for the discrepancy between studies is unclear; differences in antibody and cell line behaviour have been cited (Winey and Huneycutt, 2002). It is possible that very low levels of Mps1 activity are needed to perform the centrosome duplication function during S phase, making a defect difficult to produce (Fisk et al., 2003).

1.8.3 | Mps1 and the mitotic checkpoint

The requirement for Mps1 in the mitotic checkpoint can reasonably be described as universal: studies in yeast (He et al., 1998; Weiss and Winey, 1996), *D. melanogaster* (Fischer et al., 2004), *X. laevis* (Abrieu et al., 2001), *Danio rerio* (Poss et al., 2004) and human cells (Jelluma et al., 2008b; Liu et al., 2003; Stucke et al., 2002; Tighe et al., 2008) have concluded that Mps1 is required for the checkpoint. In human cells, Mps1 is required not only for the checkpoint response to spindle damage (e.g. nocodazole treatment), but also to restrain anaphase onset in an otherwise unperturbed mitosis (Jelluma et al., 2008b; Tighe et al., 2008). In addition to accelerated passage through an unperturbed mitosis, cells lacking Mps1 also exit mitosis with unaligned chromosomes, yielding aneuploid daughter cells (Jelluma et al., 2008b; Tighe et al., 2008).

The idea that Mps1 was at, or near, the top of the checkpoint signalling network initially came from studies in budding yeast, which showed that Mps1 overexpression activated the spindle assembly checkpoint, causing an arrest that was abolished by simultaneous mutation of other the checkpoint components Mad2, Mad2, Bub1, or Bub3 (Hardwick et al., 1996). In budding yeast, the downstream target of Mps1 appears to be Mad1, which becomes hyperphosphorylated after Mps1 overexpression (Hardwick and Murray, 1995; Hardwick et al., 1996). There is currently no evidence to support Mps1 phosphorylation of Mad1 in human cells, though localisation data does support a role for Mps1 upstream in the signalling network in vertebrates. Mps1 is required to recruit the checkpoint effector molecules Mad1 and Mad2 to kinetochores in human cells (Jelluma et al., 2008b; Liu et al., 2003; Liu et al., 2006; Martin-Lluesma et al., 2002; Tighe et al., 2008; Xu et al., 2009). Inhibition of Mps1 has also been shown to lead to BubR1 loss at kinetochores in human cells (Schmidt et al., 2005), and immunodepletion of Mps1 from *X. laevis* egg extracts reportedly perturbs Bub1, Bub3, Mad1, Mad2 and Cenp-E localisation (Abrieu et al., 2001; Vigneron et al., 2004).

Other than putative Mad1 phosphorylation in budding yeast (Hardwick et al., 1996), the targets of Mps1 that regulate checkpoint activity are yet to be fully elucidated. Some progress has been made: a recent report found that Mps1 phosphorylated several sites in the N-terminal of Ndc80/Hec1 in budding yeast (Kemmler et al., 2009). Mutation of 14 of the phosphorylation sites to alanine to prevent phosphorylation caused checkpoint failure; conversely, mutation of the same sites to phospho-mimetic aspartate residues caused metaphase arrest due to a constitutively active checkpoint. Whether this function is conserved remains to be seen. Mps1 has also been shown to phosphorylate Dam1, a protein implicated in microtubule binding at the budding yeast kinetochore (Shimogawa et al., 2006). Mps1 phosphorylation of this protein impairs coupling between Dam1 and microtubules (Shimogawa et al., 2006). As Dam1 is not conserved, it is currently unclear whether Mps1 performs an analogous function in higher organisms.

In human cells, Mps1 was reported to contribute to BubR1 phosphorylation on 4 serine residues: phospho-specific antibodies to the sites on BubR1 showed a decrease in signal after Mps1 depletion by RNAi (Huang et al., 2008). While these Mps1 sites await more rigorous validation, and the functional relevance of this phosphorylation is not fully understood, Mps1 may be one of several mitotic kinases targeting BubR1 to control checkpoint signalling. If the role of Mps1 in phosphorylation of Ndc80 is conserved in humans, this may be another example of human Aurora B and Mps1 converging upon the same substrates.

1.8.4 | Mps1 and Aurora B in error correction

The emerging relationship between Mps1 and Aurora B was the subject of a recent report from Jelluma and co-workers (2008b). The authors used an RNAi complementation approach to replace endogenous Mps1 with active (wild type, WT) or inactive (kinase dead, KD) alleles, and found that cells lacking Mps1 activity had difficulty aligning chromosomes, even after cells were kept in mitosis for an extended period by treatment with the proteasome inhibitor MG132. Jelluma et al found that these misalignments were attributable to a lack of error correction, which in turn was a consequence of decreased Aurora B activity, both globally (as shown by a decrease in immunoprecipitated Aurora B activity, and Aurora B substrate phosphorylation by western blot) and at centromeres (as shown by immunofluorescence using antibodies to Aurora B centromeric substrates). Furthermore, Mps1-catalysed phosphorylation of Borealin on 4 threonine residues was shown to be the cause of the decreased Aurora B activity (Jelluma et al., 2008b). This report presented the first evidence that Mps1 was involved in alignment in human cells, though an earlier study had concluded that Mps1 was required for error correction in

budding yeast (Maure et al., 2007). However, Maure and colleagues did not see any decrease in Ipl1 activity. Whether or not the mechanisms are fully conserved, the requirement of Mps1 activity for both checkpoint signalling and error correction adds a new facet to the relationship between chromosome alignment and checkpoint signalling. The two processes might be controlled by an interwoven web of signalling pathways, rather than operating though distinct linear molecular networks. Mps1 joins Bub1, Aurora B and BubR1 as kinases reported to have dual roles in alignment mechanics and the checkpoint surveillance mechanism.

1.8.5 | Mps1 regulation

Mps1 is maximally active and phosphorylated in mitosis (Hogg et al., 1994; Liu et al., 2003; Stucke et al., 2002). Levels of Mps1 phosphorylation increase following treatment with nocodazole or taxol, suggesting this phosphorylation is linked to checkpoint activity (Stucke et al., 2002). The amount of Mps1 protein in the cell is also cell cycle regulated: when analysed by western blot, Mps1 is visible in lysates derived from cells in all stages of the cell cycle, however its levels increase concomitant with cyclin B as cells enter mitosis, and drop again after mitotic exit (Palframan et al., 2006; Stucke et al., 2002). In budding yeast, the APC/C^{Cdc20} degrades Mps1 after anaphase (Palframan et al., 2006); it is not yet known whether this mechanism is conserved.

Several studies have reported that Mps1 can autophosphorylate, and that this autophosphorylation is required for full activity (Chu et al., 2008; Jelluma et al., 2008a; Kang et al., 2007; Mattison et al., 2007; Mills et al., 1992; Stucke et al., 2004). Moreover, autophosphorylation at threonine 676 in the activation loop of the catalytic domain is important for full activity (Jelluma et al., 2008a; Kang et al., 2007; Mattison et al., 2007). The crystal structure of the Mps1 catalytic domain has been solved, and suggests that phosphorylation in the activation loop may cause a conformational change that allows proper orientation of the adenosine triphosphate molecule (ATP) in the active site, thus increasing kinase activity (Chu et al., 2008). Mps1 is capable of trans-autophosphorylation at T676; indeed, forced dimerisation of Mps1 in cells hyperactivates the kinase (Kang et al., 2007). This led to speculation that Mps1 may dimerise and trans-activate at kinetochores, though the relationship between T676 phosphorylation, kinetochore localisation and Mps1 activity is unknown.

Like other checkpoint proteins, Mps1 localises to the kinetochores in mitosis (Abrieu et al., 2001; Stucke et al., 2002). In human cells, this is dependent on proper assembly of the outer kinetochore: depletion of components of this complex, Hec1 (Martin-Lluesma et al., 2002) or Nuf2 (Stucke et al., 2004) leads to perturbation of the outer plate (DeLuca et

al., 2005) and loss of Mps1 kinetochore localisation. The kinetochore-binding region of Mps1 has been narrowed down to amino acids 1-301 of the N-terminal domain (Liu et al., 2003; Stucke et al., 2004). This region localises to kinetochores and behaves in a dominant-negative way, preventing endogenous Mps1 from localising to kinetochores and perturbing the mitotic checkpoint (Liu et al., 2003). Analysis of fluorophore-tagged Mps1 in living cells revealed that its localisation at the kinetochores is dynamic (Howell et al., 2004).

Little is known about the regulation of Mps1 kinetochore targeting. Though the localisation of an N-terminal fragment lacking the catalytic domain to kinetochores suggests kinase activity is not intrinsically required for binding to kinetochores, it is not clear whether or not the fragment localises by virtue of interaction with the endogenous kinase (e.g. intermolecular phosphorylation). There is conflicting data regarding the importance of Mps1 kinase activity to localise to kinetochores: while some studies report that kinase-dead mutant Mps1 is reduced at kinetochores compared to wild type in human cells or *X. laevis* egg extracts depleted of Mps1 (Xu et al., 2009; Zhao and Chen, 2006), other groups have shown that kinase-dead Mps1 is readily visible at kinetochores under comparable conditions (Abrieu et al., 2001; Jelluma et al., 2008b). In *X. laevis* egg extracts and human cells, phosphorylation by MAP kinase at a conserved serine residue (S821 in human Mps1) reportedly promotes Mps1's localisation to kinetochores (Borysova et al., 2008; Zhao and Chen, 2006).

1.8.6 | The role of Mps1 kinase activity in the checkpoint and alignment

The identification of substrates is an important goal in the quest to understand the role of a kinase's activity in cells. To date, a number of Mps1 substrates have been identified. Several of these are relevant to SPB or centrosome function (see Table 1.1). Additionally, the reported phosphorylation of Smad2 and Smad3 implicated Mps1 activity in regulation of gene expression via a non-canonical Smad signalling pathway (Zhu et al., 2007). Mps1 was also reported to phosphorylate BLM (Bloom) helicase, and perturbation of this phosphorylation was associated with an increase in chromosomal instability in Bloom Syndrome (BS) cells (Leng et al., 2006); however the function of BLM helicase in mitosis is not known. Intriguingly, Mps1 was reported to phosphorylated the DNA damage checkpoint protein Chk2 in response to DNA damage, mediating G2/M arrest, and leading to speculation that the mitotic checkpoint and DNA damage sensing machinery may be linked (Wei et al., 2005).

Several substrates have been identified with direct relevance to checkpoint and/or chromosome alignment function, namely Ndc80, Mad1, Borealin, BubR1 and Mps1 itself

Mps1 substrates				
Protein	**Phosphorylation site**	**Species**	**Proposed function**	**Reference(s)**
Mad1	Multiple residues	Budding yeast	Mitotic checkpoint signalling	(Hardwick et al., 1996)
Ndc80	14 A and T residues in N-terminus	Budding yeast	Mitotic checkpoint signalling	(Kemmler et al., 2009)
Borealin	T88, T94, T169, T230	Human	Aurora B activation, error correction	(Jelluma et al., 2008b)
BubR1	S435, S543, S670, S1043	Human	S670: mediating end-on attachments	(Huang et al., 2008)
Mps1	T676 (activation loop)	Human	Auto-activation	(Jelluma et al., 2008a; Kang et al., 2007; Mattison et al., 2007)
Chk2	T68	Human	G2 arrest in response to DNA damage	(Wei et al., 2005)
BLM	S144	Human	Regulation of genome stability	(Leng et al., 2006)
TACC2	Multiple residues	Human	Centrosome function	(Dou et al., 2004)
Mortalin	Multiple residues	Human	Centrosome cycle	(Kanai et al., 2007)
Smad2/3	SSxS, C-terminal	Human	TGFβ-independent Smad signalling	(Zhu et al., 2007)
Spc42	Multiple residues	Budding yeast	Centrosome assembly	(Castillo et al., 2002)
Spc98	S60, S64, T68	Budding yeast	Centrosome assembly	(Pereira et al., 1998)
Spc110	Multiple residues	Budding yeast	Centrosome assembly	(Friedman et al., 2001)

Table 1.1 Currently known Mps1 substrates.

(see Table 1.1 and earlier sections for references and descriptions). However, it is possible that more substrates remain to be discovered, and this is likely to be a key focus of future studies.

Over the past few years, much effort has been focused upon understanding the role of Mps1 kinase activity. Researchers have employed several strategies: in *X. laevis*, Abrieu and colleagues (2001) used immunodepletion followed by addition of wild type or kinase-dead mutant alleles to show that normal levels of Cenp-E recruitment depended on Mps1 kinase activity (Abrieu et al., 2001). In human cells, RNAi complementation approaches (as opposed to simple RNAi-mediated protein repression) have been used to examine the role of Mps1 kinase activity (Jelluma et al., 2008b; Tighe et al., 2008). The

work of Tighe and co-workers (2008) illustrates how this kind of technique can reveal differences between loss of protein and loss of kinase activity only: the authors found that while Mps1 depletion led to the loss of both Mad1 and Mad2 at the kinetochores in human cells, Mad1 levels could be partially rescued with kinase dead Mps1, whereas Mad2 levels could not (Tighe et al., 2008). In other words, Mad2 localisation appeared exquisitely sensitive to loss of Mps1 activity, whereas Mad1 appeared less affected. This suggested that either Mps1 was only structurally required for Mad1 recruitment [an explanation which seems at odds with the dynamic behaviour of Mps1 at kinetochores, and the stability of Mad1 (Howell et al., 2004; Shah et al., 2004)]; or Mad1 required much lower levels of Mps1 activity to promote its kinetochore binding.

Cell-permeable small molecule inhibitors make excellent tools with which to discern the roles of kinase activity in cells, and have been used to great effect in the study of mitotic kinases like Plk1 and Aurora B (for review see Taylor and Peters, 2008). Unlike RNAi, they rapidly exert their effects in cells, and therefore allow precise temporal control of kinase activity in a dose-dependent manner. One way of achieving selective kinase inhibition is by mutagenesis of the active site of cloned kinases to render sensitivity to bulky analogues of ATP, providing specificity and potency in cells expressing the mutant form of the target kinase (reviewed in Bishop et al., 2001). Expression of this analogue sensitive mutant combined with RNAi has proved an effective approach for study of Mps1 activity in both human cells (Sliedrecht et al., 2010; Tighe et al., 2008) and budding yeast (Jones et al., 2005). Jones and colleagues were able to specifically examine Mps1's role in spindle assembly and chromosome segregation in mitosis (as distinct from its role in SPB duplication in S phase) by creating analogue-sensitive mutant strains. One potential pitfall of this approach is that mutant analogue sensitive kinases tend to lose activity, as was observed for yeast and human Mps1 (Jones et al., 2005; Sliedrecht et al., 2010), meaning cells expressing the uninhibited mutant do not provide the ideal control for normal activity levels, even if (as is the case for Mps1) lower levels of activity apparently support normal functions (Jones et al., 2005; Sliedrecht et al., 2010). Additionally, in human cells, RNAi knockdown is still required, adding a potential source of variability to experiments, though this issue has been alleviated somewhat by the creation of stable cell lines expressing Mps1 shRNA in a doxycycline-dependent manner (Sliedrecht et al., 2010). A very recent report described an extension of the analogue-sensitive approach to Mps1 study: Maciejowski and co-workers described a novel human cell line in which the endogenous Mps1 gene had been replaced with an analogue-sensitive mutant allele (Maciejowski et al., 2010).

Selective, potent small molecule inhibitors targeting endogenous kinases are desirable tools, since they can be used on unengineered cell lines, and avoid the need for RNAi. Additionally, compounds targeting endogenous enzymes can be tested against cancer cell lines to assess any potential therapeutic value. Therefore, effective small molecule inhibitors are sought for those mitotic kinases for which one is not yet available. The mitotic checkpoint kinase Mps1 is one such candidate for a small molecule tool. An inhibitor of budding yeast Mps1 has been described, however use of this compound is limited since it is ineffective in mammalian cells (Dorer et al., 2005). At the time this study commenced, only one inhibitor of human Mps1 had been reported: SP600125 (Schmidt et al., 2005), a compound originally identified as a JNK inhibitor (Bennett et al., 2001). However, the specificity of SP600125 has been called into question (Bain et al., 2007), making it a less than ideal tool. As a result, more selective Mps1 inhibitors have been sought in recent years. New compounds targeting Mps1 have been characterised and published concurrent with the one I describe here (published in Hewitt et al., 2010, appended): namely Mps1-IN-1 (Kwiatkowski et al., 2010) and Reversine (Santaguida et al., 2010).

1.9 | Aims of this study

Mps1 is a kinase with a dual role in mitosis: it controls anaphase onset, and also contributes to the mechanism of chromosome alignment. The latter function is reportedly mediated through Aurora B activation (Jelluma et al., 2008b). Despite these advances, the precise role of Mps1's catalytic activity in the maintenance of genomic stability is far from being fully understood.

The ultimate aim of this study was to examine the role of Mps1 kinase activity in cells, and by doing so shed more light upon the mechanisms by which cells ensure accurate transmission of genetic material to the next generation. AZ3146, a novel small molecule Mps1 inhibitor originally developed by AstraZeneca, was a prospective tool for these studies, but characterisation was necessary before I could confidently use the inhibitor to probe the role of Mps1 in cells. Thus, I set out to test AZ3146's ability to inhibit Mps1 *in vitro* and in cells.

2 | Materials and Methods

2.1 | Chemicals

Unless otherwise stated, chemicals were purchased from Sigma-Aldrich or Melford Laboratories.

2.2 | Cell Culture

All cell lines used in this study, and their origins, are listed in Table 2.1. Cells were cultured as adherent monolayers at 37°C in a humidified chamber with 5% CO_2. Cell culture media consisted of Dulbecco's modified Eagle's medium (DMEM; Invitrogen) supplemented with 100 U/ml penicillin, 100 μg/ml streptomycin, 2 mM L-glutamine and 10% (v/v) heat-inactivated foetal calf serum (FCS; Invitrogen). Cells were passaged and harvested by washing with warm phosphate-buffered saline (PBS) and incubating for 5 minutes with warmed trypsin solution in PBS (10%). Detached cells were resuspended in media, diluted and replated as required. To determine cell density, an aliquot of cell suspension was transferred to an Improved Neubauer haemaocytometer (VWR) for counting. For storage, cells were harvested and collected in a 15 ml tube, centrifuged at 212 × *g* (1000 rpm) for 5 minutes and resuspended in FCS with 10% (v/v) dimethyl sulfoxide (DMSO). The cell suspension was aliquotted into cryovials (Nunc) and frozen slowly by placing in a polystyrene box at -80°C for 24 hours before long-term storage in liquid nitrogen.

Cell line	Description	Source/reference
TA-HeLa	Human cervical adenocarcinoma	(Taylor and McKeon, 1997)
DLD1	Human colorectal adenocarcinoma	ATCC
HCT116	Human colorectal carcinoma	ATCC
hTERT-RPE	Human retinal pigmented epithelium	Dr S. Doxsey, Univ. of Massachusetts
HeLa FRT GFP-Histone H2B	Human cervical adenocarcinoma; stable cell line	(Morrow et al., 2005)
DLD1 FRT/TO Myc-LAP CENP-E tail, Histone-H2B-DsRed	Human colorectal adenocarcinoma; stable cell line	Dr A. Holland, UCSD (Gurden et al., 2010)
HeLa FRT/TO GFP-Mps1 WT/KD, $RNAi^R$	Human cervical adenocarcinoma; stable cell line	Dr A. Tighe (Taylor lab) (Tighe et al., 2008)

Table 2.1 – Cell lines used in this study. ATCC = American type culture collection

Drug and source	Stock concentration	Final concentration
Nocodazole	5 mg/ml	200 ng/ml
Taxol	10 mM	10 μM
Monastrol	100 mM	100 μM
MG132 (Z-leu-leu-leu-al)	20 mM	20 μM
Thymidine	200 mM	2 mM
Tetracycline	1 mg/ml	Dependent on cell line
ZM447439 (Tocris Bioscience)	10 mM	2 μM
AZ12783146 (AZ3146; AstraZeneca)	10 mM	Various (2 μM unless stated)

Table 2.2 – Drugs used in this study

2.2.1 | Drug treatments

All compounds used to treat cells in this study were made up using sterile DMSO and stored at -20 or -80°C in glass vials, except for thymidine and tetracycline which was dissolved in autoclaved water, passed through a 0.2 μm filter and stored at 4°C (short term storage of thymidine) or -20 °C (tetracycline). Unless otherwise stated, cells were treated with drugs diluted in warmed cell culture media to the final concentrations listed in Table 2.2. Drugs were purchased from Sigma-Aldrich unless indicated otherwise.

2.2.2 | Use of tetracycline-inducible stable cell lines

In this study I used two stable isogenic cell lines expressing tagged transgenes under the control of the Tet repressor. Both were made using the Flp-In™ T-REx™ system (Invitrogen) and have been described previously (see Table 2.1, bottom two rows). To induce expression of Myc-LAP-tagged CENP-E tail (amino acids 1547-2580 of Swiss-Prot entry Q02224-3) in the DLD1 cell line, media was supplemented with 50 ng/ml tetracycline and cells were cultured for 24 hours before analysis. To induce expression of wild type (WT) or kinase-dead (KD) GFP-tagged Mps1 in the HeLa cell line, 1 μg/ml tetracycline was used and cells were left for 24-48 hours until analysis. HeLa tetracycline-inducible cell lines were cultured in hygromycin (40 μg/ml, Roche) and blasticidin (4 μg/ml, Melford)

2.2.3 | Cell synchronisation

A double thymidine block was used to synchronise a cell population in early S phase. Cells were incubated with media containing thymidine for 16 hours, and then released from arrest by removing thymidine media, washing twice with PBS and replacing the media with plain media. After 8 hours, thymidine was added again, for a further 16 hours.

When released from the second block, cells proceeded through the cell cycle as a synchronised population and were harvested and processed for flow cytometry (Section 2.11) as required.

2.2.4 | Monastrol wash-out experiments

To study chromosome alignment I used a monastrol wash-out protocol. Cells grown on glass coverslips were treated with monastrol for 4 hours, then washed twice with warm complete media and once with media containing MG132 with or without the kinase inhibitors AZ3146 or ZM447439. After the third and final wash, cells were incubated in the same media (MG132 ± kinase inhibitors) for 60-90 minutes, and then cells were fixed and stained for immunofluorescence.

2.3 | Molecular Biology

2.3.1 | PCR to amplify a DNA coding sequence

To amplify an open reading frame (ORF) for cloning into a vector, polymerase chain reaction (PCR) was used. Primers were designed complementary to sequences at each end of the region of interest, with the addition of restriction enzyme cut sites to allow ligation into a vector. Primers used are listed in Table 2.3 and were purchase from Invitrogen. The template DNA for amplification of the human Mps1 catalytic domain was pcDNA5/FRT/GFP-Mps1 (originally made by P. Eyers). PCR reaction mixtures included 10 µl 10X Cloned *Pfu* DNA Polymerase Buffer (Stratagene), 10 µl dNTP mix (2.5 mM, Roche), 10 µl of 10 µM forward and reverse primers, ~600 ng of plasmid template DNA, 0.5 µl cloned *Pfu* DNA polymerase (2.5 U/µl; Stratagene) and sterile water to a total

Primer name	Sequence (5' to 3')	Restriction site	Purpose
Mps1 catalytic domain (510-857) forward	GCCGCC**GGATCC**GCATCTTCTTCAGCAAATGAATGC	BamH1	Cloning Mps1 catalytic domain (510-857) ORF into pET28a
Mps1 cat reverse	GCCGCC**GCGGCCGC**TCATTTTTTTCCCCTTTTTTTTTCAAAAGTCTTGG	Not1	
T7 Promoter (forward)	TAATACGACTCACTATAGGG	-	Sequencing – pET28a inserts from 5' vector region
T7 Terminator (reverse)	GCTAGTTATTGCTCAGCGG	-	Sequencing – pET28a inserts from 3' vector region

Table 2.3 – Primers used in this study, with restriction enzyme recognition sites in bold.

Temperature (°C)	Time (min)	Number of cycles
Thermocycling conditions for ORF amplification		
94	3:00	1
94 45 72	0:30 0:30 2:00 (2 min per kb)	2
94 55 72	0:30 0:30 2:00	25
72	5:00	1
4	∞	1
Thermocycling conditions for DNA sequencing		
96	1:00	1
96 50 60	0:10 0:15 4:00	32
4.0	∞	1

Table 2.4 – Thermocycling conditions

volume of 100 μl. Reactions were carried out in thin walled 0.2 ml PCR tubes in a GeneAmp® PCR System 2700 (Applied Biosystems). Thermocycling conditions are described in Table 2.4. 5 μl of the completed PCR reaction was run on a 1% agarose gel to check the success of the reaction (see Section 2.3.3). The PCR reaction was purified using a QIAQuick PCR Purification Kit (Qiagen) in accordance with the manufacturer's instructions.

2.3.2 | Restriction enzyme digest

To prepare DNA for ligation, a standard double digest was set up containing plasmid or insert DNA (0.5-1 μg), 10 units of each restriction enzyme, the appropriate buffer and BSA if required (enzymes, buffers and BSA were from New England Biolabs). Samples were incubated at 37 °C for 4 hours, then mixed with 5× DNA loading buffer (0.25% (w/v) bromophenol blue, 0.25% (w/v) xylene cyanol, 30% (v/v) glycerol). Digested fragments were subjected to gel electrophoresis.

2.3.3 | Gel electrophoresis and DNA purification from agarose gels

DNA molecules were separated according to size by electrophoresis. Gels were made with 1% agarose dissolved in TBE (88 mM Tris, 88 mM boric acid, 2 mM EDTA,

pH8.2). When DNA was to be excised and used directly in ligations (Section 2.3.4), low melting agarose (Flowgen) was used. Samples were mixed with DNA loading buffer before electrophoresis. A lambda phage DNA ladder (New England Biolabs) was loaded alongside samples. Gels were run at 100V for approximately 1 hour and stained with ethidium bromide, then DNA was visualised using a UV lamp. The required insert or plasmid backbone bands were excised and used in ligations.

2.3.4 | In-gel ligation

'Sticky-ended' plasmid and insert DNA was ligated by an in-gel method. First, gel slices were placed at 70 °C for 10 minutes to melt the agarose. Then 7 μl of insert, 1 μl of plasmid, and 1 μl of T4 ligase buffer (New England Biolabs) were mixed, placed on ice and allowed to set and cool. 1 μl of T4 ligase (New England Biolabs) was pipetted on top of the solidified agarose and the mixture was placed at room temperature for at least 3 hours. After the addition of 40 μl of water, the mixture was heated to 70 °C for 10 minutes and 10 μl was used to transform competent bacteria. Control ligations were performed in parallel using blank agarose in the place of either insert or plasmid.

2.3.5 | Bacterial transformation and preparation of DNA

Bacterial transformations were carried out according a standard protocol. For plasmid propagation, XL-1 Blue chemically competent *Escherichia coli* were used. A 50 μl aliquot of thawed cells was incubated on ice for 20 minutes with 1 μl of plasmid DNA or 10 μl of ligation mixture. Cells were heat-shocked at 42 °C for 90 seconds, 400 μl of LB medium was added, and the tubes were placed at 37 °C in a shaking incubator for 1 hour to allow the cells to recover. Cells were plated on agar containing 100 μg/ml carbenacillin or 50 μg/ml kanamycin, depending on the resistance conferred by the vector. Plates were incubated at 37 °C overnight. Then, single colonies were picked and grown up overnight at 37 °C in a shaking incubator in 3 ml of Luria-Bertani medium (LB) with 25 μg/ml ampicillin or 50 μg/ml kanamycin. To isolate DNA from these cultures, a QIAprep Spin Miniprep kit (Qiagen) was used as per the manufacturer's instructions.

2.3.6 | Glycerol stock preparation

To store transformed *E. coli*, a 15% glycerol stock was prepared from an overnight culture. A mixture of 200 μl sterile 50% glycerol and 466 μl bacterial cell suspension was stored at -80 °C. This stock was used to inoculate cultures or streaked on agar plates as required.

2.3.7 | Sequencing

The BigDye™ v3.1 Terminator Sequencing Kit (Applied Biosystems) was used to sequence plasmid DNA. A reaction mix was assembled containing 300-800 ng plasmid DNA, 10 pmol sequencing primer (see Table 2.3), 3.5 µl AB Buffer, 1 µl BigDye™ mix and sterile distilled water to a final volume of 20 µl. Thermocycling conditions are shown in Table 2.4. After completion of the reaction, the DNA was precipitated with ethanol as follows: the volume was made up to 100 µl with distilled water, then 10 µl of sodium acetate pH5.2, 250 µl 100% ethanol and 1 µl GlycoBlue™ (15 mg/ml, Ambion) was added. The tubes were incubated on ice for 15 minutes, and then centrifuged at 17968 × *g* (14000 rpm) for 15 minutes in a Sigma 1-15K refrigerated microfuge with rotor 12124. The pellet was washed with 500 µl 70% ethanol and centrifuged again. After careful removal of the supernatant, the pellet was air-dried at room temperature and sent to the in-house DNA Sequencing Facility.

2.4 | Production of recombinant Mps1^{CAT} in *E. coli*.

2.4.1 | Protein expression

The C-terminal catalytic domain of Mps1, corresponding to amino acids 510-857, was cloned into the bacterial expression vector pET28a (Novagen), as detailed in Section 2.3. This vector allowed expression of a fusion protein with an N-terminal 6His-tag (Mps1^{CAT}). BL21 (DE3) pLysS *E. coli* (Novagen) were transformed with the plasmid and a glycerol stock was made (see Section 2.3.5 and 2.3.6). The glycerol stock was used to inoculate 3 ml LB with 50 µg/ml kanamycin and incubated overnight at 37 °C with shaking. This culture was diluted 1:1000 into 1 litre LB media and incubated at 37 °C with shaking until the optical density measured at 600 nm (OD_{600}) was ~ 0.7. Expression was induced with 0.5 mM isopropyl-β-D-thiogalactopyranoside (IPTG) and cultures were incubated for 16 hours at 18 °C with shaking. After induction, cells were pelleted by centrifugation at 4302 × *g* (4500 rpm) in a Sigma 6K-15 centrifuge fitted with rotor 11150. The pellet was stored at -80 °C prior to purification.

2.4.2 | Bacterial cell lysis and purification of 6His-tagged Mps1^{CAT} by metal ion affinity chromatography

Pelleted bacteria were resuspended in ice-cold lysis buffer containing 50 mM Tris-HCl pH7.4, 300 mM NaCl, 0.1% (v/v) Triton X-100, 10 mM imidazole, 0.1 mM EDTA, 0.1 mM EGTA, 0.03% β-mercaptoethanol, 0.4 mM phenylmethylsulfonyl fluoride (PMSF) 1 mM benzamidine and complete EDTA-free protease inhibitor cocktail tablet (Roche) and

sonicated using a Vibracell ultrasonic processor (Sonics) on ice for 1 minute in 10 second pulses at 40% amplitude. Insoluble debris was pelleted by centrifugation at 21036 × *g* (14000 rpm) in a Sigma 6K-15 centrifuge with rotor 12166 for 45 minutes, and the resulting supernatant was incubated with 1 ml of equilibrated TALON® metal affinity resin (Clontech) for 1.5 hours at 4 °C with end-over-end rotation. The resin was washed with 50 ml wash buffer (50 mM Tris-HCl pH7.4, 500 mM NaCl, 10 mM imidazole, 0.1 mM EDTA, 0.1 mM EGTA, 0.03% β-mercaptoethanol). 6His-tagged $Mps1^{CAT}$ was eluted from the resin in 0.5-1 ml fractions with elution buffer containing 50 mM Tris-HCl pH7.4, 300 mM NaCl, 300 mM imidazole, 0.1 mM EDTA, 0.1mM EGTA and 0.01 % β-mercaptoethanol. A visual assay was performed using Coomassie Plus Bradford reagent (Pierce) to determine the fractions with the highest protein concentration. These were pooled, before changing the buffer by dialysis in a Slide-a-Lyzer dialysis cassette (3.5 kDa molecular weight cut-off, Pierce) against dialysis buffer containing 50 mM Tris-HCl pH7.4, 150 mM NaCl, 0.1 mM EGTA and 0.1 % β-mercaptoethanol. Dialysis was performed overnight at 4 °C in a volume of 500 ml with gentle stirring, with one change of buffer after 2 hours. Following dialysis, the purified 6His-$Mps1^{CAT}$ solution was concentrated by centrifugation at 4000 × *g* in a Vivaspin (Sartorius) 2 ml capacity concentrator column with a 5 kDa cut-off. Total protein concentration was determined by Bradford assay using Coomassie Plus Bradford assay reagent, using bovine serum albumin (BSA) as standards. SDS-PAGE and Coomassie staining (see Section 2.5) were used to estimate the concentration of full-length recombinant $Mps1^{CAT}$. The rest of the concentrate was split into single-use aliquots, snap-frozen on liquid nitrogen and stored at -80°C until use in initial kinase assays (see Section 2.7) with a small range of inhibitor concentrations.

For determination of AZ3146's IC_{50} by assaying a wide range of inhibitor concentrations (Figure 3.2C), purified 6His-$Mps1^{CAT}$ was obtained from Matthew Chu (Tabernero lab, University of Manchester). This was expressed and purified as described in (Chu et al., 2008).

2.5 | SDS-PAGE and western blotting

2.5.1 | SDS-PAGE

Sodium-dodedcyl-sulphate polyacrylamide gel electrophoresis (SDS-PAGE) was used to separate proteins by size. After running gels, proteins were visualised by Coomassie staining (see Section 2.5.2) or western blotting (see Section 2.5.3). To prepare samples for SDS-PAGE, they were mixed with 6X SDS-PAGE sample buffer (350 mM

Tris-HCl pH6.8, 10% SDS (w/v), 600 mM dithiothreitol (DTT), 0.06% (w/v) bromophenol blue, 30% (v/v) glycerol) and boiled for 5 minutes. For SDS-PAGE of total cell lysates, cells were harvested by trypsinisation (see Section 2.2), washed once with PBS, followed by lysis of the pelleted cells directly into SDS-PAGE sample buffer by resuspending cells in the buffer and boiling for 5 minutes. SDS-PAGE gel casting equipment and gel tanks were from Hoefer. Gels were cast in plates separated by 1.5 mm or 0.75 mm spacers with 10- or 15-well combs. The acrylamide percentage in the resolving gel was selected according to the molecular weight of the proteins to be resolved. The resolving gel was poured first and allowed to polymerise before the stacking gel was layered on top.

The polymerised gel was clamped into a Mighty Small SE250/SE260 running tank, which was filled with running buffer (25 mM Tris, 200 mM glycine and 0.1% (w/v) SDS). Protein samples and a molecular weight marker (Precision Plus Dual Colour, Bio-Rad) were loaded into wells and the gel was run at a constant voltage of 150V.

2.5.2 | Coomassie staining

To directly visualise relatively large amounts of protein after SDS-PAGE, gels were fixed and stained in Coomassie solution (0.2% (w/v) Coomassie Brilliant Blue, 40% methanol, 7% acetic acid) for up to 1 hour at room temperature whilst rocking gently. Gels were washed in destain solution (40% methanol, 7% acetic acid) at room temperature for several hours until bands were visible and background was reduced.

2.5.3 | Western blotting

For detection of a specific protein in a sample using an antibody, proteins were separated by SDS-PAGE then transferred to either an Immobilon P polyvinylidene fluoride (PVDF; Millipore) or nitrocellulose (Whatman) membrane. A standard transfer sandwich was assembled with Whatman filter paper wetted with transfer buffer (25 mM Tris, 190 mM glycine, 0.1% (w/v) SDS and 20% methanol. The membrane was placed on the anode side of the SDS-PAGE gel in a Trans-blot semi-dry transfer system (Bio-Rad), which was run at 15V for 1 h. When the protein of interest was larger than 100 kDa, a wet transfer system (Bio-Rad) was used. In this case the tank was filled with wet transfer buffer (50 mM Tris, 380 mM glycine, 0.2% (w/v) SDS, 5% methanol) and 50V was applied for 1 hour.

After transfer of the proteins to the membrane, non-specific antibody binding was prevented by incubation with a blocking solution of TBST with 5% milk solution (100 mM Tris, 150 mM NaCl, 0.1% (v/v) Tween-20, 5% (w/v) non-fat powdered milk) for 30-60

minutes. The primary antibody (see Table 2.5) was appropriately diluted in the blocking solution and incubated with the membrane overnight at 4 °C with gentle rocking.

Membranes were then washed for 5 minutes 5 times with TBST (100 mM Tris, 150 mM NaCl, 0.1% (v/v) Tween-20) before incubation for 1 h at room temperature with HRP-conjugated secondary antibody. After washing again 5 times with TBST, the membrane was incubated with SuperSignal® West Pico Chemiluminescent Substrate (Pierce) was added to the membrane. Luminescence was detected by exposure of the membrane to Biomax MR photographic film (Kodak).

2.5.4 | Phos-tag SDS-PAGE gels

To separate proteins in a total cell lysate according to their relative phosphorylation levels in addition to their size, Phos-tag (Phos-tag Consortium, Japan) was used according to the manufacturer's instructions. Briefly, Phos-tag (25 μM) and $MnCl_2$ (50 μM) were added to standard SDS-PAGE resolving gels containing 6% (for anti-Mps1) or 8% (for anti-Aurora B) acrylamide. To resolve the samples, a constant current of 30 mA was applied until the dye front reached the bottom of the gel. Following washing of the gel in wet transfer buffer with EDTA (50 mM Tris, 380 mM glycine, 0.2% (w/v) SDS, 5% methanol and 100 mM EDTA), proteins were transferred to PVDF by wet transfer and processed for western blotting as described (see Section 2.5.3).

Western blotting - primary antibodies				
Antibody	**Antigen**	**Species**	**Working dilution**	**Source/Reference**
SMP1.1	hMps1	Sheep	1:2000	(Tighe et al., 2008)
Phospho-Aurora	Phospho-hAurora A (T288)/hAurora B (T232)/hAurora C (T198)	Rabbit	1:2000	Cell Signaling Technology
Phospho-Histone H3	Phospho-S10 hHistone H3	Rabbit	1:10000	Millipore
SAA1.1	hAurora A	Sheep	1:5000	(Girdler et al., 2006)
SAB1.2	hAurora B	Sheep	1:1000	(Girdler et al., 2006)
Mps1 CT	Mps1 C-terminal	Mouse	1:1000	Millipore
His	6xHis tag	Mouse	1:1000	Sigma
Secondary antibodies				
HRP-conjugated secondary	Anti-sheep IgG	Rabbit	1:500	Invitrogen
HRP-conjugated secondary	Anti-rabbit/goat IgG	Goat	1:500	Invitrogen

Table 2.5 Antibodies used for Western blotting

2.6 | Immunoprecipitation from cell lysates

2.6.1 | Preparation of cell lysates

To prepare cell lysates for immunoprecipitation of endogenous Mps1 from mitotic TA-HeLas, cells plated on 15 cm dishes (1 dish per 5 IPs) were treated with nocodazole for 14 hours. Loosely-adherent mitotic cells were collected by shake-off, pelleted by centrifugation at 306 × *g* (1200 rpm) in a Sigma 6K15 centrifuge with rotor 11150, then washed once with chilled PBS. The washed pellet was resuspended in 1.25 ml ice-cold mammalian cell lysis buffer (250 µl per IP) consisting of 50 mM Tris-HCl pH7.4, 100 mM NaCl, 0.5% NP-40, 5 mM EDTA, 5mM EGTA, 40 mM β-glycerophosphate, 0.2 mM PMSF, 1 mM DTT, 1 mM sodium orthovanadate, 20 mM sodium fluoride, 1 µM okadaic acid (Calbiochem) and complete EDTA-free protease inhibitor cocktail tablet (Roche). Cells were lysed on ice for 30 minutes with occasional mixing, and centrifuged at 17968 × *g* (14000 rpm) for 20 minutes in a Sigma 1-15K refrigerated microfuge with rotor 12124 to pellet insoluble cell debris. The supernatant was split into 250 µl aliquots and used immediately, or snap frozen on liquid nitrogen, and stored at -80 °C until use.

2.6.2 | Covalent cross-linking of antibody to beads

Mps1 was immunoprecipitated from cell lysates using a sheep anti-Mps1 polyclonal antibody (SMP1.1, Tighe et al., 2008) coupled to a Protein G Sepharose™ 4 Fast Flow matrix (GE Healthcare). 100 µl of settled Protein G Sepharose beads was washed three times with 1 ml PBST (phosphate-buffered saline with 0.1% (v/v) Tween-20), centrifuging at 4000 × *g* at 4 °C for 2 minutes to pellet beads between washes. After resuspending the washed beads in 0.5 ml of PBST, 6 µl of SMP1.1 or sheep non-specific IgG was added. Beads and antibody were allowed to bind by incubating for 1 hour at 4 °C with end-over-end rotation. After two washes with 1 ml PBST and two washes with 1 ml 0.2 M sodium borate pH9, beads were resuspended in 1 ml of sodium borate and the cross-linker dimethylpimelimidate (DMP) was added to final concentration of 20 mM. This was incubated at room temperature for 45 minutes with end-over-end rotation. The beads were pelleted, washed twice with 1 ml of 0.2 M ethanolamine pH 8 to quench the reaction, then resuspended in 1 ml ethanolamine and rotated for 1 hour at room temperature. The coupled antibody-bead complexes were stored at 4 °C and washed three times with cell lysis buffer before use in IPs.

2.6.3 | Immunoprecipitation

All immunoprecipitation steps were performed on ice using chilled buffers and centrifugation steps were carried out at 4°C. To pre-clear the lysates of proteins binding non-specifically to the matrix, lysates were incubated with washed Protein G Sepharose beads (20 µl of 50% slurry per 250 µl lysate) and rotated at 4 °C for 30 minutes. Beads were pelleted, and the pre-cleared supernatant was removed. An aliquot of this lysate was removed for analysis and labelled as the IP input. Antibody-coupled beads were added (20 µl of 50% slurry per 250 µl lysate), and samples were incubated at 4 °C for 2 hours with end-over-end rotation. Non-specific sheep IgG-coupled beads were used alongside SMP1.1 as control IPs. After binding of antibody-bead complexes to the target protein, the complexes were pelleted and washed once with 1 ml high salt wash buffer (50 mM Tris-HCl pH7.4, 400 mM NaCl, 0.5% NP-40, 5 mM EDTA, 5mM EGTA, 40 mM β-glycerophosphate, 0.2 mM PMSF, 1 mM DTT, 1 mM sodium orthovanadate, 20 mM sodium fluoride) and twice with 1 ml wash buffer (as high salt wash buffer, but with 100 mM NaCl). Pelleted immune complexes were used in kinase assays (see Section 2.7) or boiled in sample buffer for SDS-PAGE analysis (see Section 2.5)

2.7 | γ^{32}P incorporation assays (kinase assays)

Radioactive *in vitro* assays were used to measure the effect of various concentrations of AZ3146 on the kinase activity of Mps1. To measure the activity of recombinant $Mps1^{CAT}$, the purified enzyme was added to an assay buffer containing 25 mM Tris-HCl pH7.4, 100 mM NaCl, 50 mg/ml BSA, 0.1 mM EGTA, 0.1% β-mercaptoethanol, 10 mM $MgCl_2$ and 0.5 mg/ml of the exogenous substrate myelin basic protein (MBP; Upstate). The final assay volume was 40 µl. In initial assays testing AZ3146 over a small concentration range (see Figure 3.2B), ~1 µg of $Mps1^{CAT}$ was used per assay. For determination of the IC_{50} for AZ3146 in this assay (see Figure 3.2C) 500 ng of recombinant $Mps1^{CAT}$ was used. Pelleted bead complexes were used in assays to measure the activity of immunoprecipitated Mps1 from cells (see Section 2.6). 1 µl of AZ3146 diluted in DMSO was added to the assay mix to achieve the required final inhibitor concentration, and DMSO was included in control assays to account for the solvent. Assays were started by addition of [γ^{32}P] ATP (Perkin Elmer) to a final concentration of 100 µM (2 µCi per assay), followed by incubation at 30 °C for 20 minutes. When assays contained bead-bound Mps1 from cells, samples were incubated with shaking at 250 rpm. Assays were then processed depending on the required read-out, as described below.

2.7.1 | Quantitation of Mps1 kinase activity by Cerenkov counting

For determination AZ3146's IC_{50}, proteins phosphorylated during the assay were captured on phosphocellulose paper to measure their radioactivity. After completion of the incubation time, assays were spotted onto labelled squares of P81 paper (Whatman), then dropped into a beaker of 0.5% phosphoric acid containing a magnetic stir bar. The papers were left to wash for 10 minutes before replacing the phosphoric acid and washing for 5 minutes a further three times. Papers were submerged in acetone for 2 minutes, air-dried, placed inside vials without scintillation fluid and the incorporated $\gamma^{32}P$ was measured by Cerenkov counting in a Packard 2100 scintillation counter for 1 minute per sample. The background level of radioactivity, as determined by a no-kinase control, was subtracted from the sample readings. All AZ3146-treated samples were normalised to the level of radioactivity in the solvent-only assay. IC_{50}s were determined by fitting a sigmoidal dose-response curve using Prism v4.0 software (GraphPad Software).

2.7.2 | Quantification of Mps1 kinase activity by 2D densitometry

The activity of immunoprecipitated Mps1 from cells was measured by 2D densitometry of the MBP or Mps1 after separating proteins in the kinase assay by SDS-PAGE. After incubation at 30 °C, assays were stopped by addition of 10 µl 6X sample buffer, heated at 75 °C for 10 minutes and spun down. Samples were loaded onto a 15% acrylamide gel and run as described in Section 2.5. After resolving the proteins, the gel was Coomassie stained (Section 2.5.2) and dried down. The dried gel was exposed to a Fugi phosphorimaging plate and imaged using a Fugi FLA 3000 phosphorimager. Quantification of ^{32}P signal intensity was carried out using AIDA software (Raytest Isotopenmessgerate GmbH). The background level of phosphorylation, as determined by a non-specific sheep IgG control IP, was subtracted from the values for each sample. AZ3146-treated samples were normalised to the signal in the Mps1 IP treated with DMSO alone, and graphs were drawn as above.

2.8 | Selectivity screen

To assess the selectivity of AZ3146, a single point screen was carried out by Invitrogen's SelectScreen™ Kinase Profiling service. A panel of 50 kinases were selected from those available and assayed with 1 µM AZ3146.

2.9 | Colony formation assays

To test the effect of various concentrations of AZ3146 on viability of cultured human cell lines, colony formation assays were carried out. TA-HeLa, RPE-hTERT and HCT116

cells were seeded on 6-well plates at a density of 21 cells/cm^2 (200 cells/well) and left 24 hours to adhere. Fresh media was then added, either without drug, or containing AZ3146 at concentrations of 10, 5, 2, 1, and 0.5 μM. After 8-9 days, cells were washed with PBS, fixed in 4% formaldehyde for 20 minutes, washed with distilled water and stained with 0.1% (w/v) crystal violet solution for 5 minutes. After further washes, plates were dried in an oven before counting the visible colonies and solubilising the stain with 10% (v/v) acetic acid (1 ml per well). Aliquots of solubilised stain from each well were transferred to a microtitre plate, and the absorbance at 595 nm was read on a Biotek Synergy HT plate reader with KC4™ software. The background absorbance of 10% acetic acid-filled blank wells was subtracted from each sample measurement, and absorbance readings were normalised to control (no AZ3146) levels.

2.10 | Flow cytometry

Propidium iodide and anti-MPM2 (anti-phospho-Ser/Thr-Pro, Upstate) staining was used to analyse DNA content and mitotic index of a population of fixed cells. Cells were grown on 10 cm dishes, treated with drugs when appropriate and harvested by trypsinisation, collecting all media and washes. Harvested cells were washed with 5 ml cold PBS and pelleted by centrifugation at 212 × *g* (1000 rpm) for 5 minutes. The pellet was resuspended in 100 μl cold PBS and 350 μl ice-cold ethanol was added drop-wise whilst gently vortexing. Fixed cells were stored at -20 °C for at least 16 hours prior to staining. Immediately before staining, cells were washed twice with PBS, centrifuging at 478 × *g* (1500 rpm) to pellet cells. Pellets were resuspended in 500 μl anti-MPM2 diluted 1:2000 in PBS, then incubated with the antibody for 1-2 hours at 4 °C. After further washing with PBS, the cells were incubated with FITC-conjugated donkey anti-mouse secondary antibody (Jackson Labs) for 1 hour at 4 °C in darkness. Cells were then washed again with PBS. To stain the DNA, cells were resuspended in 500 μl of propidium iodide (40 μg/ml) and ribonuclease A (RNase A, 50 μg/ml) in PBS and incubated for 30 minutes at room temperature in darkness. Stained cells were analysed on a CyAn™ flow cytometer (Dako) with Summit software.

2.11 | Immunofluorescence

To allow visualisation of specific cellular proteins using antibody labelling, cells were seeded onto 19 mm glass coverslips at 5.4 × 10^4 per coverslip for analysis 24 hours later, or 3.6 × 10^4 per coverslip for analysis 48 hours later. Cells were treated with compounds as required, washing coverslips once with drug-containing media before

addition of the final media. Cells were fixed and stained by one of three protocols as detailed below.

For most applications, the following fixation conditions were used: Coverslips were washed once with PBS, fixed in 1% formaldehyde in PBS for 10 minutes, and then washed a further three times with PBS. After incubation for 5 minutes in ~10 mM glycine block solution (1 drop of 1M glycine-Tris HCl pH8.5 in 4 ml PBS), cells were permeabilised by washing with 0.1% (v/v) Triton X-100 in PBS (PBS-T). Primary antibodies were diluted in glycine block solution (see Table 2.6) and coverslips were incubated with antibodies for 1 hour at room temperature. Next, coverslips were washed twice with PBST and then incubated with the appropriate fluorophore-conjugated secondary antibodies for 1 hour at room temperature in darkness. Following further washes with PBST, 1 μg/ml Hoechst 33258 diluted in PBST was placed on coverslips for 2 minutes to stain DNA. After two more washes, coverslips were mounted on slides on a drop of mounting media (90% glycerol, 20 mM Tris-HCl pH8.0). The edges were sealed with clear nail varnish.

To visualise tubulin, a microtubule-kinetochore stabilising buffer (MT-KC buffer: 100 mM PIPES, 1 mM $MgCl_2$, 0.1 mM $CaCl_2$, 0.1% Triton X-100) was used to pre-extract the cells. First, coverslips were washed once with PBS, then MT-KC buffer was added to the coverslips for 90 seconds at room temperature, followed by fixation in 4% formaldehyde in the same buffer for 10 minutes. Blocking and staining proceeded as described in the previous paragraph.

For staining of Cenp-E and components of the RZZ/Zwint complex, kinetochore buffer (KB: 20 mM Tris-HCl pH7.4, 150 mM NaCl, 0.1% BSA and 0.2% Triton X-100, Chan et al., 2000) was used to pre-extract cells. After washing with PBS, coverslips were incubated with KB for 2 minutes at room temperature. Cells were fixed in 4% formaldehyde in PBS for 7-10 minutes, then blocked and stained as detailed above.

Slides were stored at -20 °C prior to viewing cells by fluorescence microscopy as described in Section 2.13.

2.12 | Microscopy

After fixation and staining, cells were analysed on a microscope. Two microscope systems were used in this study. For routine analysis (referred to as 'standard fluorescence microscopy' in subsequent chapters), cells were viewed using a Zeiss Axioskop 2 upright microscope and images captured used a CoolSNAP HQ CCD camera (Photometrics). MetaMorph (Universal Imaging) software was used for image acquisition. For high-quality, deconvolved images and where quantification was required, a Delta Vision

Immunofluorescence				
Antibody name	**Antigen**	**Species**	**Dilution**	**Source/Reference**
Primary antibodies				
ACA	Centromeres	Human	1:500	Bill Earnshaw, University of Edinburgh, UK
TAT1	α-Tubulin	Mouse	1:100	Keith Gull, University of Oxford, UK
Cenp-E	hCenp-E	Rabbit	1:2000	Don Cleveland, UCSD, USA
SCF.2	hCenp-F	Sheep	1:800	(Holt et al., 2005)
SB1.3	hBub1	Sheep	1:1000	(Taylor et al., 2001)
SBR1.1	hBubR1	Sheep	1:1000	(Taylor et al., 2001)
SAA.1	hAurora A	Sheep	1:5000	(Girdler et al., 2006)
SAB.1	hAurora B	Sheep	1:1000	(Girdler et al., 2006)
Phospho-Aurora	Phospho-hAurora A (T288)/hAurora B (T232)/hAurora C (T198)	Rabbit	1:500	Cell Signaling Technology
9B10	hMad1	Mouse	1:1000	Abcam
SM2.2	hMad2	Sheep	1:500	(Johnson et al., 2004)
Cenp-A	hCenp-A	Rabbit	1:200	Millipore
Phospho-Cenp-A	Phospho-S7 hCenp-A	Rabbit	1:1000	Millipore
Phospho-Histone H3	Phospho-S10 hHistone H3	Rabbit	1:500	Millipore
MCAK	MCAK	Rabbit	1:1000	Cytoskeleton
Rod	hRod	Rabbit	1:1000	Gordon Chan, University of Alberta, Canada
ZW10	hZW10	Rat	1:1000	Gordon Chan, University of Alberta, Canada
Zwich	hZwilch	Rat	1:500	Gordon Chan, University of Alberta, Canada
Zwint	hZwint	Rabbit	1:5000	Gordon Chan, University of Alberta, Canada
GFP	GFP	Rabbit	1:3000	Abcam
Secondary Antibodies				
Cy2-, Cy3- and Cy5-conjugated secondaries	Anti-sheep/mouse/ rabbit/human/rat IgG	Donkey	1:500 (1:250 for Cy5)	Jackson Immunoresearch

Table 2.6 Antibodies used for immunofluorescence.

RT (Applied Precision) restoration microscope was used, equipped with a 100×/1.40 UPlan S Apo objective, a Sedat Quad 86000v2 filter set (Chroma Technology Corp.) and an API XYZ stage. Images were captured using a CoolSNAP HQ CCD camera, with a Z-optical spacing of 0.2 μm. Raw image stacks were deconvolved using SoftWoRx software (Applied Precision). Maximum intensity projections were created from deconvolved stacks; these images were used for quantification where required, and are shown in the Results.

2.12.1 | Quantitation of kinetochore protein localisation

Protein levels at kinetochores were quantified by normalising to the ACA signal of each kinetochore pair. SoftWoRx software was used to capture the total pixel intensity of wavelengths in the kinetochore region, and background readings were taken in non-kinetochore areas. The background pixel intensity per pixel was calculated for each wavelength and appropriate values subtracted from the reading for each kinetochore pair. A ratio was calculated (protein of interest/ACA) for each kinetochore, and these were used to compare levels between control and drug-treated cells. Datasets were normalised to the mean control ratio and graphs drawn using Prism software.

2.13 | Live cell imaging

HeLa cells stably expressing a GFP-tagged Histone H2B (see Table 2.1) were filmed to analyse mitotic timing and monitor chromosome segregation. Twenty-four hours before filming, cells were plated onto either a 4-well glass bottomed chamber slide (LabTek®) at 7 × 10^4 cells per well, or onto a clear 24-well plate (Corning) at 9.6 × 10^4 cell per well. On the day of filming, cells were treated with drugs or solvent alone as required, and filming commenced ~2 hours later. Cells were viewed using a Zeiss Axiovert 200 microscope system with a 32×/0.4 LD A-Plan objective. The microscope was equipped with an environmental control chamber (Solent Scientific) and a PZ-2000 motorised stage (Applied Scientific Instrumentation) to enable multiple XY point visiting. Cells were maintained at 37 °C with a humidified stream of 5% CO_2. Images were captured every 2 minutes with a CoolSNAP HQ camera (Photometrics), and acquisition was controlled by MetaMorph software. Mitoses were analysed manually using MetaMorph. Movies and sequential TIFFs were made in MetaMorph and exported to QuickTime (Apple) or Photoshop (Adobe).

2.14 | Mps1 RNAi add-back experiments

Endogenous Mps1 expression was perturbed in cells using a shRNA-based approach, followed by induction of an RNAi-resistant GFP-Mps1 transgene using tetracycline (Tighe

et al 2008, and see Section 2.2.2). The procedure was essentially the same as that described previously (Tighe et al 2008). Twenty-four hours prior to transfection, 4×10^4 HeLa FRT/TO GFP-Mps1 WT^R/KD^R cells were seeded onto a 24-well plate in antibiotic-free media. Cells were transfected with pRS HuSH shRNA vectors (Origene) containing a 21 nt Mps1 targeting sequence (target locus: nucleotides 1686-1706 of Mps1 coding sequence, NCBI ID CCDS4993.1) or a control pRS vector, mixed in a ratio of 9:1 with pcDNA5 DsRed-Histone H2B (Tighe et al., 2008). Lipofectamine™ PLUS™ (Invitrogen) was used for transfections according the manufacturer's instructions. Briefly, 1 μl Lipofectamine™ and 4 μl PLUS™ reagent were used to form DNA-lipid complexes with 400 ng total DNA per well (360 ng : 40 ng). Media was replaced with 200 μl of serum and antibiotic-free media, and complexes were added to wells in a volume of 50 μl. Complexes were left on cells for ~6 hours before addition of 250 μl 20% serum media, with or without 2 μg/ml tetracycline, in order that final well concentrations were 10% serum and 1 μg/ml tetracycline. Twenty-four hours later, cells were replated to coverslips for immunofluorescence, or 6 well plates for western blotting. Cells were maintained in tetracycline where appropriate. A further 24 hours later, coverslips were treated with nocodazole and MG132 for 2 hours before fixing and staining for immunofluorescence (Section 2.12). Six-well plates were harvested by trypsinisation and lysed directly in SDS-PAGE sample buffer before SDS-PAGE and western blotting (Section 2.5).

3 | *Results Chapter I:* AZ3146, a novel inhibitor of Mps1

3.1 | Introduction

A great deal of insight has been gained into the roles of human Mps1 in the mitotic checkpoint and chromosome alignment using RNAi-based techniques (Fisk et al., 2003; Jelluma et al., 2008b; Liu et al., 2003; Sliedrecht et al., 2010; Stucke et al., 2002; Tighe et al., 2008). Despite these advances, the role of Mps1 kinase activity is far from fully understood. When this study began, only one inhibitor of endogenous human Mps1 had been described: SP600125 (Schmidt et al., 2005). However, this inhibitor is of limited use since it inhibits a broad range of kinases in cells (Bain et al., 2007). Thus, new inhibitors of endogenous human Mps1 would be of great value.

AZ3146 was developed at AstraZeneca, Macclesfield, after a high-throughput screen for inhibitors of Mps1 activity. The original hit compound has been modified to increase potency and specificity, resulting in AZ3146, which is depicted in Figure 3.1A. The initial aims of this study were to assess the ability of this compound to inhibit Mps1. In this chapter, I describe kinase assays designed to test the inhibitors potency and selectivity, followed by analysis of its effect on Mps1 in cells.

3.2 | AZ3146 inhibits recombinant Mps1^{CAT} *in vitro*

To determine whether AZ3146 can indeed inhibit Mps1's enzymatic activity, I set up an *in vitro* kinase assay using recombinant Mps1 purified from bacteria, MBP as an artificial substrate and γ^{32}P-labelled ATP. Instead of expressing and purifying the full-length kinase, I used a C-terminal fragment encompassing the catalytic domain (amino acids 310-857) with an N-terminal 6xHis-tag (Mps1^{CAT}) that has previously been shown to be active *in vitro* (Chu et al., 2008). This fusion protein was expressed in *E. coli* and isolated from the bacterial cell lysate by metal ion affinity chromatography using Talon™ resin. To assess the purity of the eluted protein, it was resolved by SDS-PAGE and the gel was stained with Coomassie Brilliant Blue. The protein appeared largely free from contaminants and migrated at a position consistent with its expected molecular mass (Figure 3.1B, marked by an arrowhead). The band appeared as a smear, consistent with reports that Mps1 purified from bacteria is highly phosphorylated (Mattison et al., 2007). To confirm that the affinity-purified protein was 6xHis-tagged Mps1^{CAT}, I processed protein samples for western blot and probed them with antibodies against the Mps1 C-terminal and the 6xHis-tag. A band was detectable at the expected molecular weight with

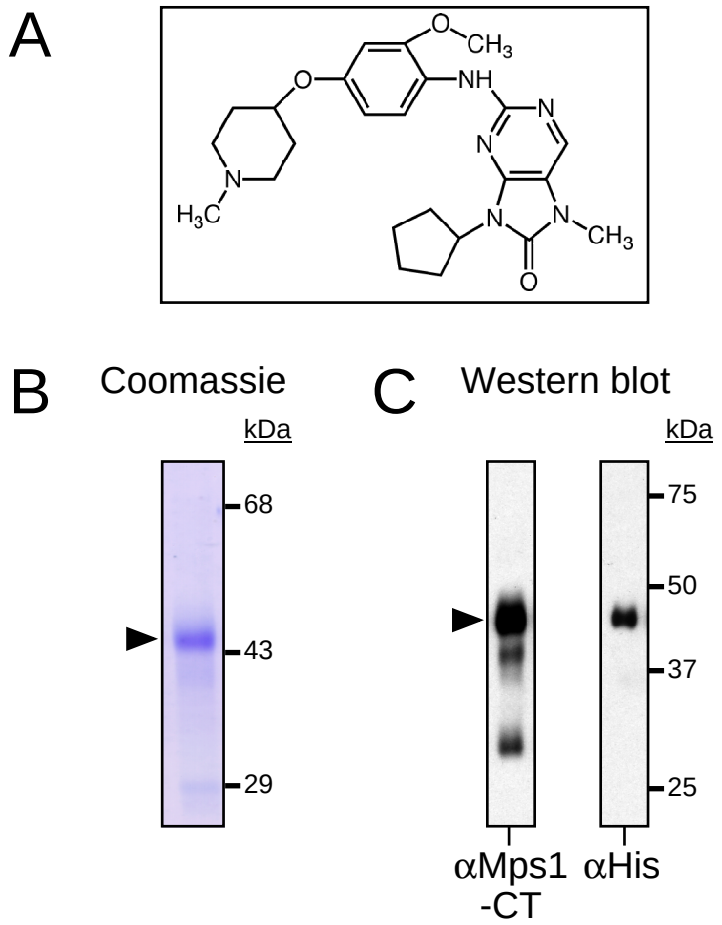

Figure 3.1 The structure of AZ3146 and the purification of recombinant Mps1^{CAT} from *E. coli*
(A) The chemical structure of AZ3146.
(B) Purified 6xHis-tagged Mps1^{CAT} was expressed in *E. coli* and purified by metal ion affinity chromatography using Talon® resin. The eluted protein was resolved by SDS-PAGE, and gel was Coomassie stained to visualise total protein. The major band, which appears at the predicted molecular weight for 6xHis-tagged Mps1^{CAT}, is marked by an arrowhead.
(C) The purified protein was processed for western blotting and probed with antibodies raised against the C-terminal domain of Mps1 (αMps1-CT, left panel) and the 6xHis-tag (right panel, αHis). The arrowhead marks the band corresponding to the full-length 6xHis-tagged protein. The lower molecular weight bands visible in the Mps1-CT blot are likely to represent degradation products.

both antibodies (Figure 3.1C), indicating that the protein I had purified was indeed 6xHis-tagged $Mps1^{CAT}$, and could be used in kinase assays.

Several physiologically relevant substrates have been reported for human Mps1 (Dou et al., 2004; Jelluma et al., 2008b; Kanai et al., 2007; Leng et al., 2006; Wei et al., 2005; Zhu et al., 2007), and both full-length Mps1 and its catalytic domain have been shown to autophosphorylate (Chu et al., 2008; Jelluma et al., 2008a; Kang et al., 2007; Mattison et al., 2007; Mills et al., 1992; Stucke et al., 2004). However, for convenience, I chose to use the non-specific substrate MBP in assays, since this acts as a good substrate for Mps1 *in vitro* (Lauze et al., 1995; Stucke et al., 2002). Kinase assays were started by addition of [γ^{32}P]ATP, incubated at 30°C for 20 minutes, then the reactions were stopped by addition of SDS-PAGE sample buffer and proteins were separated by SDS-PAGE. ^{32}P incorporation was visualised by exposing the dried gel to photographic film. When $Mps1^{CAT}$ was included in the assays, bands corresponding to radiolabelled MBP and $Mps1^{CAT}$ were readily detectable by autoradiography (Figure 3.2A, lane 1), consistent with phosphorylation of the exogenous substrate and the kinase itself. To rule out the presence of contaminants in the assay components, a no-kinase control was included (lane 8). No radiolabelled MBP could be detected in the absence of the kinase, showing that the MBP phosphorylation relied upon the addition of affinity-purified $Mps1^{CAT}$. While I cannot completely exclude the presence of co-purifying kinases in the $Mps1^{CAT}$ prep, the lack of visible contaminants in the eluted protein (see Figure 3.1B), plus prior reports (Lauze et al., 1995; Stucke et al., 2002), allows a reasonable level of confidence that $Mps1^{CAT}$ kinase activity is responsible for MBP phosphorylation. Therefore, these assays provide a useful read-out of Mps1 activity *in vitro*.

Having set up a suitable *in vitro* assay of Mps1 activity, I tested the ability of AZ3146 to inhibit this activity. Increasing concentrations of the compound were added to the assay mix before the reactions were started with [γ^{32}P]ATP, producing a dose-dependent decrease in ^{32}P incorporation into both MBP and $Mps1^{CAT}$ itself when the proteins were visualised by autoradiography (Figure 3.2A). The reduction in ^{32}P-MBP and ^{32}P-$Mps1^{CAT}$ in response to AZ3146 treatment is consistent with the notion that the compound inhibits the catalytic activity of Mps1. Taken together with data provided by AstraZeneca (Stephen Green, personal communication), these data verify that AZ3146 is a reasonably potent Mps1 inhibitor, justifying further investigation.

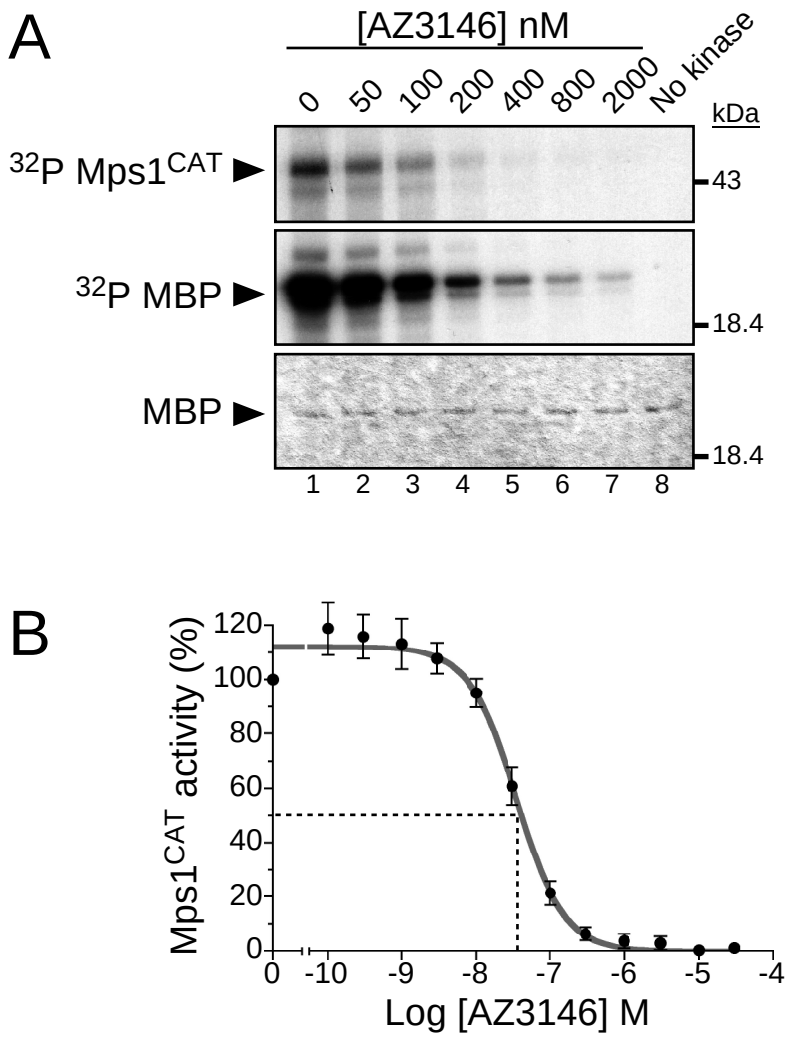

Figure 3.2 AZ3146 inhibits Mps1^{CAT} kinase activity in vitro.

(A) Kinase assays were performed with bacterially-expressed Mps1^{CAT} and concentrations of the inhibitor ranging from 50 nM to 2 μM. Solvent only (lane 1) and no kinase (lane 8) controls were included. After incubation with [γ^{32}P]ATP, proteins were separated by SDS-PAGE and radiolabelled Mps1^{CAT} (upper panel) and MBP (middle panel) were visualised by autoradiography. The Coomassie-stained gel (lower panel) shows roughly equal loading of MBP.

(B) In vitro kinase assays were carried out with Mps1^{CAT} and a range of AZ3146 concentrations (0.1, 0.3, 1, 3, 10, 30 nM, 0.1, 0.3, 1, 3, 10, 30 μM) Mps^{CAT} activity was measured by spotting assays onto P81 paper followed by scintillation counting. Background readings were subtracted and values were normalised to the solvent only control, and a sigmoidal dose response curve was fitted using Prism software. The dashed line approximates the position of the IC_{50} calculated from the curve. Data points represent the mean values from 3 independent experiments, ± s.e.m.(error bars).

Having shown that AZ3146 is indeed capable of inhibiting Mps1 *in vitro*, I sought to quantify its potency by establishing an IC_{50} for the compound. To facilitate a more quantitative approach, I turned to Cerenkov counting, which measures the blue light given off by high-energy beta emitters such as ^{32}P. Kinase assays were carried out essentially as described above, except I used $Mps1^{CAT}$ provided by Matthew Chu (University of Manchester, purified as in Chu et al., 2008), and spotted the reactions onto negatively charged phosphocellulose paper before immersing the papers in phosphoric acid solution. This simultaneously stopped the reaction and conferred a positive charge to the proteins in the assays, causing them to stick to the phosphocellulose paper. Unbound [$\gamma^{32}P$]ATP was washed away, and the dry papers were placed in vials and counted in a scintillation counter (Hastie et al., 2006). The background level of radioactivity in the no-kinase control was subtracted from each reading and the solvent-only control readings were set to 100% before plotting the data points on a graph, and fitting a sigmoidal dose-response curve using Prism v4.0 software (Figure 3.2B).

The IC_{50} value calculated for the AZ3146 dose-response curve was 35 nM (Figure 3.2B, marked on the graph by a dashed line). It is noteworthy that at concentrations below 3 nM, the radioactivity of the samples increased reproducibly to 115-120% of the control, solvent-only levels. It is possible that the presence of the inhibitor, or some contaminant contained within the solution, may have had a stimulatory effect on kinase activity leading to an increase in radiolabelling in those samples. Nevertheless, it is reasonable to conclude that their effect on the calculated IC_{50} would be relatively slight, so I proceeded to use the data to generate the IC_{50} value.

The IC_{50} of 35 nM suggested a reasonable level of potency. While it is difficult to compare the IC_{50}s obtained for distinct kinase-inhibitor combinations under different assay conditions, it is nevertheless worth noting that this value is similar to the reported IC_{50} of an ATP-competitive Aurora B inhibitor, ZM447439 [50 nM, assayed at the same ATP concentration as this study (Girdler et al., 2006)]. ZM447439 potently inhibits Aurora B in cells at 2 μM (Ditchfield et al., 2003) and indeed has been widely used to investigate Aurora B function (Taylor and Peters, 2008). It therefore seemed reasonable to speculate that AZ3146 might be able to yield similarly potent Mps1 inhibition. Also noteworthy is the observation that AZ3146's IC_{50} is value is ~10-fold lower than that of the other published human Mps1 inhibitor SP600125 (Schmidt et al., 2005) when used to inhibit $Mps1^{CAT}$ under identical assay conditions (356 nM – Matthew Chu, personal communication), indicating that AZ3146 is more potent than SP600125, and therefore

potentially more effective in cells at lower concentrations, which would make AZ3146 a preferential tool for study of Mps1 function.

In summary, under the assay conditions used in this study, AZ3146 inhibits $Mps1^{CAT}$ with an IC_{50} of ~35 nM. While it can be difficult to extrapolate *in vitro* data to predict efficacy in cells, this *in vitro* IC_{50} suggests that the potency of AZ3146 may indeed be sufficient to produce potent Mps1 inhibition in cells at low micromolar concentrations.

3.3 | AZ3146 inhibits full-length Mps1 from cells

The capacity of AZ3146 to inhibit recombinant $Mps1^{CAT}$ *in vitro* was encouraging. However, before moving on to cell-based assays, I wanted to check that AZ3146 could inhibit full-length Mps1 isolated from human cells. For this purpose, I used endogenous Mps1 immunoprecipitated from cells in kinase assays. HeLa cells were challenged with the microtubule-depolymerising drug nocodazole to arrest the population in mitosis, then harvested and a soluble lysate produced. Mps1 was immunoprecipitated from these mitotic lysates and pelleted bead complexes were used in kinase assays. A fraction of the reaction mix was analysed by western blot (Figure 3.3A, upper panel), indicating that the kinase was present in roughly equal amounts in each assay (lanes 1-8), unless a non-specific IgG was used for immunoprecipitations, in which case Mps1 was absent (lane 9). To visualise and quantify the incorporation of ^{32}P into both the MBP and the Mps1, the proteins were resolved by SDS-PAGE and exposed to a phosphorimaging plate. Representative images are shown in Figure 3.3A (middle and lower panels).

Endogenous human Mps1 is maximally active and phosphorylated in mitosis (Liu et al., 2003; Stucke et al., 2002). When immunoprecipitated Mps1 was used in kinase assays, ^{32}P was incorporated into both the MBP (Figure 3.3A, bottom panel) and the immunoprecipitated Mps1 (middle panel), consistent with the notion that the kinase is active against both the exogenous substrate and itself. Note however that I am unable to rule out the contribution of co-immunoprecipitated kinases to this phosphorylation. When a control immunoprecipitation was performed, no ^{32}P-Mps1 was discernable (middle panel, lane 9). I was, however, able to detect radiolabelled MBP (bottom panel, lane 9), indicating that contaminant MBP kinase(s) that bind non-specifically to the Protein G Sepharose™ beads or control sheep IgG were present in the assays. However, when Mps1-bead complexes were assayed, ^{32}P-MBP levels increased more than 5-fold compared to levels in the control assay (compare lanes 1 and 9, bottom panel), consistent with the notion that the immunoprecipitated Mps1 phosphorylates the substrate. Therefore, I was able to use radiolabelling of both immunoprecipitated Mps1 itself and MBP as a read-out

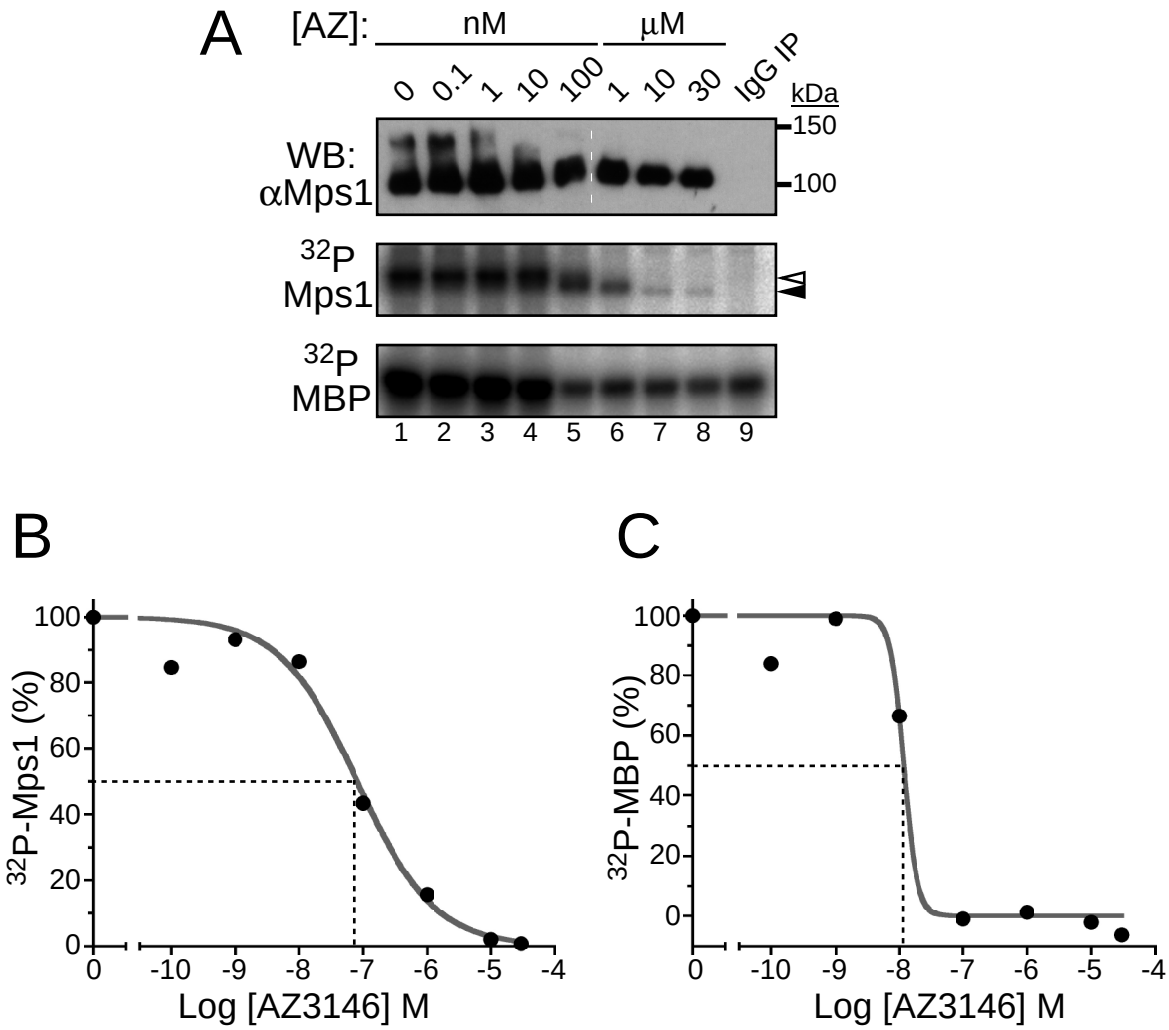

Figure 3.3 AZ3146 inhibits endogenous Mps1 immunoprecipitated from mitotic cells.
Mps1 was immunoprecipitated from nocodazole-treated HeLa lysates. The bead-bound proteins were used in kinase assays with the indicated concentrations of AZ3146. **(A)** A fraction of the assay was resolved by SDS-PAGE and blotted for Mps1 (upper panel). Note the absence of Mps1 in the control IgG IP (lane 9). Assays were also processed by SDS-PAGE followed by phosphorimaging to visualise both radiolabelled Mps1 (middle panel) and MBP (lower panel). **(B)** Mps1 phosphorylation and **(C)** MBP phosphorylation was quantified by 2D densitometry. Background readings from the IgG control were subtracted, and values were normalised to the solvent only control. The dashed line approximates the position of the IC_{50} calculated from the curve.

of Mps1 activity in this assay.

To verify the ability of AZ3146 to inhibit the immunoprecipitated Mps1, I included increasing doses of the compound in the assay mixes. Radiolabelling of Mps1 and MBP was quantified by 2D densitometry, the background levels from the IgG IP were subtracted, the control solvent-only readings were set to 100% and the data was graphed (Figure 3.3 B and C). As predicted, the amount of ^{32}P incorporated into both the Mps1 and the MBP fell in response to higher concentrations of AZ3146 (Figure 3.3 A and B). ^{32}P-Mps1 levels dropped markedly with 100 nM AZ3146, and decreased further at higher concentrations, becoming very low at 10 μM (Figure 3.3A, middle panel and 3.3B). Concurrent with the decrease in radiolabelling, a distinct band-shift from a slower mobility form of Mps1 (middle panel, marked by the open arrowhead) towards a faster mobility species (closed arrowhead) was evident as AZ3146 concentration in the assay increased, suggesting that this band-shift may be due to phosphorylation. The decrease in ^{32}P-MBP signal was more sudden, with a sharp fall in radiolabelling of the substrate between 10 nM and 100 nM AZ3146, after which levels plateaued (Figure 3.3A, bottom panel and 3.3C). The IC_{50}s for AZ3146 in this assay were calculated to be ~80 nM and ~12 nM for Mps1 phosphorylation and MBP phosphorylation respectively, which is in the same broad range as that determined using Mps1^{CAT} (Figure 3.2B). There are clearly slight differences between the IC_{50}s and dose response curves obtained for MBP and Mps1 (Figure 3.3B and C), however more work would be required to establish whether or not these differences are reproducible and if so, what this might mean. Taken together, these data provide evidence for AZ3146-mediated inhibition of full-length Mps1 immunoprecipitated from mitotic cells leading to a decrease in both Mps1 autophosphorylation and phosphorylation of the exogenous substrate MBP.

3.4 | AZ3146 is a reasonably selective Mps1 inhibitor

Having established that AZ3146 could inhibit the kinase activity of both recombinant Mps1^{CAT} and also Mps1 immunoprecipitated from mitotic HeLa cells, I set out to gain an insight into its selectivity. The selectivity of an inhibitor refers to its ability to inhibit its target kinase (or kinases) with a higher level of potency compared to other kinases. Selectivity is a desirable quality in most kinase inhibitors, since it means that the compound's effect in cells are more likely to be specifically attributable to inhibition of the target, rather than to off-target effects. Although the original hit compound had been optimised for enhanced selectivity and potency (Stephen Green, personal communication), I wanted to obtain an independent assessment of AZ3146's selectivity. To achieve this, I made use of Invitrogen's SelectScreen™ Kinase Profiling Service, and screened panel of

50 diverse kinases with 1 μM AZ3146 (Figure 3.4). A broad range of both serine/threonine and tyrosine kinases were selected, including representatives from 7 of the 9 conventional kinase groups as classified by sequence homology (Manning et al., 2002). Kinases with reported roles in control of mitotic events were selected for inclusion the screen, such as the Aurora kinases (Carmena and Earnshaw, 2003), cyclin dependent kinases (Malumbres and Barbacid, 2005), Tao1 (Draviam et al., 2007), Gsk3β (Tighe et al., 2007), Plk1 (Archambault and Glover, 2009), Erk2 (Borysova et al., 2008; Chen, 2004; Chung and Chen, 2003; Zhao and Chen, 2006). Unfortunately the mitotic checkpoint kinases Bub1 and BubR1 were not available, and so could not be tested in this screen. Mps1 was also unavailable for selection, and so could not be included in the panel as a control. However, as shown in Figure 3.2B, the concentration used for the screen almost completely inhibited $Mps1^{CAT}$ *in vitro* (96%). The majority of kinases in the screen, 46 out of the 50, were not greatly affected by 1 μM AZ3146, with inhibition levels <40% (Figure 3.4).

Four kinases were inhibited by more than 40%, namely FAK (43%), KIT (58%), JNK1 (68%) and JNK2 (64%). FAK is cytosolic tyrosine kinase with roles in the regulation of proliferation, survival, adhesion and migration (Hauck et al., 2002). KIT is a receptor tyrosine kinase of the platelet-derived growth factor receptor family particularly associated with haematopoietic stem cells, with reported roles in regulation of proliferation and survival (Masson and Ronnstrand, 2009). JNK1 and JNK2 are MAP kinases associated with the JNK/p38 pathway, which are implicated in regulation of transcription in response to environmental stress, and have also been shown to regulate apoptosis (Weston and Davis, 2007). To the best of my knowledge, none of these kinases have been implicated in the regulation of mitosis, so there is no precedent to suggest inhibition of these kinases could have cellular effects attributable to Mps1 inhibition. However, it is interesting to note that both AZ3146 and SP600125 are capable of inhibiting both Mps1 and JNK (this study and Schmidt et al., 2005), pointing to a level of similarity between the catalytic domain of JNK1/2 and Mps1 (Chu et al., 2008; Schmidt et al., 2005), and perhaps the mechanism of inhibitor binding.

In summary, the selectivity screen described above allows AZ3146 to be considered a reasonably selective inhibitor, since at a concentration that potently inhibits the kinase activity of Mps1, only a small fraction of the kinases screened were inhibited to moderate levels. This confirmed data from AstraZeneca (Stephen Green, personal communication) and provided further support for the notion that AZ3146 will be a useful tool for studying Mps1 in cells.

Kinase	% inhibition	Kinase	% inhibition
ABL1	9	LYN A	-1
AKT1	11	MAP4K4	19
AURORA A	9	MAPK14	30
AURORA B	10	MARK2	13
AURORA C	14	MEK1	8
AXL	6	MEK2	10
BRAF	12	MST1R	20
CDK1/cyclin B	9	mTOR	-8
CDK2/cyclin A	10	NEK1	17
CHK1	29	NEK2	7
CHK2	23	PAK4	23
EPHA2	21	PDGFR β	19
ERBB1	15	PHKG2	26
ERBB2	2	PIM1	14
ERK2	19	PKA	5
FAK	43	PKC β I	22
FGFR1	24	PLK1	39
FYN	11	ROCK1	23
GSK3 β	9	ROCK2	6
IKK β	4	SRC	12
JAK3	16	SYK	20
JNK1	68	TAO1	-3
JNK2	64	VEGFR1	16
KIT	58	VEGFR2	22
LCK	10	ZAP70	15
		MPS1	96

Legend		
< 40%	40% - 80%	≥ 80%

Figure 3.4 AZ3146 has limited activity against a panel of 50 kinases.
A single point screen with 1 μM AZ3146 was carried out by Invitrogen's SelectScreen™ Kinase Profiling Service. 50 diverse kinases were selected from the available list. Kinases were assayed at the approximate K_m for ATP, except B-RAF, MEK1, MEK2, MAPK14, JNK1 and JNK2, which were assayed with 100 μM ATP. The Mps1 data included in the table is from the assays described in this study, where ATP was at 100 μM.

3.5 | AZ3146 affects Mps1 phosphorylation in cells

Having determined AZ3146's potency and selectivity *in vitro*, I determined to assess its effect on Mps1 in cells. Currently, there are no reliable phosphospecific antibodies with which to estimate Mps1 activity in cells, so instead I looked for changes in the electrophoretic mobility of the kinase itself when AZ3146 was added to the culture medium. To prepare extracts for analysis by western blot, HeLa cells were treated with nocodazole overnight, then collected by mitotic shake-off and replated into nocodazole or Taxol, with or without 2 μM AZ3146. The proteasome inhibitor MG132 was also included to prevent mitotic exit, since the predicted effect of an Mps1 inhibitor would be to override the checkpoint-mediated mitotic arrest in the presence of spindle toxins, resulting in changes in the phosphorylation as a result of mitotic exit and obscuring the effect of Mps1 inhibition. After incubation with the indicated drug combinations, harvested cells were lysed in SDS-PAGE sample buffer, and then resolved on a polyacrylamide gel supplemented with the phosphate-binding ligand Phos-tag (Phos-tag Consortium), which enhances phosphorylation-induced mobility shifts in SDS-PAGE by facilitating separation of differentially phosphorylated forms (Kinoshita et al., 2006). Consequently, a ladder of bands was visible when the blot was probed with an anti-Mps1 antibody (Figure 3.5). When the lysate blotted was from interphase cells (adherent cells left behind after mitotic shake-off), Mps1 appeared as 3 relatively fast migrating bands (lane 1, marked with asterisks). When nocodazole or Taxol-treated lysates were probed (lanes 2 and 4), the majority of Mps1 now largely appeared as 2 shifted, slower-mobility bands (marked by arrowheads). Importantly, when mitotic cells were treated with 2 μM AZ3146, the uppermost band decreased markedly (lanes 3 and 5, white arrowhead). This was true for both nocodazole and Taxol-treated samples. The banding pattern produced from the Phos-tag gel can be interpreted to mean that in nocodazole- or Taxol treated mitotic cells, the majority of Mps1 is more highly phosphorylated than in interphase cells (compare lane 1 with lanes 2 and 4). When mitotic cells are treated with AZ3146, the disappearance of this slow-mobility band likely reflects a decrease in phosphorylation of Mps1. In support of this, work carried out by my colleague, Anthony Tighe, has confirmed using phosphatase treatment that the ladder of Mps1 bands observed after running mitotic samples on Phos-tag gels are indeed due to phosphorylation (Hewitt et al., 2010). While the identity of the site(s) in Mps1 which might be dephosphorylated with AZ3146 treatment are unknown, and I cannot rule out indirect effects, this provides evidence of an effect on Mps1

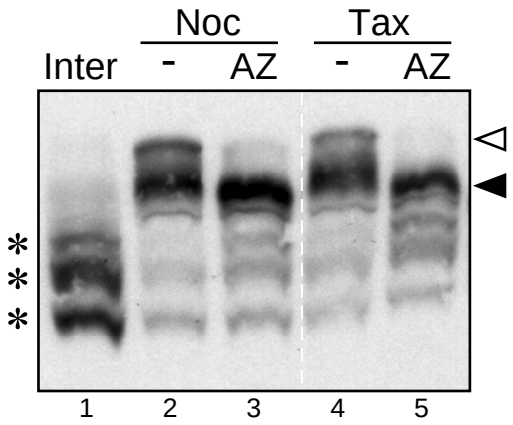

Figure 3.5 AZ3146 affects Mps1 autophosphorylation in cells.
HeLa cells were treated with nocodazole for 12 hours. Mitotic cells were collected and replated into the indicated drug combinations (plus MG132 to prevent mitotic exit) for 2 hours. Adherent cells left behind after mitotic shake-off were harvested and constituted the interphase sample (lane 1). AZ3146 was used at 2 μM and DMSO was used in controls to account for the solvent. Harvested cells were lysed directly in SDS-PAGE sample buffer and run on gels containing Phos-tag. Proteins were transferred to a PVDF membrane and probed with an anti-Mps1 antibody. Asterisks mark the 3 bands evident in interphase samples; the closed arrowhead indicates the major Mps1 band in mitotic lysates; the open arrowhead indicates the slowest-mobility band which virtually disappears from mitotic samples on treatment with AZ3146.

Contributions to this figure:
Cells were treated with drugs and harvested by Anthony Tighe. Samples were run on Phos-tag gels and immunoblotted by Laura Hewitt.

phosphorylation in response to AZ3146, in both nocodazole and Taxol. As such, this is entirely consistent with AZ3146-mediated inhibition of Mps1 in cells.

3.6 | Summary

This chapter describes the initial stages in the characterisation of the novel Mps1 inhibitor AZ3146. The compound inhibited recombinant $Mps1^{CAT}$ in kinase assays, with an IC_{50} of ~35 nM. At a concentration that inhibited Mps1 activity by 96%, the compound exhibited relatively low inhibition of a panel of 46 out of 50 diverse kinases, indicating some selectivity for Mps1. Inhibition of full-length Mps1 immunoprecipitated from HeLa cells was also observed. Importantly, when mitotic cells were cultured with media containing AZ3146, the banding pattern on a Phos-tag gel suggested that endogenous Mps1 phosphorylation was reduced. Since Mps1 autophosphorylation has been shown to correlate with kinase activity (Jelluma et al., 2008a; Kang et al., 2007; Mattison et al., 2007), this decrease in phosphorylation might correlate with a reduction in activity. Encouragingly, the effect was achieved with 2 μM AZ3146, a relatively low molarity, meaning the risk of off-target effects in cells is reduced. Taken together, the above data show that AZ3146 is a potentially useful tool for studying the function of Mps1 kinase activity in cells. I next sought to extend my characterisation of the inhibitor by establishing its effect on the viability and mitotic checkpoint response of cultured tumour cell lines.

4 | *Results Chapter II:* AZ3146 affects cell viability and leads to mitotic checkpoint override

4.1 | Introduction

Mps1 is a conserved component of the mitotic checkpoint, which delays anaphase in the presence of unattached or maloriented kinetochores, and thereby helps to safeguard against missegregation and the subsequent production of aneuploid daughter cells. Several reports focusing on cultured human cancer cell lines have shown that complete abrogation of the spindle checkpoint by siRNA-mediated depletion of Mad2 or BubR1 results in widespread death in a cell population after 6 or 7 days due to catastrophic segregation errors (Kops et al., 2004; Michel et al., 2004). Consistent with this, complete depletion of Mps1 by RNAi (Janssen et al., 2009), its replacement with a kinase-dead mutant (Jelluma et al., 2008a; Jelluma et al., 2008b), or replacement of endogenous Mps1 with a bulky ATP analogue-sensitive form (Sliedrecht et al., 2010) causes loss of viability in tumour cells. There has been some confusion in the literature regarding the effect of loss of Mps1 activity on untransformed 'normal' cells: BJ-TERT fibroblasts were shown to be resistant to checkpoint override induced by the non-specific Mps1 inhibitor SP600125 (Schmidt et al., 2005), and, unlike tumour cell lines, VH-10 fibroblasts were resistant to death when treated with taxol concurrent with partial Mps1 depletion (Janssen et al., 2009). However, recent work showed that ablation of Mps1 catalytic activity negatively affects proliferation and viability in both tumour cells lines and 'normal' untransformed cells lines (Kwiatkowski et al., 2010; Maciejowski et al., 2010).

In this chapter, I sought to establish whether AZ3146-treated cells behaved as predicted for treatment with an Mps1 inhibitor. The existing body of work on Mps1's role in the mitotic checkpoint provided a clear framework with which to test the compound, and enabled me to make several predictions. An inhibitor of Mps1 should: (1) kill tumour cells, and probably untransformed cells (Janssen et al., 2009; Jelluma et al., 2008b; Kwiatkowski et al., 2010; Maciejowski et al., 2010); (2) prevent cells arresting in the presence of drugs known to perturb the mitotic spindle (Jelluma et al., 2008b; Liu et al., 2003; Schmidt et al., 2005; Stucke et al., 2002; Tighe et al., 2008); (3) hasten mitotic progression in an otherwise unperturbed mitosis, and lead to errors in chromosome segregation (Jelluma et al., 2008b; Maure et al., 2007; Tighe et al., 2008).

4.2 | AZ3146 affects the viability of cultured human cancer cell lines and immortalised untransformed cells

To compare the effect of AZ3146 with published reports (Janssen et al., 2009; Jelluma et al., 2008a; Kwiatkowski et al., 2010; Maciejowski et al., 2010; Sliedrecht et al., 2010), I sought to find out if AZ3146 treatment was detrimental to the survival of different cell lines. I wanted to observe the compound's effect on more than one class of tumour-derived cell line, so I chose to test one aneuploid cervical adenocarcinoma cell line (HeLa) and one near-diploid colon carcinoma cell line (HCT116). I also included the immortalised retinal pigmented epithelium cell line (hTERT-RPE) as an example of a non-transformed human cell line (Jiang et al., 1999).

To obtain a read-out of the viability of these cell lines in response to AZ3146-treatment, I used colony-formation assays. These assays measure the ability of single cells to give rise to colonies when cells are plated at low density and cultured for several days, i.e. the cloning efficiency. Two hundred cells were plated into each well of a 6-well culture plate, allowed to adhere, then cultured in media containing a range of AZ3146 concentrations for 8-9 days. The colonies were visualised by fixing and staining the cells with crystal violet and photographed. Representative images of stained plates are shown in Figure 4.1. Stained colonies were readily visible in the control wells for all 3 cell lines (top left well of each plate). The mean colony number ± s.e.m. for the HeLa, HCT116 and hTERT-RPE untreated controls were 157.3 ± 6.0, 142.7 ± 11.8, and 91.3 ± 6.8 respectively, suggesting that, while the cloning efficiency was reasonably high for both HeLa and HCT116s, a more significant amount of cell death may have occurred in the hTERT-RPE controls. However, it is also plausible that the hTERT-RPE colony number was slightly underestimated due to merging of the relatively widespread, less dense colonies seen in this cell type (Figure 4.1C).

In order to quantify the cell number in each well without introducing inaccuracies due to counting difficulties, the crystal violet stain was solubilised and the absorbance at 595 nm was read. A further advantage of this method over simply counting the colonies is that differences in colony size, as well as number, are reflected in the absorbance readings. The A_{595} values for control, untreated wells were set to 100% and data for each cell line was graphed (Figure 4.1). For all 3 cell lines tested, addition of AZ3146 concentrations of 1 μM or higher to the wells produced a marked decrease in staining, reflecting decreased cell viability. At 2 μM, 5 μM and 10 μM, very little colony staining was evident for any cell line; reflecting this, A_{595} readings plateaued at a low level. It should be noted that small increases in A_{595} were observed for both HeLa (Figure 4.1A) and

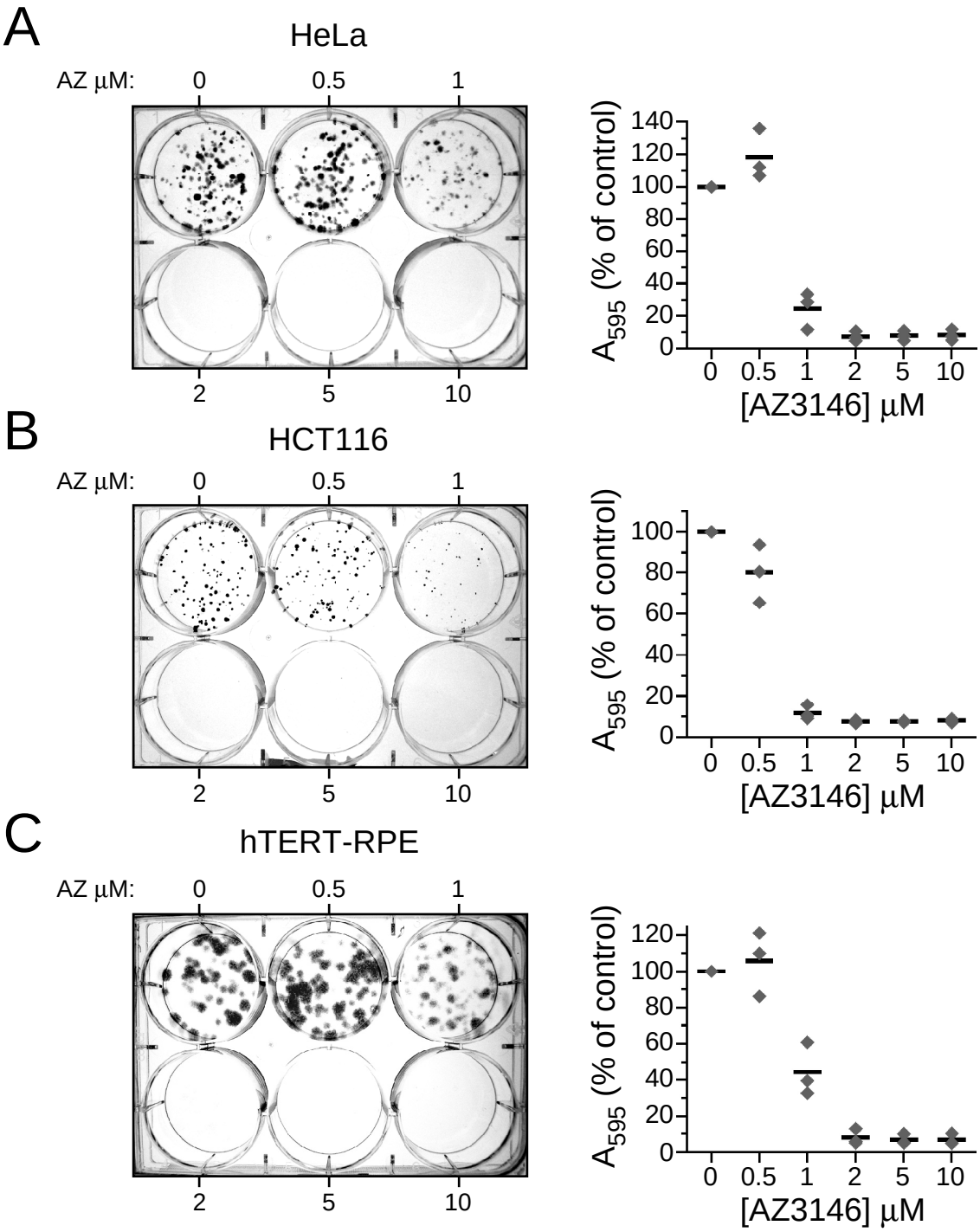

Figure 4.1 AZ3146 affects the viability of human cancer cells and immortalised untransformed cells. HeLa **(A)**, HCT116 **(B)**, and hTERT-RPE **(C)** cells were cultured in 6-well plates for 8-9 days in the presence of AZ3146 at the indicated molarities, before fixation and staining with crystal violet to visualise colonies. Representative images of stained plates are shown (left panel). To quantify cell survival, the crystal violet was solubilised and the absorbance at 595 nm was read (see graphs, right panel). The black line represents the mean level of absorbance from 3 independent experiments. The value for each independent replicate (grey diamond) is itself a mean derived from 2 duplicate wells. Values are normalised to the absorbance reading from untreated wells.

hTERT-RPE (Figure 4.1C) when cells were cultured with 0.5 μM AZ3146. Whilst I cannot rule out a stimulatory effect of AZ3146 on cell proliferation at low molarity, perhaps due to some unknown off target-effect, it is also possible that this increase is caused by slight inaccuracies in cell distribution between wells.

To summarise, at concentrations of 1 μM or higher, AZ3146 had a severely detrimental affect on HeLa, HCT116 and hTERT-RPE cell viability in these colony formation assays. The hTERT-RPEs appeared to be slightly more resistant to AZ3146-induced cell death than HeLa and HCT116 cells, based on the comparatively large number of surviving hTERT-RPE cells after culture in 1 μM AZ3146 (44.5 ± 8.5% of control levels, compared to 24.6 ± 6.7 % for HeLa cells and 11.7 ± 2% for HCT116 cells; compare Figure 4.1C to A and B), but the differences between the cell lines was not large. These data suggest that Mps1 inhibition by AZ3146 treatment can affect the viability of both cancer cell lines and immortalised untransformed cells.

4.3 | AZ3146 causes degeneration of DNA content profiles in a dose-dependent manner

A plausible explanation for the reduction in of HeLa, HCT116 and hTERT-RPE cells after long term AZ3146 treatment is that perturbation of Mps1 activity at ≥1 μM AZ3146 caused missegregation events which, over the 9-10 day duration of the assay, were not compatible with survival or growth of colonies. To see if there were indeed segregation errors after AZ3146 treatment, I treated asynchronous populations of each cell line with a range of AZ3146 concentrations for 24 hours, which would allow for 1-2 divisions in the presence of the drug, then analysed the DNA content of the population by flow cytometry (Figure 4.2). This kind of DNA content analysis is a relatively low-resolution method of detecting segregation errors, but it does provide a view of a relatively large cell population (in this case ~10,000 cells). The DNA content profiles for the control populations showed slight variability between cell lines, presumably reflecting differences in the lengths of cell cycle phases, but all control profiles appeared to reflect a normal, cycling asynchronous population: 2N and 4N peaks were well defined, and an S-phase population was evident in between these (Figure 4.2, top row). After 24 hours treatment with 1 μM AZ3146, profiles still appeared largely normal (second row). When 2 μM of AZ3146 was used, the profiles for all 3 cell lines showed signs of deviation from the norm (third row): the 2N and 4N peaks were wider than those in the control profiles. Of the 3 cell lines tested, hTERT-RPEs (right panel) appeared least severely affected by the compound in this assay; 2 μM AZ3146 caused only a slight effect on the DNA profile of this cell line. At 5 μM and 10 μM AZ3146, further deterioration of the profiles was evident for all 3 cell lines. The

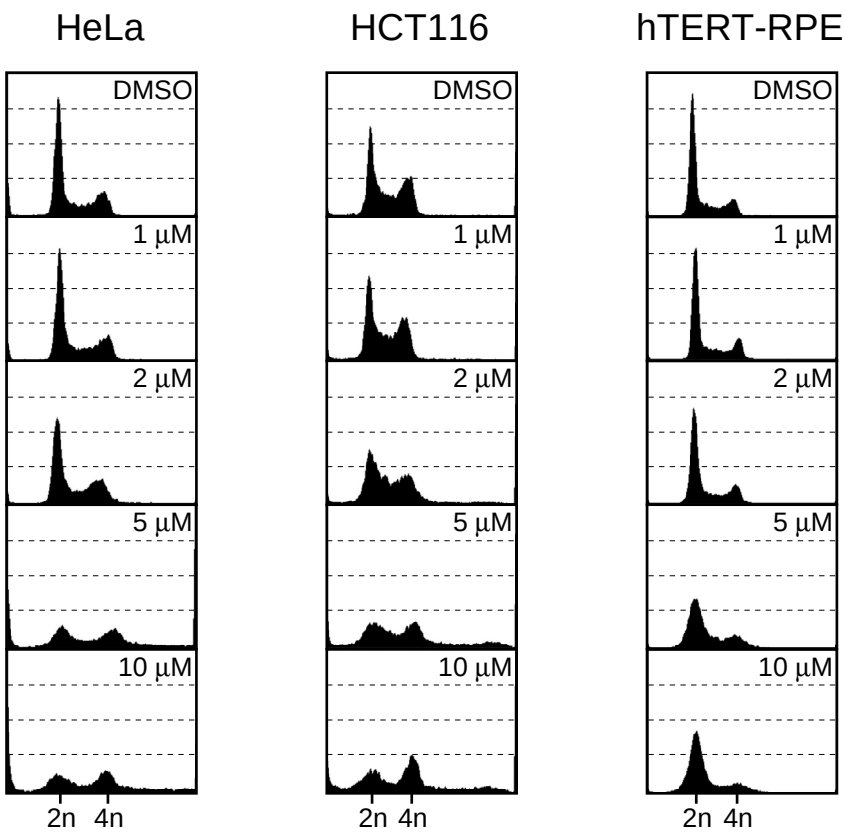

Figure 4.2 AZ3146 causes degeneration of DNA content profiles in a dose-dependent manner
Asynchronous HeLa (left panel), HCT116 (middle panel) and hTERT-RPE cells (right panel) were cultured with DMSO as a solvent-only control, or AZ3146 at the indicated molarities for 24 hours then harvested and processed for DNA content analysis by flow cytometry.

widening of the 2N and 4N peaks reflects an increase in the number of cells with chromosome complements deviating from the normal copy number, and is therefore consistent with the notion that AZ3146-mediated Mps1 inhibition causes chromosome missegregation, giving rise to aneuploid cells.

When treated with 5 μM or 10 μM AZ3146, the HCT116 population (middle panel) contained some cells abnormally high DNA contents of up to ~8N. A fraction of HeLa cells treated with 5 μM or 10 μM of the compound (left panel) also had DNA contents of more than 4N. These fractions presumably contain cells that have failed to segregate their chromosomes, but exited mitosis in a tetraploid state and proceeded into the next cell cycle, re-entering S phase. There are at least two possible explanations for the existence of tetraploid cells. Firstly, at the highest AZ3146 concentrations, Mps1 inhibition (and checkpoint override) may be more complete, meaning a larger proportion of cells might exit mitosis before bipolar spindle formation and cytokinesis can occur, as has been reported for DLD1 cells depleted of BubR1 (Morrow et al., 2005). This might leave more tetraploid cells after exit from mitosis. Alternatively, perhaps higher concentrations of AZ3146 prevent cytokinesis itself from occurring in small subset of cells, through direct or indirect inhibition of pathways required for its completion. Either way, since no prolonged mitotic arrest has occurred, some or all of these tetraploid cells may be capable of progression into the next S phase (Uetake and Sluder, 2007), as a similar effect was observed in cells where cytokinesis is prevented by depolymerising microtubules and inactivating the mitotic checkpoint (Kops et al., 2004; Taylor and McKeon, 1997), or inhibition of Aurora B (Ditchfield et al., 2003). It is not possible to determine the mechanism governing formation of these >4N cells from the data shown here, however it seems reasonable to say that cytokinesis failure and/or the production of octaploid cells is a minor effect of AZ3146 treatment in asynchronous cells, but can occur in a subset of cells, most noticeably when AZ3146 is used at concentrations over 2 μM.

The profiles shown in Figure 4.2 indicate that when cells were treated with 1 μM AZ3146 for 24 hours, the population appeared to be relatively unaffected. However, the colony formation assays in Figure 4.1 showed that in the long term (9-10 days) cell viability was adversely affected by 1 μM of the compound in all 3 of the cell lines tested. How might this apparent contradiction be reconciled? On possible answer is that with 1 μM AZ3146, each mitosis produces only mild segregation errors leading to only very small deviations from the 2N and 4N populations, perhaps only in a proportion of cells. Such mild errors might be imperceptible in the DNA content profile of the cell population after only 24 hours, but might accumulate in the population over several rounds of division and be detrimental to survival over a longer period.

In summary, after incubation with AZ3146 at 2 μM or higher for 24 hours, HeLa, HCT116 and hTERT-RPE cells exhibit DNA content profiles consistent with chromosome loss or gain. This is entirely consistent with premature inactivation of the mitotic checkpoint and an increased rate of missegregation as a consequence of Mps1 kinase activity reduction.

4.4 | 2 μM AZ3146 causes degeneration of DNA content profiles over time.

Having established the effect of a range of doses of AZ3146 on the DNA content of cells at a single time point, I wanted to see what effect AZ3146 treatment had on the cell population over a longer time period. For this, I used 2 μM of the drug, since this molarity causes phenotypes consistent with Mps1 inhibition in cells: it affects the phosphorylation of Mps1 in cells (Figure 3.5), leads to loss of viability in colony formation assays (Figure 4.1), and causes a phenotype consistent with checkpoint override when DNA content was analysed by flow cytometry (Figure 4.2). HeLa, HCT116 and hTERT-RPE cells were cultured in the presence of 2 μM AZ3146 and harvested at 24 h, 48 h and 72 h time points before analysis by flow cytometry. The control populations appeared as expected for the duration of the experiment (Figure 4.3, DMSO profiles). When cells were treated with 2 μM AZ3146 for 24 hours, aneuploid cells were evident in the DNA content profiles for all 3 cell lines, in keeping with the results shown in Figure 4.2. For HeLa and HCT116 cells, the widening of the 2N and 4N peaks became more pronounced after 48 and 72 hour treatment, signifying more severe aneuploidy; this was accompanied by an increase in sub-2N DNA, suggestive of cell death by apoptosis. This was particularly marked in HCT116 cells, where the DNA content profile had degenerated considerably after 72 hours with 2 μM AZ3146. The hTERT-RPE cell population also exhibited DNA contents suggestive of aneuploidy over the course of the experiment, but the deterioration of the profiles over time was less marked. The hTERT-RPE cells did not exhibit a noticeable increase in sub-2N DNA, which can be interpreted to mean there was less cell death in the population.

These data strongly suggest that 2 μM AZ3146 treatment causes chromosome loss or gain, which, certainly in HeLa and HCT116 cells, leads to production of increasingly aneuploid cells over 3 days in culture. The increase in sub-2N DNA is indictative of apoptosis, suggesting that in some cases this aneuploidy is lethal. hTERT-RPE cells also showed signs of aneuploidy, but less evidence of lethality, suggesting that changes chromosome number were largely tolerated by the cell population over the 3 day duration of the experiment. The loss of viability observed in the colony formation assays with hTERT-RPE cells (Figure 4.1) could indicate that the chromosome gains and losses

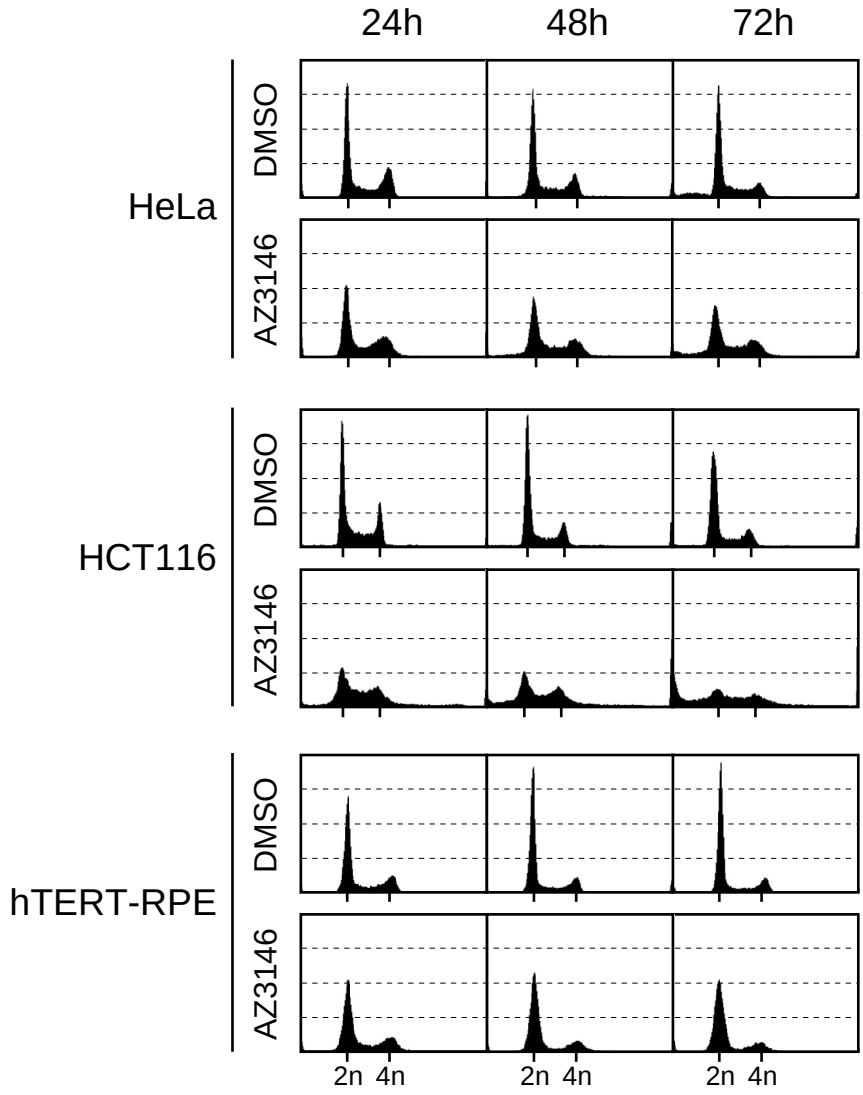

Figure 4.3 AZ3146 treatment causes degeneration of DNA content profiles over time.
Asynchronous HeLa (top panel), HCT116 (middle panel), or hTERT-RPE (bottom panel) cells were cultured in the presence of either DMSO (solvent-only control) or 2 μM AZ3146 for 24, 48 or 72 hours. Cells were harvested and processed for DNA content analysis by flow cytometry.

induced by 2 μM AZ3146 are not compatible with viability over a longer period. Overall, the data from all 3 cell lines supports the idea AZ3146 treatment leads to accumulation of aneuploidy as a result of impaired Mps1 function. It also seems likely that the reduced colony formation of these cells (Figure 4.1) is caused, at least in part, by missegregation events as a consequence of Mps1 inhibition.

4.5 | AZ3146 treatment results in bypass of a nocodazole-induced mitotic checkpoint

Next, I sought to investigate a likely contributing factor to chromosome missegregation: mitotic checkpoint malfunction. The catalytic activity of Mps1 is required for the mitotic checkpoint-mediated arrest in the presence of microtubule toxins that prevent spindle assembly (Jelluma et al., 2008b; Kwiatkowski et al., 2010; Schmidt et al., 2005; Tighe et al., 2008). Therefore, AZ3146 treatment is predicted to override the checkpoint-mediated arrest induced by nocodazole treatment. To test this, I treated an asynchronous population of HeLa cells with nocodazole and 2 μM AZ3146 for 24 hours, then analysed the DNA content of the population by flow cytometry, and determined the fraction of the cell population with DNA content over 4N. The DNA content profiles obtained for the various combinations of drug treatments are shown in Figure 4.4A, with the percentage of DNA >4N indicated in the upper right corner of each profile. The control population appeared as expected, with a clear 2N and 4N peak and very few cells with a DNA quota exceeding 4N (1.0%; Figure 4.4A). With AZ3146 alone, DNA contents diverging from 2N and 4N were observed, as seen in Figure 4.2 and 4.3, and the proportion of cells with >4N DNA very slightly increased (4.4%). Twenty-four hours of nocodazole treatment caused accumulation of tetraploid cells, consistent with a checkpoint-induced mitotic arrest, and very few cells (1.3%) contained more than 4N DNA. Importantly, when AZ3146 was combined with nocodazole, 52% of cells had a DNA complement of more that 4N, implying that the mitotic checkpoint response to nocodazole had failed. Checkpoint-deficient cells had exited mitosis without segregating DNA, avoided arrest or activation of pro-death pathways and proceeded into the next cell cycle, reduplicating their DNA in the subsequent S phase (Kops et al., 2004; Taylor and McKeon, 1997). This is consistent with an AZ1346-mediated mitotic checkpoint override, and inhibition of Mps1 catalytic activity (Jelluma et al., 2008b; Kwiatkowski et al., 2010; Schmidt et al., 2005; Tighe et al., 2008).

To confirm the apparent mitotic checkpoint override induced by AZ3146, I wanted to observe its effect on a synchronised cell population. To achieve this, I arrested HeLa cells in early S phase using a double thymidine block-and-release method, and then

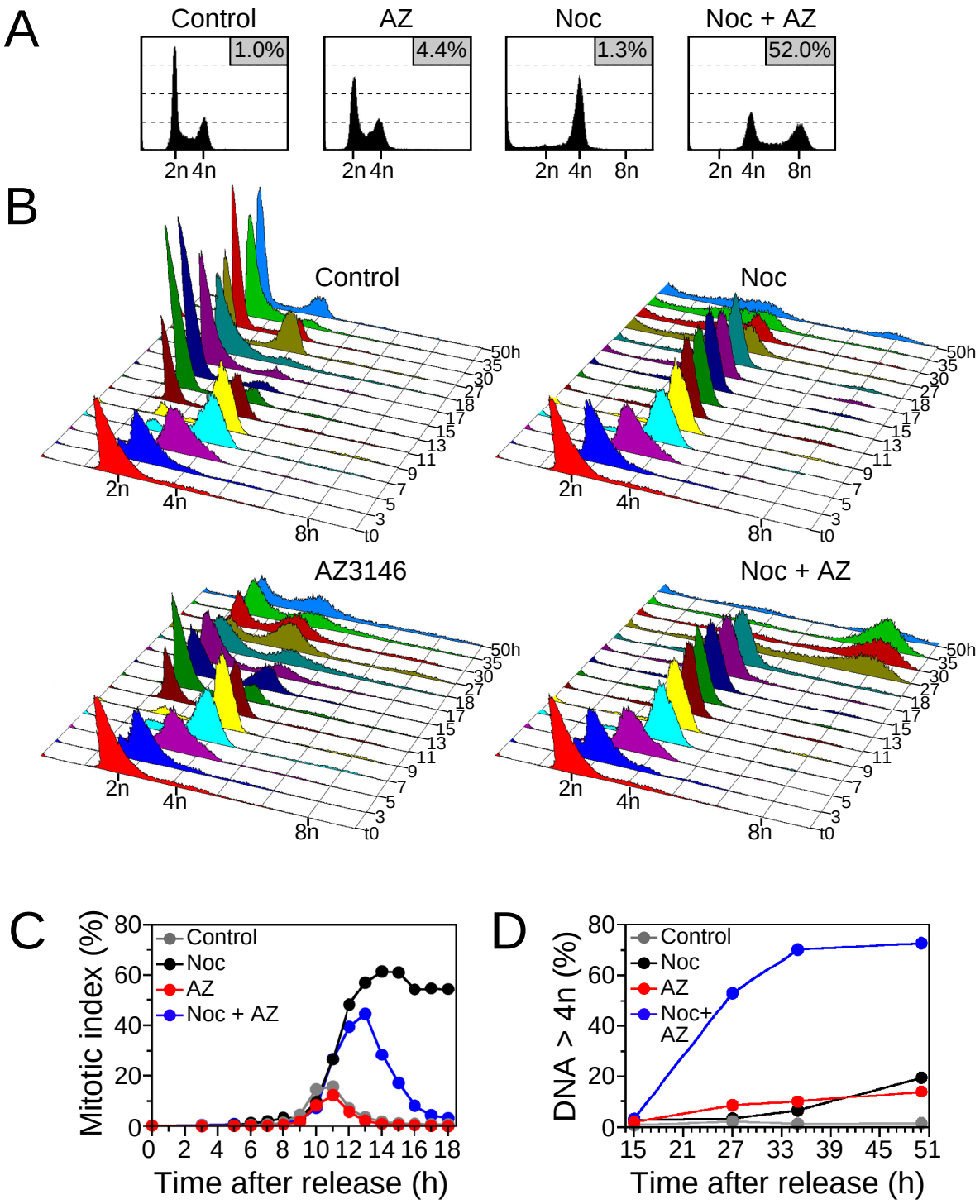

Figure 4.4 AZ3146 treatment compromises a nocodazole-induced mitotic checkpoint.
(A) Asynchronous HeLa cells were cultured with DMSO (control) or the indicated combinations of AZ3146 (2 μM) and nocodazole for 24 hours before harvesting and processing for DNA content analysis by flow cytometry. The percentage of cells with DNA content over 4N is shown in the top corner of each profile. **(B, C, and D)** HeLa cells were synchronised in early S phase using a double thymidine block protocol, then released into DMSO (control) or the indicated drug combinations. Cells were harvested at time points post-release, and analysed by flow cytometry. **(B)** DNA content profiles from the indicated timepoints (t=0 to 50 h post-release). **(C)** Mitotic indices in the first 18 h post-release. Mitotic cells were defined as those with 4N DNA content and MPM2 positivity. **(D)** The percentage of cells with DNA contents of more than 4N were determined from DNA content profiles.

released them into media containing the indicated combinations of nocodazole and 2 μM AZ3146. Cells were harvested at subsequent time points and analysed to determine DNA content (Figure 4.4B). Control DNA content profiles revealed cells progressing through S phase after release from thymidine block, then returning to 2N around 11 hours post-release as cells went through mitosis. Staining with the mitosis-specific phospho-antibody MPM2 confirmed that the mitotic index of the control population peaked around 10-11 hours after release (Figure 4.4C). Control cells then continued to cycle for the remainder of the experiment, and had lost synchrony by the final 50 hour time point (Figure 4.4B). Treatment with 2 μM AZ3146 alone caused the appearance of cells with abnormal DNA quotas after 1 or more rounds of division (11 hours post-release onwards), confirming previous observations (Figure 4.2, 4.3, 4.4A). As predicted, cells released from thymidine into nocodazole arrested with 4N DNA content, with a mitotic index of ~50-60% up to 18 hours after release (Figure 4.4B, C), indicative of a mitotic arrest due to spindle perturbation. After 27 hours post-release, the appearance of sub-2N DNA suggested that many nocodazole-treated cells died (Figure 4.4B), while only a small fraction appeared to progress into the next cell cycle, reduplicating DNA (Figure 4.4D). When cells were released into nocodazole and AZ3146, tetraploid cells began to accumulate in mitosis at a similar rate to cells treated with nocodazole alone, but, importantly, the mitotic index of AZ3146 and nocodazole treated cells fell dramatically after the 13 hour time point (Figure 4.4B, C). Furthermore, a large proportion of AZ3146 and nocodazole-treated cells went on to exhibit >4N DNA content (Figure 4.4B, C). Strikingly, 27 hours after release from thymidine, 53% of AZ3146 and nocodazole-treated cells had >4N DNA, compared to only 3% of cells that were released into nocodazole alone (Figure 4.4D). These data indicate that AZ3146-treated cells fail to mount a robust mitotic checkpoint response to nocodazole, and continue to cycle in its presence. This is in keeping with the previous data from asynchronous cells (Figure 4.4A). Taken together, the data in Figure 4.4 strongly support the idea that AZ3146 treatment causes a mitotic checkpoint override, as one would expect from an Mps1 inhibitor.

4.6 | AZ3146 accelerates mitotic exit in the presence of antimitotic drugs with varying mechanisms of action

To extend the population-based analysis of AZ3146's ability to induce mitotic checkpoint override in response to nocodazole (Figure 4.4), I next employed a direct, single cell approach to observe the compound's effect in the presence of antimitotic drugs that target the spindle. All three of these drugs prevent satisfaction of the mitotic checkpoint, leading to a mitotic arrest dependent on inhibition of the APC/C^{Cdc20}.

However, the mechanism of action for each drug differs. Nocodazole causes depolymerisation of microtubules, and thus a multitude of unattached kinetochores. Taxol, on the other hand, prevents microtubule disassembly, leading to stabilised, non-dynamic microtubules that can form attachments at kinetochores, but their ability to form stable, amphitelic, checkpoint-satisfying attachments is severely compromised (Yang et al., 2009). Thirdly, the Eg5 kinesin inhibitor monastrol does not affect microtubule dynamics, but prevents centrosome separation, leading to monopolar spindles, syntelic attachments consequently and mitotic checkpoint activation (Kapoor et al., 2000; Mayer et al., 1999).

To observe the effect of AZ3146 treatment on the duration of the mitotic arrest caused by these compounds, asynchronous HeLa cells stably expressing GFP-tagged Histone H2B were treated with the antimitotic drugs with or without 2 μM AZ3146, and filmed by timelapse microscopy. Mitotic entry was defined as the point of NEBD, and mitotic exit was judged to have occurred when chromatin visibly began to decondense. Survival curves were plotted to visualise the data (Figure 4.5). In nocodazole, the vast majority of cells (69 out of 71) remained in mitosis, with condensed chromatin, for at least 500 minutes, consistent with mitotic checkpoint-mediated arrest. In contrast, almost all AZ3146-treated cells analysed (76 out of 81) had decondensed their chromatin by 500 minutes post-NEBD. The variation in length of mitotic delay was wide, but concurs with the mitotic index values exhibited in Figure 4.4C: most cells remained in mitosis for at least ~180 minutes, after which the number of cells in mitosis dropped steadily. Taxol treatment also led to a prolonged mitosis as measured by chromatin condensation: most cells (83 out of 91) kept their chromatin condensed for 500 minutes or more. When AZ3146 was present, all cells (139 out of 139) had exited mitosis by ~220 minutes after NEBD. Monastrol caused a comparatively transient arrest, with 65 out of 92 cells exiting mitosis after fewer than 500 minutes arrest. Many of these cells divided, albeit often aberrantly (data not shown). This might be a reflection of monastrol's somewhat low potency: despite the continued presence of the drug, spindles can frequently bipolarise, and in cells that cannot resolve the merotelic attachments that arise during monopolar arrest, satisfy the spindle checkpoint (Gascoigne and Taylor, 2008). Nevertheless, it is clear that AZ3146 markedly accelerated mitotic exit in the presence of monastrol: all cells had decondensed their chromatin by ~350 minutes post-NEBD.

The data described above suggest that the mitotic checkpoint response to different types of drug that target microtubule dynamics, namely nocodazole and taxol, is attenuated by AZ3146 treatment. AZ3146-treated cells exited mitosis fastest in taxol; all cells analysed left mitosis after a delay of less than ~220 minutes. Nocodazole- and AZ3146-

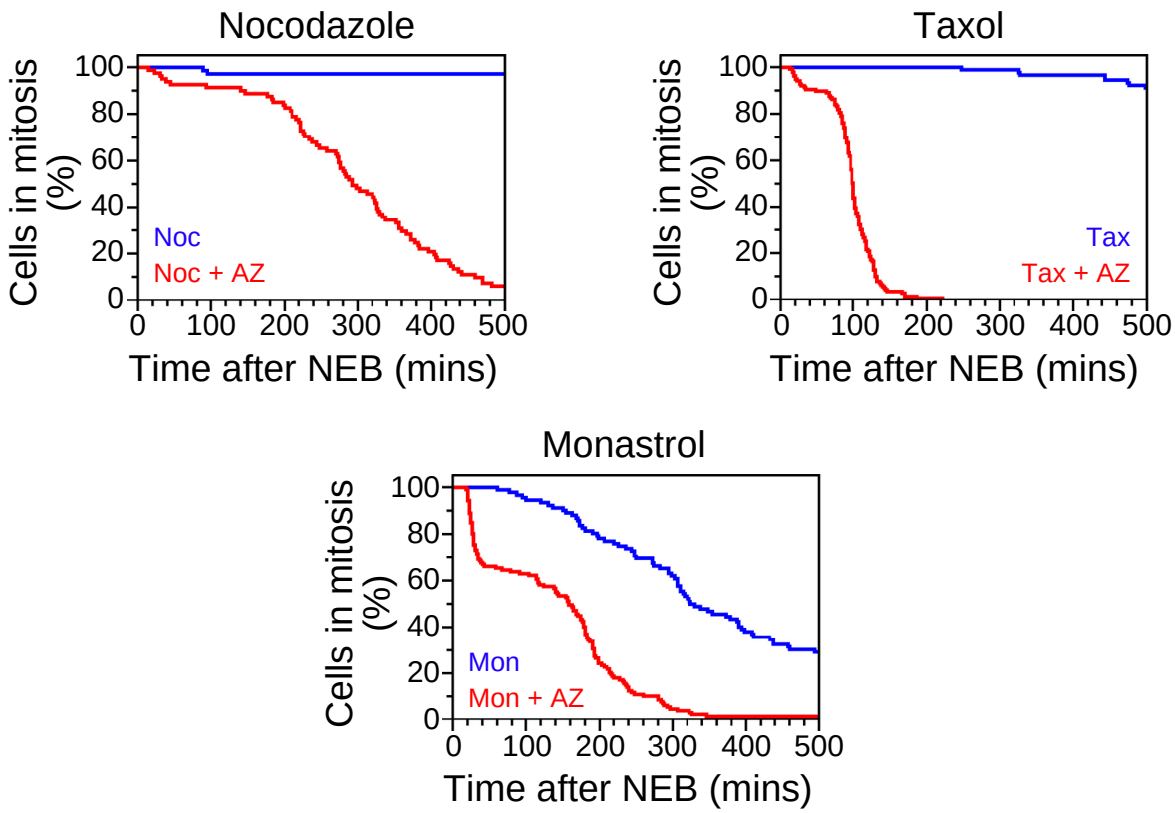

Figure 4.5 AZ3146 accelerates mitotic exit in the presence of anti-mitotic drugs
Asynchronous HeLa cells stably expressing GFP-tagged Histone H2B were treated with nocodazole (top left), taxol (top right) or monastrol (bottom centre), along with either DMSO (solvent-only control, blue lines), or 2 μM AZ3146 (red lines) before tracking mitotic progression with fluorescence timelapse microscopy. The time each cell spent in mitosis was determined by recording the point of mitotic entry (NEB) and exit (chromatin decondensation). Survival curves were plotted for each dataset.

treated cells took longer to exit mitosis (up to 350 minutes), and showed much wider variation in the duration of arrest, as shown by the gently sloping survival curve (Figure 4.5). One possible explanation for this is that the checkpoint in taxol is somehow easier to silence than the checkpoint in nocodazole, resulting in more rapid mitotic exit when cells are treated with taxol and AZ3146. Perhaps the presence of microtubules allows more efficient trafficking of checkpoint components off the kinetochore, meaning the signal can be extinguished more efficiently (Howell et al., 2001; Musacchio and Salmon, 2007). Or, because kinetochores occupied by taxol-stabilised microtubules stimulate much less Mad2 recruitment than unoccupied kinetochores (Waters et al., 1998), and have even been shown to be able to eventually cause checkpoint satisfaction (Yang et al., 2009), AZ3146 treatment might more easily counteract the checkpoint in taxol. Additional inputs into the downstream signalling cascade may exist in nocodazole-treated cells: Bub1 is reported to monitor kinetochore-microtubule attachment, and is therefore activated by nocodazole but not taxol (Morrow et al., 2005). This extra positive influence on checkpoint signalling might mean cells treated with AZ3146 are able to sustain an arrest for longer in nocodazole than in taxol. However, even if such additional input/s are able to delay mitotic exit in nocodazole, they are not sufficient to prevent checkpoint override in nocodazole when cells are treated with AZ3146. In both nocodazole and taxol, almost all cells analysed were unable to sustain a checkpoint-mediated arrest when AZ3146 was present.

Taken together, the timelapse microscopy data shown in Figure 4.5 strongly suggests that 2 μM AZ3146 treatment leads to inactivation of the mitotic checkpoint and consequently mitotic exit, despite the presence of antimitotic compounds that usually cause a more prolonged delay in mitosis. This is entirely consistent with Mps1 inhibition.

4.7 | AZ3146 accelerates passage through an unperturbed mitosis and causes missegregations

As well as mediating mitotic arrest in response to spindle perturbations which inhibit the formation of checkpoint-satisfying microtubule-kinetochore attachments, the mitotic checkpoint is active in a 'normal', unperturbed mitosis to delay the onset of anaphase until all sister kinetochore pairs have achieved biorientation (Rieder et al., 1995). RNAi complementation assays have been used to show that Mps1 catalytic activity is required to stop premature anaphase initiation in human tumour cell lines (Jelluma et al., 2008b; Kwiatkowski et al., 2010; Sliedrecht et al., 2010; Tighe et al., 2008). Therefore, I asked whether 2 μM AZ3146 treatment accelerated passage through mitosis. I used timelapse microscopy to film asynchronous cells and recorded the duration of mitosis (NEB to chromatin decondensation), and extended my analysis to include both hTERT-RPE and

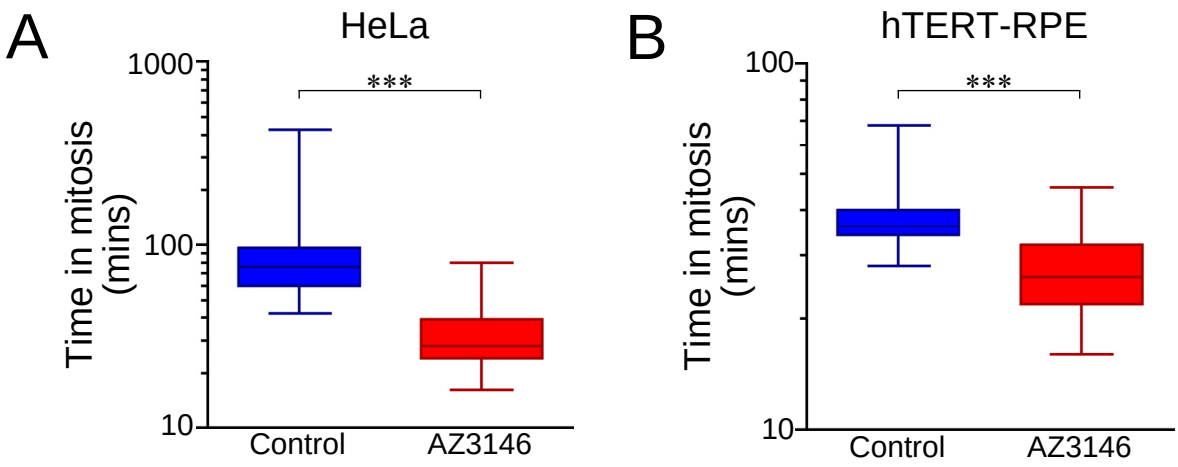

Figure 4.6 AZ3146 accelerates passage through an unperturbed mitosis
Asynchronous HeLa **(A)** and hTERT-RPE **(B)** cells stably expressing GFP-Histone H2B were cultured in the presence of DMSO (control) or 2 μM AZ3146 and filmed using fluorescence microscopy. Time in mitosis was defined as the time from NEB to chromatin decondensation. Data is displayed as box and whisker plots, where the box shows the interquartile range and the median, and the whiskers show the full range. In **(A)**, the data shown is combined from 2 independent experiments; with a total of at least 75 HeLa cells analysed per condition. In **(B)**, the data shown is combined from 3 independent experiments, with a total of 150 hTERT-RPE cells analysed per conditon. (***$P < 0.0001$, Mann-Whitney U-test.)

HeLa cells stably expressing GFP-tagged Histone H2B (Figure 4.6). Control HeLa cells took a mean time of 90 min to complete mitosis; strikingly, the mean duration of mitosis was reduced to 32 minutes when AZ3146 was present (Figure 4.6A). Control hTERT-RPEs completed mitosis in a mean time of 37 min, in keeping with reports that untransformed cells take less time in mitosis than transformed cells (Rieder and Maiato, 2004). Again, AZ3146 addition reduced the mean duration of mitosis: hTERT-RPE cells now took an average of only 27 min from NEB to chromatin decondensation (Figure 4.6B). These data indicate that, in both a tumour cell line (HeLa) and immortalised "normal" cell line (hTERT-RPE), AZ3146 accelerated mitotic exit. This effect is attributable to Mps1 inhibition via AZ3146, and suggests that Mps1 activity is required to restrain mitotic exit in both transformed and untransformed cells.

As well as causing accelerated passage through mitosis, loss of Mps1 kinase activity (and consequently mitotic checkpoint function) is also associated with missegregation events in human tumour cells lines (Jelluma et al., 2008b; Kwiatkowski et al., 2010; Sliedrecht et al., 2010; Tighe et al., 2008). To assess the mitotic phenotype of AZ3146-treated cells, I classified the same HeLa and hTERT-RPE cells analysed in Figure 4.6 according to the presence or absence of certain mitotic abnormalities. The vast majority of untreated HeLa cells appeared to complete a normal mitosis, restraining the onset of anaphase until all chromosomes were properly aligned at the metaphase plate and cleanly segregating chromatin into two new daughter cells (Figure 4.7 A, montage *i*). A fraction of untreated HeLa cells had mitotic abnormalities (21%), predominantly anaphase bridges; however, when cells were filmed in the presence of AZ3146 the proportion of cells with visible mitotic abnormalities increased dramatically, reaching 91%. Two major phenotypes were evident. Of these, segregation of DNA in the presence of misaligned chromosomes was the most common: 53% of AZ3146-treated HeLa cells exhibited this defect. The severity of the defect varied from anaphase in the presence of one or more unaligned chromosomes at the poles (montage *ii*), to the absence of visible metaphase plate formation, with chromatin apparently cleaved by ingression of the furrow at cytokinesis (montage *iii*). This resembles a 'cut'-like phenotype that has been described in Mps1-depleted cells (Jelluma et al., 2008b). Missegregations like these could clearly produce aneuploid cells, in concurrence with the flow cytometry data (Figures 4.2-4.4). The second most common phenotype in AZ3146-treated HeLa cells is illustrated in montage *iv*: 32% of cells failed to segregate their DNA, exiting mitosis with a single mass of chromatin. These cells frequently appeared to initiate anaphase prior to bipolar spindle formation, in a similar manner to cells depleted of BubR1 (Morrow et al., 2005). Although cells with >4N

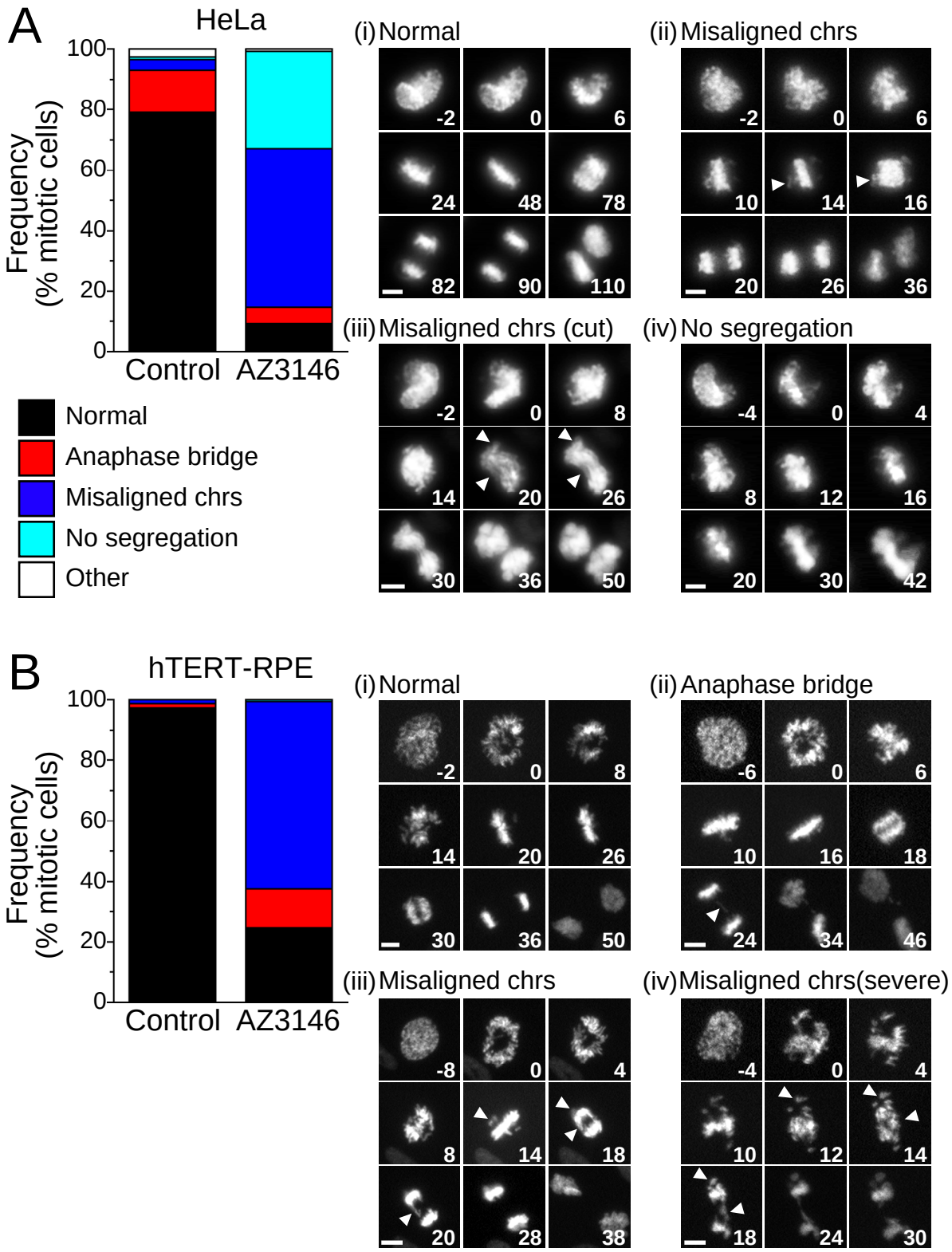

Figure 4.7 AZ3146 causes mitotic abnormalities consistent with mitotic checkpoint override
Asynchronous HeLa (**A**) and hTERT-RPE (**B**) cells stably expressing GFP-Histone H2B were cultured in the presence of DMSO (control) or 2 μM AZ3146 and imaged using fluorescence timelapse microscopy. Mitotic defects were classified and represented as bar graphs (**A** and **B** left panel; the legend in **A** also applies to **B**). Representative examples are shown as image sequences (**A** and **B** ***i-iv***). The time from NEB in minutes is shown for each image. Arrowheads point to mis-aligned chromosomes and anaphase bridge-like structures. Scale bars, 5 μm.

DNA contents were uncommon in asynchronous AZ3146-treated HeLa cells analysed by flow cytometry (Figures 4.2-4.4), some of the tetraploid cells produced by treatment with 2 μM AZ3146 might be capable of progression into the next S phase: a modest increase in cells with >4N DNA content was apparent by flow cytometry in asynchronous AZ3146-treated HeLa cells (Figure 4.4A), and when synchronised HeLa cells were released into 2 μM AZ3146 (Figure 4.4B, D). This timelapse data is consistent with AZ3146-mediated mitotic checkpoint override in HeLa cells, in agreement with the flow cytometry data.

Analysis of the control population of hTERT-RPE cells revealed that almost every mitoses was normal in appearance (97%; Figure 4.7B, montage *i*). Strikingly, treatment with 2 μM AZ3146 meant 75% of mitoses were classified as abnormal, with two distinct phenotypes. A relatively small fraction of cells (13%) appeared to have an anaphase bridge-like structure, as shown in montage *ii*. However, the principal abnormality in AZ3146-treated hTERT-RPE cells was anaphase initiation in the presence of misaligned chromosomes (62% of mitoses), ranging in severity as exemplified in montages *iii* and *iv*. Divisions like these are likely to lead to loss or gain of a few chromosomes, resulting in the relatively minor aneuploidy seen by DNA content analysis of these cells when treated with 2 μM AZ3146 for 24 hours (Figures 4.2 and 4.3). Taken together, the data in Figure 4.6 and 4.7 back up the DNA content analysis in Figures 4.2-4.4, providing direct evidence of a mitotic phenotype consistent with Mps1 inhibition.

4.8 | Summary

In this chapter I tested the effect of AZ3146 on three different human cell lines. Whilst this is not a comprehensive examination of the compound's effects on various cell types, it enabled me to gain some insight into the response of both tumour cell lines and untransformed cell lines to Mps1 inhibition. Overall, the results show that hTERT-RPE cells, like HeLa and HCT116s, are sensitive to Mps1 inhibition: all cell lines showed signs of mitotic checkpoint override and a decrease in viability in the presence of the drug. However, it is noteworthy that the mitotic defect exhibited by the hTERT-RPEs was less severe than that observed in HeLa cells, which is possibly why the untransformed cells appeared to tolerate treatment with 2 μM AZ3146 better then the tumour cell lines in the shorter term (Figure 4.3) and seemed slightly more resistant to long term treatment (Figure 4.2).

The major aim of this chapter was to characterise AZ3146's effect in cells by using various read-outs of mitotic checkpoint inhibition. To summarise, the data in this chapter provides evidence that AZ3146 treatment (1) decreases viability in both transformed and untransformed human cells; (2) abrogates the mitotic checkpoint response induced by

spindle-perturbing agents, and; (3) overrides the mitotic checkpoint in asynchronous cells, leading to accelerated passage through mitosis and aneuploidy. Importantly, these observations are all wholly consistent with Mps1 inhibition. Therefore, I am confident that AZ3146 is indeed a useful tool to probe Mps1 biology.

5 | *Results Chapter III:* AZ3146 leads to loss of Mad2 and accumulation of Mps1 at kinetochore

5.1 | Introduction

In the previous chapter, I found that AZ3146-mediated Mps1 inhibition abrogated mitotic checkpoint signalling. In order to establish a possible mechanism for this, I focused my attention on the origin of the checkpoint signal: the unattached kinetochore (Rieder et al., 1995). Proteins involved in the mitotic checkpoint localise to the fibrous corona of unattached kinetochores, and abolishing kinetochore localisation of core checkpoint proteins perturbs the checkpoint response (e.g. Taylor and McKeon, 1997; Zhao and Chen, 2006). The work in this chapter focuses on the unattached kinetochore, and describes the effect of AZ3146 treatment on its components. By making these observations, I hoped to gain some insight into the function of Mps1 catalytic activity in the mitotic checkpoint.

5.2 | Mad2 localisation is highly sensitive to AZ3146 treatment

To explore the cellular effects of AZ3146-mediated Mps1 inhibition, I used a simple, indirect immunofluorescence-based assay to observe the effect of AZ3146 treatment on localisation of several kinetochore proteins. Briefly, HeLa cells were treated simultaneously with nocodazole, MG132 and 2 μM AZ3146 (or DMSO in controls) for 2 hours before fixation and staining with antibodies to detect kinetochore proteins of interest. The addition of nocodazole created unattached kinetochores, and MG132 prevented mitotic exit, thereby keeping a proportion of the cells arrested in prometaphase where, under normal circumstances, the mitotic checkpoint is active and checkpoint proteins are recruited. In these cells, selected protein levels were qualitatively assessed after fixation and staining with appropriate antibodies. Standard fluorescence microscopy was used to view the cells, and levels were assessed by eye then classified as high, medium or low. I intended the categories to correspond roughly to kinetochore staining levels of 100-66%, 66-33% and 33-0% respectively.

Loss of Mad2 at the prometaphase kinetochore is a relatively well-established indicator of loss of Mps1 function. Mps1 depletion leads to loss of Mad2 at kinetochores in Xenopus egg extracts and in human cells (Abrieu et al., 2001; Fisk et al., 2003; Jelluma et al., 2008b; Liu et al., 2003; Martin-Lluesma et al., 2002; Tighe et al., 2008); furthermore, the use of kinase-dead and ATP analogue-sensitive mutants, along with the

Kinetochore protein levels after treatment with nocodazole and 2 μM AZ3146			
Protein	**Level after AZ**	**Protein**	**Level after AZ**
Mad2	*Low*	Bub1	*High*
Mad1	*Med*	BubR1	*High*
Rod	*Med*	Aurora B	*High*
ZW10	*Med*	Cenp-F	*Med*
Zwilch	*Med/Low*	Cenp-E	*Med*
Zwint	*High*	Cenp-A	*High*

Table 5.1 Summary of kinetochore protein levels in HeLa cells after treatment with AZ3146, nocodazole and MG132, derived from the data presented in Figure 5.1.

recently-published Mps1-IN-1 inhibitor, has revealed that the catalytic activity of the kinase is necessary for Mad2 recruitment (Kwiatkowski et al., 2010; Sliedrecht et al., 2010; Tighe et al., 2008). Therefore, I would predict decreased levels of Mad2 staining after AZ3146 treatment in my immunofluorescence-based assay. The majority of AZ3146-treated, prometaphase-arrested cells (66%) had faint or undetectable kinetochore Mad2, in stark contrast to the readily visible kinetochore staining pattern in control cells, where 83% of cells had high levels of staining (Figure 5.1A and Table 5.1). In parallel with my analysis, A. Tighe's quantification of pixel intensities in AZ3146-treated cells showed that this equates to an 85% reduction, on average (Hewitt et al., 2010). Importantly, these observations fit with previous work and confirm that Mps1 kinase activity is required for Mad2 recruitment and/or maintenance at the kinetochore.

The effect of Mps1 depletion or inhibition on Mad1 localisation is somewhat controversial. Whilst it is established that Mps1 RNAi leads to Mad1 loss (Jelluma et al., 2008b; Liu et al., 2003; Tighe et al., 2008), there is some conflicting data regarding the requirement for Mps1 kinase activity for Mad1 localisation (Jelluma et al., 2008b; Schmidt et al., 2005; Tighe et al., 2008). Therefore, I was particularly interested in finding out whether AZ3146 caused loss of Mad1 signal at kinetochores. Mad1 is clearly affected by AZ3146 treatment in this assay: 36% or 42% of prometaphase cells had low or medium kinetochore staining levels, respectively (Figure 5.1B and Table 5.1). Notably, however, the effect of AZ3146 on Mad1 is certainly less severe than on Mad2, which had almost twice the number of cells with low levels of staining (Figure 5.1A). Therefore, it seems that Mps1 kinase activity is differentially required for Mad2 and Mad1 recruitment. One possible explanation for this difference is that Mad1 kinetochore localisation may require less Mps1 activity: perhaps any residual catalytic activity remaining after treatment with 2 μM AZ3146 is enough to recruit or maintain Mad1 at easily detectable levels in many

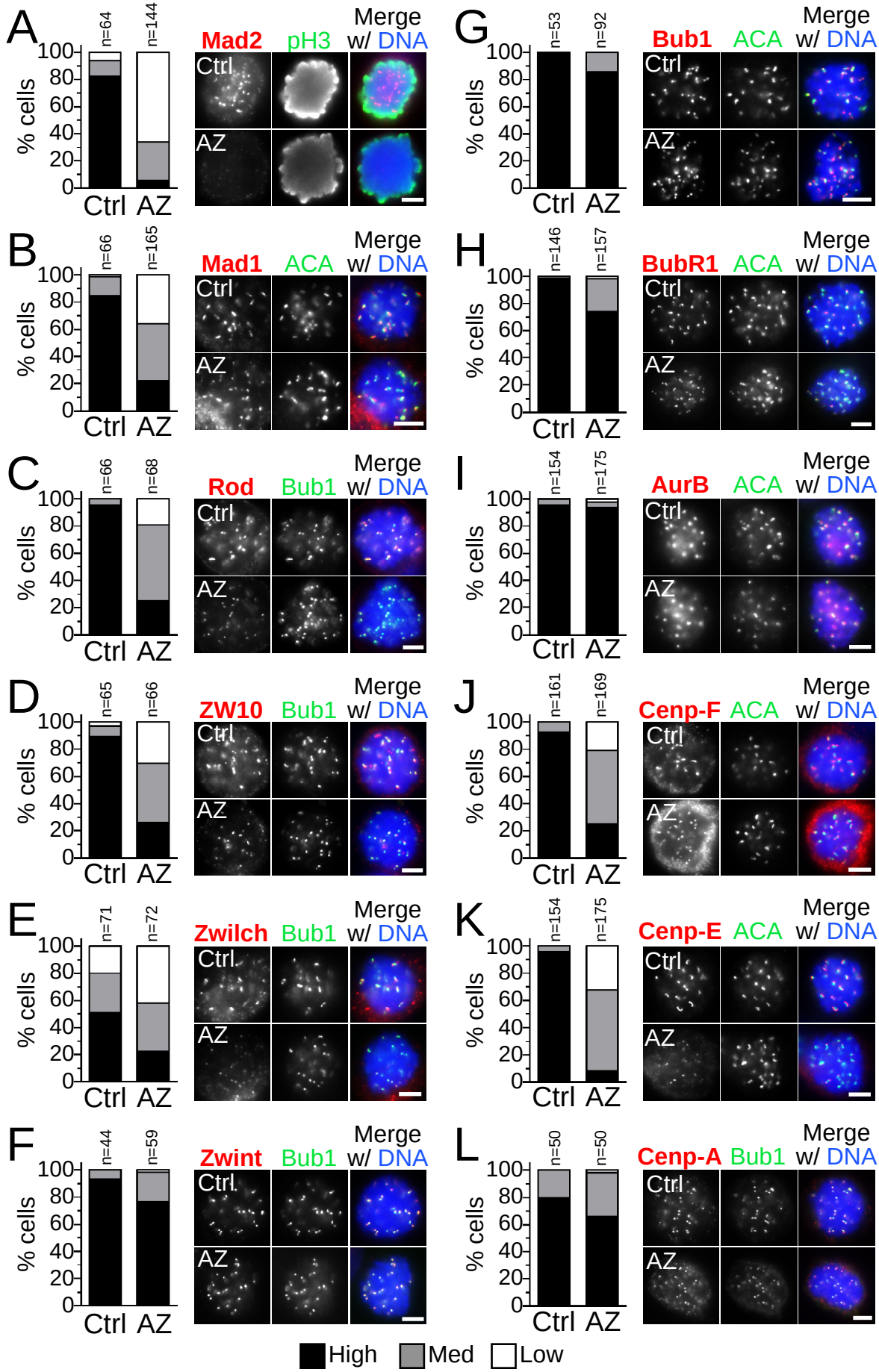

Figure 5.1 Localisation of kinetochore proteins after Mps1 inhibition with AZ3146
HeLa cells were treated with nocodazole, MG132 and DMSO or AZ3146 (2 µM), fixed after 2 h and processed for immunofluorescence. Kinetochore levels of the protein shown in red were assessed by eye and the results shown as bar graphs. Cells were co-stained with antibodies to phospho-histone H3 (pH3), Bub1, or anticentromere marker (ACA), shown in green. Representative images are shown for each protein. Values of *n* refer to number of cells counted per condition; datasets are combined from 2 experiements. Bars: 5 µm.

cells, but not sufficient for detectable Mad2 localisation. However, this may not be a complete explanation, since when higher molarities of AZ3146 are used, presumably minimising residual activity, there remains a difference between Mad2 and Mad1 kinetochore levels: almost all prometaphase cells treated with 4 μM and 8 μM AZ3146 have low levels of Mad2 staining at kinetochores (83% and 98% respectively, Figure 5.2A), whereas medium levels of Mad1 staining are observed in ~50% of cells under the same conditions (Figure 5.2B). In agreement with this variability in the population assessed in my assays, recent work carried out by A. Tighe suggests that inhibition of Mps1 activity can prevent Mad1's recruitment to unattached kinetochore, but has less effect on Mad1 if it has already been recruited prior to Mps1 inhibition (Hewitt et al., 2010). This may provide an explanation for the data presented here, since the cells in my assay are likely to be a mixture of mitotic cells that had already recruited Mad1 to prometaphase kinetochores, and those which were in prophase or metaphase and therefore had no Mad1 at the kinetochore at the time of drug treatment. Overall, my data provides evidence that, in mixed cell population, Mad1 localisation is clearly affected by AZ3146 treatment, but in some cells is less sensitive to loss of Mps1 activity than Mad2, likely because of the different mitotic stages at which Mps1 inhibition takes place.

After establishing the effect of AZ3146-meditated Mps1 inhibition on Mad1 and Mad2, I turned my attention to the RZZ complex. The RZZ complex (Rod, ZW10 and Zwilch) is found in the fibrous corona region, interacts with the outer kinetochore plate component Zwint, and is required for Mad1-Mad2 recruitment to the kinetochore (reviewed in Karess, 2005). After AZ3146 treatment, I observed a partial decrease in kinetochore staining for all three components of the RZZ complex (Figure 5.2C-E and Table 5.1). There are minor differences between the data for the three constituents of the complex, possibly due to differences in antibody sensitivity. Notably however, AZ3146's effect on the RZZ complex closely resembles its effect on Mad1 staining. This observation is corroborated by recently published work using the small molecule inhibitor Reversine, which implicates Mps1 activity in Zwilch recruitment (Santaguida et al., 2010). The decrease in RZZ staining cannot be explained by a fall in kinetochore-bound Zwint, since treatment with AZ3146 produced only a relatively small fraction of cells with notably decreased Zwint signal (Figure 5.1F and Table 5.1). Taken together, these data suggest a role for Mps1 kinase activity in the recruitment of Mad1-Mad2 via the RZZ complex.

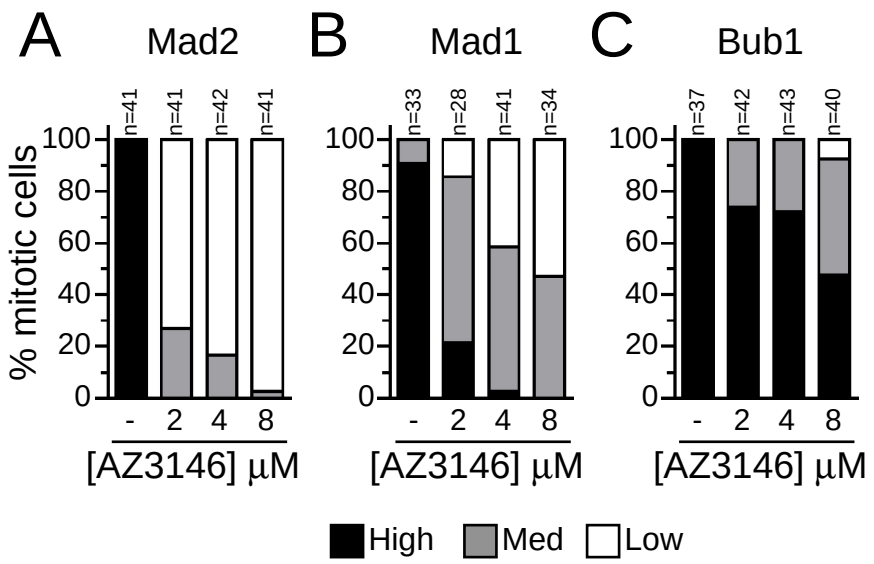

Figure 5.2 Levels of Mad2, Mad1, and Bub1 at kinetochores after treatment with higher concentrations of AZ3146

HeLa cells were treated simultaneously with nocodazole, MG132 and DMSO or AZ3146 (2 μM, 4 μM, or 8 μM), fixed after 2 h and processed for immunofluorescence. Kinetochore levels of the indicated protein were assessed by eye and the results shown as bar graphs. Values at the top of each bar refer to the number of cells counted for each drug concentration.

5.3 | Bub1, BubR1 and Aurora B are relatively unaffected by AZ3146-mediated Mps1 inhibition

There are some discrepancies in the literature regarding the requirement of Mps1 for the kinetochore localisation of Bub1 (Jelluma et al., 2008b; Liu et al., 2006; Martin-Lluesma et al., 2002; Santaguida et al., 2010; Sliedrecht et al., 2010; Tighe et al., 2008). When cells were treated with nocodazole, MG132 and 2 μM AZ3146, a small increase in the frequency of medium levels of kinetochore staining was observed (from 0% in the control population to 14% in AZ3146-treated cells). It should also be noted that many cells classified as having high levels exhibited a small reduction in Bub1 levels. In keeping with this, when pixel intensities were quantified by A. Tighe in identically treated cells, an average reduction of 25% was seen (Hewitt et al., 2010). This suggests Bub1 recruitment and/or maintenance at the kinetochore is largely unaffected by inhibition of Mps1 kinase activity. The relatively mild nature of the defect may be partly due to residual Mps1 activity in cells treated with 2 μM AZ3146: when the AZ3146 dosage is increased to 8 μM, 52.5% of cells had either low or medium Bub1 levels (Figure 5.2C). Overall however, the results presented here do not exclude a role for Mps1 catalytic activity in Bub1 localisation, but they suggest a comparatively minor role.

Like its role in Bub1 localisation, the role for Mps1 in BubR1 localisation has also been subject to debate (Jelluma et al., 2008b; Kang et al., 2007; Liu et al., 2006; Martin-Lluesma et al., 2002; Santaguida et al., 2010; Schmidt et al., 2005; Sliedrecht et al., 2010; Tighe et al., 2008). Several reports have suggested that perturbation of Mps1 kinase activity leads to a significant decrease in BubR1 kinetochore staining (Kang et al., 2007; Schmidt et al., 2005), however others have reported that the effect of inhibition on kinetochore-bound BubR1 is only marginal (Santaguida et al., 2010; Sliedrecht et al., 2010). When I analysed BubR1 levels in a population of 2 μM AZ3146-, nocodazole- and MG132-treated cells and compared them to control cells, I observed only a small fraction with significantly decreased, medium or low levels of BubR1 (26% compared to 1% in the control population, Figure 5.1H). As with Bub1, many cells appeared to have slightly reduced BubR1 staining, but were still within the range considered ‘high’. Whilst I cannot exclude the possibility that a more major defect may reveal itself at higher molarities of AZ3146, this data suggests at most a small, relatively minor role for Mps1 kinase activity in BubR1 recruitment and maintenance at kinetochores.

Aurora B localises to the centromere/kinetochore region at prometaphase, and its kinase activity is known to be required for the recruitment of several other kinetochore

components (Ditchfield et al., 2003; Hauf et al., 2003). Mps1 RNAi is reported to have very little effect on Aurora B's immunolocalisation pattern (Jelluma et al., 2008b; Tighe et al., 2008). When I analysed Aurora B staining following inhibition of Mps1 with AZ3146, I saw virtually no difference between the control and AZ3146-treated populations (Figure 5.1I). This data suggests that Mps1 kinase activity has no discernable role in recruitment or maintenance of Aurora B at the prometaphase centromere/kinetochore region, in agreement with published RNAi-based data.

5.4 | Cenp-F and Cenp-E are reduced at kinetochores after AZ3146 treatment

I also used my immunofluorescence-based assay to look at the localisation of Cenp-F, a component of the fibrous corona that is required for chromosome alignment (Holt et al., 2005; Yang et al., 2005). After AZ3146-treatment, the population of prometaphase-arrested cells exhibited noticeably lower levels of Cenp-F kinetochore staining than the control population (Figure 5.1J): 75% of cells analysed had medium or low levels. Mps1 knockdown by RNAi has been reported to have no effect on Cenp-F localisation (Liu et al., 2006), or cause a 35% reduction (Tighe et al., 2008); the data presented here is in broad agreement with the latter. This suggests Mps1 kinase activity has at least a partial role in recruitment and/or maintenance of Cenp-F at the kinetochore.

The role of Mps1 in Cenp-E kinetochore localisation is somewhat controversial. Work in the Xenopus egg extract model system implicates Mps1 kinase activity in Cenp-E kinetochore localisation (Abrieu et al., 2001), and Mps1 RNAi in HeLa cells is reported to cause improper Cenp-E localisation during mitosis (Fisk et al., 2003). However, several reports have concluded that Mps1 RNAi has no effect on Cenp-E immunolocalisation (Jelluma et al., 2008b; Martin-Lluesma et al., 2002; Tighe et al., 2008), and one recent report saw no effect on Cenp-E after inhibition of Mps1 kinase activity (Sliedrecht et al., 2010). In my assay, AZ3146-treatment clearly led to a reduction in Cenp-E staining at kinetochores: 92% of cells analysed had either medium or low levels (Figure 5.1K). Thus, in contrast to a previous report (Sliedrecht et al., 2010), these data suggest that Mps1 kinase activity contributes to Cenp-E kinetochore localisation in human cells. This might be mediated via Cenp-F, since Cenp-F has been shown to interact with Cenp-E and promote its kinetochore localisation (Chan et al., 1998; Johnson et al., 2004; Yang et al., 2005; Yao et al., 2000).

I also wanted to extend my analysis to a structural component of the inner kinetochore, so I analysed the effect of AZ3146 on the histone H3 homologue, and constitutive centromere-binding protein, Cenp-A (Cheeseman and Desai, 2008). AZ3146-

mediated Mps1 inhibition had no effect on the levels of Cenp-A staining in the majority of AZ3146-treated cells, where levels were classified as high (Figure 5.1L and Table 5.1). However, a small increase in cells with medium or low Cenp-A staining levels was observed (from 20% in controls to 34% in AZ3146-treated cells). This might indicate a small reduction in kinetochore levels in some cells. However, it is unlikely that a small decrease would cause problems with subsequent assembly of other kinetochore components, since Cenp-A is thought to be in excess at the human kinetochore (Liu et al., 2006). Whilst more detailed analysis would be required to fully confirm the presence of other structural kinetochore proteins, this data, along with the near-normal Zwint levels described earlier (Figure 5.1F), means I have no evidence to suggest underlying inner and outer kinetochore structure is perturbed by AZ3146.

Taken together, the data presented in the chapter so far show that AZ3146 treatment leads to kinetochore recruitment defects that could contribute to mitotic checkpoint malfunction (Chapter 4). Crucially, Mad2 appeared exquisitely sensitive to AZ3146 treatment; Mad1, while partially mislocalised, was less sensitive. The requirement for Mps1 activity in Mad1 localisation might be indirect, since I also observed a decrease in kinetochore levels of the RZZ complex. Cenp-E and Cenp-F staining levels were notably lower at kinetochores following AZ3146 treatment; interestingly, both of these proteins are involved in chromosome alignment, a process in which Mps1 is also implicated. Other components of the kinetochore (Bub1, BubR1, Aurora B, Cenp-A, Zwint) were largely unaffected by AZ3146 treatment.

5.5 | Mps1 accumulates at prometaphase kinetochores following AZ3146 treatment

Having established at AZ3146's effect on the above kinetochore components, I turned my attention to Mps1 itself. Mps1 localises to the kinetochore via its N-terminal domain (Liu et al., 2003; Stucke et al., 2004), and its interaction with the kinetochore is a dynamic one, with a half-life of recovery of 13 s (Howell et al., 2004). However, the mechanism by which this interaction is regulated remains elusive. I wanted to test the effect of loss of kinase activity on the kinetochore localisation of endogenous Mps1, so I used my indirect immunofluorescence assay to look at Mps1 localisation in nocodazole, MG132 and AZ3146-treated HeLa cells. In control cells, Mps1 staining is evident at the kinetochore region, but the signal is rather weak (Figure 5.3A, top panel). Strikingly, on addition of AZ3146, the signal increases markedly (Figure 5.3A, bottom panel). Quantification of pixel intensities revealed that Mps1 staining at the kinetochore increased 5-fold on average in AZ3146-treated cells, suggesting that Mps1's kinase activity

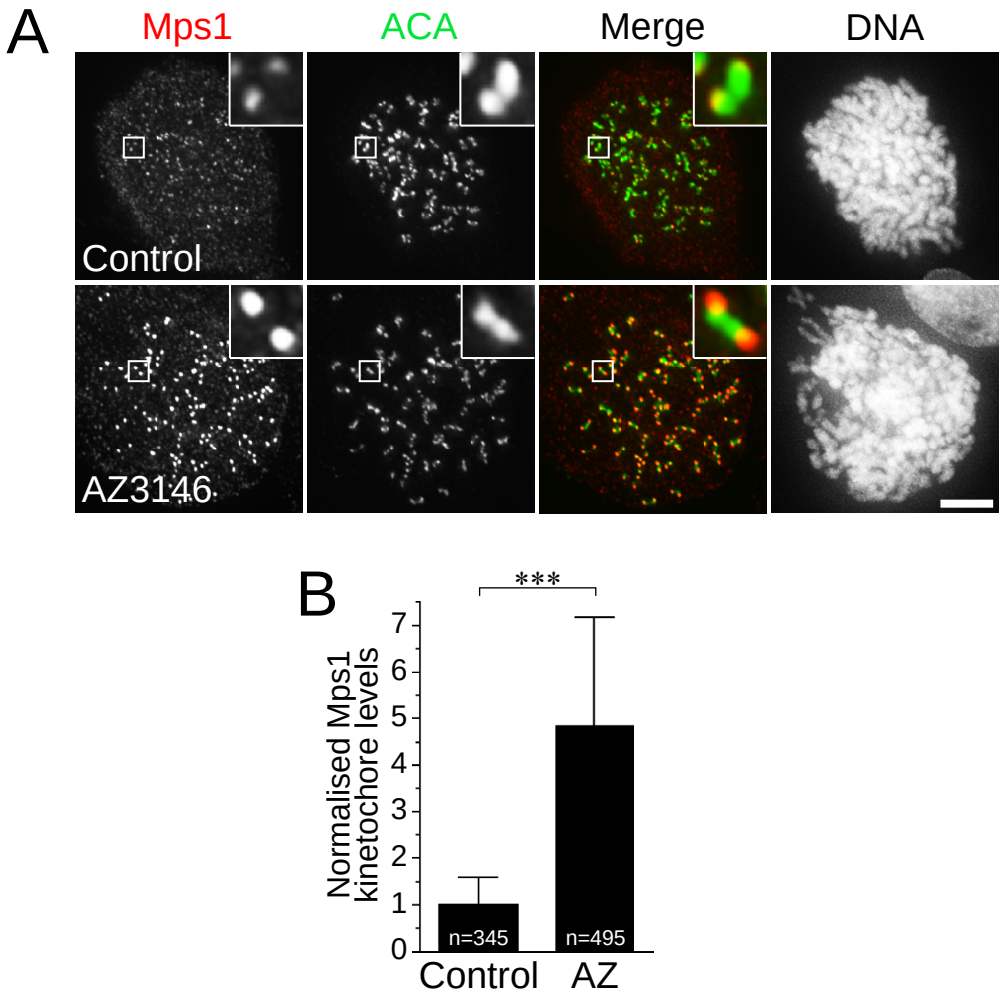

Figure 5.3 Endogenous Mps1 accumulates at kinetochores after AZ3146 treatment.
(**A**) HeLa cells were treated with either DMSO (Control) or 2 μM AZ3146 plus nocodazole and MG132 for 2 h, then processed for immunofluorescence with antibodies against Mps1 (red) and ACA (green). DNA was visualised with Hoechst staining. Representative examples of a control and AZ3146-treated cell are shown. Images are maximum intensity projections of deconvolved *z*-section stacks. Enlargements of boxed kinetochore pairs show enhanced Mps1 staining with AZ3146 treatment. Scale bar: 5 μm.
(**B**) Quantification of cells treated as in A. Mps1 pixel intensities at each kinetochore pair were quantified as a ratio to the ACA signal. The data shown in the bar graph is combined from 3 independent experiments, in which a total of 19 control cells or 18 AZ3146-treated cells were analysed. Numbers within bars refer to the total kinetochore pairs in dataset. Ratios were normalised to the mean control value for each experiment. Error bars represent the standard deviation. (***$P < 0.0001$, Mann-Whitney U-test.)

may be involved in regulating its localisation.

In the above experiments, I detected endogenous Mps1 using a polyclonal antibody raised against an N-terminal 242-amino acid fragment of Mps1 (Tighe et al., 2008). It is possible that the apparent accumulation I observed might be due to changes in the antibody's affinity for kinetochore-bound Mps1 caused by epitope unmasking, perhaps due to changes in phosphorylation. With this in mind, I set out to firmly establish whether the increase in signal seen in Figure 5.3 was indeed a consequence of raised levels of kinetochore-bound protein. For this, I used HeLa cells stably expressing tetracycline-inducible GFP-tagged wild type Mps1 (GFP-Mps1-WT, Tighe et al., 2008).

Firstly, I tested the propensity of GFP-Mps1-WT to accumulate after AZ3146 treatment. Levels of the exogenous kinase were detected by immunostaining with an anti-GFP antibody. In control cells, the kinetochore signal from GFP-Mps1^{WT} staining was often so low that it was virtually undetectable after deconvolution (see Figure 5.4A, top panel). Importantly, when cells were cultured with AZ3146, the anti-GFP signal increased, and was frequently readily detectable (Figure 5.4A, bottom panel). When quantified, an average ~2-fold increase in GFP-Mps1-WT kinetochore staining was observed (Figure 5.4B). As the standard deviation of the datasets indicates (error bars), there was wide variation in GFP-Mps1-WT levels in these experiments. This was largely due to variability in transgene expression levels from cell to cell, a characteristic of the HeLa stable cells lines being used (data not shown and A. Tighe, personal communication). In order to exclude any possibility that the ~2-fold increase observed in Figure 5.4B was due to sampling differences rather than a real trend towards higher GFP-Mps1-WT staining after AZ3146 treatment, I assessed the kinetochore levels of the control and treated cell populations by eye. As shown in Figure 5.4C, there was a clear shift towards brighter kinetochore staining when cell when AZ3146 was used. Thus, I was able to recapitulate the kinetochore accumulation of inhibitor-treated Mps1 with a second antibody against the GFP-tag of stably expressed wild-type Mps1, further supporting the idea that AZ3146-treatment leads to Mps1 accumulation at kinetochores.

As a second way of assessing the effect of AZ3146 on kinetochore levels of GFP-Mps1-WT, I turned to an antibody-free approach. GFP-Mps1-WT fluorescence was observed directly by standard fluorescence microscopy and levels assessed by eye. Control cells stably expressing GFP-Mps1-WT frequently had undetectable kinetochore levels, but in some cells, expression was high enough to allow visualisation of GFP-Mps1^{WT} at the kinetochore, and levels were classified as medium (Figure 5.4D, top panel). When cells were treated with AZ3146, cells frequently had intensely fluorescent

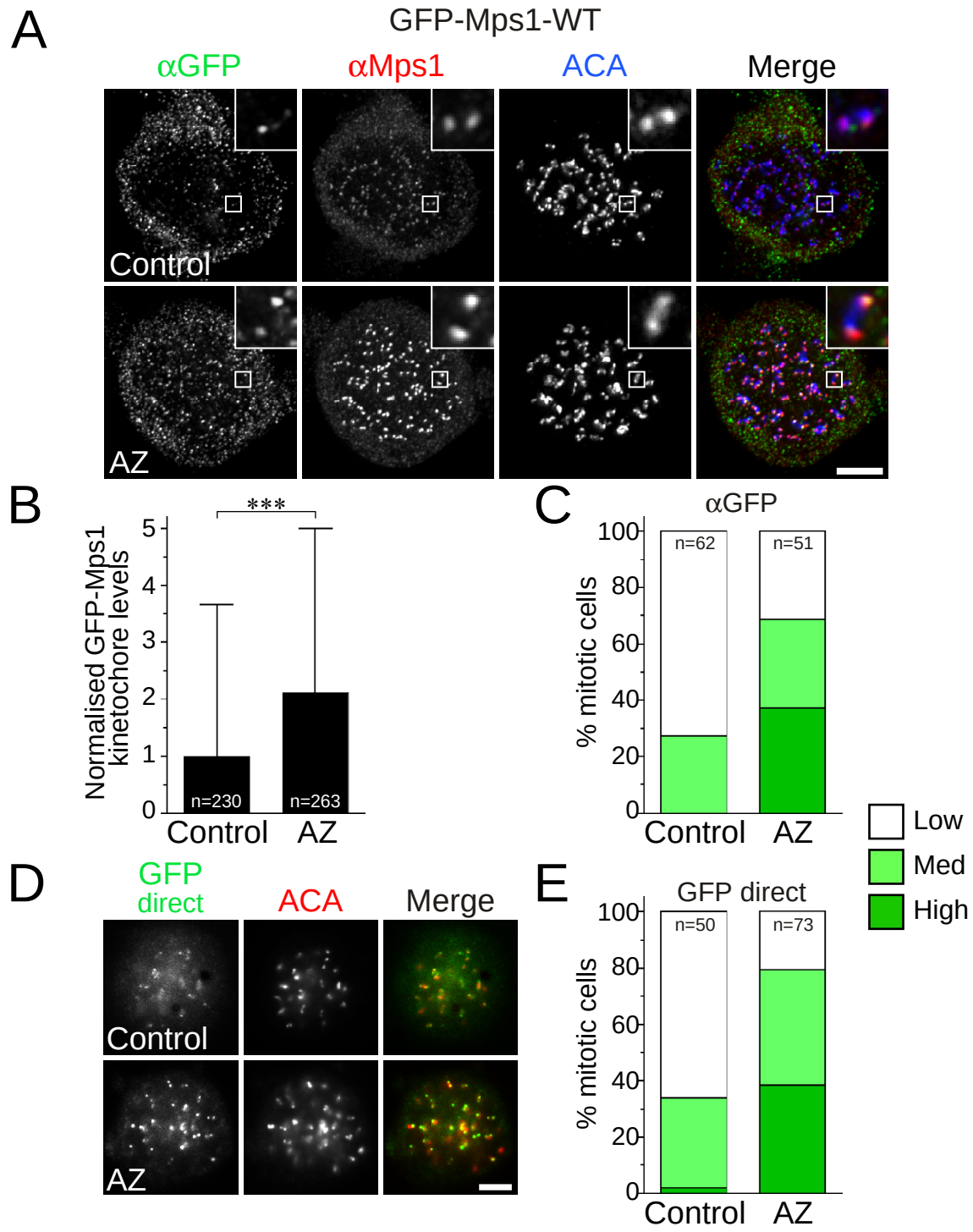

Figure 5.4 GFP-tagged wild-type Mps1 accumulates at kinetochores after AZ3146 treatment.
(**A**) HeLa cells expressing tet-inducible GFP-tagged wild-type Mps1 (GFP-Mps1-WT) were treated with either DMSO (Control) or 2 μM AZ3146 plus nocodazole and MG132 for 2 h, then processed for immunofluorescence with antibodies against GFP (green), Mps1 (red) and ACA (blue). Representative examples of a control and AZ3146-treated cell are shown. Images are maximum intensity projections of deconvolved *z*-section stacks. Enlargements of boxed kinetochore pairs show enhanced GFP and Mps1 staining with AZ3146 treatment. (**B**) Quantification of kinetochore GFP-Mps1-WT levels in cells treated as in A. GFP pixel intensities at each kinetochore pair were quantified as a ratio to the ACA signal. The data shown in the bar graph is combined from 3 independent experiments, in which a total of 19 control cells and 18 AZ-treated cells were analysed. Numbers within bars refer to the total kinetochore pairs in each dataset. Ratios were normalised to the mean control value in each experiment. Error bars represent the standard deviation. (***$P < 0.0001$, Mann-Whitney U-test.) (**C**) Levels of GFP-Mps1-WT were assessed by eye in the same cells described in A and B. Data from one of the three repeats is shown. Values within the bars refer to the number of cells counted. (**D**) GFP-Mps1-WT at kinetochores was visualised directly by virtue of GFP fluorescence, in cells treated as in A, but by standard fluorescence microscopy. Cells were co-stained with ACA (red). (**E**) Quantitation of GFP-Mps1-WT levels in cells treated and visualised as in D. Scale bars: 5 μm

points of GFP-Mps1-WT at the kinetochore, as in the example shown in Figure 5.4D (bottom panel), where levels were classed as high. There was a clear increase in the proportion of cells with either medium or high GFP-Mps1-WT levels at kinetochores after AZ3146 treatment (Figure 5.4E). Importantly, this confirms that the enhanced staining in Figure 5.3 and 5.4A-D is not caused by changes in antibody affinity, but by an increase in Mps1 protein levels at kinetochores following inhibition.

5.6 | Kinase-dead Mps1 accumulates at unattached kinetochores following AZ3146 treatment

In parallel with experiments to determine that wild type GFP-Mps1 was enriched at kinetochores, I also carried out the same experiments with cells expressing catalytically inactive, mutant GFP-Mps1 (GFP-Mps1-KD, Tighe et al., 2008). Originally, I hypothesised that the kinetochore localisation of the catalytically inactive kinase would not be enhanced on addition of the inhibitor, since the kinase is already inherently inactive. If lack of catalytic activity caused the kinetochore accumulation observed in Figure 5.3 and 5.4, the GFP-Mps1-KD would already be maximally enriched at kinetochores before inhibitor treatment. However, like GFP-Mps1-WT, GFP-Mps1-KD was frequently virtually undetectable when stained with an anti-GFP antibody in control cells (Figure 5.5A, top panel). Furthermore, when cells were treated with AZ3146, the anti-GFP signal at the kinetochores became substantially higher than in control cells, with GFP-Mps1-KD now readily visible (Figure 5.5A, bottom panel). Quantification of the GFP signal showed an average ~5-fold increase at the kinetochore following AZ3146 treatment (Figure 5.5B), though levels were once again highly variable due to cell to cell expression level differences. As with GFP-Mps1-WT, I was able to confirm the increase in kinetochore bound GFP-Mps1-KD by analysis of a larger sample of cells from the two populations by eye (Figure 5.5C). Contrary to my original hypothesis, these data indicate that, like GFP-Mps1-WT, GFP-Mps1-KD accumulates at prometaphase kinetochores after AZ3146 treatment.

One possible explanation for this observation is that the kinetochore accumulation of Mps1 is not dependent on the intrinsic activity of a single molecule, but instead on the level of Mps1 activity in the cell. Thus, in the presence of endogenous Mps1 activity, GFP-Mps1-KD remains at a low level at the kinetochore, and only accumulates following AZ3146 treatment, presumably because it can no longer interact with active endogenous Mps1. To further confirm this effect, I turned to an RNAi complementation approach, in which I repressed endogenous Mps1 with shRNA, and induced expression of RNAi-

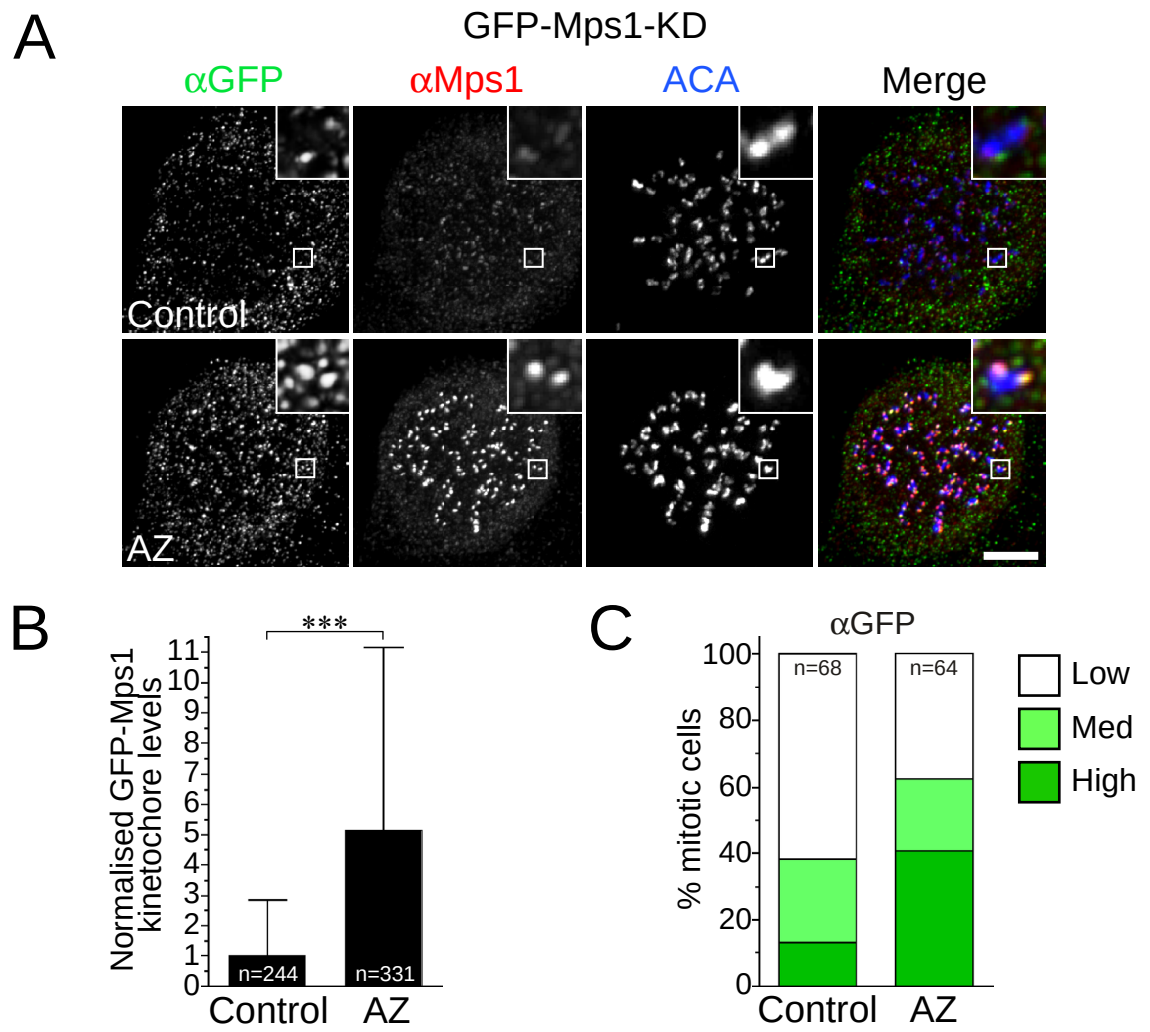

Figure 5.5 GFP-tagged kinase-dead Mps1 accumulates at kinetochores after AZ3146 treatment.
(**A**) HeLa cells expressing tet-inducible GFP-tagged kinase-dead Mps1 (GFP-Mps1-KD) were treated with either DMSO (Control) or 2 μM AZ3146 plus nocodazole and MG132 for 2 h, then processed for immunofluorescence with antibodies against GFP (green), Mps1 (red) and ACA (blue). Representative examples of a control and AZ3146-treated cell are shown. Images are maximum intensity projections of deconvolved *z*-section stacks. Enlargements of boxed kinetochore pairs show enhanced GFP and Mps1 staining with AZ3146 treatment. Scale bar: 5 μm (**B**) Quantification of kinetochore GFP-Mps1-KD levels in cells treated as in A. GFP pixel intensities at each kinetochore pair were quantified as a ratio to the ACA signal. The data shown in the bar graph is combined from 3 independent experiments, in which a total of 17 control cells and 16 AZ-treated cells were analysed. Numbers within bars refer to the total kinetochore pairs in dataset. Ratios were normalised to the mean control value in each experiment. Error bars represent the standard deviation. (***$P < 0.0001$, Mann-Whitney U-test.) (**C**) Levels of GFP-Mps1-KD were assessed by eye in the same cells described in A and B. Data from one of the three repeats is shown. Values within the bars refer to the number of cells counted.

resistant GFP-Mps1-WT or GFP-Mps1-KD (Tighe et al., 2008). Western blots (Figure 5.6A) confirmed that transfection with shRNA targeting Mps1 caused a fall in endogenous protein levels, whilst levels of resistant GFP-Mps1 were unaffected. When cells transfected with control shRNA were treated with nocodazole and MG132, staining with an anti-GFP antibody revealed virtually undetectable kinetochore levels of both WT and KD GFP-Mps1 (data not shown), in agreement with data from control cells in Figures 5.4 and 5.5. Following repression of endogenous Mps1, GFP-Mps1-WT levels at kinetochores remained very low; although the GFP-tagged form was now predominant in the cells, accumulation did not occur. Importantly however, GFP-Mps1-KD levels increased markedly in shRNA-transfected cells (Figure 5.6B, C). Quantification of anti-GFP pixel intensities indicated an ~8.5 fold increase in kinetochore-bound GFP-Mps1-KD on average (Figure 5.6C). Again, the datasets had high levels of variability, but additional qualitative analysis of kinetochore GFP levels in each cell population showed a clear increase in the proportion of cells with high levels in Mps1-depleted, GFP-Mps1-KD expressing cells. Taken together, this data confirms that decreasing cellular levels of Mps1 catalytic activity leads to its accumulation at the kinetochore, and since kinase dead Mps1 only accumulates markedly following Mps1 shRNA, hints at the importance of inter-molecular interactions in regulating Mps1 localisation.

5.7 | Summary

To summarise, the data in this chapter provide evidence that AZ3146 treatment affects the localisation of kinetochore proteins essential for mitotic checkpoint function (Mad2, Mad1, RZZ complex). Conversely, I also show that the levels of Mps1 itself increase markedly at kinetochores after ablation of the kinase's activity: this novel observation may reflect an important aspect of the mechanism by which Mps1 inhibition causes mitotic checkpoint override.

AZ3146 treatment also leads to an apparent decrease in kinetochore levels of proteins with a role in chromosome alignment (Cenp-E and Cenp-F). The effect of AZ3146 treatment on this aspect of Mps1 function will be explored further in Chapter 6.

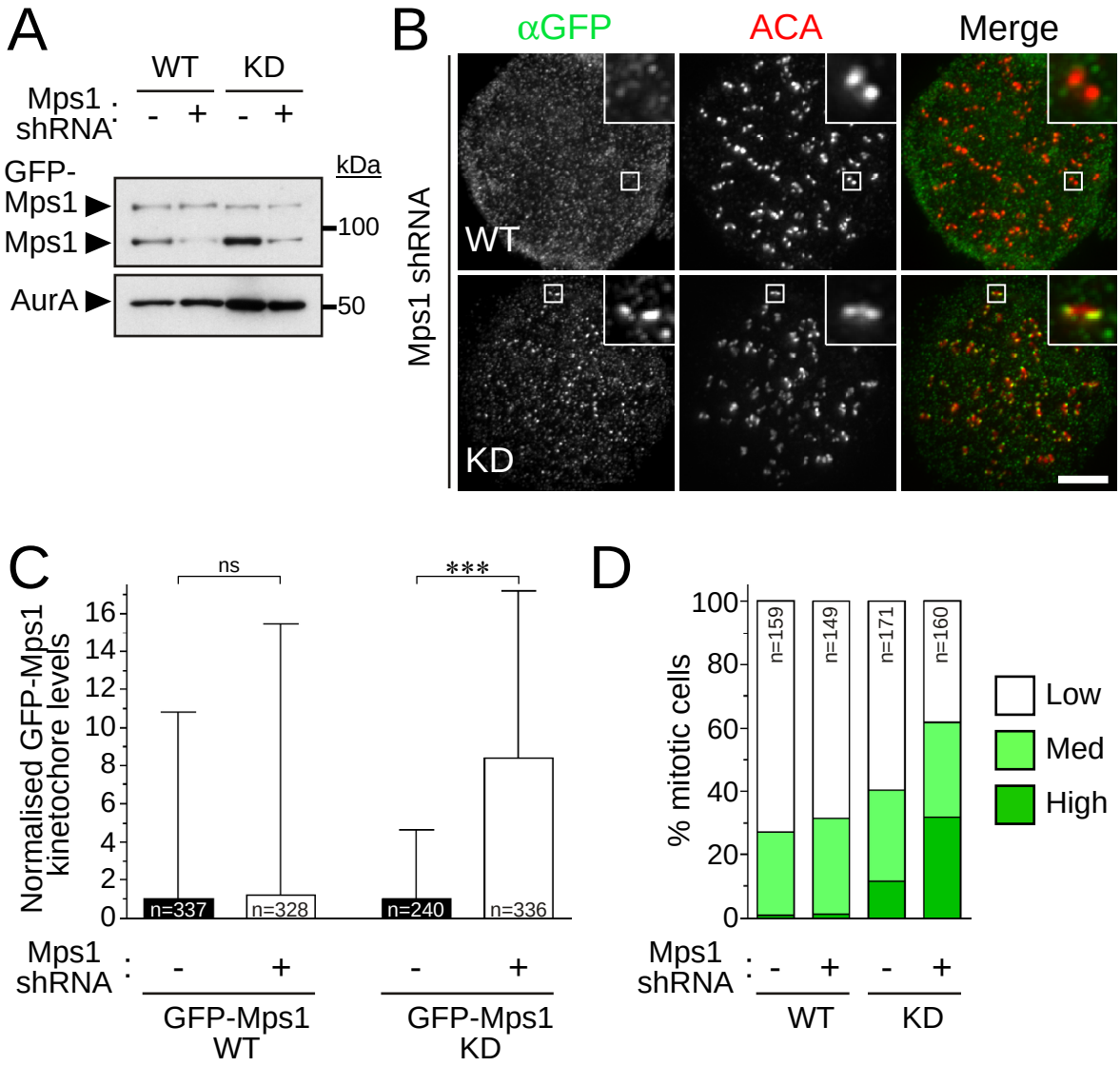

Figure 5.6 Kinase-dead GFP-Mps1 accumulates at kinetochores after depletion of endogenous Mps1
(**A**) HeLa cells stably expressing tet-inducible RNAi-resistant GFP-Mps1 wild-type (WT) or kinase-dead (KD) were transfected with plasmids encoding shRNA targetting Mps1, or a control plasmid. Samples were processed for western blot and probed with antibodies against Mps1 (top panel) or Aurora A (bottom panel) as a loading control. (**B**) After endogenous Mps1 depletion and induction of GFP-Mps1 expression as in A, cells were treated with nocodazole and MG132 for 2 hours. Cells were then fixed and processed for immunofluorescence, staining with antibodies against GFP (green) and ACA (red). In each cell analysed, shRNA/control plasmid transfection was confirmed by expression of co-transfected DsRed-histone H2B (not shown). Representative examples of cells lacking endogenous Mps1, but expressing either wild-type or kinase-dead GFP-Mps1 are shown. Note the enhanced kinetochore localisation of GFP-Mps1-KD. Scale bar: 5 µm. (**C**) Quantification of kinetochore GFP-Mps1 levels in cells treated as in B. GFP pixel intensities at each kinetochore pair were quantified as a ratio to the ACA signal. The data shown in the bar graph is combined from 3 independent experiments, in which at least 16 cells were analysed for each condition. Numbers within bars refer to the total kinetochore pairs in the dataset. WT and KD ratios were normalised to their respective mean control value in each experiment. Error bars represent the standard deviation. (***$P <$ 0.0001, Mann-Whitney U-test) (**D**) Levels of GFP-Mps1 WT and KD were assessed by eye in the same cells described in B and C. Values within the bars refer to the number of cells counted.

6 | *Results Chapter IV:* Inhibition of Mps1 perturbs chromosome alignment by inducing mislocalisation of Cenp-E

6.1 | Introduction

Over the last few years, a dual role for Mps1 in mitosis has emerged. Not only does it promote mitotic checkpoint signalling to delay anaphase until the appropriate time, but it also functions in the mechanics of chromosome alignment. Some reports have found that Mps1's role in chromosome alignment is mediated via phosphorylation of Borealin, a member of the chromosomal passenger complex (Jelluma et al., 2008b; Sliedrecht et al., 2010). This phosphorylation is said to be required for full activation of Aurora B, which itself has a well-documented role in error correction, promoting the destabilisation of erroneous kinetochore-microtubule attachments (reviewed in Ruchaud et al., 2007). In addition, some of the observations documented in the previous chapter, namely Cenp-E and Cenp-F reduction, hinted at possible alternative ways in which Mps1 could influence alignment by its effect on the mitotic kinetochore. The work described in this chapter focuses on the effect of AZ3146 on the mechanics of chromosome alignment, and the relationship between Mps1 and Aurora B.

6.2 | Mps1 inhibition leads to alignment problems after enrichment for errors

In order to detect problems with alignment, I treated cells with the proteasome inhibitor MG132. Assays I have used in the previous chapters could not distinguish this type of defect, since either a spindle toxin was present, or premature mitotic exit was induced due to checkpoint malfunction. By blocking proteolysis, MG132 prevents anaphase onset downstream of spindle checkpoint inactivation. In normal cells, chromosomes will align, forming a metaphase plate, but chromatids will not separate. If AZ3146-treated cells have problems with alignment, this will manifest as an inability to form a fully aligned metaphase plate, despite the extended time in mitosis afforded by MG132 treatment. I assessed alignment in MG132-treated cell populations by fixing cells, staining to visualise DNA, kinetochores and the mitotic spindle to allow classification of cells according to their stage of mitosis (prophase, prometaphase, metaphase, or anaphase). A cell with one or more unaligned chromosomes was classified as being in prometaphase. When I treated either HeLa cells or DLD1 cells with MG132 (Figure 6.1A), a large proportion of control cells reached a fully aligned metaphase (39% of HeLa cells and 68% of DLD1s). Surprisingly, this did not significantly decrease when cells were treated with

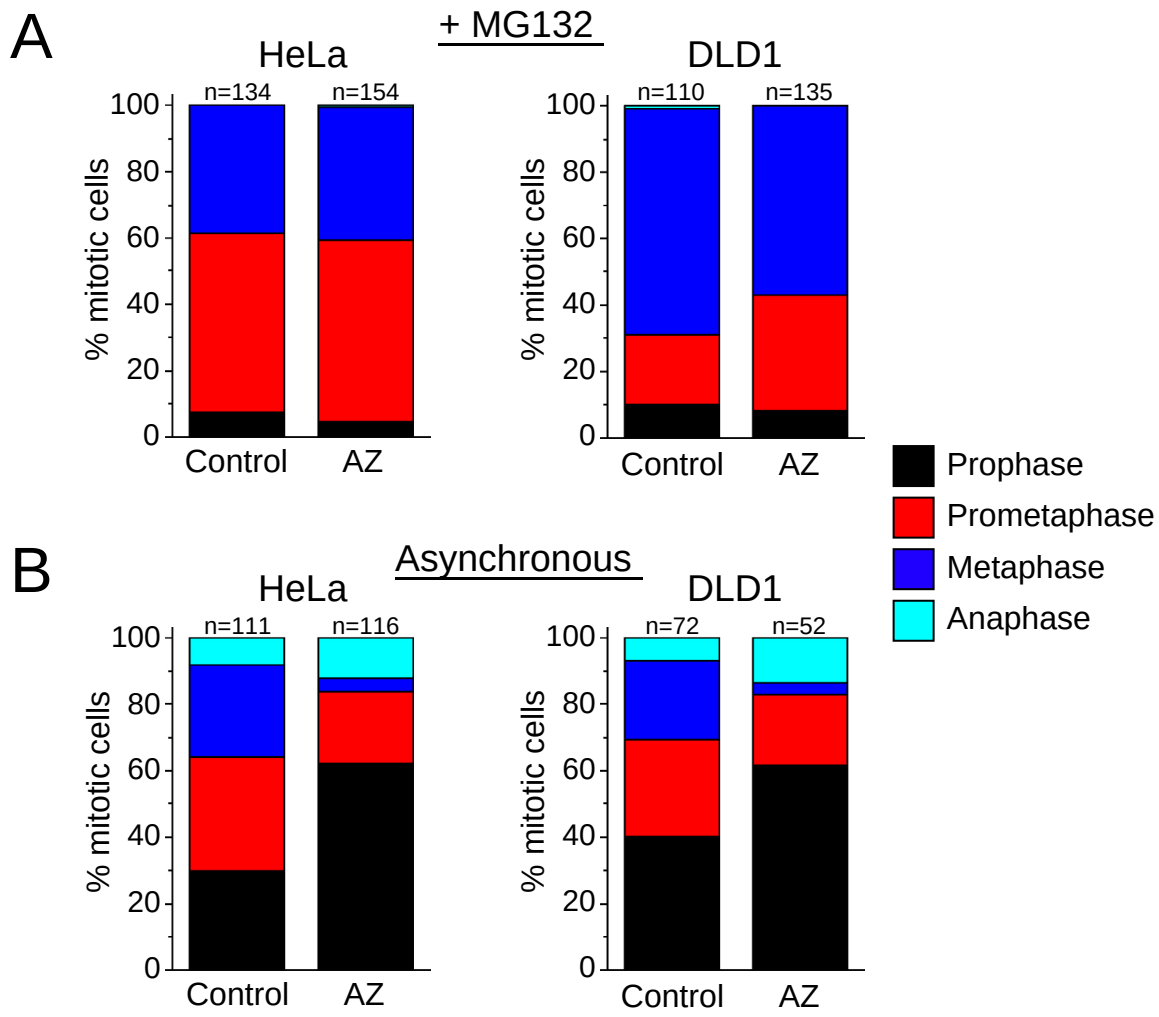

Figure 6.1 Inhibition of Mps1 does not affect alignment in an unperturbed prometaphase
(**A**) HeLa and DLD1 cells were treated with DMSO (Control) or 2 μM AZ3146 for 2 hours, and then fixed and stained. The mitotic population was classified according to the phase of mitosis, and the results are represented in bar graphs. Note the decreased proportion of metaphase cells in when cells are treated with AZ3146. HeLa data is combined from 2 independent experiments.
(**B**) HeLa and DLD1 cells were treated with MG132 and DMSO (Control) or 2 μM AZ3146 for 2 hours, fixed, analysed and represented as in A.

MG132 and AZ3146: 40% of HeLa cells and 57% of DLD1s had aligned all chromosomes. Though an alignment defect did not appear to manifest under these conditions, Mps1 was inhibited in these cells: the mitotic checkpoint was compromised, as shown by analysis of the mitotic population of asynchronous cells (Figure 6.1B). In both cell types, the proportion of cells in metaphase or prometaphase decreased, indicating cells rarely achieved alignment and were accelerated through prometaphase, as predicted following Mps1 inhibition.

The lack of alignment defect observed after Mps1 inhibition was somewhat surprising. To see if Mps1 activity really was entirely dispensable for alignment, I used a monastrol wash-out approach to enrich for erroneous attachments (Kapoor et al., 2000; Mayer et al., 1999). When spindle pole separation is prevented using monastrol, kinetochore pairs frequently become attached to the same spindle pole (syntelic attachment). Monastrol can be efficiently washed out of cells, allowing spindle pole separation and correction of the erroneous attachments so that alignment can be achieved (Kapoor et al., 2000). The mechanism of alignment after monastrol wash-out has been dissected (see Figure 1.6): Aurora B activity mediates the first steps towards alignment by promoting K-fibre disassembly, moving the chromosome polewards (Lampson et al., 2004). Mono-oriented chromosomes can then congress from the polar region towards the spindle equator via the action of the plus-end directed kinesin Cenp-E, and in doing so, increase their chances of becoming bioriented (Kapoor et al., 2006). To detect any problems in this process following Mps1 inhibition, HeLa cells were released from monastrol into MG132 with or without AZ3146, then fixed and stained to allow classification of the mitotic population. Cells were also released into ZM447439 and MG132 to provide examples of the phenotype induced by direct Aurora B inhibition. Ninety minutes after monastrol removal, the majority of control cells had formed a bipolar spindle and a fully aligned metaphase plate (65.1%; Figure 6.2A, B). By contrast, 96.9% of cells released into ZM447439 were still in prometaphase with many misaligned chromosomes spread along the spindle. Strikingly, AZ3146-treated cells also rarely achieved alignment: 85.9% of mitotic cells remained in prometaphase, sometimes with numerous unaligned chromosomes in the polar region (e.g. Figure 6.2A, 'AZ major') and sometimes with just a few unaligned chromosomes (e.g. 'AZ minor'). Thus, though 2 μM AZ3146 does not elicit an alignment defect in cells treated with MG132 alone (Figure 6.1), this level of Mps1 inhibition does lead to an alignment defect in the presence of an artificially high number of incorrect attachments. There are several possible explanations for the emergence of the alignment defect following monastrol treatment. Perhaps residual Mps1 activity in cells treated with 2 μM AZ3146 is enough to ensure alignment of any

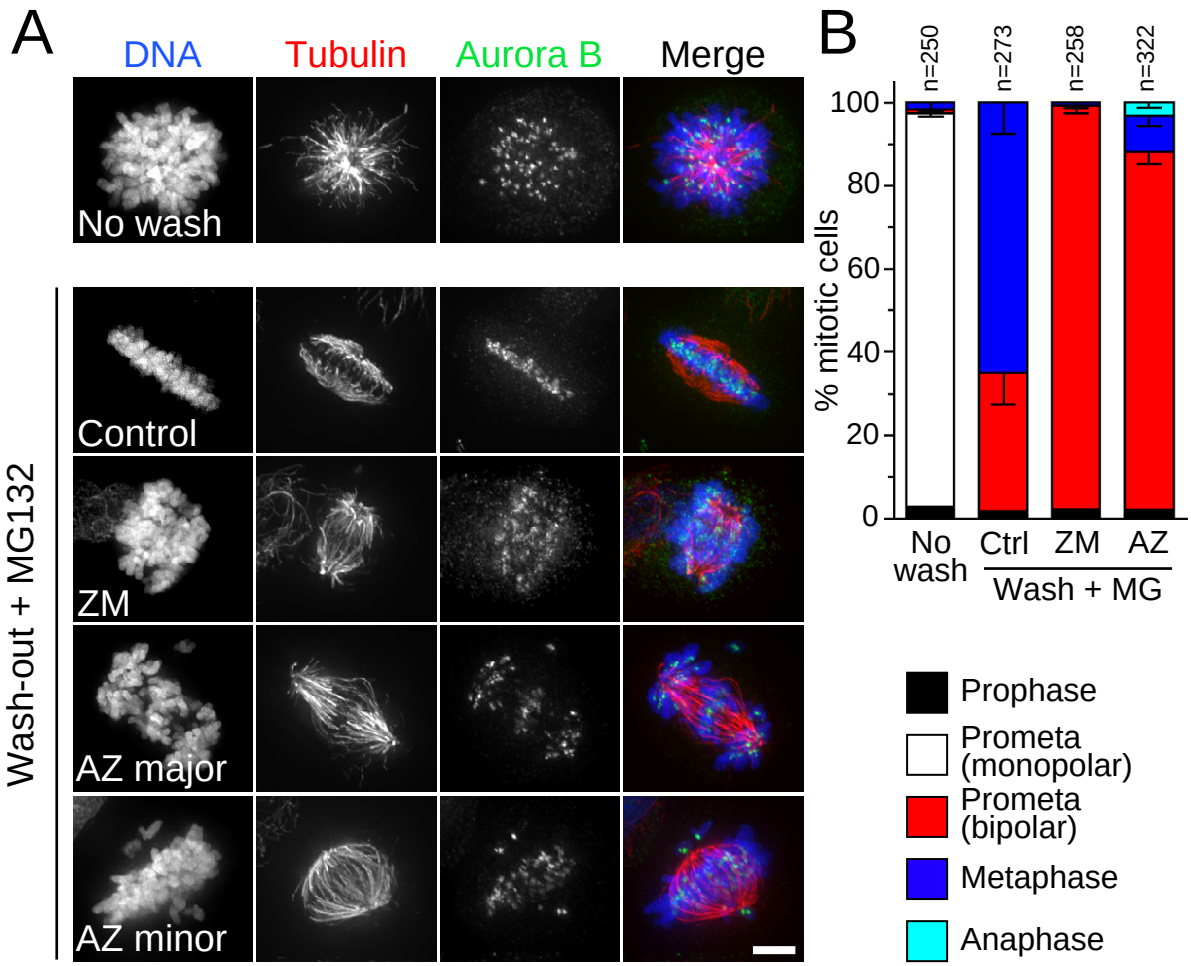

Figure 6.2 Inhibition of Mps1 perturbs alignment after enrichment for errors by monastrol wash-out
(**A**) HeLa cells were treated with monastrol for 4 hours, then the monastrol was removed by washing and cells were incubated with media containing MG132 to arrest cells at metaphase, and either DMSO (Control), AZ3146 or ZM447439 (both at 2 μM) for 90 minutes. Some cells remained in monastrol for the duration of the experiment ("No wash"). Cells were fixed, stained to detect DNA and with antibodies against α-tubulin (TAT1; red) to visualise the spindle and Aurora B to mark centromeres (green). Representative images are shown for each treatment; two examples of AZ3146-treated cells are shown to refect the varying severity of the misalignments observed. Images are maximum intensity projections of deconvolved *z*-section stacks. Scale bar: 5 μm.
(**B**) Mitotic cells were treated as in A were classified according to their phase of mitosis, and the results are shown as a bar graph. Cells with any number of unaligned chromosomes were called prometaphase cells. Data shown reflects the mean derived from 3 independent experiments, error bars show the standard deviation. Values of *n* refer to the total number of cells classified per treatment. Note that while most control cells achieve full alignment after monastrol wash-out (metaphase), cells treated with AZ3146 or ZM447439 still exhibit unaligned chromosomes (prometaphase).

erroneous attachments in an unperturbed metaphase, though insufficient to support full mitotic checkpoint function (Figure 6.1). It is also possible that in the cells I used, during a normal prometaphase where the spindle poles are allowed to move apart normally, so few erroneous attachments actually occur that Mps1 activity may not be required at all. Arrest with a monopolar spindle may be required to increase the number of mono-oriented chromosomes in order for the defect to become visible. Whatever the explanation, it is clear that AZ3146-mediated Mps1 inhibition does indeed compromise the alignment process, as previously reported (Jelluma et al., 2008b; Sliedrecht et al., 2010).

6.3 | Aurora B activity remains high after Mps1 inhibition

The alignment defect exhibited after loss of Mps1 activity was previously explained by decreased Aurora B activity (Jelluma et al., 2008b; Sliedrecht et al., 2010). With this in mind, I set out to see if I could detect Aurora B inhibition in AZ3146-treated cells. My first strategy was to treat nocodazole-arrested HeLa cells with AZ3146 or ZM447439, along with MG132 to prevent mitotic exit, then harvest cells and probe the lysates with phospho-specific antibodies against markers of global Aurora B activity, namely the autoactivation site Thr232 (Yasui et al., 2004) and the endogenous Aurora B substrate Ser10 of Histone H3 (Fischle et al., 2005; Hirota et al., 2005). To look at phospho-Thr232, I used a phospho-antibody with reactivity against the phosphorylated autoactivation residue of Aurora A, B and C. In control lysates, the antibodies recognised bands at the expected sizes for both phospho-Thr232 Aurora B and phospho-Ser10 Histone H3 (Figure 6.3A). Direct inhibition of Aurora B with ZM447439 abolished the phospho-T232 signal, and significantly reduced the phospho-Ser10 Histone H3 signal. However, AZ3146 did not noticeably affect the signal from either phospho-antibody, even at the highest concentration tested (10 μM). Although this data not absolutely conclusive, Figure 6.3A suggests that under these conditions, Mps1 inhibition does not significantly affect Aurora B autoactivation or Ser10 Histone H3 phosphorylation in cells.

To extend my analysis of Aurora B activity in cells with inhibited Mps1, I turned to an immunofluorescence-based approach, which allowed me to look specifically at mitotic cells in an asynchronous population. Again, I used reactivity of an antibody against phosphorylated Histone H3 as a read-out of Aurora B activity in asynchronous HeLa cells treated with either only ZM447439 or AZ3146. As expected, prometaphase cells stained brightly for phospho-Histone H3 around the condensed chromatin (Figure 6.3B); ZM447439 effectively abolished this staining. By contrast, prometaphase cells treated with AZ3146 still had high levels of phospho-Histone H3 staining, suggestive of comparatively high levels of Aurora B activity. I also looked at the localisation of the

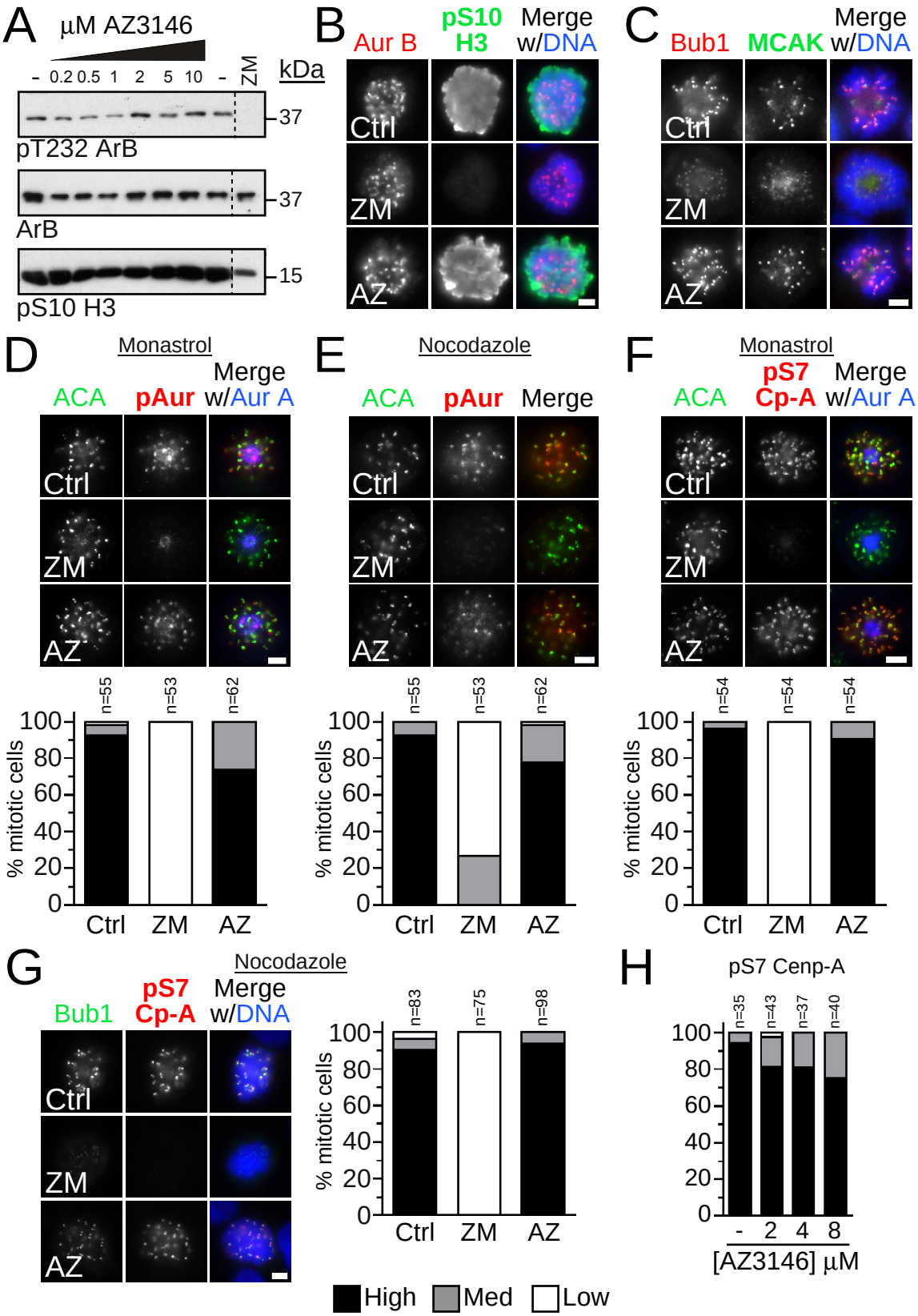

Figure 6.3 Aurora B does not appear significantly inhibited following AZ3146 treatment.
(**A**) HeLa cells were treated with nocodazole for 14 h, then with nocodazole, MG132 plus the indicated concentrations of AZ3146, ZM447439 (5 μM) or DMSO (control) for 2 h. Cells were harvested, lysed in SDS-PAGE sample buffer and processed for western blotting. A phospho-Aurora A/B/C antibody was used but only the pT232 Aur B band is shown. The dotted line indicates an excised lane. (**B,C**) HeLas were treated with AZ or ZM alone (both 2 μM) for 2 h. Cells were fixed and stained to visualise DNA, and the indicated proteins by IF. (**D-G**) HeLas were treated with monastrol (D and F) or nocodazole (E and G) along with MG132 and either AZ3146 or ZM447439 (both 2 μM) for 2 h. Cells were fixed and processed for IF using the indicated antibodies. Kinetochore/centromere levels of phospho-Aurora (D,E) or phospho-Ser7 Cenp-A staining (F,G) were assessed by eye and the data shown as bar graphs, along with representative images. (**H**) HeLa cells were treated as in G, but various concentrations of AZ3146 were used. Values of *n* refer to cells counted in each dataset. Scale bars: 5 μm.

microtubule-depolymerising kinesin MCAK in the centromere/kinetochore region as a read-out for Aurora B activity in prometaphase cells (Andrews et al., 2004; Lan et al., 2004): as shown in Figure 6.3C, while centromeric MCAK staining was much reduced after ZM447439 treatment, AZ3146 had no discernable effect, implying the cells had sufficient Aurora B activity to support recruitment of the kinesin.

Although the western blot shown in Figure 6.3A did not show a global decrease in phospho-Thr232 Aurora B signal following AZ3146 treatment, it could be argued that the western blot analysis might lack the sensitivity to detect changes in Aurora B activation at the centromere. To address this, I used the Aurora autoactivation residue phospho-antibody described above to stain fixed HeLa cells for immunofluorescence. This antibody detects phospho-Thr232 Aurora B at the centromere, as well as the active forms of the other Aurora family members. Cells were arrested in prometaphase, either with normal microtubule dynamics but erroneous, unstable kinetochore-microtubule attachments (monastrol) or with depolymerised microtubules and unattached kinetochores (nocodazole). Levels of centromeric staining were assessed by eye as previously described (Chapter 5). In both monastrol (Figure 6.3D) and nocodazole (Figure 6.3E), the majority of control cells exhibited high levels of staining in the centromeric region, reflecting the expected localisation of active, phospho-Thr232 Aurora B. As predicted, most ZM447439-treated cells had low levels of centromeric staining in both monastrol and nocodazole, pointing to loss of phospho-Thr232 and inactivation of Aurora B. By contrast, the majority of AZ3146-treated cells had high levels of centromeric phospho-Aurora staining, suggesting Aurora B was phosphorylated at Thr232 and therefore active. It is worth noting that I cannot rule out the contribution of phospho-Thr198 on Aurora C to the centromeric staining pattern: while the lesser-studied Aurora family member is usually associated with male meiosis (e.g. Tang et al., 2006), it is also expressed in several human cancer cell lines derived from different tissues, including HeLa cells (Kimura et al., 1999) and is reported to localise to centromeres (Li et al., 2004; Sasai et al., 2004). However, I saw little effect on the centromeric phospho-threonine pattern after AZ3146 treatment.

I also carried out a similar analysis using another read-out of Aurora B activity at the centromere: phosphorylation of the Ser7 of the Histone H3 variant, Cenp-A (Zeitlin et al., 2001). In monastrol (Figure 6.3F) and nocodazole (Figure 6.3G), brightly stained kinetochores were evident in control cells; this staining largely disappeared on treatment with ZM447439, but was still present at high levels in cells treated with AZ3146. In keeping with the data presented above, this suggests Aurora B is relatively active at centromeres when Mps1 is inhibited.

Taken together, the data in Figure 6.3 suggest that, contrary to previous reports (Jelluma et al., 2008b; Kwiatkowski et al., 2010; Sliedrecht et al., 2010), Aurora B activity remains relatively high after Mps1 inhibition. One possible explanation for this is that residual Mps1 activity in cells treated with 2 μM AZ3146 is enough to promote sufficient Borealin phosphorylation which, in turn, supports relatively normal levels of Aurora B catalytic activity towards the substrates I looked at. However, phospho-Ser7 Cenp-A levels at kinetochores were still high in most nocodazole-treated HeLa cells at concentrations of AZ3146 up to 8 μM (Figure 6.3H), and phospho-Thr232 Aurora B levels by western blot remain high in nocodazole-treated cells at 10 μM AZ3146 (Figure 6.3A). While I have not been able to look directly at the phosphorylation of Borealin itself, and cannot rule out effects on specific Aurora B substrates that I have not examined, I have no evidence to suggest Aurora B's kinase activity is decreased after Mps1 inhibition.

6.4 | Aurora B inhibition affects Mps1 phosphorylation in cells and its kinetochore localisation

To extend my investigations into the relationship between Mps1 and Aurora B, I used Phos-tag gels to look at the phosphorylation status of both kinases in nocodazole-arrested mitotic HeLa cells following treatment with AZ3146 and ZM447439. Both Mps1 and Aurora B appeared as a ladder of multiple bands after immunoblotting of mitotic samples run on Phos-tag gel, likely representing differentially phosphorylated forms (Figure 6.4A). As previously described in Chapter 3 (Figure 3.5), treatment of mitotic cells with the Mps1 inhibitor AZ3146 led to the loss of the slowest-mobility band on the Mps1 blot (compare lanes 2 and 3); most Mps1 migrates as a major, faster-mobility band in samples treated with AZ3146, which suggests a decrease in phosphorylation. Similarly, treatment with the Aurora B inhibitor ZM447439 led to a marked decrease in intensity of the two slowest-mobility Aurora B bands (compare lanes 2 and 4), leaving the majority of protein as two faster-migrating bands, and suggesting the kinase becomes dephosphorylated following direct inhibition. AZ3146 had little effect on the Aurora B banding pattern (lane 3), which agrees with data presented above (Figure 6.3A) and supports the notion that Aurora B activity remains high after Mps1 inhibition.

Surprisingly, direct inhibition of Aurora B caused a clear loss of the uppermost Mps1 band; this suggests Aurora B inhibition affects the phosphorylation of Mps1 in cells (Figure 6.4A, lane 4). It is not possible to determine whether Aurora B itself influences Mps1 phosphorylation directly or indirectly from this data; however, it strongly suggests that Aurora B is positioned upstream from Mps1 in a mitotic signalling cascade. Furthermore, while Aurora B's localisation in nocodazole-treated cells is unaffected by

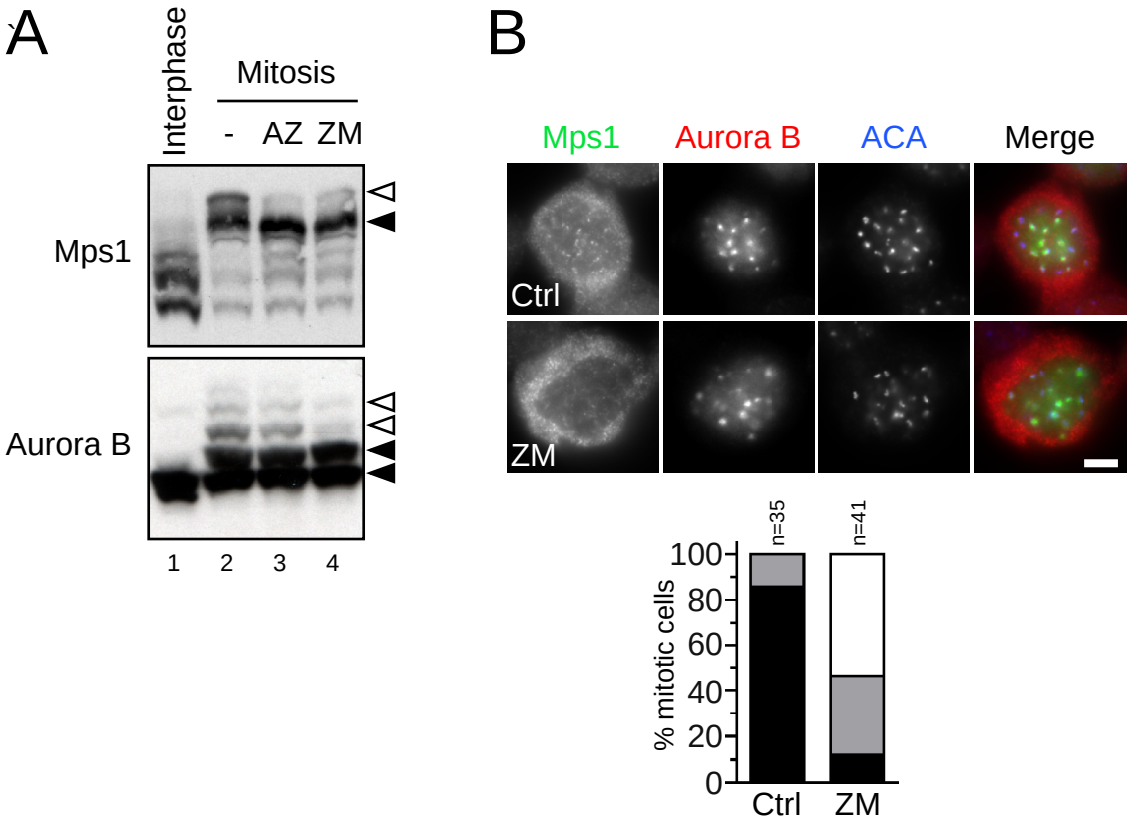

Figure 6.4 Aurora B inhibition leads to a decrease in Mps1 phosphorylation and mislocalisation of kinetochore-bound Mps1

(**A**) HeLa cells were treated with nocodazole for 12 hours. Mitotic cells were collected and replated into the indicated drug combinations (plus MG132 to prevent mitotic exit) for 2 hours. Adherent cells left behind after mitotic shake-off were harvested and constituted the interphase sample (lane 1). AZ3146 and ZM447439 was used at 2 µM and DMSO was used in controls to account for the solvent. Harvested cells were lysed directly in SDS-PAGE sample buffer and run on gels containing Phos-tag. Proteins were transferred to a PVDF membrane and probed with anti-Mps1 or anti-Aurora B antibodies. Several bands were visible for both proteins in mitotic lysates. Bands decreased in mitotic samples following direct inhibition of the respective kinases are marked by open arrowheads. Faster-migrating bands remaining after inhibition are marked by closed arrowheads. Note than the slowest-migrating species on the Mps1 blot disappears after inhibition of Aurora B with ZM447439, as well as after direct inhibition with AZ3146. Part of the anti-Mps1 blot was also presented in Figure 3.5.

(**B**) HeLa cells were treated with nocodazole, MG132 and DMSO (control) or 2 µM ZM447439 for 2 h, then fixed and processed for IF using antibodies against the indicated proteins. Mps1 kinetochore staining levels were assessed by eye in prometaphase-arrested cells; data is represented as a bar graph. Scale bar: 5 µm.

Contributions to part A of this figure:
Cells were treated with drugs and harvested by Anthony Tighe. Samples were run on Phos-tag gels and immunoblotted by Laura Hewitt.

Mps1 inhibition (see Figure 6.3B, also Jelluma et al., 2008b; Tighe et al., 2008), Mps1 kinetochore staining is reduced when cells are treated with ZM447439 (Figure 6.4B): only 12% of cells assessed had high levels Mps1 at kinetochores after ZM447439 treatment, compared to 86% of control cells. This data implicates Aurora B activity in Mps1 recruitment and/or maintenance at unattached kinetochores, possibly through a direct or indirect effect on its phosphorylation.

Taken together, the data presented in this Chapter so far point to a model where Mps1 inhibition compromises chromosome alignment, as previously reported (Jelluma et al., 2008b), but I have seen no evidence that this is mediated via reduced Aurora B activity. It is not immediately clear why this discrepancy should exist, though other groups have recently published similar findings using different methods of Mps1 inhibition (Maciejowski et al., 2010; Santaguida et al., 2010). With Aurora B inhibition not apparent, I sought alternative explanations for the alignment problem seen in Figure 6.2.

6.5 | Mps1 inhibition reduces Cenp-E levels at unaligned chromosomes

The alignment defect seen after monastrol wash-out (Figure 6.2) shared some characteristics with the defect seen after Cenp-E depletion (Kapoor et al., 2006; Weaver et al., 2003; Wood et al., 1997; Yao et al., 2000), and Mps1 activity has been shown to be required for maximal Cenp-E localisation in Xenopus egg extracts (Abrieu et al., 2001). This, along with the reduction in Cenp-E staining in AZ3146 and nocodazole-treated cells (Figure 5.1K), prompted me to investigate Cenp-E localisation in AZ3146-treated unaligned chromosomes. To do this, I performed monastrol wash-outs as described earlier, and released cells into MG132 with or without 2 μM AZ3146 for 1 hour before fixation and staining to detect Cenp-E (Figure 6.5A). Control cells still in the process of aligning their chromosomes had kinetochores with bright staining for Cenp-E; however, in AZ3146 cells, despite the presence of numerous unaligned chromosomes, very little Cenp-E was apparent at kinetochores. To compare levels in control and Mps1-inhibited cells, I quantified Cenp-E pixel intensities at unaligned kinetochores judged to be in the polar region of the spindle (see inset schematic in Figure 6.5B). Strikingly, in AZ3146-treated cells, kinetochore Cenp-E levels fell dramatically, to an average 7% of control levels. This decrease in Cenp-E is more drastic than that which I observed in nocodazole (Figure 5.1K): this may, at least in part, be due to the presence of polymerised microtubules, which have been shown to facilitate loss of microtubule motors from kinetochores (Murata-Hori and Wang, 2002). In support of this, I observed near-disappearance of Cenp-E at kinetochores in monastrol- and AZ3146-treated cells (Figure 6.5C). Cenp-E could

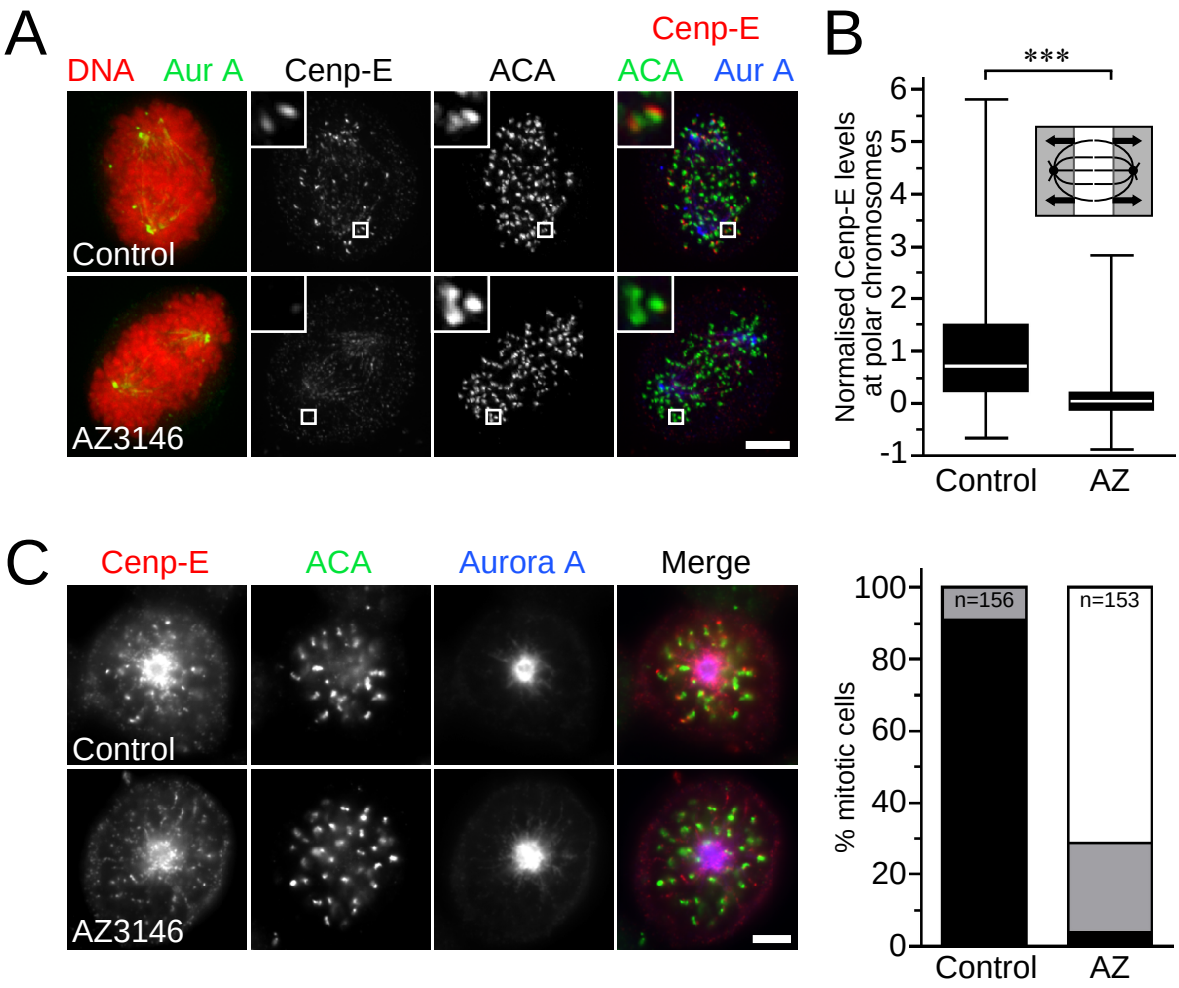

Figure 6.5 Cenp-E is absent from unaligned chromosomes when Mps1 is inhibited

(**A**) HeLa cells were treated with monastrol for 4 hours, followed by wash-out and incubation with MG132 and DMSO (control) or 2 μM AZ3146 for 1 h. Cells were fixed and stained to detect DNA and with antibodies against the proteins indicated. Representative examples of a control and AZ3146-treated cell are shown. Images are maximum intensity projections of deconvolved *z*-section stacks. Enlargements of boxed polar kinetochore pairs show absence of Cenp-E following AZ3146 treatment.

(**B**) Quantification of polar kinetochore Cenp-E levels in cells treated as in A. Polar kinetochores were defined as those situated in the approximate equivalent of the shaded region on the schematic diagram. Cenp-E pixel intensities at each kinetochore pair were quantified as a ratio to the ACA signal. The data shown in the box-and-whiskers plot is combined from 3 independent experiments, in which a total of 23 control cells (315 kinetochores) and 23 AZ-treated cells (308 kinetochores) were analysed. Ratios were normalised to the mean control value in each experiment. Whiskers represent the full range; boxes the interquartile range, and the line shows the median. (***$P < 0.0001$, Mann-Whitney U-test.)

(**C**) HeLa cells were treated with monastrol, MG132 and DMSO (control) or 2 μM AZ3146 for 2 h, then fixed and processed for IF using antibodies against the indicated proteins. Cenp-E kinetochore staining levels were assessed by eye in monopolar cells; data is represented as a bar graph. Values of *n* refer to the number of cells counted. Scale bars: 5 μm.

sometimes be seen decorating what appear to be microtubules instead (Figure 6.5C, lower panel). Taken together, this implicates Mps1 activity in the promotion of proper Cenp-E localisation.

Cenp-E binds kinetochores via a region within its carboxyl-terminus tail domain (Chan et al., 1998). To investigate whether this interaction might be perturbed after Mps1 inhibition, and so help to confirm the requirement for Mps1 activity in Cenp-E localisation, I used a DLD1 stable cell line expressing a GFP- and Myc-tagged ~122 kDa Cenp-E tail fusion protein which has been described previously (Gurden et al., 2010). This tool allowed me visualise Cenp-E tail's subcellular localisation directly via the GFP tag, and therefore potentially exclude the contribution of epitope masking following Mps1 inhibition. After fixation of the cells and visualisation of the GFP, I could clearly see Cenp-E tail at kinetochores in nocodazole-treated cells (Figure 6.6A). Importantly, when AZ3146 was present, the GFP tagged protein was markedly decreased at kinetochores. When GFP-Cenp-E tail levels were assessed by eye, the vast majority of AZ3146-treated cells had either low or medium levels (70%), compared to only 12 % of control cells (Figure 6.6B). This strongly suggests that Mps1 inhibition does indeed result in a loss of Cenp-E protein from unattached kinetochores. Importantly, work carried out by my colleague Anthony Tighe shows that perturbation of Mps1 activity by replacement of the endogenous kinase with an inhibitable, ATP analogue-sensitive mutant also causes loss of Cenp-E at unaligned kinetochores (Hewitt et al., 2010). This is consistent with Cenp-E loss being an on-target effect of AZ3146, and supports the existence of a link between Mps1 kinase activity and Cenp-E localisation in human cells.

6.6 | Summary

This chapter has focused on the role of Mps1 catalytic activity in chromosome alignment. Using AZ3146, I have confirmed that inhibition of Mps1 leads to an alignment defect after enrichment for mono-oriented chromosomes using a monastrol wash-out protocol. Previously, reduced Aurora B activity has been shown to be the cause of this defect; however, I was unable to detect any decrease in Aurora B activity levels in cells treated with AZ3146. In fact, it appeared that Aurora B was upstream of Mps1, since direct inhibition of Aurora B affected both Mps1's phosphorylation status and its kinetochore localisation. Interestingly, as a possible alternative explanation for the alignment problem observed after Mps1 inhibition, I found that Cenp-E levels were drastically reduced at unaligned kinetochores when Mps1 was inhibited. This might indicate either an indirect link between the two, or a direct phosphorylation event, as has been shown *in vitro* for Xenopus Cenp-E and Mps1 (Espeut et al., 2008). Loss of

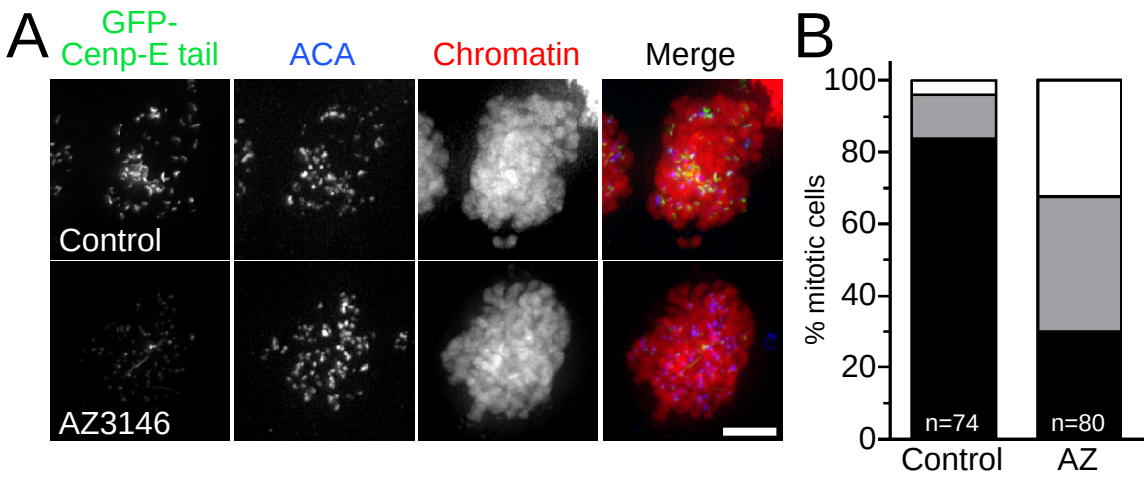

Figure 6.6 Exogenous Cenp-E tail is displaced from kinetochores when Mps1 is inhibited

(**A**) DLD1 cells expressing GFP-tagged Cenp-E tail were treated with nocodazole, MG132 and either DMSO (control) or 2 μM AZ3146, then fixed and processed for immunofluorescence, staining to visualise centromeres (ACA, blue). Cenp-E tail was detected directly via GFP fluorescence, and chromatin was visualised by DsRed-histone H2B fluorescence. Representative examples of a control and AZ3146-treated cell are shown. Images are maximum intensity projections of deconvolved *z*-section stacks. (**B**) In cells treated as in A, Cenp-E tail levels at kinetochores were assessed by eye and the results depicted as bar graphs; *n* values refer to the number of cells counted.

Cenp-E from unaligned kinetochores may, at least in part, explain the inability of Mps1 treated cells to achieve a fully aligned metaphase.

7 | Discussion

The ultimate aim of this study was to investigate the role of Mps1 in mitotic checkpoint signalling and the process of chromosome alignment, two key aspects of mitotic control that contribute towards the fidelity of genome propagation. To achieve this, I used the small molecule inhibitor AZ3146, a novel compound originally developed by AstraZeneca. Initial characterisation of the compound gave me confidence that AZ3146 was a useful tool with which to dissect the role of Mps1's kinase activity in cells: the compound appeared relatively selective and potent in *in vitro* assays, and affected the phosphorylation status of Mps1 in HeLa cells (Chapter 3). Furthermore, the compound decreased the viability of cultured human cell lines, and perturbed the mitotic checkpoint (Chapter 4). I turned to an immunofluorescence-based approach to assess the effect of Mps1 inhibition on various components of the kinetochore. In agreement with previous studies, the localisation of the checkpoint effector molecule Mad2 was exquisitely sensitive to Mps1 inhibition (Chapter 5). Interestingly, Mps1 abundance at unattached kinetochores markedly increased following AZ3146 treatment. This novel finding implied that Mps1's release from kinetochores might be regulated by its activity. Additionally, kinase-dead Mps1 accumulated at kinetochores, but only after removal of endogenous Mps1 activity, suggesting inter-molecular interactions may regulate Mps1's release from the kinetochore (Chapter 5). Finally, I used AZ3146 to investigate the role of Mps1 kinase activity in chromosome alignment: an alignment defect was apparent, but in contrast to other studies (Jelluma et al., 2008b; Sliedrecht et al., 2010) I was unable to detect Aurora B inhibition (Chapter 6). Mps1 inhibition also caused levels of the plus-end directed kinesin Cenp-E to decrease markedly at kinetochores of unaligned chromosomes, providing a novel possible alternative cause of the chromosome alignment defects in human cells.

In this chapter, I will discuss: firstly, the merits of AZ3146 as a tool to investigate Mps1 function; secondly, my findings with respect to checkpoint regulation in human cells; thirdly, my observations pertaining to Mps1's role in chromosome alignment and the link between Mps1 and Aurora B; fourthly, and lastly, data relating to Mps1 and cell viability.

7.1 | AZ3146: a novel tool to probe Mps1 function

In this study, I present AZ3146, a novel Mps1 inhibitor originally developed at AstraZeneca. AZ3146 has proved a useful tool, and enabled me to make several novel observations relating to Mps1's role in the regulation of mitosis (see above). Small molecule kinase inhibitors are desirable tools: they are a favourable alternative to RNAi-

based strategies, since they avoid variability and technical challenges associated with these approaches, and offer exquisite temporal control over target inhibition. Ideally, small molecule inhibitors should be both potent and selective, to enable complete inhibition of the target kinase and minimise the potential for confusing off-target effects in cells. AZ3146 is potent enough to be useful in cells: *in vitro*, the compound perturbed $Mps1^{CAT}$ dependent phosphorylation with an IC_{50} of ~35 nM (Figure 3.2), and elicited effects in cells consistent with Mps1 inhibition at 2 μM (Figures 3.5-5.1). There may be some residual activity in cells treated with 2 μM AZ3146, as implied by the increase in the severity of the phenotype when cells were treated with higher molarities (see Figure 4.2 and 5.2). A reliable biomarker for Mps1 activity would facilitate accurate assessment of Mps1 activity levels.

In vitro selectivity screens are commonly used to gain some insight into the ability of a compound to inhibit a wide range of kinases, and can help to predict selectivity in cells (Knight and Shokat, 2005; Smyth and Collins, 2009). The Invitrogen SelectScreen™ data (Figure 3.4) indicated that 1 μM AZ3146 was capable of partially inhibiting several kinases out of a diverse panel of 50 *in vitro*: Fak, Kit, and the two JNK isoforms were inhibited by more that 40%, and several other kinases were inhibited by more than 20% (Figure 3.4). However, it was encouraging that none of the kinases tested in the panel were inhibited to the same degree as Mps1, which is almost completely inactive in the presence of 1 μM AZ3146 under my assay conditions (Figure 3.4). To place this data in context, although some kinase inhibitors have been described with a higher degree of selectivity [e.g. the Plk inhibitors BI 2536 (Steegmaier et al., 2007) or Cyclapolin 9 (McInnes et al., 2006) which have minimal activity against a kinase panel at 10 or 100 μM, and very potently inhibit Plks], AZ3146 can be considered a reasonably selective Mps1 inhibitor. While I cannot rule out AZ3146-mediated inhibition of kinases other than the fifty I included in my panel, the screen gave me confidence that the cellular phenotypes I observed were likely to be due to Mps1 inhibition.

Further support for AZ3146's validity as an Mps1 inhibitor comes from the observation that AZ3146-treated cells behaved similarly to cells in which endogenous Mps1 was replaced with an exogenous kinase-dead mutant form of the kinase (Jelluma et al., 2008b; Tighe et al., 2008) in several important respects. As well as abrogating the mitotic checkpoint and leading to errors in chromosome segregation (see Chapter 4), AZ3146 led to the loss of anti-Mad2 staining at the kinetochore (Figure 5.1). This has been observed following Mps1 inhibition in our laboratory and others (Jelluma et al., 2008b; Tighe et al., 2008). By comparing the results of AZ3146 treatment with Mps1 RNAi followed by kinase-dead mutant add-back, I have also been able to support the idea

that the accumulation of Mps1 at kinetochores is an on-target effect (Figure 5.6). Additionally, my colleague A. Tighe has shown that Cenp-E loss at unaligned kinetochores is common to both AZ3146-treated cells and those in which analogue-sensitive Mps1 is inhibited using the ATP-analogue 1NM-PP1 (Hewitt et al., 2010), suggesting that this too is an on-target effect.

Whilst these approaches have proved helpful, an AZ3146-resistant Mps1 mutant would aid confirmation that the effects in cells are caused by on-target Mps1 inhibition. Mutation of the Mps1 active site gatekeeper residue from methionine to glutamine (M602Q) imparts a degree of resistance to both SP600125 (Schmidt et al., 2005) and Mps1-IN-1 (Kwiatkowski et al., 2010); expression of the mutant kinase was shown to lessen the severity of some of the drug-induced effects. However, expression of Mps1 M602Q in HeLa cells did not lessen the severity of the mitotic defects caused by 2 μM AZ3146 treatment when cells were observed by timelapse microscopy (data not shown). Future efforts might include a search for an AZ3146-resistant mutant form of Mps1, perhaps by conducting a screen for resistance in hypermutagenic HCT116 cells (e.g. Girdler et al., 2008), or by a systematic mutation of residues in the active site, where the inhibitor is likely to bind (e.g. Scutt et al., 2009). The crystal structure of the Mps1 kinase domain in complex with AZ3146 should be informative for the latter approach.

Whilst further work could help to firmly establish the degree of inhibition in cells, and strengthen the case for selectivity, as it stands AZ3146 is an important part of the newly-expanded toolbox for investigation of Mps1's role in cells. Until very recently, only the relatively nonspecific compound SP600125 (Schmidt et al., 2005) was available for inhibition of endogenous Mps1 in human cells; now, AZ3146 (this study and Hewitt et al., 2010), Reversine (Santaguida et al., 2010), and Mps-IN-1 (Kwiatkowski et al., 2010) have been introduced. Reversine also directly inhibits Aurora B (D'Alise et al., 2008), albeit less potently than Mps1 (Santaguida et al., 2010). This may have the potential to cause problems with the dissection of the two kinases' roles. AZ3146 and Mps1-IN-1 do not appear to target Aurora B (this study and Kwiatkowski et al., 2010). The existence of several small molecule inhibitors targeting Mps1, as well as cell lines engineered to express ATP-analogue sensitive Mps1 alleles, (Maciejowski et al., 2010; Sliedrecht et al., 2010) means data can be corroborated and off-target effects are more likely to be recognised as such. However, this does not entirely preclude discrepancies between groups, such as those discussed in Section 7.8.

Much of the data I present in this study has been built upon and extended by further work using AZ3146 in the Taylor laboratory. Along with data presented in this thesis,

some of this work is published in the appended journal article (Hewitt et al., 2010). Discussion of data presented in this study will be followed by reference to, and discussion of, relevant data obtained by my colleague Anthony Tighe and published in Hewitt et al (2010).

7.2 | Mps1 and checkpoint signalling

Mps1 is an established member of the signalling network governing mitotic checkpoint activation (Abrieu et al., 2001; Stucke et al., 2002; Weiss and Winey, 1996). Recently published work has implicated Mps1 kinase activity in the establishment and maintenance of the mitotic checkpoint (Hewitt et al., 2010; Jelluma et al., 2008a; Kwiatkowski et al., 2010; Santaguida et al., 2010; Sliedrecht et al., 2010; Tighe et al., 2008), and the data I presented in Chapter 4 is consistent with the notion that Mps1 activity is required for checkpoint function.

The kinetochore has long been understood play a critical role in mitotic checkpoint signalling (Rieder et al., 1995). Kinetochore protein recruitment is known to be crucial for the mitotic checkpoint to restrain anaphase in the presence of unaligned chromosomes (Meraldi et al., 2004). However, evidence exists for a preformed APC/C inhibitor, which acts as a kinetochore independent 'timer', preventing anaphase onset in early mitosis, before kinetochores have reached maturity (Meraldi et al., 2004; Sudakin et al., 2001). Reports suggest cytosolic MCC-like complexes containing Cdc20, Mad2 and/or BubR1 (Kulukian et al., 2009; Sudakin et al., 2001) exist in interphase and determine the minimum length of mitosis, independently of kinetochore-derived checkpoint signalling. Perturbing solely kinetochore-based checkpoint signalling (e.g. by depletion of Mad1) does not cause a significant shortening of an unperturbed mitosis comparative to controls; however, depletion of components of the proposed timer does drastically reduce mitotic timing (Meraldi et al., 2004). Interestingly, Mps1 inhibition by via AZ3146 hastens mitotic exit in an unperturbed mitosis, in both HeLa and hTERT-RPE cells (Figure 4.6), consistent with a role in formation of the cytosolic timer. This study has not examined this aspect of Mps1 function, but a recent publication has: Maciejowski and colleagues (2010) report that cells in which Mps1 is potently inhibited have reduced levels of cytosolic Cdc20-bound Mad2 and BubR1 in interphase and mitotic cell extracts, implicating Mps1 activity in the creation of an APC/C inhibitory complex both outside and within mitosis. Furthermore, a mutant form of Mps1 lacking its kinetochore targeting region ($Mps1^{\Delta N}$) could restore formation of Cdc20-Mad2, mitotic timing, and partially rescue the mitotic checkpoint defect in response to nocodazole, though not the alignment defect caused by Mps1 inhibition (Maciejowski et al., 2010). The apparent functionality of the

predominantly cytosolic Mps1$^{\Delta N}$ mutant seems to contradict earlier work, which found the kinetochore localisation of Mps1 was important for spindle checkpoint function (Liu et al., 2003; Zhao and Chen, 2006). However, Mps1$^{\Delta N}$ was only partially competent to restore checkpoint function when challenged with nocodazole, implying that active Mps1 at the kinetochore is necessary for sustained checkpoint signalling (Maciejowski et al., 2010). It will be interesting to see if this new data implicating cytosolic Mps1 activity in mitotic timing can be replicated with other Mps1 inhibitors.

7.2.1 | Mps1 regulates Mad1 and Mad2 levels at the kinetochore

Although the newly-emerging cytosolic role of Mps1 may contribute to mitotic timing, evidence suggests the recruitment of the checkpoint effectors molecules Mad1 and Mad2 to unattached kinetochores is a critical step in the amplification and maintenance of the checkpoint signal (Musacchio and Salmon, 2007), and one that Mps1 has been proposed to regulate in human cells (Jelluma et al., 2008b; Liu et al., 2003; Martin-Lluesma et al., 2002; Sliedrecht et al., 2010; Xu et al., 2009). Previous work from our laboratory using an RNAi complementation approach had observed a difference between Mad1 and Mad2 localisation in terms of the requirement for Mps1 kinase activity: while Mad2 was exquisitely sensitive to loss of Mps1 activity, Mad1 localisation was only partially decreased (Tighe et al., 2008). This implied that either Mps1's role in Mad1 recruitment was predominantly structural, or that a far lower level of enzymatic activity was necessary for Mad1 recruitment than for Mad2 recruitment. In keeping with this, I saw a similar effect with AZ3146 treatment: with 2 μM AZ3146, most cells had low levels of Mad2 staining at kinetochores, whereas Mad1 levels were less severely affected (Figure 5.1). However, while both Mad1 and Mad2 are decreased after treatment with AZ3146, the apparent difference between Mad1 and Mad2 sensitivity to Mps1 inhibition is maintained even when higher molarities of AZ3146 are used in cells (Figure 5.2), indicating that the difference is unlikely to be solely attributable to residual Mps1 activity. The data I present in this study confirms a role for Mps1 kinase activity in both Mad1 and Mad2 kinetochore localisation, and points to a more critical role for Mps1 activity in Mad2 recruitment. The implications of this data, along with recent work extending the analysis of Mad1 and Mad2 recruitment after Mps1 inhibition, are discussed below.

The apparent difference in requirement for Mps1 catalytic activity in Mad1 and Mad2 recruitment (Figure 5.1 and Hewitt et al., 2010) is at odds with data from other laboratories, where both Mad1 and Mad2 were lost from kinetochores following Mps1 inhibition (Santaguida et al., 2010). However, this difference might be explained by differences between assay designs, affecting the timing of Mps1 inhibition. The

immunofluorescence-based assay I used to assess kinetochore protein localisation involved simultaneous treatment with AZ3146, nocodazole and MG132. All cells undergo microtubule depolymerisation via nocodazole, and proteasome inhibition via MG132 prevents cells from either leaving or entering mitosis. As a result, a mixed population of mitotic cells, undistinguishable from one another, is created for analysis: some were already in prometaphase at the time of treatment, some were at metaphase with kinetochores stripped of Mad1/2 (DeLuca et al., 2003), and some were in early mitosis, prior to recruitment of checkpoint proteins to kinetochores. The question arises: could the reason for the variability in Mad1 levels following AZ3146 treatment (Figure 5.1), which leads to the partial effect when staining levels are quantified (Hewitt et al., 2010), stem from differences between the sub-populations of mitotic cells? Work carried out by A. Tighe and published in Hewitt et al (2010) suggests that this is indeed the case. When cells were pre-treated with nocodazole to trigger recruitment of checkpoint protein to unattached kinetochores, then incubated with AZ3146 and MG132 to inhibit Mps1 and prevent mitotic entry/exit respectively, Mad1 levels remained high. By contrast, when cells were treated first with MG132 to arrest cells at metaphase (with Mad1 gone from kinetochores), then with nocodazole to destroy the spindle, control cells re-recruited Mad1 to newly unattached kinetochores, whereas Mps1-inhibited cells did not. Thus, it appears that high levels of Mps1 activity are required to recruit (or re-recruit) Mad1 to unattached kinetochores, but Mps1 activity is less important for the maintenance of Mad1 at kinetochores at which it is already established. Notably, Mad2 levels were always predominantly low when Mps1 was inhibited; implying sustained Mps1 activity is critical for both recruitment (via Mad1) and maintenance of Mad2 at unattached kinetochores.

When this data is placed in the context of the currently favoured Mad2 template model (see Intro Figure 1.5 and De Antoni et al., 2005a; Musacchio and Salmon, 2007), further questions arise. As discussed in detail in the Chapter 1, Mad2 is capable of forming two very different conformations, which can dimerise: an open conformation (O-Mad2) and a closed conformation (C-Mad2). At the unattached kinetochore, Mad1 and C-Mad2 form a stable core complex consisting of Mad1 and C-Mad2, which then acts as a receptor for soluble O-Mad2, facilitating its conversion to C-Mad2 bound to Cdc20, and consequently APC/C^{Cdc20} inhibition (De Antoni et al., 2005a; Fang et al., 1998; Luo et al., 2004; Mapelli et al., 2007; Yang et al., 2008). Importantly, the Mad1-C-Mad2 core complex is highly stable (Howell et al., 2004; Shah et al., 2004; Vink et al., 2006), and exists at the nuclear pore in interphase (Campbell et al., 2001; Shah et al., 2004), suggesting it might be recruited to the kinetochore pre-complexed. Thus, biochemical and cell-based data implies that the interaction between Mad1 and C-Mad2 is an improbable

candidate for regulation by Mps1 activity. Rather, it seemed more likely that the recruitment of O-Mad2 might be the step at which Mps1 acts. So, why does the Mad2 signal at kinetochores largely disappear after AZ3146 treatment, when Mad1 remains relatively high (this study and Hewitt et al., 2010)? One possible explanation is that the antibody with which Mad2 was detected in these assays (SM2.2, Tighe et al., 2008) may only detect Mad2 in cells when it is in the open conformation. C-Mad2 may either be masked in cells, or have no affinity for the antibody. If this is indeed the case, C-Mad2 might be present at the kinetochore when Mps1 is inhibited, but remain undetectable by immunofluorescence with SM2.2, reconciling the immunofluorescence data with current knowledge regarding the biochemical behaviour of the Mad1-Mad2 complex (see Figure 7.1).

Work carried out by A. Tighe and described in Hewitt et al (2010) has provided substantial data to support this hypothesis. Using stable cell lines expressing Myc-tagged Mad2 fusion proteins, it was found that anti-Myc antibodies could readily detect Myc-Mad2 at the nuclear envelope in interphase cells, in contrast to SM2.2. This supports the notion that SM2.2 has low affinity for C-Mad2, the conformer present at the nuclear pore (Shah et al., 2004), and suggests the anti-Myc antibody recognises C-Mad2. Both SM2.2 and anti-Myc antibodies yielded a kinetochore staining pattern in mitotic cells; crucially, however, AZ3146 treatment only partially ablated the anti-Myc signal, while the SM2.2 signal disappeared almost completely. Thus, unlike SM2.2, the anti-Myc antibody recognises both conformers formed by the exogenous Myc-Mad2 pool: the anti-Myc kinetochore signal decreases as Myc-O-Mad2 is absent, but Mad1-bound Myc-C-Mad2 remains at readily detectable, relatively high levels (Hewitt et al., 2010).

The hypothesis was further confirmed by examining the kinetochore localisation of two Myc-Mad2 mutants initially characterised by Mapelli et al (2007): Mad2ΔC, which cannot form the closed conformation or bind to Mad1, represents an ‘open only’ form of Mad2; and Mad2RQ, which cannot dimerise, only binds kinetochores via Mad1, therefore only adopts the closed conformation (Mapelli et al., 2007). As predicted, AZ3146 treatment severely compromised Myc-Mad2ΔC kinetochore localisation, decreasing it to levels comparable to that seen when SM2.2 was used. Conversely, Myc-Mad2RQ showed only a slight decrease after AZ3146 treatment (Hewitt et al., 2010). Taken together, this data indicates that C-Mad2, presumably as part of the core complex with Mad1, is not severely affected by AZ3146-mediated Mps1 inhibition (unless Mps1 is inhibited prior to mitotic entry); however, O-Mad2 is exquisitely sensitive to Mps1 inhibition, and requires sustained Mps1 activity to both recruit and maintain it at unattached kinetochores.

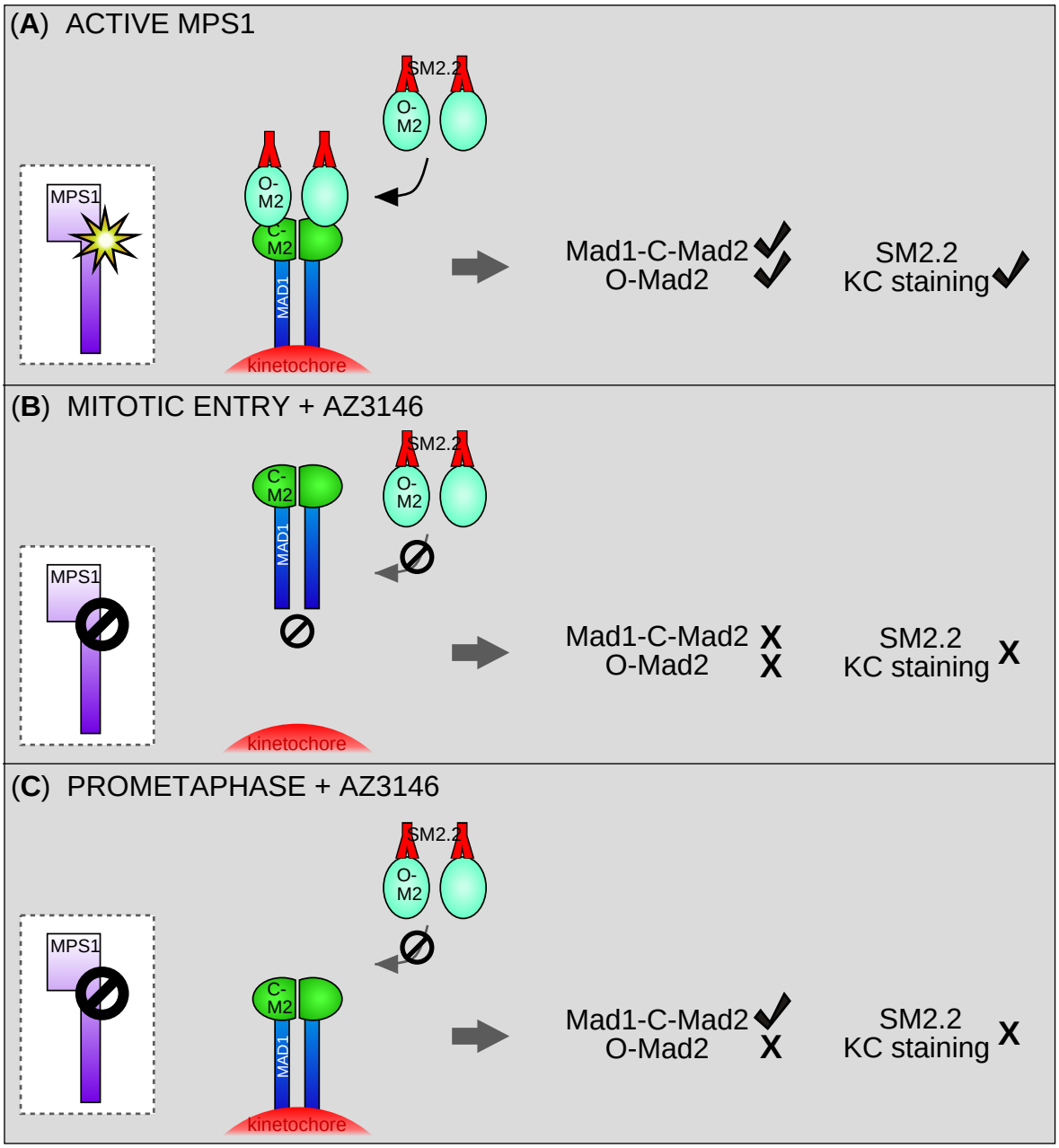

Figure 7.1 Schematic describing the role of Mps1 in Mad1 and Mad2 recruitment at the kinetochore
(A) Mps1 activity recruits and maintains the stable Mad1-C-Mad2 core complex and O-Mad2 at unattached kinetochores during mitosis. O-Mad2 at the kinetochore is recognised by the anti-Mad2 antibody SM2.2 (Hewitt et al, 2010), which I used in this study (Figure 5.3).
(B) Mps1 activity is required to recruit Mad1-C-Mad2 to unattached kinetochores in early mitosis. This can be inferred from data showing that when unattached kinetochores are created in cells where Mad1 and Mad2 have been stripped from kinetochores, Mps1 inhibition via AZ3146 prevents re-recruitment of the proteins to unattached kinetochores (Hewitt et al, 2010). When Mad1-C-Mad2 cannot be recruited, O-Mad2 cannot dimerise at the kinetochore, and the SM2.2 does not stain kinetochores.
(C) Mps1 activity is required to maintain O-Mad2 levels at unattached kinetochores during mitosis. When cells are arrested with nocodazole to induce Mad1 and Mad2 recruitment to unattached kinetochores, then treated with AZ3146 to inhibit Mps1, Mad1-C-Mad2 levels remain relatively high, whereas O-Mad2 levels (and consequently SM2.2 kinetochore staining) are very low (Hewitt et al, 2010). The specificity of SM2.2 for O-Mad2 in cells explains the low levels of SM2.2 staining compared to Mad1 staining, and the difference in effect of Mps1 inhibition depending on the point of inhibition contributes to the variability in Mad1 levels in the mixed mitotic population analysed in Figure 5.3.

7.2.2 | Mps1 appears to have an indirect role in Mad1-Mad2 core complex recruitment

The data discussed above, along with work from other groups highlighting the importance of Mps1 kinase activity in recruiting Mad1 and Mad2 to kinetochores (Jelluma et al., 2008b; Kwiatkowski et al., 2010; Liu et al., 2003; Maciejowski et al., 2010; Martin-Lluesma et al., 2002; Santaguida et al., 2010; Sliedrecht et al., 2010; Tighe et al., 2008; Xu et al., 2009), provides a mechanistic explanation for the spindle checkpoint malfunction in Mps1-inhibited cells. How exactly Mps1 might promote initial recruitment of the Mad1-C-Mad2 core complex to the kinetochore in prometaphase is unknown; notably, however, data in this study (Figure 5.1) and concurrently from others (Maciejowski et al., 2010; Santaguida et al., 2010) indicated that kinetochore levels of the RZZ complex, which is necessary for full Mad1 recruitment (Buffin et al., 2005; Kops et al., 2005), are also lowered following Mps1 inhibition. Therefore, Mps1's role in Mad1 recruitment might be indirect, perhaps by mediating the interaction between RZZ and Zwint: along with other members of the outer kinetochore KMN network, Zwint remains at kinetochores following Mps1 inhibition (this study, Figure 5.1 and Santaguida et al., 2010). The kinetochore binding sites for the RZZ complex are not fully understood (Civril et al., 2010), and further understanding of specific requirements for kinetochore assembly could help clarify any role for Mps1.

7.2.3 | Regulation of Mad2 dimerisation – the "cap" hypothesis

As well as it's role in initial recruitment of the core Mad1-C-Mad2 complex to kinetochores, likely via mediation of RZZ localisation, Mps1 kinase activity seems to be important in both the recruitment and subsequent maintenance of soluble O-Mad2 levels at the kinetochore (Hewitt et al., 2010). How O-Mad2 recruitment is promoted remains a key question. The fact that the dynamics of Mad1-Mad2 binding can be recreated *in vitro* (Vink et al., 2006) suggests that promotion of Mad2 dimerisation in cells likely involves removal of some inhibitory element that is not present in the *in vitro* experiments. Structural and biochemical data have led to the hypothesis that $p31^{comet}$ acts as a kind of "cap" on the core complex, inactivating the checkpoint (Mapelli et al., 2006; Vink et al., 2006; Yang et al., 2007a). It is hypothesised that some factor(s) at kinetochores might regulate $p31^{comet}$, perhaps via post-translational modification, to allow Mad2 dimerisation and checkpoint signalling when unattached kinetochores are present. The subsequent reactivation of $p31^{comet}$ might contribute to the cessation of checkpoint signalling when all chromosomes have aligned (Musacchio and Salmon, 2007). Mps1 is a candidate $p31^{comet}$

regulator: conceivably, its sustained activity could prevent association of p31^{comet} with C-Mad2, allowing Mad2 dimerisation. Currently, this remains speculation, but work is underway to elucidate the mechanism by which p31^{comet} regulates the checkpoint.

A striking novel observation described in this study suggests a possible alternative mechanism controlling O-Mad2's association with C-Mad2. When Mps1 activity was decreased in nocodazole-arrested cells, either by inhibition of Mps1 with AZ3146 or by expressing a kinase-dead mutant and depleting the endogenous kinase by RNAi, Mps1 increases in abundance at the kinetochores (Figure 5.3-5.6). As FRAP-based experiments have shown, Mps1 is not a stable resident at unattached kinetochores: it cycles with an apparent half-life of recovery of 13 seconds (Howell et al., 2004). Therefore, the increased levels of Mps1 at kinetochores I observed by immunofluorescence might reflect a decrease in the rate at which Mps1 cycles on and off the kinetochore. In the future, FRAP experiments might prove useful to determine whether or not Mps1's residency at kinetochores is extended after inhibition of its kinase activity.

One important implication of this data is that Mps1 activity might regulate its own kinetochore localisation, and that this may relate to checkpoint signalling. Since Mps1 activity levels peak as cells enter mitosis (Liu et al., 2003; Stucke et al., 2002), it is plausible that Mps1 itself might act as the inhibitory cap on the Mad1-C-Mad2 core complex: its activation on mitotic entry could trigger its release from kinetochores, enabling Mad2 dimerisation and activating checkpoint signalling (see schematic diagram in Figure 7.2). Following checkpoint satisfaction, Mps1 levels at kinetochores decrease (Howell et al., 2004; Liu et al., 2003; Stucke et al., 2002), as do levels of Mad1 and Mad2 at kinetochores due to Dynein-dependent stripping (Howell et al., 2001). Perhaps Mps1 reprises its role as a cap on the core complex as the proteins are stripped from aligned kinetochores, as has been suggested for p31^{comet} (Musacchio and Salmon, 2007). There is currently a lack of biochemical data to support the Mps1 cap hypothesis: no physical interactions between Mps1 and members of the core complex have been reported. Indeed, none were detected in immunoprecipitations performed in this laboratory (A. Tighe, unpublished results). Nevertheless, it is possible that such interactions may exist despite these negative results, since they may be relatively weak and difficult to detect by immunoprecipitation.

7.2.4 | Mps1 molecules interact with each other in cells

The increase in Mps1 levels at kinetochores also pointed to important aspects of Mps1 regulation. Specifically, the fact that the exogenous kinase-dead GFP-Mps1 levels did not increase significantly relative to wild-type levels at kinetochores, unless

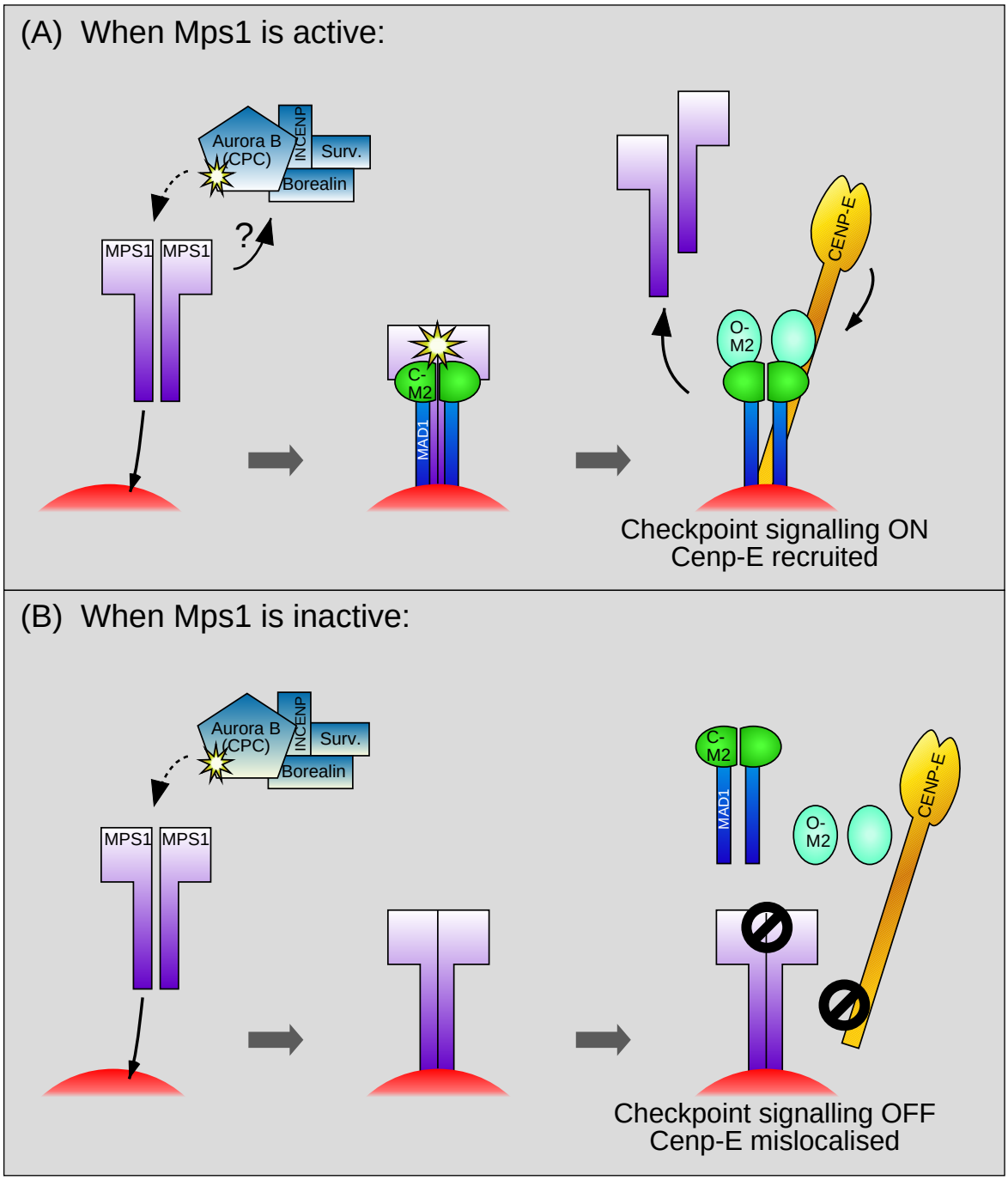

Figure 7.2 A speculative model for Mps1's kinetochore based role in mitotic checkpoint signalling and Cenp-E recruitment

(A) Mps1's recruitment to unattached kinetochores (shown in red) is promoted, indirectly or directly, by centromeric Aurora B activity, which associates with INCENP, Survivin and Borealin to form the chromosomal passenger complex (CPC). It has been reported that Mps1 phosphorylates Borealin, but I see no evidence for this. Mps1 activity recruits the Mad1-C-Mad2 core complex to unattached kinetochores (probably indirectly via the RZZ complex - not shown on this schematic). At kinetochores, Mps1 dimerises and trans-autophosphorylates, triggering its own auto-release, and allowing O-Mad2 to dimerise with C-Mad2 in the core complex. This facilitates downstream checkpoint signalling. Note that Mps1 activity is required for the initial recruitment of both Mad1-C-Mad2 core complex and O-Mad2 to unattached kinetochores, but its sustained activity is a critical requirement for continued O-Mad2 recruitment (Hewitt et al, 2010). Mps1's auto-release also exposes the Cenp-E tail's kinetochore binding site, allowing Cenp-E to be recruited and contributing to proper alignment of chromosomes at the metaphase plate.

(**B**) When Mps1 is inactive, it can still be recruited to kinetochores by Aurora B. Inactive Mps1 can dimerise (Hewitt et al, 2010) but cannot trans-autophosphorylate and accumulates at kinetochores. This prevents kinetochore-based checkpoint signalling and perturbs alignment, by stopping the Cenp-E tail domain from accessing its binding site.

endogenous activity was removed by RNAi (Figure 5.6), or ablated by AZ3146 treatment (Figure 5.5), was intriguing. The inactive transgene was apparently prevented from accumulating when active, endogenous Mps1 was present, which hinted at some interaction between the two pools of Mps1 in the cell. Evidence from several laboratories implies that Mps1 molecules do indeed interact with each other: the kinase is capable of trans-molecular autophosphorylation, and this autophosphorylation is required for full kinase activity (Jelluma et al., 2008a; Kang et al., 2007; Mattison et al., 2007; Tyler et al., 2009). Artificially induced dimerisation leads to hyperactivity of immunoprecipitated Mps1 (Kang et al., 2007). A hypothesis presents itself based on these findings: perhaps Mps1 functions as a dimer, which comes together at the kinetochore, trans-autophosphorylates, activates and also triggers its own release from kinetochores. One might therefore predict that dimers in which both Mps1 molecules are inactive fail to trans-autophosphorylate and are retained at the kinetochore.

Work published in Hewitt et al (2010) supports this hypothesis. Importantly, my colleague A. Tighe found the first evidence of Mps1 dimers in mitotic cells, observing an interaction between immunoprecipitated Myc- and GFP-tagged Mps1. If at least one of the members of the immunoprecipitated dimer was active, wild type Mps1, the immunoprecipitated kinase appeared to be phosphorylated, as measured by band-shift on an SDS-PAGE gel. However, when both members of the dimer were inactive kinase dead mutants, this apparent phosphorylation was markedly reduced. This work supports Mps1 dimerisation and trans-phosphorylation in cells, but the significance of these findings with regard to regulation of Mps1 kinetochore localisation is as yet unknown. The identity of the Mps1 target phosphorylation site(s), whether autophosphorylation or otherwise, will be important in helping to understand the regulation of its localisation.

7.3 | Mps1 and chromosome alignment

As detailed in Chapter 1, Mps1 has a dual role in mitosis, regulating the mitotic checkpoint via Mad1/Mad2, and also facilitating chromosome alignment (Jelluma et al., 2008b; Maciejowski et al., 2010; Santaguida et al., 2010; Sliedrecht et al., 2010). In agreement with this, AZ3146-treated cells failed to reach metaphase after removal of monastrol (Figure 6.2). However, in contrast to some previous reports (Jelluma et al., 2008b; Kwiatkowski et al., 2010; Sliedrecht et al., 2010), I did not see any evidence of Aurora B inhibition in Mps1 inhibited cells (Figure 6.3; discussed below), but I did see a significant decrease in Cenp-E levels at kinetochores in both nocodazole- and monastrol-treated cells, and at unaligned chromosomes after monastrol wash-out. Previous reports indicate Cenp-E is relatively unaffected after RNAi of Mps1 (Jelluma et al., 2008b; Tighe

et al., 2008), raising the possibility that Cenp-E loss after AZ3146 treatment may be caused by Mps1 accumulation at the kinetochore. Cenp-E and Mps1 may occupy mutually exclusive binding sites at kinetochores, meaning Cenp-E can localise via its tail domain relatively normally when Mps1 is active and rapidly cycling, but is prevented from binding when inactive Mps1 does not auto-release from kinetochores (see Figure 7.2).

The above hypothesis is speculative, but if true, suggests that Mps1's role in Cenp-E recruitment is not through direct protein-protein interaction. However, evidence does exist to support a direct substrate-kinase interaction between Xenopus Mps1 and the Cenp-E tail domain, at least *in vitro* (Espeut et al., 2008). In this system, Mps1 phosphorylation of the Cenp-E tail is proposed to relieve autoinhibition of the kinesin, thereby presumably activating it at the kinetochore (Espeut et al., 2008). Cdk1 is also known to phosphorylate the Cenp-E tail domain (Espeut et al., 2008; Liao et al., 1994), and out of the 4 mitotic phospho-sites identified in the Cenp-E tail by phosphoprotemic methods (Dephoure et al., 2008; Nousiainen et al., 2006), 2 match the consensus site for proline-directed kinases (Cdk1 or MAPKs). The fact that 2 of these sites are not in proline-directed motifs suggests Cenp-E's kinetochore localisation domain is phosphorylated by other kinase(s) in mitotic human cells: Mps1 is a possible candidate. However, to date there is no evidence that Mps1 phosphorylates Cenp-E in cells. Preliminary data I obtained from mass spectrometry on Cenp-E tail from mitotic cells identified one of these non-Cdk1 sites (S2651 in the full-length protein), and saw no change in its phosphorylation level after AZ3146 treatment, though the level of phosphorylation at a Cdk1 consensus site (S2654) was increased slightly (data not shown). This preliminary data requires both repetition and consolidation before any conclusions can be confidently drawn from it, however it is tempting to speculate that the increase in phosphorylation at S2654 might be a consequence of Cenp-E tail's mislocalisation from kinetochores into the cytoplasm where Cdk1 has access to the substrate. Further analysis of Cenp-E phosphorylation in both Mps1-inhibited and Cdk1-inhibited cells will be required to determine whether or not this holds true.

Whether or not it is regulated by phosphorylation, Cenp-E's disappearance from kinetochores may at least partly explain the problems with alignment in Mps1 inhibitor-treated cells. Notably, Mps1 activity is a requirement for efficient Cenp-E recruitment to kinetochores in *X. laevis* egg extracts (Abrieu et al., 2001), and my observations have recently been corroborated in hTERT-RPE cells expressing analogue-sensitive Mps1^{as} (Maciejowski et al., 2010). Lack of Cenp-E at kinetochores would prevent chromosomes from congressing from the poles toward the metaphase plate. It is likely, however, that Mps1-deficient cells might have multiple problems with the mechanism of alignment. Kinetochores in AZ3146-treated cells also have lowered levels of Cenp-F (Figure 5.1),

which, in addition to binding Cenp-E (Chan et al., 1998; Johnson et al., 2004; Yang et al., 2005; Yao et al., 2000), has also been linked to Dynein-dynactin recruitment via Nde1 (Vergnolle and Taylor, 2007). This may mean AZ3146-treated cells have a reduced ability to move chromosomes polewards prior to biorientation, a process that is thought to contribute to the efficiency of alignment (Yang et al., 2007b). More detailed analysis of AZ3146-treated cells could shed light on the contributions of these proteins to the alignment defect.

7.3.1 | Mps1 and Aurora B – who regulates whom?

As previously mentioned, Mps1 has previously been placed upstream of Aurora B in a signalling network controlling the correction of erroneous kinetochore-microtubule attachments, thereby facilitating alignment (Jelluma et al., 2008b; Sliedrecht et al., 2010). In the process of conducting this study, I found no evidence that Aurora B activity is diminished in cells treated with an Mps1 inhibitor (Figure 6.3). On the contrary, both Mps1's phosphorylation status and its kinetochore localisation were affected by treatment with the Aurora B inhibitor ZM447439, positioning Aurora B upstream of Mps1 (Figure 6.4). It remains to be determined whether Mps1 is a direct substrate for Aurora B, or whether the decrease in phosphorylation is linked to the lowered kinetochore levels of Mps1. This, in turn, might reflect an increase in the rate of cycling Mps1, or a lower level of Mps1 cycling normally: FRAP experiments would be necessary to distinguish between these two possibilities.

The apparent lack of Aurora B inhibition after AZ3146 treatment was surprising in light of previous publications (Jelluma et al., 2008b; Kwiatkowski et al., 2010; Sliedrecht et al., 2010). However, concurrent with the publication of our report (Hewitt et al., 2010), two other laboratories published similar findings, arrived at by different means: Santaguida and colleagues (2010) used another small molecule, Reversine; Maciejowski et al (2010) used targeted gene deletion followed by replacement with bulky purine analogue-sensitive Mps1^{as}. Both reports show that potent Mps1 inhibition had no appreciable effect on Aurora B activation levels, meaning the lack of Aurora B inhibition I observed is unlikely to be due to be solely attributable to residual Mps1 activity. The contrasting conclusions concerning who regulates whom might point to a non-linear signalling network involving the kinases, maybe involving cross-talk between the two. But why would different labs produce such divergent results? The answer is currently unclear, but one possibility is that differences between cells lines may be important. Aurora B appears to be regulated by Mps1 in U2OS and HCT116-derived cell lines (Sliedrecht et al., 2010), but not in HeLa cells (Hewitt et al., 2010, and this study; Santaguida et al., 2010) or in untransformed

hTERT-RPE cells (Maciejowski et al., 2010). This suggests the differences are not simply due to use of transformed versus untransformed cell lines. However, it is still conceivable that other differences between cell lines might explain these results. Perhaps Aurora B activity is regulated in RPE and HeLa cells by Mps1-independent mechanism(s) that are non-functional in U2OS and HCT116 cells. Another possible explanation is that expression, or regulation of Aurora C, the third, lesser-studied member of the Aurora family, might differ between cells lines, potentially masking Aurora B inhibition in Mps1 treated cells. Aurora C might be able to compensate for loss of Aurora B activity in Mps1-inhibited cells (Li et al., 2004; Sasai et al., 2004; Slattery et al., 2008), meaning Aurora B appears active, but is not. Aurora C expression has been reported in an untransformed human fibroblast cell line (WI-38 cells), plus several cancer cell lines including both HeLa and HCT116 cells (Sasai et al., 2004), suggesting the explanation may not be as simple as presence or absence of the kinase. The situation is further complicated by the fact that, like Aurora B, Aurora C can also form a complex with the apparent Mps1 substrate Borealin, along with other members of the CPC (Li et al., 2004; Slattery et al., 2008), but it is not known whether these complexes are regulated identically, or whether Aurora C only functions as part of the CPC. This situation certainly warrants further exploration: it would be interesting to find out if Aurora C expression or activation levels might differ between cell lines, and whether these correlate with Aurora B activity levels following Mps1 inhibition. Whilst the relationship between Mps1 and Aurora B is far from completely understood, newly described tools for Mps1 inhibition, including AZ3146, should facilitate further investigation into the function of the two kinases in mitosis.

7.4 | Mps1 inhibition and cell viability

The discovery that inactivation of the mitotic checkpoint cause cell death due to catastrophic errors in segregation (Kops et al., 2004; Michel et al., 2004) gave rise to the idea that inhibition of the mitotic checkpoint could represent a useful anti-cancer strategy. However, evidence suggests that Mps1 inhibition kills both cancer cells lines and "normal" untransformed cell lines (Figure 4.1 and Kwiatkowski et al., 2010; Maciejowski et al., 2010), making it less than ideal for therapeutic use, where drugs that are selective for tumour cells are desirable. Another important caveat is that effective checkpoint inhibition might be difficult to achieve *in vivo* without a more potent drug than those currently available.

Prior publications have shown that a low level of Mps1 activity (~10-40%) is sufficient to maintain viability of cultured cells (Janssen et al., 2009; Jelluma et al., 2008a; Maciejowski et al., 2010). My data appears to conflict with this: colony formation assays

showed that treatment with 1 μM AZ3146, a concentration that does not cause significant aneuploidy after 24 hour treatment (as measured by the appearance of the DNA content profile of treated cells, Figure 4.2) significantly affected the long-term viability of HeLa, HCT116 and hTERT-RPE cells (Figure 4.1). In the absence of a more detailed analysis of the level of inhibition caused by 1 μM AZ3146 in cells, and a more sensitive measurement of chromosome missegregations it may cause, it is difficult to compare my data with earlier publications. However, it has been shown that even relatively severe chromosome missegregations can take several doublings to cause widespread death in a population (Kops et al., 2004), so if 1 μM AZ3146 causes loss or gain of a few chromosomes with each division (which may not be visible by the relatively insensitive DNA content profiling I used in Figure 4.2) it seems reasonable that this may have a detrimental effect on cell survival over 9-10 days (Figure 4.1). While the contribution of off-target effects to the decrease in viability in AZ3146-treated cells cannot be excluded, taking together my data and that from other laboratories, (Janssen et al., 2009; Jelluma et al., 2008a; Kwiatkowski et al., 2010; Maciejowski et al., 2010) it is clear that Mps1 activity is necessary for the survival of both transformed and untransformed cell lines.

Although current data casts doubt upon its selectivity for cancer cell lines, AZ3146 and other new Mps1 inhibitors will allow further evaluation of Mps1 targeting as an anti-cancer strategy by assessing its effect in more tumour cell lines and in tumour models. It has been suggested that Mps1's dual role in chromosome alignment and checkpoint signalling can be exploited to selectively kill cancer cells: RNAi-based studies indicate that partial Mps1 depletion combined with a low, sub-lethal dose of Taxol leads to an increased rate of chromosome missegregation, providing selective toxicity towards cultured cancer cell lines (Janssen et al., 2009). The fact that *partial* depletion of Mps1 was enough to synergise with Taxol treatment in cancer cells is encouraging, since partial inhibition is likely to be easier to achieve *in vivo* than complete inhibition. It remains to be seen whether AZ3146 or other Mps1 inhibitors will also have a selective synergy with Taxol, and more importantly whether this strategy of enhancing the rate of chromosome missegregation will prove selective for tumour cells in *in vivo* models.

7.5 | Perspectives and future directions

Mps1 activity has a dual role in the maintenance of genomic stability and cell viability: it is involved in both the mechanism of chromosome alignment and control of mitotic timing in human cells. The dynamic nature of Mps1's interaction with the kinetochore may prove critical in the regulation of both of these processes. Further dissection of the relationship between Mps1 and Aurora B is a key challenge for the future:

it has become apparent that the two kinases are closely linked and converge upon some of the same substrates: for example, Ndc80 and BubR1 are targets of both kinases (Cheeseman et al., 2002; Ditchfield et al., 2003; Hauf et al., 2003; Huang et al., 2008; Kemmler et al., 2009). Interestingly, a key Mps1 substrate appears to be Mps1 itself: a role for dimerisation and trans-autophosphorylation in regulation of Mps1 activity has emerged (Hewitt et al., 2010; Kang et al., 2007), and might also be involved in regulation of Mps1's kinetochore localisation (see speculative model in Figure 7.2). It seems likely that further Mps1 substrates remain to be discovered, and AZ3146, along with other Mps1 inhibitors, should prove valuable in this endeavour and help to further understanding of the processes of mitotic checkpoint regulation and chromosome alignment.

8 | Bibliography

Abrieu, A., L. Magnaghi-Jaulin, J.A. Kahana, M. Peter, A. Castro, S. Vigneron, T. Lorca, D.W. Cleveland, and J.C. Labbe. 2001. Mps1 is a kinetochore-associated kinase essential for the vertebrate mitotic checkpoint. Cell. 106:83-93.

Ahonen, L.J., M.J. Kallio, J.R. Daum, M. Bolton, I.A. Manke, M.B. Yaffe, P.T. Stukenberg, and G.J. Gorbsky. 2005. Polo-like kinase 1 creates the tension-sensing 3F3/2 phosphoepitope and modulates the association of spindle-checkpoint proteins at kinetochores. Curr Biol. 15:1078-89.

Allan, L.A., and P.R. Clarke. 2007. Phosphorylation of caspase-9 by CDK1/cyclin B1 protects mitotic cells against apoptosis. Mol Cell. 26:301-10.

Amon, A. 2008. A decade of Cdc14--a personal perspective. Delivered on 9 July 2007 at the 32nd FEBS Congress in Vienna, Austria. FEBS J. 275:5774-84.

Andrews, P.D., Y. Ovechkina, N. Morrice, M. Wagenbach, K. Duncan, L. Wordeman, and J.R. Swedlow. 2004. Aurora B regulates MCAK at the mitotic centromere. Dev Cell. 6:253-68.

Antonarakis, S.E., R. Lyle, E.T. Dermitzakis, A. Reymond, and S. Deutsch. 2004. Chromosome 21 and down syndrome: from genomics to pathophysiology. Nat Rev Genet. 5:725-38.

Archambault, V., and D.M. Glover. 2009. Polo-like kinases: conservation and divergence in their functions and regulation. Nat Rev Mol Cell Biol. 10:265-75.

Arnaud, L., J. Pines, and E.A. Nigg. 1998. GFP tagging reveals human Polo-like kinase 1 at the kinetochore/centromere region of mitotic chromosomes. Chromosoma. 107:424-9.

Bain, J., L. Plater, M. Elliott, N. Shpiro, C.J. Hastie, H. McLauchlan, I. Klevernic, J.S. Arthur, D.R. Alessi, and P. Cohen. 2007. The selectivity of protein kinase inhibitors: a further update. Biochem J. 408:297-315.

Bakhoum, S.F., S.L. Thompson, A.L. Manning, and D.A. Compton. 2009. Genome stability is ensured by temporal control of kinetochore-microtubule dynamics. Nat Cell Biol. 11:27-35.

Barber, T.D., K. McManus, K.W. Yuen, M. Reis, G. Parmigiani, D. Shen, I. Barrett, Y. Nouhi, F. Spencer, S. Markowitz, V.E. Velculescu, K.W. Kinzler, B. Vogelstein, C. Lengauer, and P. Hieter. 2008. Chromatid cohesion defects may underlie chromosome instability in human colorectal cancers. Proc Natl Acad Sci U S A. 105:3443-8.

Barr, A.R., and F. Gergely. 2007. Aurora-A: the maker and breaker of spindle poles. J Cell Sci. 120:2987-96.

Basto, R., R. Gomes, and R.E. Karess. 2000. Rough deal and Zw10 are required for the metaphase checkpoint in Drosophila. Nat Cell Biol. 2:939-43.

Bennett, B.L., D.T. Sasaki, B.W. Murray, E.C. O'Leary, S.T. Sakata, W. Xu, J.C. Leisten, A. Motiwala, S. Pierce, Y. Satoh, S.S. Bhagwat, A.M. Manning, and D.W. Anderson. 2001. SP600125, an anthrapyrazolone inhibitor of Jun N-terminal kinase. Proc Natl Acad Sci U S A. 98:13681-6.

Biggins, S., and A.W. Murray. 2001. The budding yeast protein kinase Ipl1/Aurora allows the absence of tension to activate the spindle checkpoint. Genes Dev. 15:3118-29.

Bishop, A.C., O. Buzko, and K.M. Shokat. 2001. Magic bullets for protein kinases. Trends Cell Biol. 11:167-72.

Blethrow, J.D., J.S. Glavy, D.O. Morgan, and K.M. Shokat. 2008. Covalent capture of kinase-specific phosphopeptides reveals Cdk1-cyclin B substrates. Proc Natl Acad Sci U S A. 105:1442-7.

Borysova, M.K., Y. Cui, M. Snyder, and T.M. Guadagno. 2008. Knockdown of B-Raf impairs spindle formation and the mitotic checkpoint in human somatic cells. Cell Cycle. 7:2894-901.

Brinkley, B.R. 2001. Managing the centrosome numbers game: from chaos to stability in cancer cell division. Trends Cell Biol. 11:18-21.

Buffin, E., C. Lefebvre, J. Huang, M.E. Gagou, and R.E. Karess. 2005. Recruitment of Mad2 to the kinetochore requires the Rod/Zw10 complex. Curr Biol. 15:856-61.

Burke, D.J., and P.T. Stukenberg. 2008. Linking kinetochore-microtubule binding to the spindle checkpoint. Dev Cell. 14:474-9.

Burton, J.L., and M.J. Solomon. 2007. Mad3p, a pseudosubstrate inhibitor of APCCdc20 in the spindle assembly checkpoint. Genes Dev. 21:655-67.

Cahill, D.P., C. Lengauer, J. Yu, G.J. Riggins, J.K. Willson, S.D. Markowitz, K.W. Kinzler, and B. Vogelstein. 1998. Mutations of mitotic checkpoint genes in human cancers. Nature. 392:300-3.

Campbell, M.S., G.K. Chan, and T.J. Yen. 2001. Mitotic checkpoint proteins HsMAD1 and HsMAD2 are associated with nuclear pore complexes in interphase. J Cell Sci. 114:953-63.

Campbell, M.S., and G.J. Gorbsky. 1995. Microinjection of mitotic cells with the 3F3/2 anti-phosphoepitope antibody delays the onset of anaphase. J Cell Biol. 129:1195-204.

Carmena, M., and W.C. Earnshaw. 2003. The cellular geography of aurora kinases. Nat Rev Mol Cell Biol. 4:842-54.

Carmena, M., S. Ruchaud, and W.C. Earnshaw. 2009. Making the Auroras glow: regulation of Aurora A and B kinase function by interacting proteins. Curr Opin Cell Biol. 21:796-805.

Castillo, A.R., J.B. Meehl, G. Morgan, A. Schutz-Geschwender, and M. Winey. 2002. The yeast protein kinase Mps1p is required for assembly of the integral spindle pole body component Spc42p. J Cell Biol. 156:453-65.

Chan, G.K., S.A. Jablonski, D.A. Starr, M.L. Goldberg, and T.J. Yen. 2000. Human Zw10 and ROD are mitotic checkpoint proteins that bind to kinetochores. Nat Cell Biol. 2:944-7.

Chan, G.K., S.A. Jablonski, V. Sudakin, J.C. Hittle, and T.J. Yen. 1999. Human BUBR1 is a mitotic checkpoint kinase that monitors CENP-E functions at kinetochores and binds the cyclosome/APC. J Cell Biol. 146:941-54.

Chan, G.K., B.T. Schaar, and T.J. Yen. 1998. Characterization of the kinetochore binding domain of CENP-E reveals interactions with the kinetochore proteins CENP-F and hBUBR1. J Cell Biol. 143:49-63.

Chan, Y.W., L.L. Fava, A. Uldschmid, M.H. Schmitz, D.W. Gerlich, E.A. Nigg, and A. Santamaria. 2009. Mitotic control of kinetochore-associated dynein and spindle orientation by human Spindly. J Cell Biol. 185:859-74.

Cheeseman, I.M., S. Anderson, M. Jwa, E.M. Green, J. Kang, J.R. Yates, 3rd, C.S. Chan, D.G. Drubin, and G. Barnes. 2002. Phospho-regulation of kinetochore-microtubule attachments by the Aurora kinase Ipl1p. Cell. 111:163-72.

Cheeseman, I.M., J.S. Chappie, E.M. Wilson-Kubalek, and A. Desai. 2006. The conserved KMN network constitutes the core microtubule-binding site of the kinetochore. Cell. 127:983-97.

Cheeseman, I.M., and A. Desai. 2008. Molecular architecture of the kinetochore-microtubule interface. Nat Rev Mol Cell Biol. 9:33-46.

Chen, R.H. 2002. BubR1 is essential for kinetochore localization of other spindle checkpoint proteins and its phosphorylation requires Mad1. J Cell Biol. 158:487-96.

Chen, R.H. 2004. Phosphorylation and activation of Bub1 on unattached chromosomes facilitate the spindle checkpoint. EMBO J. 23:3113-21.

Chen, R.H., D.M. Brady, D. Smith, A.W. Murray, and K.G. Hardwick. 1999. The spindle checkpoint of budding yeast depends on a tight complex between the Mad1 and Mad2 proteins. Mol Biol Cell. 10:2607-18.

Chen, R.H., A. Shevchenko, M. Mann, and A.W. Murray. 1998. Spindle checkpoint protein Xmad1 recruits Xmad2 to unattached kinetochores. J Cell Biol. 143:283-95.

Chen, R.H., J.C. Waters, E.D. Salmon, and A.W. Murray. 1996. Association of spindle assembly checkpoint component XMAD2 with unattached kinetochores. Science. 274:242-6.

Chu, M.L., L.M. Chavas, K.T. Douglas, P.A. Eyers, and L. Tabernero. 2008. Crystal structure of the catalytic domain of the mitotic checkpoint kinase Mps1 in complex with SP600125. J Biol Chem. 283:21495-500.

Chung, E., and R.H. Chen. 2002. Spindle checkpoint requires Mad1-bound and Mad1-free Mad2. Mol Biol Cell. 13:1501-11.

Chung, E., and R.H. Chen. 2003. Phosphorylation of Cdc20 is required for its inhibition by the spindle checkpoint. Nat Cell Biol. 5:748-53.

Ciferri, C., S. Pasqualato, E. Screpanti, G. Varetti, S. Santaguida, G. Dos Reis, A. Maiolica, J. Polka, J.G. De Luca, P. De Wulf, M. Salek, J. Rappsilber, C.A. Moores, E.D. Salmon, and A. Musacchio. 2008. Implications for kinetochore-microtubule attachment from the structure of an engineered Ndc80 complex. Cell. 133:427-39.

Cimini, D. 2008. Merotelic kinetochore orientation, aneuploidy, and cancer. Biochim Biophys Acta. 1786:32-40.

Civril, F., A. Wehenkel, F.M. Giorgi, S. Santaguida, A. Di Fonzo, G. Grigorean, F.D. Ciccarelli, and A. Musacchio. 2010. Structural analysis of the RZZ complex reveals common ancestry with multisubunit vesicle tethering machinery. Structure. 18:616-26.

Crasta, K., H.H. Lim, T.H. Giddings, Jr., M. Winey, and U. Surana. 2008. Inactivation of Cdh1 by synergistic action of Cdk1 and polo kinase is necessary for proper assembly of the mitotic spindle. Nat Cell Biol. 10:665-75.

D'Alise, A.M., G. Amabile, M. Iovino, F.P. Di Giorgio, M. Bartiromo, F. Sessa, F. Villa, A. Musacchio, and R. Cortese. 2008. Reversine, a novel Aurora kinases inhibitor, inhibits colony formation of human acute myeloid leukemia cells. Mol Cancer Ther. 7:1140-9.

De Antoni, A., C.G. Pearson, D. Cimini, J.C. Canman, V. Sala, L. Nezi, M. Mapelli, L. Sironi, M. Faretta, E.D. Salmon, and A. Musacchio. 2005a. The Mad1/Mad2 complex as a template for Mad2 activation in the spindle assembly checkpoint. Curr Biol. 15:214-25.

De Antoni, A., V. Sala, and A. Musacchio. 2005b. Explaining the oligomerization properties of the spindle assembly checkpoint protein Mad2. Philos Trans R Soc Lond B Biol Sci. 360:637-47, discussion 447-8.

De Boer, L., V. Oakes, H. Beamish, N. Giles, F. Stevens, M. Somodevilla-Torres, C. Desouza, and B. Gabrielli. 2008. Cyclin A/cdk2 coordinates centrosomal and nuclear mitotic events. Oncogene. 27:4261-8.

De Souza, C.P., and S.A. Osmani. 2007. Mitosis, not just open or closed. Eukaryot Cell. 6:1521-7.

DeLuca, J.G., Y. Dong, P. Hergert, J. Strauss, J.M. Hickey, E.D. Salmon, and B.F. McEwen. 2005. Hec1 and nuf2 are core components of the kinetochore outer plate essential for organizing microtubule attachment sites. Mol Biol Cell. 16:519-31.

DeLuca, J.G., W.E. Gall, C. Ciferri, D. Cimini, A. Musacchio, and E.D. Salmon. 2006. Kinetochore microtubule dynamics and attachment stability are regulated by Hec1. Cell. 127:969-82.

DeLuca, J.G., B.J. Howell, J.C. Canman, J.M. Hickey, G. Fang, and E.D. Salmon. 2003. Nuf2 and Hec1 are required for retention of the checkpoint proteins Mad1 and Mad2 to kinetochores. Curr Biol. 13:2103-9.

den Elzen, N., and J. Pines. 2001. Cyclin A is destroyed in prometaphase and can delay chromosome alignment and anaphase. J Cell Biol. 153:121-36.

Dephoure, N., C. Zhou, J. Villen, S.A. Beausoleil, C.E. Bakalarski, S.J. Elledge, and S.P. Gygi. 2008. A quantitative atlas of mitotic phosphorylation. Proc Natl Acad Sci U S A. 105:10762-7.

Ditchfield, C., V.L. Johnson, A. Tighe, R. Ellston, C. Haworth, T. Johnson, A. Mortlock, N. Keen, and S.S. Taylor. 2003. Aurora B couples chromosome alignment with anaphase by targeting BubR1, Mad2, and Cenp-E to kinetochores. J Cell Biol. 161:267-80.

Dobles, M., V. Liberal, M.L. Scott, R. Benezra, and P.K. Sorger. 2000. Chromosome missegregation and apoptosis in mice lacking the mitotic checkpoint protein Mad2. Cell. 101:635-45.

Dohadwala, M., E.F. da Cruz e Silva, F.L. Hall, R.T. Williams, D.A. Carbonaro-Hall, A.C. Nairn, P. Greengard, and N. Berndt. 1994. Phosphorylation and inactivation of protein phosphatase 1 by cyclin-dependent kinases. Proc Natl Acad Sci U S A. 91:6408-12.

Dong, Y., K.J. Vanden Beldt, X. Meng, A. Khodjakov, and B.F. McEwen. 2007. The outer plate in vertebrate kinetochores is a flexible network with multiple microtubule interactions. Nat Cell Biol. 9:516-22.

Dorer, R.K., S. Zhong, J.A. Tallarico, W.H. Wong, T.J. Mitchison, and A.W. Murray. 2005. A small-molecule inhibitor of Mps1 blocks the spindle-checkpoint response to a lack of tension on mitotic chromosomes. Curr Biol. 15:1070-6.

Dou, Z., X. Ding, A. Zereshki, Y. Zhang, J. Zhang, F. Wang, J. Sun, H. Huang, and X. Yao. 2004. TTK kinase is essential for the centrosomal localization of TACC2. FEBS Lett. 572:51-6.

Draviam, V.M., F. Stegmeier, G. Nalepa, M.E. Sowa, J. Chen, A. Liang, G.J. Hannon, P.K. Sorger, J.W. Harper, and S.J. Elledge. 2007. A functional genomic screen identifies a role for TAO1 kinase in spindle-checkpoint signalling. Nat Cell Biol. 9:556-64.

Elowe, S., S. Hummer, A. Uldschmid, X. Li, and E.A. Nigg. 2007. Tension-sensitive Plk1 phosphorylation on BubR1 regulates the stability of kinetochore microtubule interactions. Genes Dev. 21:2205-19.

Espeut, J., A. Gaussen, P. Bieling, V. Morin, S. Prieto, D. Fesquet, T. Surrey, and A. Abrieu. 2008. Phosphorylation relieves autoinhibition of the kinetochore motor Cenp-E. Mol Cell. 29:637-43.

Fang, G. 2002. Checkpoint protein BubR1 acts synergistically with Mad2 to inhibit anaphase-promoting complex. Mol Biol Cell. 13:755-66.

Fang, G., H. Yu, and M.W. Kirschner. 1998. The checkpoint protein MAD2 and the mitotic regulator CDC20 form a ternary complex with the anaphase-promoting complex to control anaphase initiation. Genes Dev. 12:1871-83.

Fischer, M.G., S. Heeger, U. Hacker, and C.F. Lehner. 2004. The mitotic arrest in response to hypoxia and of polar bodies during early embryogenesis requires Drosophila Mps1. Curr Biol. 14:2019-24.

Fischle, W., B.S. Tseng, H.L. Dormann, B.M. Ueberheide, B.A. Garcia, J. Shabanowitz, D.F. Hunt, H. Funabiki, and C.D. Allis. 2005. Regulation of HP1-chromatin binding by histone H3 methylation and phosphorylation. Nature. 438:1116-22.

Fisk, H.A., C.P. Mattison, and M. Winey. 2003. Human Mps1 protein kinase is required for centrosome duplication and normal mitotic progression. Proc Natl Acad Sci U S A. 100:14875-80.

Fisk, H.A., C.P. Mattison, and M. Winey. 2004. A field guide to the Mps1 family of protein kinases. Cell Cycle. 3:439-42.

Fisk, H.A., and M. Winey. 2001. The mouse Mps1p-like kinase regulates centrosome duplication. Cell. 106:95-104.

Flemming, W. 1882. Zellsubstanz, Kern und Zelltheilung. Vogel, F .C. W., Liepzig.

Foltz, D.R., L.E. Jansen, B.E. Black, A.O. Bailey, J.R. Yates, 3rd, and D.W. Cleveland. 2006. The human CENP-A centromeric nucleosome-associated complex. Nat Cell Biol. 8:458-69.

Friedman, D.B., J.W. Kern, B.J. Huneycutt, D.B. Vinh, D.K. Crawford, E. Steiner, D. Scheiltz, J. Yates, 3rd, K.A. Resing, N.G. Ahn, M. Winey, and T.N. Davis. 2001. Yeast Mps1p phosphorylates the spindle pole component Spc110p in the N-terminal domain. J Biol Chem. 276:17958-67.

Furuno, N., N. den Elzen, and J. Pines. 1999. Human cyclin A is required for mitosis until mid prophase. J Cell Biol. 147:295-306.

Ganem, N.J., S.A. Godinho, and D. Pellman. 2009. A mechanism linking extra centrosomes to chromosomal instability. Nature. 460:278-82.

Gascoigne, K.E., and S.S. Taylor. 2008. Cancer cells display profound intra- and interline variation following prolonged exposure to antimitotic drugs. Cancer Cell. 14:111-22.

Gavet, O., and J. Pines. 2010a. Activation of cyclin B1-Cdk1 synchronizes events in the nucleus and the cytoplasm at mitosis. J Cell Biol. 189:247-59.

Gavet, O., and J. Pines. 2010b. Progressive activation of CyclinB1-Cdk1 coordinates entry to mitosis. Dev Cell. 18:533-43.

Girdler, F., K.E. Gascoigne, P.A. Eyers, S. Hartmuth, C. Crafter, K.M. Foote, N.J. Keen, and S.S. Taylor. 2006. Validating Aurora B as an anti-cancer drug target. J Cell Sci. 119:3664-75.

Girdler, F., F. Sessa, S. Patercoli, F. Villa, A. Musacchio, and S. Taylor. 2008. Molecular basis of drug resistance in aurora kinases. Chem Biol. 15:552-62.

Glotzer, M., A.W. Murray, and M.W. Kirschner. 1991. Cyclin is degraded by the ubiquitin pathway. Nature. 349:132-8.

Gorbsky, G.J., and W.A. Ricketts. 1993. Differential expression of a phosphoepitope at the kinetochores of moving chromosomes. J Cell Biol. 122:1311-21.

Guimaraes, G.J., Y. Dong, B.F. McEwen, and J.G. Deluca. 2008. Kinetochore-microtubule attachment relies on the disordered N-terminal tail domain of Hec1. Curr Biol. 18:1778-84.

Gurden, M.D.J., A.J. Holland, W. van Zon, A. Tighe, M.A. Vergnolle, D.A. Andres, H.P. Spielmann, M. Malumbres, R.M.F. Wolthuis, D.W. Cleveland, and S.S. Taylor. 2010. Cdc20 is required for the post-anaphase, KEN-dependent degradation of centromere protein F. J Cell Sci. 123:321-30.

Habu, T., S.H. Kim, J. Weinstein, and T. Matsumoto. 2002. Identification of a MAD2-binding protein, CMT2, and its role in mitosis. EMBO J. 21:6419-28.

Hanks, S., K. Coleman, S. Reid, A. Plaja, H. Firth, D. Fitzpatrick, A. Kidd, K. Mehes, R. Nash, N. Robin, N. Shannon, J. Tolmie, J. Swansbury, A. Irrthum, J. Douglas, and N. Rahman. 2004. Constitutional aneuploidy and cancer predisposition caused by biallelic mutations in BUB1B. Nat Genet. 36:1159-61.

Hardwick, K.G., and A.W. Murray. 1995. Mad1p, a phosphoprotein component of the spindle assembly checkpoint in budding yeast. J Cell Biol. 131:709-20.

Hardwick, K.G., E. Weiss, F.C. Luca, M. Winey, and A.W. Murray. 1996. Activation of the budding yeast spindle assembly checkpoint without mitotic spindle disruption. Science. 273:953-6.

Hartwell, L.H., and T.A. Weinert. 1989. Checkpoints: controls that ensure the order of cell cycle events. Science. 246:629-34.

Hastie, C.J., H.J. McLauchlan, and P. Cohen. 2006. Assay of protein kinases using radiolabeled ATP: a protocol. Nat Protoc. 1:968-71.

Hauck, C.R., D.A. Hsia, and D.D. Schlaepfer. 2002. The focal adhesion kinase--a regulator of cell migration and invasion. IUBMB Life. 53:115-9.

Hauf, S., R.W. Cole, S. LaTerra, C. Zimmer, G. Schnapp, R. Walter, A. Heckel, J. van Meel, C.L. Rieder, and J.M. Peters. 2003. The small molecule Hesperadin reveals a role for Aurora B in correcting kinetochore-microtubule attachment and in maintaining the spindle assembly checkpoint. J Cell Biol. 161:281-94.

Hauf, S., E. Roitinger, B. Koch, C.M. Dittrich, K. Mechtler, and J.M. Peters. 2005. Dissociation of cohesin from chromosome arms and loss of arm cohesion during early mitosis depends on phosphorylation of SA2. PLoS Biol. 3:e69.

He, X., M.H. Jones, M. Winey, and S. Sazer. 1998. Mph1, a member of the Mps1-like family of dual specificity protein kinases, is required for the spindle checkpoint in S. pombe. J Cell Sci. 111 (Pt 12):1635-47.

Hershko, A., and A. Ciechanover. 1998. The ubiquitin system. Annu Rev Biochem. 67:425-79.

Herzog, F., I. Primorac, P. Dube, P. Lenart, B. Sander, K. Mechtler, H. Stark, and J.M. Peters. 2009. Structure of the anaphase-promoting complex/cyclosome interacting with a mitotic checkpoint complex. Science. 323:1477-81.

Hewitt, L., A. Tighe, S. Santaguida, A.M. White, C.D. Jones, A. Musacchio, S. Green, and S.S. Taylor. 2010. Sustained Mps1 activity is required in mitosis to recruit OMad2 to the Mad1-C-Mad2 core complex. J Cell Biol. 190:25-34.

Hirota, T., J.J. Lipp, B.H. Toh, and J.M. Peters. 2005. Histone H3 serine 10 phosphorylation by Aurora B causes HP1 dissociation from heterochromatin. Nature. 438:1176-80.

Hogg, D., C. Guidos, D. Bailey, A. Amendola, T. Groves, J. Davidson, R. Schmandt, and G. Mills. 1994. Cell cycle dependent regulation of the protein kinase TTK. Oncogene. 9:89-96.

Holland, A.J., and D.W. Cleveland. 2009. Boveri revisited: chromosomal instability, aneuploidy and tumorigenesis. Nat Rev Mol Cell Biol. 10:478-87.

Holloway, S.L., M. Glotzer, R.W. King, and A.W. Murray. 1993. Anaphase is initiated by proteolysis rather than by the inactivation of maturation-promoting factor. Cell. 73:1393-402.

Holt, S.V., M.A.S. Vergnolle, D. Hussein, M.J. Wozniak, V.J. Allan, and S.S. Taylor. 2005. Silencing Cenp-F weakens centromeric cohesion, prevents chromosome alignment and activates the spindle checkpoint. J Cell Sci. 118:4889-900.

Howell, B.J., D.B. Hoffman, G. Fang, A.W. Murray, and E.D. Salmon. 2000. Visualization of Mad2 dynamics at kinetochores, along spindle fibers, and at spindle poles in living cells. J Cell Biol. 150:1233-50.

Howell, B.J., B.F. McEwen, J.C. Canman, D.B. Hoffman, E.M. Farrar, C.L. Rieder, and E.D. Salmon. 2001. Cytoplasmic dynein/dynactin drives kinetochore protein transport to the spindle poles and has a role in mitotic spindle checkpoint inactivation. J Cell Biol. 155:1159-72.

Howell, B.J., B. Moree, E.M. Farrar, S. Stewart, G. Fang, and E.D. Salmon. 2004. Spindle checkpoint protein dynamics at kinetochores in living cells. Curr Biol. 14:953-64.

Hoyt, M.A., L. Totis, and B.T. Roberts. 1991. S. cerevisiae genes required for cell cycle arrest in response to loss of microtubule function. Cell. 66:507-17.

Huang, H., J. Hittle, F. Zappacosta, R.S. Annan, A. Hershko, and T.J. Yen. 2008. Phosphorylation sites in BubR1 that regulate kinetochore attachment, tension, and mitotic exit. J Cell Biol. 183:667-80.

Hwang, L.H., L.F. Lau, D.L. Smith, C.A. Mistrot, K.G. Hardwick, E.S. Hwang, A. Amon, and A.W. Murray. 1998. Budding yeast Cdc20: a target of the spindle checkpoint. Science. 279:1041-4.

Iwanaga, Y., Y.H. Chi, A. Miyazato, S. Sheleg, K. Haller, J.M. Peloponese, Jr., Y. Li, J.M. Ward, R. Benezra, and K.T. Jeang. 2007. Heterozygous deletion of mitotic arrest-deficient protein 1 (MAD1) increases the incidence of tumors in mice. Cancer Res. 67:160-6.

Janssen, A., G.J. Kops, and R.H. Medema. 2009. Elevating the frequency of chromosome mis-segregation as a strategy to kill tumor cells. Proc Natl Acad Sci U S A. 106:19108-13.

Jeganathan, K., L. Malureanu, D.J. Baker, S.C. Abraham, and J.M. van Deursen. 2007. Bub1 mediates cell death in response to chromosome missegregation and acts to suppress spontaneous tumorigenesis. J Cell Biol. 179:255-67.

Jelluma, N., A.B. Brenkman, I. McLeod, J.R. Yates, 3rd, D.W. Cleveland, R.H. Medema, and G.J. Kops. 2008a. Chromosomal instability by inefficient Mps1 auto-activation due to a weakened mitotic checkpoint and lagging chromosomes. PLoS One. 3:e2415.

Jelluma, N., A.B. Brenkman, N.J. van den Broek, C.W. Cruijsen, M.H. van Osch, S.M. Lens, R.H. Medema, and G.J. Kops. 2008b. Mps1 phosphorylates Borealin to control Aurora B activity and chromosome alignment. Cell. 132:233-46.

Jiang, X.R., G. Jimenez, E. Chang, M. Frolkis, B. Kusler, M. Sage, M. Beeche, A.G. Bodnar, G.M. Wahl, T.D. Tlsty, and C.P. Chiu. 1999. Telomerase expression in human somatic cells does not induce changes associated with a transformed phenotype. Nat Genet. 21:111-4.

Johnson, V.L., M.I.F. Scott, S.V. Holt, D. Hussein, and S.S. Taylor. 2004. Bub1 is required for kinetochore localization of BubR1, Cenp-E, Cenp-F and Mad2, and chromosome congression. J Cell Sci. 117:1577-89.

Jokelainen, P.T. 1967. The ultrastructure and spatial organization of the metaphase kinetochore in mitotic rat cells. J Ultrastruct Res. 19:19-44.

Jones, M.H., B.J. Huneycutt, C.G. Pearson, C. Zhang, G. Morgan, K. Shokat, K. Bloom, and M. Winey. 2005. Chemical genetics reveals a role for Mps1 kinase in kinetochore attachment during mitosis. Curr Biol. 15:160-5.

Kalitsis, P., E. Earle, K.J. Fowler, and K.H. Choo. 2000. Bub3 gene disruption in mice reveals essential mitotic spindle checkpoint function during early embryogenesis. Genes Dev. 14:2277-82.

Kallio, M.J., M.L. McCleland, P.T. Stukenberg, and G.J. Gorbsky. 2002. Inhibition of aurora B kinase blocks chromosome segregation, overrides the spindle checkpoint, and perturbs microtubule dynamics in mitosis. Curr Biol. 12:900-5.

Kan, Z., B.S. Jaiswal, J. Stinson, V. Janakiraman, D. Bhatt, H.M. Stern, P. Yue, P.M. Haverty, R. Bourgon, J. Zheng, M. Moorhead, S. Chaudhuri, L.P. Tomsho, B.A. Peters, K. Pujara, S. Cordes, D.P. Davis, V.E. Carlton, W. Yuan, L. Li, W. Wang, C. Eigenbrot, J.S. Kaminker, D.A. Eberhard, P. Waring, S.C. Schuster, Z. Modrusan, Z. Zhang, D. Stokoe, F.J. de Sauvage, M. Faham, and S. Seshagiri. 2010. Diverse somatic mutation patterns and pathway alterations in human cancers. Nature. 466:869-73.

Kanai, M., Z. Ma, H. Izumi, S.H. Kim, C.P. Mattison, M. Winey, and K. Fukasawa. 2007. Physical and functional interaction between mortalin and Mps1 kinase. Genes Cells. 12:797-810.

Kang, J., Y. Chen, Y. Zhao, and H. Yu. 2007. Autophosphorylation-dependent activation of human Mps1 is required for the spindle checkpoint. Proc Natl Acad Sci U S A. 104:20232-7.

Kang, J., M. Yang, B. Li, W. Qi, C. Zhang, K.M. Shokat, D.R. Tomchick, M. Machius, and H. Yu. 2008. Structure and substrate recruitment of the human spindle checkpoint kinase Bub1. Mol Cell. 32:394-405.

Kapoor, T.M., M.A. Lampson, P. Hergert, L. Cameron, D. Cimini, E.D. Salmon, B.F. McEwen, and A. Khodjakov. 2006. Chromosomes can congress to the metaphase plate before biorientation. Science. 311:388-91.

Kapoor, T.M., T.U. Mayer, M.L. Coughlin, and T.J. Mitchison. 2000. Probing spindle assembly mechanisms with monastrol, a small molecule inhibitor of the mitotic kinesin, Eg5. J Cell Biol. 150:975-88.

Karess, R. 2005. Rod-Zw10-Zwilch: a key player in the spindle checkpoint. Trends Cell Biol. 15:386-92.

Kemmler, S., M. Stach, M. Knapp, J. Ortiz, J. Pfannstiel, T. Ruppert, and J. Lechner. 2009. Mimicking Ndc80 phosphorylation triggers spindle assembly checkpoint signalling. EMBO J. 28:1099-110.

Kim, S.H., D.P. Lin, S. Matsumoto, A. Kitazono, and T. Matsumoto. 1998. Fission yeast Slp1: an effector of the Mad2-dependent spindle checkpoint. Science. 279:1045-7.

Kimura, M., Y. Matsuda, T. Yoshioka, and Y. Okano. 1999. Cell cycle-dependent expression and centrosome localization of a third human aurora/Ipl1-related protein kinase, AIK3. J Biol Chem. 274:7334-40.

Kinoshita, E., E. Kinoshita-Kikuta, K. Takiyama, and T. Koike. 2006. Phosphate-binding tag, a new tool to visualize phosphorylated proteins. Mol Cell Proteomics. 5:749-57.

Kirschner, M., and T. Mitchison. 1986. Beyond self-assembly: From microtubules to morphogenesis. Cell. 45:329-342.

Knight, Z.A., and K.M. Shokat. 2005. Features of selective kinase inhibitors. Chem Biol. 12:621-37.

Kops, G.J., D.R. Foltz, and D.W. Cleveland. 2004. Lethality to human cancer cells through massive chromosome loss by inhibition of the mitotic checkpoint. Proc Natl Acad Sci U S A. 101:8699-704.

Kops, G.J., Y. Kim, B.A. Weaver, Y. Mao, I. McLeod, J.R. Yates, 3rd, M. Tagaya, and D.W. Cleveland. 2005. ZW10 links mitotic checkpoint signaling to the structural kinetochore. J Cell Biol. 169:49-60.

Kops, G.J., A.T. Saurin, and P. Meraldi. 2010. Finding the middle ground: how kinetochores power chromosome congression. Cell Mol Life Sci. 67:2145-61.

Kraft, C., F. Herzog, C. Gieffers, K. Mechtler, A. Hagting, J. Pines, and J.M. Peters. 2003. Mitotic regulation of the human anaphase-promoting complex by phosphorylation. EMBO J. 22:6598-609.

Kulukian, A., J.S. Han, and D.W. Cleveland. 2009. Unattached kinetochores catalyze production of an anaphase inhibitor that requires a Mad2 template to prime Cdc20 for BubR1 binding. Dev Cell. 16:105-17.

Kwiatkowski, N., N. Jelluma, P. Filippakopoulos, M. Soundararajan, M.S. Manak, M. Kwon, H.G. Choi, T. Sim, Q.L. Deveraux, S. Rottmann, D. Pellman, J.V. Shah, G.J. Kops, S. Knapp, and N.S. Gray. 2010. Small-molecule kinase inhibitors provide insight into Mps1 cell cycle function. Nat Chem Biol.

Kwon, Y.G., S.Y. Lee, Y. Choi, P. Greengard, and A.C. Nairn. 1997. Cell cycle-dependent phosphorylation of mammalian protein phosphatase 1 by cdc2 kinase. Proc Natl Acad Sci U S A. 94:2168-73.

Lampson, M.A., and T.M. Kapoor. 2005. The human mitotic checkpoint protein BubR1 regulates chromosome-spindle attachments. Nat Cell Biol. 7:93-8.

Lampson, M.A., K. Renduchitala, A. Khodjakov, and T.M. Kapoor. 2004. Correcting improper chromosome-spindle attachments during cell division. Nat Cell Biol. 6:232-7.

Lan, W., X. Zhang, S.L. Kline-Smith, S.E. Rosasco, G.A. Barrett-Wilt, J. Shabanowitz, D.F. Hunt, C.E. Walczak, and P.T. Stukenberg. 2004. Aurora B phosphorylates centromeric MCAK and regulates its localization and microtubule depolymerization activity. Curr Biol. 14:273-86.

Lauze, E., B. Stoelcker, F.C. Luca, E. Weiss, A.R. Schutz, and M. Winey. 1995. Yeast spindle pole body duplication gene MPS1 encodes an essential dual specificity protein kinase. Embo J. 14:1655-63.

Lenart, P., M. Petronczki, M. Steegmaier, B. Di Fiore, J.J. Lipp, M. Hoffmann, W.J. Rettig, N. Kraut, and J.M. Peters. 2007. The small-molecule inhibitor BI 2536 reveals novel insights into mitotic roles of polo-like kinase 1. Curr Biol. 17:304-15.

Leng, M., D.W. Chan, H. Luo, C. Zhu, J. Qin, and Y. Wang. 2006. MPS1-dependent mitotic BLM phosphorylation is important for chromosome stability. Proc Natl Acad Sci U S A. 103:11485-90.

Lengauer, C., K.W. Kinzler, and B. Vogelstein. 1997. Genetic instability in colorectal cancers. Nature. 386:623-7.

Li, M., X. Fang, Z. Wei, J.P. York, and P. Zhang. 2009. Loss of spindle assembly checkpoint-mediated inhibition of Cdc20 promotes tumorigenesis in mice. J Cell Biol. 185:983-94.

Li, R., and A.W. Murray. 1991. Feedback control of mitosis in budding yeast. Cell. 66:519-31.

Li, X., and R.B. Nicklas. 1995. Mitotic forces control a cell-cycle checkpoint. Nature. 373:630-2.

Li, X., G. Sakashita, H. Matsuzaki, K. Sugimoto, K. Kimura, F. Hanaoka, H. Taniguchi, K. Furukawa, and T. Urano. 2004. Direct association with inner centromere protein (INCENP) activates the novel chromosomal passenger protein, Aurora-C. J Biol Chem. 279:47201-11.

Li, Y., and R. Benezra. 1996. Identification of a human mitotic checkpoint gene: hsMAD2. Science. 274:246-8.

Li, Y., C. Gorbea, D. Mahaffey, M. Rechsteiner, and R. Benezra. 1997. MAD2 associates with the cyclosome/anaphase-promoting complex and inhibits its activity. Proc Natl Acad Sci U S A. 94:12431-6.

Liao, H., G. Li, and T.J. Yen. 1994. Mitotic regulation of microtubule cross-linking activity of CENP-E kinetochore protein. Science. 265:394-8.

Lindberg, R.A., W.H. Fischer, and T. Hunter. 1993. Characterization of a human protein threonine kinase isolated by screening an expression library with antibodies to phosphotyrosine. Oncogene. 8:351-9.

Lindqvist, A., V. Rodriguez-Bravo, and R.H. Medema. 2009. The decision to enter mitosis: feedback and redundancy in the mitotic entry network. J Cell Biol. 185:193-202.

Lingle, W.L., S.L. Barrett, V.C. Negron, A.B. D'Assoro, K. Boeneman, W. Liu, C.M. Whitehead, C. Reynolds, and J.L. Salisbury. 2002. Centrosome amplification drives chromosomal instability in breast tumor development. Proc Natl Acad Sci U S A. 99:1978-83.

Liu, D., G. Vader, M.J. Vromans, M.A. Lampson, and S.M. Lens. 2009. Sensing chromosome bi-orientation by spatial separation of aurora B kinase from kinetochore substrates. Science. 323:1350-3.

Liu, S.T., G.K. Chan, J.C. Hittle, G. Fujii, E. Lees, and T.J. Yen. 2003. Human MPS1 kinase is required for mitotic arrest induced by the loss of CENP-E from kinetochores. Mol Biol Cell. 14:1638-51.

Liu, S.T., J.B. Rattner, S.A. Jablonski, and T.J. Yen. 2006. Mapping the assembly pathways that specify formation of the trilaminar kinetochore plates in human cells. J Cell Biol. 175:41-53.

Lowe, M., C. Rabouille, N. Nakamura, R. Watson, M. Jackman, E. Jamsa, D. Rahman, D.J. Pappin, and G. Warren. 1998. Cdc2 kinase directly phosphorylates the cis-Golgi matrix protein GM130 and is required for Golgi fragmentation in mitosis. Cell. 94:783-93.

Luo, X., G. Fang, M. Coldiron, Y. Lin, H. Yu, M.W. Kirschner, and G. Wagner. 2000. Structure of the Mad2 spindle assembly checkpoint protein and its interaction with Cdc20. Nat Struct Biol. 7:224-9.

Luo, X., Z. Tang, J. Rizo, and H. Yu. 2002. The Mad2 spindle checkpoint protein undergoes similar major conformational changes upon binding to either Mad1 or Cdc20. Mol Cell. 9:59-71.

Luo, X., Z. Tang, G. Xia, K. Wassmann, T. Matsumoto, J. Rizo, and H. Yu. 2004. The Mad2 spindle checkpoint protein has two distinct natively folded states. Nat Struct Mol Biol. 11:338-45.

Maciejowski, J., K.A. George, M.E. Terret, C. Zhang, K.M. Shokat, and P.V. Jallepalli. 2010. Mps1 directs the assembly of Cdc20 inhibitory complexes during interphase and mitosis to control M phase timing and spindle checkpoint signaling. J Cell Biol. 190:89-100.

Malumbres, M., and M. Barbacid. 2005. Mammalian cyclin-dependent kinases. Trends Biochem Sci. 30:630-41.

Malureanu, L.A., K.B. Jeganathan, M. Hamada, L. Wasilewski, J. Davenport, and J.M. van Deursen. 2009. BubR1 N terminus acts as a soluble inhibitor of cyclin B degradation by APC/C(Cdc20) in interphase. Dev Cell. 16:118-31.

Manchester, K.L. 1995. Theodor Boveri and the origin of malignant tumours. Trends Cell Biol. 5:384-7.

Manning, G., D.B. Whyte, R. Martinez, T. Hunter, and S. Sudarsanam. 2002. The protein kinase complement of the human genome. Science. 298:1912-34.

Mao, Y., A. Abrieu, and D.W. Cleveland. 2003. Activating and silencing the mitotic checkpoint through CENP-E-dependent activation/inactivation of BubR1. Cell. 114:87-98.

Mao, Y., A. Desai, and D.W. Cleveland. 2005. Microtubule capture by CENP-E silences BubR1-dependent mitotic checkpoint signaling. J Cell Biol. 170:873-80.

Mapelli, M., F.V. Filipp, G. Rancati, L. Massimiliano, L. Nezi, G. Stier, R.S. Hagan, S. Confalonieri, S. Piatti, M. Sattler, and A. Musacchio. 2006. Determinants of conformational dimerization of Mad2 and its inhibition by p31comet. EMBO J. 25:1273-84.

Mapelli, M., L. Massimiliano, S. Santaguida, and A. Musacchio. 2007. The Mad2 conformational dimer: structure and implications for the spindle assembly checkpoint. Cell. 131:730-43.

Maresca, T.J., and E.D. Salmon. 2009. Intrakinetochore stretch is associated with changes in kinetochore phosphorylation and spindle assembly checkpoint activity. J Cell Biol. 184:373-81.

Maresca, T.J., and E.D. Salmon. 2010. Welcome to a new kind of tension: translating kinetochore mechanics into a wait-anaphase signal. J Cell Sci. 123:825-35.

Martin-Lluesma, S., V.M. Stucke, and E.A. Nigg. 2002. Role of Hec1 in spindle checkpoint signaling and kinetochore recruitment of Mad1/Mad2. Science. 297:2267-70.

Masson, K., and L. Ronnstrand. 2009. Oncogenic signaling from the hematopoietic growth factor receptors c-Kit and Flt3. Cell Signal. 21:1717-26.

Matsumura, S., F. Toyoshima, and E. Nishida. 2007. Polo-like kinase 1 facilitates chromosome alignment during prometaphase through BubR1. J Biol Chem. 282:15217-27.

Matsuura, S., Y. Matsumoto, K. Morishima, H. Izumi, H. Matsumoto, E. Ito, K. Tsutsui, J. Kobayashi, H. Tauchi, Y. Kajiwara, S. Hama, K. Kurisu, H. Tahara, M. Oshimura, K. Komatsu, T. Ikeuchi, and T. Kajii. 2006. Monoallelic BUB1B mutations and defective mitotic-spindle checkpoint in seven families with premature chromatid separation (PCS) syndrome. Am J Med Genet A. 140:358-67.

Mattison, C.P., W.M. Old, E. Steiner, B.J. Huneycutt, K.A. Resing, N.G. Ahn, and M. Winey. 2007. Mps1 activation loop autophosphorylation enhances kinase activity. J Biol Chem. 282:30553-61.

Maure, J.F., E. Kitamura, and T.U. Tanaka. 2007. Mps1 kinase promotes sister-kinetochore bi-orientation by a tension-dependent mechanism. Curr Biol. 17:2175-82.

May, K.M., and K.G. Hardwick. 2006. The spindle checkpoint. J Cell Sci. 119:4139-42.

Mayer, T.U., T.M. Kapoor, S.J. Haggarty, R.W. King, S.L. Schreiber, and T.J. Mitchison. 1999. Small molecule inhibitor of mitotic spindle bipolarity identified in a phenotype-based screen. Science. 286:971-4.

McEwen, B.F., G.K. Chan, B. Zubrowski, M.S. Savoian, M.T. Sauer, and T.J. Yen. 2001. CENP-E is essential for reliable bioriented spindle attachment, but chromosome alignment can be achieved via redundant mechanisms in mammalian cells. Mol Biol Cell. 12:2776-89.

McEwen, B.F., C.E. Hsieh, A.L. Mattheyses, and C.L. Rieder. 1998. A new look at kinetochore structure in vertebrate somatic cells using high-pressure freezing and freeze substitution. Chromosoma. 107:366-75.

McInnes, C., A. Mazumdar, M. Mezna, C. Meades, C. Midgley, F. Scaerou, L. Carpenter, M. Mackenzie, P. Taylor, M. Walkinshaw, P.M. Fischer, and D. Glover. 2006. Inhibitors of Polo-like kinase reveal roles in spindle-pole maintenance. Nat Chem Biol. 2:608-17.

McIntosh, J.R. 1991. Structural and mechanical control of mitotic progression. Cold Spring Harb Symp Quant Biol. 56:613-9.

Meraldi, P., V.M. Draviam, and P.K. Sorger. 2004. Timing and checkpoints in the regulation of mitotic progression. Dev Cell. 7:45-60.

Meraldi, P., and P.K. Sorger. 2005. A dual role for Bub1 in the spindle checkpoint and chromosome congression. EMBO J. 24:1621-33.

Michel, L., E. Diaz-Rodriguez, G. Narayan, E. Hernando, V.V. Murty, and R. Benezra. 2004. Complete loss of the tumor suppressor MAD2 causes premature cyclin B degradation and mitotic failure in human somatic cells. Proc Natl Acad Sci U S A. 101:4459-64.

Michel, L.S., V. Liberal, A. Chatterjee, R. Kirchwegger, B. Pasche, W. Gerald, M. Dobles, P.K. Sorger, V.V. Murty, and R. Benezra. 2001. MAD2 haplo-insufficiency causes premature anaphase and chromosome instability in mammalian cells. Nature. 409:355-9.

Mills, G.B., R. Schmandt, M. McGill, A. Amendola, M. Hill, K. Jacobs, C. May, A.M. Rodricks, S. Campbell, and D. Hogg. 1992. Expression of TTK, a novel human protein kinase, is associated with cell proliferation. J Biol Chem. 267:16000-6.

Morrow, C.J., A. Tighe, V.L. Johnson, M.I.F. Scott, C. Ditchfield, and S.S. Taylor. 2005. Bub1 and aurora B cooperate to maintain BubR1-mediated inhibition of APC/CCdc20. J Cell Sci. 118:3639-52.

Murata-Hori, M., and Y.L. Wang. 2002. The kinase activity of aurora B is required for kinetochore-microtubule interactions during mitosis. Curr Biol. 12:894-9.

Murray, A.W., and M.W. Kirschner. 1989. Cyclin synthesis drives the early embryonic cell cycle. Nature. 339:275-80.

Murray, A.W., M.J. Solomon, and M.W. Kirschner. 1989. The role of cyclin synthesis and degradation in the control of maturation promoting factor activity. Nature. 339:280-6.

Musacchio, A., and E.D. Salmon. 2007. The spindle-assembly checkpoint in space and time. Nat Rev Mol Cell Biol. 8:379-93.

Nasmyth, K. 2002. Segregating sister genomes: the molecular biology of chromosome separation. Science. 297:559-65.

Nezi, L., and A. Musacchio. 2009. Sister chromatid tension and the spindle assembly checkpoint. Curr Opin Cell Biol. 21:785-95.

Nicklas, R.B., S.C. Ward, and G.J. Gorbsky. 1995. Kinetochore chemistry is sensitive to tension and may link mitotic forces to a cell cycle checkpoint. J Cell Biol. 130:929-39.

Nilsson, J., M. Yekezare, J. Minshull, and J. Pines. 2008. The APC/C maintains the spindle assembly checkpoint by targeting Cdc20 for destruction. Nat Cell Biol. 10:1411-20.

Nousiainen, M., H.H. Sillje, G. Sauer, E.A. Nigg, and R. Korner. 2006. Phosphoproteome analysis of the human mitotic spindle. Proc Natl Acad Sci U S A. 103:5391-6.

O'Connell, C.B., J. Loncarek, P. Hergert, A. Kourtidis, D.S. Conklin, and A. Khodjakov. 2008. The spindle assembly checkpoint is satisfied in the absence of interkinetochore tension during mitosis with unreplicated genomes. J Cell Biol. 183:29-36.

O'Connell, K.F., C. Caron, K.R. Kopish, D.D. Hurd, K.J. Kemphues, Y. Li, and J.G. White. 2001. The C. elegans zyg-1 gene encodes a regulator of centrosome duplication with distinct maternal and paternal roles in the embryo. Cell. 105:547-58.

Palframan, W.J., J.B. Meehl, S.L. Jaspersen, M. Winey, and A.W. Murray. 2006. Anaphase inactivation of the spindle checkpoint. Science. 313:680-4.

Paweletz, N. 2001. Walther Flemming: pioneer of mitosis research. Nat Rev Mol Cell Biol. 2:72-5.

Percy, M.J., K.A. Myrie, C.K. Neeley, J.N. Azim, S.P. Ethier, and E.M. Petty. 2000. Expression and mutational analyses of the human MAD2L1 gene in breast cancer cells. Genes Chromosomes Cancer. 29:356-62.

Pereira, G., M. Knop, and E. Schiebel. 1998. Spc98p directs the yeast gamma-tubulin complex into the nucleus and is subject to cell cycle-dependent phosphorylation on the nuclear side of the spindle pole body. Mol Biol Cell. 9:775-93.

Perera, D., and S.S. Taylor. 2010. Sgo1 establishes the centromeric cohesion protection mechanism in G2 before subsequent Bub1-dependent recruitment in mitosis. J Cell Sci.

Perera, D., V. Tilston, J.A. Hopwood, M. Barchi, R.P. Boot-Handford, and S.S. Taylor. 2007. Bub1 maintains centromeric cohesion by activation of the spindle checkpoint. Dev Cell. 13:566-79.

Peter, M., J. Nakagawa, M. Doree, J.C. Labbe, and E.A. Nigg. 1990a. Identification of major nucleolar proteins as candidate mitotic substrates of cdc2 kinase. Cell. 60:791-801.

Peter, M., J. Nakagawa, M. Doree, J.C. Labbe, and E.A. Nigg. 1990b. In vitro disassembly of the nuclear lamina and M phase-specific phosphorylation of lamins by cdc2 kinase. Cell. 61:591-602.

Peters, J.M. 2006. The anaphase promoting complex/cyclosome: a machine designed to destroy. Nat Rev Mol Cell Biol. 7:644-56.

Petersen, J., and I.M. Hagan. 2003. S. pombe aurora kinase/survivin is required for chromosome condensation and the spindle checkpoint attachment response. Curr Biol. 13:590-7.

Petronczki, M., P. Lenart, and J.M. Peters. 2008. Polo on the Rise-from Mitotic Entry to Cytokinesis with Plk1. Dev Cell. 14:646-59.

Pfarr, C.M., M. Coue, P.M. Grissom, T.S. Hays, M.E. Porter, and J.R. McIntosh. 1990. Cytoplasmic dynein is localized to kinetochores during mitosis. Nature. 345:263-5.

Pines, J. 2006. Mitosis: a matter of getting rid of the right protein at the right time. Trends Cell Biol. 16:55-63.

Pines, J., and T. Hunter. 1991. Human cyclins A and B1 are differentially located in the cell and undergo cell cycle-dependent nuclear transport. J Cell Biol. 115:1-17.

Pines, J., and C.L. Rieder. 2001. Re-staging mitosis: a contemporary view of mitotic progression. Nat Cell Biol. 3:E3-6.

Pinsky, B.A., and S. Biggins. 2005. The spindle checkpoint: tension versus attachment. Trends Cell Biol. 15:486-93.

Pinsky, B.A., C. Kung, K.M. Shokat, and S. Biggins. 2006. The Ipl1-Aurora protein kinase activates the spindle checkpoint by creating unattached kinetochores. Nat Cell Biol. 8:78-83.

Poss, K.D., A. Nechiporuk, K.F. Stringer, C. Lee, and M.T. Keating. 2004. Germ cell aneuploidy in zebrafish with mutations in the mitotic checkpoint gene mps1. Genes Dev. 18:1527-32.

Putkey, F.R., T. Cramer, M.K. Morphew, A.D. Silk, R.S. Johnson, J.R. McIntosh, and D.W. Cleveland. 2002. Unstable kinetochore-microtubule capture and chromosomal instability following deletion of CENP-E. Dev Cell. 3:351-65.

Qi, W., Z. Tang, and H. Yu. 2006. Phosphorylation- and polo-box-dependent binding of Plk1 to Bub1 is required for the kinetochore localization of Plk1. Mol Biol Cell. 17:3705-16.

Queralt, E., and F. Uhlmann. 2008. Cdk-counteracting phosphatases unlock mitotic exit. Curr Opin Cell Biol. 20:661-8.

Rahmani, Z., M.E. Gagou, C. Lefebvre, D. Emre, and R.E. Karess. 2009. Separating the spindle, checkpoint, and timer functions of BubR1. J Cell Biol. 187:597-605.

Rieder, C.L., R.W. Cole, A. Khodjakov, and G. Sluder. 1995. The checkpoint delaying anaphase in response to chromosome monoorientation is mediated by an inhibitory signal produced by unattached kinetochores. J Cell Biol. 130:941-8.

Rieder, C.L., A. Khodjakov, L.V. Paliulis, T.M. Fortier, R.W. Cole, and G. Sluder. 1997. Mitosis in vertebrate somatic cells with two spindles: implications for the metaphase/anaphase transition checkpoint and cleavage. Proc Natl Acad Sci U S A. 94:5107-12.

Rieder, C.L., and H. Maiato. 2004. Stuck in division or passing through: what happens when cells cannot satisfy the spindle assembly checkpoint. Dev Cell. 7:637-51.

Rieder, C.L., and R.E. Palazzo. 1992. Colcemid and the mitotic cycle. J Cell Sci. 102 (Pt 3):387-92.

Rieder, C.L., A. Schultz, R. Cole, and G. Sluder. 1994. Anaphase onset in vertebrate somatic cells is controlled by a checkpoint that monitors sister kinetochore attachment to the spindle. J Cell Biol. 127:1301-10.

Rischitor, P.E., K.M. May, and K.G. Hardwick. 2007. Bub1 is a fission yeast kinetochore scaffold protein, and is sufficient to recruit other spindle checkpoint proteins to ectopic sites on chromosomes. PLoS One. 2:e1342.

Roberts, B.T., K.A. Farr, and M.A. Hoyt. 1994. The Saccharomyces cerevisiae checkpoint gene BUB1 encodes a novel protein kinase. Mol Cell Biol. 14:8282-91.

Ruchaud, S., M. Carmena, and W.C. Earnshaw. 2007. The chromosomal passenger complex: one for all and all for one. Cell. 131:230-1.

Santaguida, S., A. Tighe, A.M. D'Alise, S.S. Taylor, and A. Musacchio. 2010. Dissecting the role of MPS1 in chromosome biorientation and the spindle checkpoint through the small molecule inhibitor Reversine. J Cell Biol. 190:73-87.

Sasai, K., H. Katayama, D.L. Stenoien, S. Fujii, R. Honda, M. Kimura, Y. Okano, M. Tatsuka, F. Suzuki, E.A. Nigg, W.C. Earnshaw, W.R. Brinkley, and S. Sen. 2004. Aurora-C kinase is a novel chromosomal passenger protein that can complement Aurora-B kinase function in mitotic cells. Cell Motil Cytoskeleton. 59:249-63.

Schaar, B.T., G.K. Chan, P. Maddox, E.D. Salmon, and T.J. Yen. 1997. CENP-E function at kinetochores is essential for chromosome alignment. J Cell Biol. 139:1373-82.

Schmidt, M., Y. Budirahardja, R. Klompmaker, and R.H. Medema. 2005. Ablation of the spindle assembly checkpoint by a compound targeting Mps1. EMBO Rep. 6:866-72.

Scholey, J.M., I. Brust-Mascher, and A. Mogilner. 2003. Cell division. Nature. 422:746-52.

Scutt, P.J., M.L. Chu, D.A. Sloane, M. Cherry, C.R. Bignell, D.H. Williams, and P.A. Eyers. 2009. Discovery and exploitation of inhibitor-resistant aurora and polo kinase mutants for the analysis of mitotic networks. J Biol Chem. 284:15880-93.

Shah, J.V., E. Botvinick, Z. Bonday, F. Furnari, M. Berns, and D.W. Cleveland. 2004. Dynamics of centromere and kinetochore proteins; implications for checkpoint signaling and silencing. Curr Biol. 14:942-52.

Sharp-Baker, H., and R.H. Chen. 2001. Spindle checkpoint protein Bub1 is required for kinetochore localization of Mad1, Mad2, Bub3, and CENP-E, independently of its kinase activity. J Cell Biol. 153:1239-50.

Shimogawa, M.M., B. Graczyk, M.K. Gardner, S.E. Francis, E.A. White, M. Ess, J.N. Molk, C. Ruse, S. Niessen, J.R. Yates, 3rd, E.G. Muller, K. Bloom, D.J. Odde, and T.N. Davis. 2006. Mps1 phosphorylation of Dam1 couples kinetochores to microtubule plus ends at metaphase. Curr Biol. 16:1489-501.

Simonetta, M., R. Manzoni, R. Mosca, M. Mapelli, L. Massimiliano, M. Vink, B. Novak, A. Musacchio, and A. Ciliberto. 2009. The influence of catalysis on mad2 activation dynamics. PLoS Biol. 7:e10.

Sironi, L., M. Mapelli, S. Knapp, A. De Antoni, K.T. Jeang, and A. Musacchio. 2002. Crystal structure of the tetrameric Mad1-Mad2 core complex: implications of a 'safety belt' binding mechanism for the spindle checkpoint. Embo J. 21:2496-506.

Sirri, V., D. Hernandez-Verdun, and P. Roussel. 2002. Cyclin-dependent kinases govern formation and maintenance of the nucleolus. J Cell Biol. 156:969-81.

Skinner, J.J., S. Wood, J. Shorter, S.W. Englander, and B.E. Black. 2008. The Mad2 partial unfolding model: regulating mitosis through Mad2 conformational switching. J Cell Biol. 183:761-8.

Slattery, S.D., R.V. Moore, B.R. Brinkley, and R.M. Hall. 2008. Aurora-C and Aurora-B share phosphorylation and regulation of CENP-A and Borealin during mitosis. Cell Cycle. 7:787-95.

Sliedrecht, T., C. Zhang, K.M. Shokat, and G.J. Kops. 2010. Chemical genetic inhibition of Mps1 in stable human cell lines reveals novel aspects of Mps1 function in mitosis. PLoS One. 5:e10251.

Smyth, L.A., and I. Collins. 2009. Measuring and interpreting the selectivity of protein kinase inhibitors. J Chem Biol. 2:131-51.

Steegmaier, M., M. Hoffmann, A. Baum, P. Lenart, M. Petronczki, M. Krssak, U. Gurtler, P. Garin-Chesa, S. Lieb, J. Quant, M. Grauert, G.R. Adolf, N. Kraut, J.M. Peters, and W.J. Rettig. 2007. BI 2536, a potent and selective inhibitor of polo-like kinase 1, inhibits tumor growth in vivo. Curr Biol. 17:316-22.

Stern, B.M., and A.W. Murray. 2001. Lack of tension at kinetochores activates the spindle checkpoint in budding yeast. Curr Biol. 11:1462-7.

Stucke, V.M., C. Baumann, and E.A. Nigg. 2004. Kinetochore localization and microtubule interaction of the human spindle checkpoint kinase Mps1. Chromosoma. 113:1-15.

Stucke, V.M., H.H. Sillje, L. Arnaud, and E.A. Nigg. 2002. Human Mps1 kinase is required for the spindle assembly checkpoint but not for centrosome duplication. Embo J. 21:1723-32.

Sudakin, V., G.K. Chan, and T.J. Yen. 2001. Checkpoint inhibition of the APC/C in HeLa cells is mediated by a complex of BUBR1, BUB3, CDC20, and MAD2. J Cell Biol. 154:925-36.

Sumara, I., E. Vorlaufer, P.T. Stukenberg, O. Kelm, N. Redemann, E.A. Nigg, and J.M. Peters. 2002. The dissociation of cohesin from chromosomes in prophase is regulated by Polo-like kinase. Mol Cell. 9:515-25.

Tanaka, T.U., N. Rachidi, C. Janke, G. Pereira, M. Galova, E. Schiebel, M.J. Stark, and K. Nasmyth. 2002. Evidence that the Ipl1-Sli15 (Aurora kinase-INCENP) complex promotes chromosome bi-orientation by altering kinetochore-spindle pole connections. Cell. 108:317-29.

Tang, C.J., C.Y. Lin, and T.K. Tang. 2006. Dynamic localization and functional implications of Aurora-C kinase during male mouse meiosis. Dev Biol. 290:398-410.

Tang, Z., R. Bharadwaj, B. Li, and H. Yu. 2001. Mad2-Independent inhibition of APCCdc20 by the mitotic checkpoint protein BubR1. Dev Cell. 1:227-37.

Tang, Z., H. Shu, D. Oncel, S. Chen, and H. Yu. 2004. Phosphorylation of Cdc20 by Bub1 provides a catalytic mechanism for APC/C inhibition by the spindle checkpoint. Mol Cell. 16:387-97.

Taylor, S., and J.M. Peters. 2008. Polo and Aurora kinases: lessons derived from chemical biology. Curr Opin Cell Biol. 20:77-84.

Taylor, S.S., E. Ha, and F. McKeon. 1998. The human homologue of Bub3 is required for kinetochore localization of Bub1 and a Mad3/Bub1-related protein kinase. J Cell Biol. 142:1-11.

Taylor, S.S., D. Hussein, Y. Wang, S. Elderkin, and C.J. Morrow. 2001. Kinetochore localisation and phosphorylation of the mitotic checkpoint components Bub1 and BubR1 are differentially regulated by spindle events in human cells. J Cell Sci. 114:4385-95.

Taylor, S.S., and F. McKeon. 1997. Kinetochore localization of murine Bub1 is required for normal mitotic timing and checkpoint response to spindle damage. Cell. 89:727-35.

Taylor, S.S., M.I.F. Scott, and A.J. Holland. 2004. The spindle checkpoint: a quality control mechanism which ensures accurate chromosome segregation. Chromosome Res. 12:599-616.

Thompson, S.L., S.F. Bakhoum, and D.A. Compton. 2010. Mechanisms of chromosomal instability. Curr Biol. 20:R285-95.

Thompson, S.L., and D.A. Compton. 2008. Examining the link between chromosomal instability and aneuploidy in human cells. J Cell Biol. 180:665-72.

Tighe, A., V.L. Johnson, M. Albertella, and S.S. Taylor. 2001. Aneuploid colon cancer cells have a robust spindle checkpoint. EMBO Rep. 2:609-14.

Tighe, A., A. Ray-Sinha, O.D. Staples, and S.S. Taylor. 2007. GSK-3 inhibitors induce chromosome instability. BMC Cell Biol. 8:34.

Tighe, A., O. Staples, and S. Taylor. 2008. Mps1 kinase activity restrains anaphase during an unperturbed mitosis and targets Mad2 to kinetochores. J Cell Biol. 181:893-901.

Torres, E.M., T. Sokolsky, C.M. Tucker, L.Y. Chan, M. Boselli, M.J. Dunham, and A. Amon. 2007. Effects of aneuploidy on cellular physiology and cell division in haploid yeast. Science. 317:916-24.

Torres, E.M., B.R. Williams, and A. Amon. 2008. Aneuploidy: cells losing their balance. Genetics. 179:737-46.

Tyler, R.K., M.L. Chu, H. Johnson, E.A. McKenzie, S.J. Gaskell, and P.A. Eyers. 2009. Phosphoregulation of human Mps1 kinase. Biochem J. 417:173-81.

Uchida, K.S., K. Takagaki, K. Kumada, Y. Hirayama, T. Noda, and T. Hirota. 2009. Kinetochore stretching inactivates the spindle assembly checkpoint. J Cell Biol. 184:383-90.

Uetake, Y., and G. Sluder. 2007. Cell-cycle progression without an intact microtuble cytoskeleton. Curr Biol. 17:2081-6.

Vader, G., C.W. Cruijsen, T. van Harn, M.J. Vromans, R.H. Medema, and S.M. Lens. 2007. The chromosomal passenger complex controls spindle checkpoint function independent from its role in correcting microtubule kinetochore interactions. Mol Biol Cell. 18:4553-64.

Vader, G., and S.M. Lens. 2008. The Aurora kinase family in cell division and cancer. Biochim Biophys Acta. 1786:60-72.

Vergnolle, M.A.S., and S.S. Taylor. 2007. Cenp-F links kinetochores to Ndel1/Nde1/Lis1/dynein microtubule motor complexes. Curr Biol. 17:1173-9.

Vermeulen, K., D.R. Van Bockstaele, and Z.N. Berneman. 2003. The cell cycle: a review of regulation, deregulation and therapeutic targets in cancer. Cell Prolif. 36:131-49.

Vigneron, S., S. Prieto, C. Bernis, J.C. Labbe, A. Castro, and T. Lorca. 2004. Kinetochore localization of spindle checkpoint proteins: who controls whom? Mol Biol Cell. 15:4584-96.

Vink, M., M. Simonetta, P. Transidico, K. Ferrari, M. Mapelli, A. De Antoni, L. Massimiliano, A. Ciliberto, M. Faretta, E.D. Salmon, and A. Musacchio. 2006. In vitro FRAP identifies the minimal requirements for Mad2 kinetochore dynamics. Curr Biol. 16:755-66.

Walczak, C.E., and R. Heald. 2008. Mechanisms of mitotic spindle assembly and function. Int Rev Cytol. 265:111-58.

Waldeyer, H.W.G. 1888. Über Karyokinese und ihre Beziehungen zu den Befruchtungsvorgängen. Archiv für mikroskopische Anatomie und Entwicklungsmechanik. 32:1-122.

Wan, X., R.P. O'Quinn, H.L. Pierce, A.P. Joglekar, W.E. Gall, J.G. DeLuca, C.W. Carroll, S.T. Liu, T.J. Yen, B.F. McEwen, P.T. Stukenberg, A. Desai, and E.D. Salmon. 2009. Protein architecture of the human kinetochore microtubule attachment site. Cell. 137:672-84.

Wang, Q., T. Liu, Y. Fang, S. Xie, X. Huang, R. Mahmood, G. Ramaswamy, K.M. Sakamoto, Z. Darzynkiewicz, M. Xu, and W. Dai. 2004. BUBR1 deficiency results in abnormal megakaryopoiesis. Blood. 103:1278-85.

Wang, Y., F. Hu, and S.J. Elledge. 2000. The Bfa1/Bub2 GAP complex comprises a universal checkpoint required to prevent mitotic exit. Curr Biol. 10:1379-82.

Ward, G.E., and M.W. Kirschner. 1990. Identification of cell cycle-regulated phosphorylation sites on nuclear lamin C. Cell. 61:561-77.

Waters, J.C., R.H. Chen, A.W. Murray, and E.D. Salmon. 1998. Localization of Mad2 to kinetochores depends on microtubule attachment, not tension. J Cell Biol. 141:1181-91.

Weaver, B.A., Z.Q. Bonday, F.R. Putkey, G.J. Kops, A.D. Silk, and D.W. Cleveland. 2003. Centromere-associated protein-E is essential for the mammalian mitotic checkpoint to prevent aneuploidy due to single chromosome loss. J Cell Biol. 162:551-63.

Weaver, B.A., and D.W. Cleveland. 2006. Does aneuploidy cause cancer? Curr Opin Cell Biol. 18:658-67.

Weaver, B.A., A.D. Silk, C. Montagna, P. Verdier-Pinard, and D.W. Cleveland. 2007. Aneuploidy acts both oncogenically and as a tumor suppressor. Cancer Cell. 11:25-36.

Wei, J.H., Y.F. Chou, Y.H. Ou, Y.H. Yeh, S.W. Tyan, T.P. Sun, C.Y. Shen, and S.Y. Shieh. 2005. TTK/hMps1 participates in the regulation of DNA damage checkpoint response by phosphorylating CHK2 on threonine 68. J Biol Chem. 280:7748-57.

Weiss, E., and M. Winey. 1996. The Saccharomyces cerevisiae spindle pole body duplication gene MPS1 is part of a mitotic checkpoint. J Cell Biol. 132:111-23.

Weston, C.R., and R.J. Davis. 2007. The JNK signal transduction pathway. Curr Opin Cell Biol. 19:142-9.

Williams, B.C., Z. Li, S. Liu, E.V. Williams, G. Leung, T.J. Yen, and M.L. Goldberg. 2003. Zwilch, a new component of the ZW10/ROD complex required for kinetochore functions. Mol Biol Cell. 14:1379-91.

Williams, B.R., V.R. Prabhu, K.E. Hunter, C.M. Glazier, C.A. Whittaker, D.E. Housman, and A. Amon. 2008. Aneuploidy affects proliferation and spontaneous immortalization in mammalian cells. Science. 322:703-9.

Winey, M., L. Goetsch, P. Baum, and B. Byers. 1991. MPS1 and MPS2: novel yeast genes defining distinct steps of spindle pole body duplication. J Cell Biol. 114:745-54.

Winey, M., and B.J. Huneycutt. 2002. Centrosomes and checkpoints: the MPS1 family of kinases. Oncogene. 21:6161-9.

Wolthuis, R., L. Clay-Farrace, W. van Zon, M. Yekezare, L. Koop, J. Ogink, R. Medema, and J. Pines. 2008. Cdc20 and Cks direct the spindle checkpoint-independent destruction of cyclin A. Mol Cell. 30:290-302.

Wong, O.K., and G. Fang. 2005. Plx1 is the 3F3/2 kinase responsible for targeting spindle checkpoint proteins to kinetochores. J Cell Biol. 170:709-19.

Wong, O.K., and G. Fang. 2007. Cdk1 phosphorylation of BubR1 controls spindle checkpoint arrest and Plk1-mediated formation of the 3F3/2 epitope. J Cell Biol. 179:611-7.

Wood, K.W., R. Sakowicz, L.S. Goldstein, and D.W. Cleveland. 1997. CENP-E is a plus end-directed kinetochore motor required for metaphase chromosome alignment. Cell. 91:357-66.

Wu, J.Q., J.Y. Guo, W. Tang, C.S. Yang, C.D. Freel, C. Chen, A.C. Nairn, and S. Kornbluth. 2009. PP1-mediated dephosphorylation of phosphoproteins at mitotic exit is controlled by inhibitor-1 and PP1 phosphorylation. Nat Cell Biol. 11:644-51.

Xia, G., X. Luo, T. Habu, J. Rizo, T. Matsumoto, and H. Yu. 2004. Conformation-specific binding of p31(comet) antagonizes the function of Mad2 in the spindle checkpoint. EMBO J. 23:3133-43.

Xu, Q., S. Zhu, W. Wang, X. Zhang, W. Old, N. Ahn, and X. Liu. 2009. Regulation of kinetochore recruitment of two essential mitotic spindle checkpoint proteins by Mps1 phosphorylation. Mol Biol Cell. 20:10-20.

Yang, M., B. Li, C.J. Liu, D.R. Tomchick, M. Machius, J. Rizo, H. Yu, and X. Luo. 2008. Insights into mad2 regulation in the spindle checkpoint revealed by the crystal structure of the symmetric mad2 dimer. PLoS Biol. 6:e50.

Yang, M., B. Li, D.R. Tomchick, M. Machius, J. Rizo, H. Yu, and X. Luo. 2007a. p31comet blocks Mad2 activation through structural mimicry. Cell. 131:744-55.

Yang, Z., J. Guo, Q. Chen, C. Ding, J. Du, and X. Zhu. 2005. Silencing mitosin induces misaligned chromosomes, premature chromosome decondensation before anaphase onset, and mitotic cell death. Mol Cell Biol. 25:4062-74.

Yang, Z., A.E. Kenny, D.A. Brito, and C.L. Rieder. 2009. Cells satisfy the mitotic checkpoint in Taxol, and do so faster in concentrations that stabilize syntelic attachments. J Cell Biol. 186:675-84.

Yang, Z., U.S. Tulu, P. Wadsworth, and C.L. Rieder. 2007b. Kinetochore dynein is required for chromosome motion and congression independent of the spindle checkpoint. Curr Biol. 17:973-80.

Yao, X., A. Abrieu, Y. Zheng, K.F. Sullivan, and D.W. Cleveland. 2000. CENP-E forms a link between attachment of spindle microtubules to kinetochores and the mitotic checkpoint. Nat Cell Biol. 2:484-91.

Yasui, Y., T. Urano, A. Kawajiri, K. Nagata, M. Tatsuka, H. Saya, K. Furukawa, T. Takahashi, I. Izawa, and M. Inagaki. 2004. Autophosphorylation of a newly identified site of Aurora-B is indispensable for cytokinesis. J Biol Chem. 279:12997-3003.

Yen, T.J., G. Li, B.T. Schaar, I. Szilak, and D.W. Cleveland. 1992. CENP-E is a putative kinetochore motor that accumulates just before mitosis. Nature. 359:536-9.

Zachariae, W., M. Schwab, K. Nasmyth, and W. Seufert. 1998. Control of cyclin ubiquitination by CDK-regulated binding of Hct1 to the anaphase promoting complex. Science. 282:1721-4.

Zeitlin, S.G., R.D. Shelby, and K.F. Sullivan. 2001. CENP-A is phosphorylated by Aurora B kinase and plays an unexpected role in completion of cytokinesis. J Cell Biol. 155:1147-57.

Zhao, Y., and R.H. Chen. 2006. Mps1 phosphorylation by MAP kinase is required for kinetochore localization of spindle-checkpoint proteins. Curr Biol. 16:1764-9.

Zhu, S., W. Wang, D.C. Clarke, and X. Liu. 2007. Activation of Mps1 promotes transforming growth factor-beta-independent Smad signaling. J Biol Chem. 282:18327-38.

Zich, J., and K.G. Hardwick. 2010. Getting down to the phosphorylated 'nuts and bolts' of spindle checkpoint signalling. Trends Biochem Sci. 35:18-27.

9 | Appendix

Publication:

Hewitt, L.*, A. Tighe*, S. Santaguida, A.M. White, C.D. Jones, A. Musacchio, S. Green, and S.S. Taylor. 2010. Sustained Mps1 activity is required in mitosis to recruit OMad2 to the Mad1-C-Mad2 core complex. *J Cell Biol*. 190:25-34.
**equal contribution*

Published July 12, 2010

Sustained Mps1 activity is required in mitosis to recruit O-Mad2 to the Mad1–C-Mad2 core complex

Laura Hewitt,[1] Anthony Tighe,[1] Stefano Santaguida,[2] Anne M. White,[3] Clifford D. Jones,[3] Andrea Musacchio,[2] Stephen Green,[3] and Stephen S. Taylor[1]

[1]Faculty of Life Sciences, University of Manchester, Manchester M13 9PT, England, UK
[2]Department of Experimental Oncology, European Institute of Oncology, I-20139 Milan, Italy
[3]Cancer and Infection Research Area, AstraZeneca, Cheshire SK10 4TG, England, UK

Mps1 is an essential component of the spindle assembly checkpoint. In this study, we describe a novel Mps1 inhibitor, AZ3146, and use it to probe the role of Mps1's catalytic activity during mitosis. When Mps1 is inhibited before mitotic entry, subsequent recruitment of Mad1 and Mad2 to kinetochores is abolished. However, if Mps1 is inhibited after mitotic entry, the Mad1–C-Mad2 core complex remains kinetochore bound, but O-Mad2 is not recruited to the core. Although inhibiting Mps1 also interferes with chromosome alignment, we see no obvious effect on aurora B activity. In contrast, kinetochore recruitment of centromere protein E (CENP-E), a kinesin-related motor protein, is severely impaired. Strikingly, inhibition of Mps1 significantly increases its own abundance at kinetochores. Furthermore, we show that Mps1 can dimerize and transphosphorylate in cells. We propose a model whereby Mps1 transphosphorylation results in its release from kinetochores, thus facilitating recruitment of O-Mad2 and CENP-E and thereby simultaneously promoting checkpoint signaling and chromosome congression.

Introduction

The Mps1 protein kinase plays an essential role in the spindle assembly checkpoint (SAC; Weiss and Winey, 1996), an inhibitory network that restrains anaphase until all kinetochores are stably attached to spindle microtubules (Musacchio and Salmon, 2007). Recent efforts have revealed that its catalytic activity is required for SAC function and chromosome alignment (Jelluma et al., 2008a,b; Tighe et al., 2008; Kwiatkowski et al., 2010; Sliedrecht et al., 2010; see Santaguida et al. in this issue). Exactly how Mps1 does this is unclear; although its SAC function is linked to kinetochore recruitment of Mad1 and Mad2 (Martin-Lluesma et al., 2002; Liu et al., 2003), Mps1 has also been implicated in aurora B regulation (Jelluma et al., 2008b), possibly explaining its role in chromosome alignment.

Previously, when we used an RNAi complementation assay to inhibit Mps1's catalytic activity, Mad2 was largely undetectable at kinetochores (Tighe et al., 2008). However, Mad1 recruitment was only partially affected, suggesting two possibilities: either Mps1 recruits Mad1 via a noncatalytic role or only low level Mps1 activity is required for Mad1 recruitment. Either way, because Mad1 directly recruits Mad2 to the kinetochore (Chung and Chen, 2002), the simplest explanation was that Mps1 activity promotes the Mad1–Mad2 interaction.

This notion is at odds with current views of Mad2 function (Mapelli et al., 2007). The Mad2 template model posits that a Mad1 dimer acts as the kinetochore receptor for Mad2, which can adopt two conformations, open (O-Mad2) and closed (C-Mad2). When Mad2 binds Mad1, it adopts the closed conformation, forming the Mad1–C-Mad2 core complex. Because Mad2 can dimerize, this core complex in turn recruits two O-Mad2 molecules. These are handed over to Cdc20, and in doing so, Mad2 closes, generating two Cdc20–C-Mad2 complexes. Because the Mad1–C-Mad2 complex is very stable (Howell et al., 2004; Shah et al., 2004; Vink et al., 2006) and probably present in interphase where it binds the

L. Hewitt and A. Tighe contributed equally to this paper.

Correspondence to Stephen S. Taylor: stephen.taylor@manchester.ac.uk

A.M. White's present address is Faculty of Human and Medical Sciences, University of Manchester, Manchester M13 9PT, England, UK.

Abbreviations used in this paper: CENP-E, centromere protein E; RZZ, Rod–Zw10–Zwilch; SAC, spindle assembly checkpoint.

Supplemental Material can be found at:
http://jcb.rupress.org/content/suppl/2010/07/07/jcb.201002133.DC1.html

The Rockefeller University Press $30.00
J. Cell Biol. Vol. 190 No. 1 25–34
www.jcb.org/cgi/doi/10.1083/jcb.201002133

Published July 12, 2010

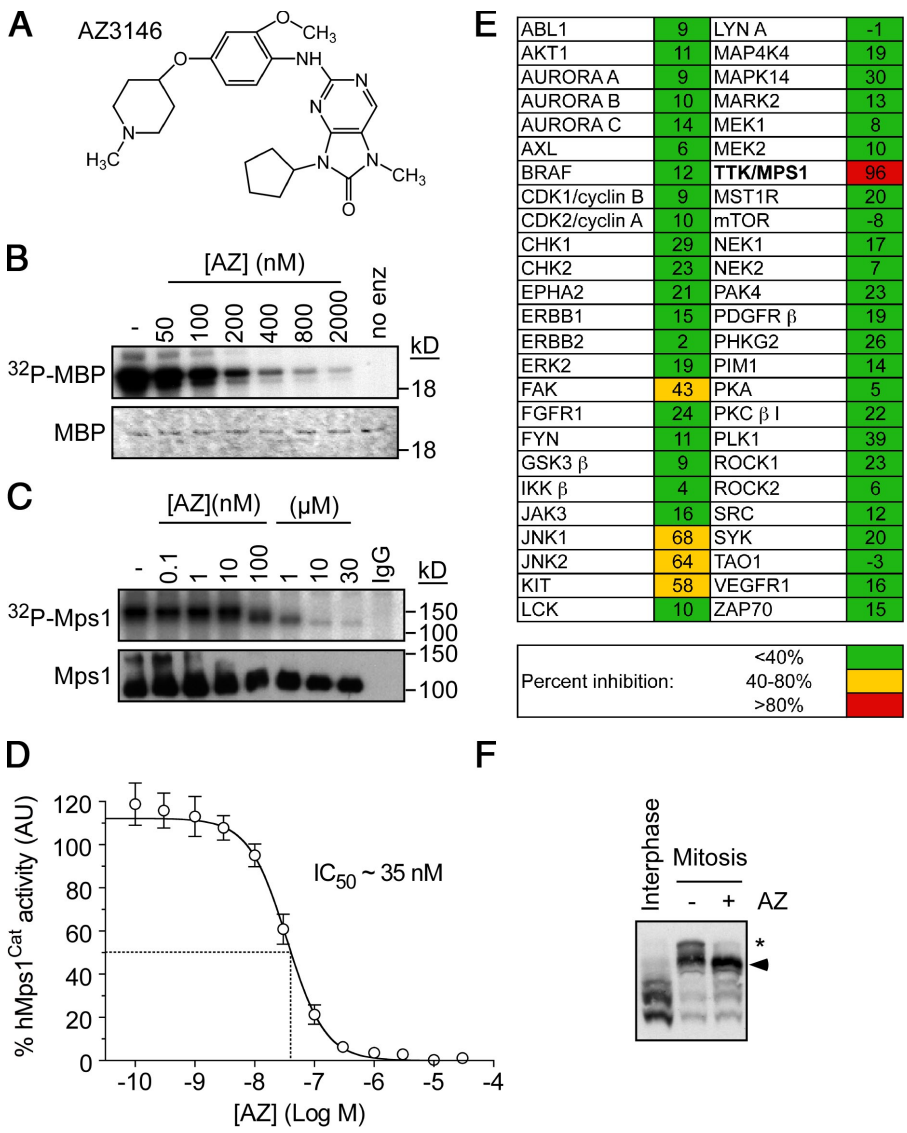

Figure 1. **AZ3146, a novel Mps1 inhibitor.** (A) AZ3146 (AZ) is shown. (B) In vitro kinase assay measuring the ability of $Mps1^{Cat}$ to phosphorylate myelin basic protein (MBP). (C) In vitro kinase assays measuring the activity of Mps1 immunoprecipitated from nocodazole-arrested HeLa cells. (D) Dose–response curve showing inhibition of $Mps1^{Cat}$ by AZ3146. (E) Activity of AZ3146 against a kinase panel. (F) Phos tag immunoblot of Mps1 isolated from interphase cells or nocodazole-arrested cells treated with MG132 ± 2 μM AZ3146 for 2 h. Arrowhead, major band; asterisk, minor band. Error bars indicate SEM derived from three experiments.

nuclear envelope (Campbell et al., 2001), it seems unlikely that Mps1 promotes binding of Mad2 to Mad1.

An alternative explanation comes from the fact that our observations were derived using an antibody against Mad2, called SM2.2 (Tighe et al., 2008). Because kinetochore-bound Mad2 effectively represents two different species, we reasoned that the effect observed in Mps1-deficient cells was not necessarily caused by a complete inability to recruit Mad2, but may reflect an inability to detect it using SM2.2 either because the antibody is conformation specific (i.e., it cannot bind C-Mad2) or possibly because C-Mad2 is masked. If either possibility is true, an attractive hypothesis emerges; if SM2.2 only detects O-Mad2 at kinetochores for whatever reason, perhaps Mps1 kinase activity is required to recruit O-Mad2 to the Mad1–C-Mad2 core complex. In this study, we test this hypothesis using a novel small molecule Mps1 inhibitor.

Results and discussion

AZ3146, a novel Mps1 inhibitor

To identify Mps1 inhibitors, we used a high throughput in vitro kinase assay to screen a compound collection, yielding an inhibitor that was modified to enhance potency and selectivity, resulting in AZ3146 (Fig. 1 A). In in vitro kinase assays, AZ3146 inhibited human $Mps1^{Cat}$ with an IC_{50} (50% inhibitory concentration) of ~35 nM (Fig. 1, B and D). AZ3146 also efficiently inhibited autophosphorylation of full-length Mps1 immunoprecipitated from human cells (Fig. 1 C). Screening a panel of 50 other kinases demonstrated minimal activity against 46 enzymes (Fig. 1 E). Only four kinases were inhibited by >40%, namely FAK, JNK1, JNK2, and KIT. Together, these data suggest that AZ3146 is a reasonably potent and selective Mps1 inhibitor. To measure the effect on Mps1 in cells, we used Phos tag gels to resolve phosphorylated isoforms (Kinoshita et al., 2006). When isolated from mitotic cells, Mps1 appeared as a major band and a minor, slower-migrating band (Fig. 1 F). Upon exposure to AZ3146, the minor band largely disappeared, demonstrating that it clearly inhibits phosphorylation of Mps1 in cells (Fig. 1 F and Fig. S1 B). Mitotic-specific phospho forms of aurora B and BubR1 were not affected by AZ3146 (Fig. S1 C), and AZ3146 did not inhibit Cdk1 or aurora B in mitotic cells (Fig. S1, A and D).

Published July 12, 2010

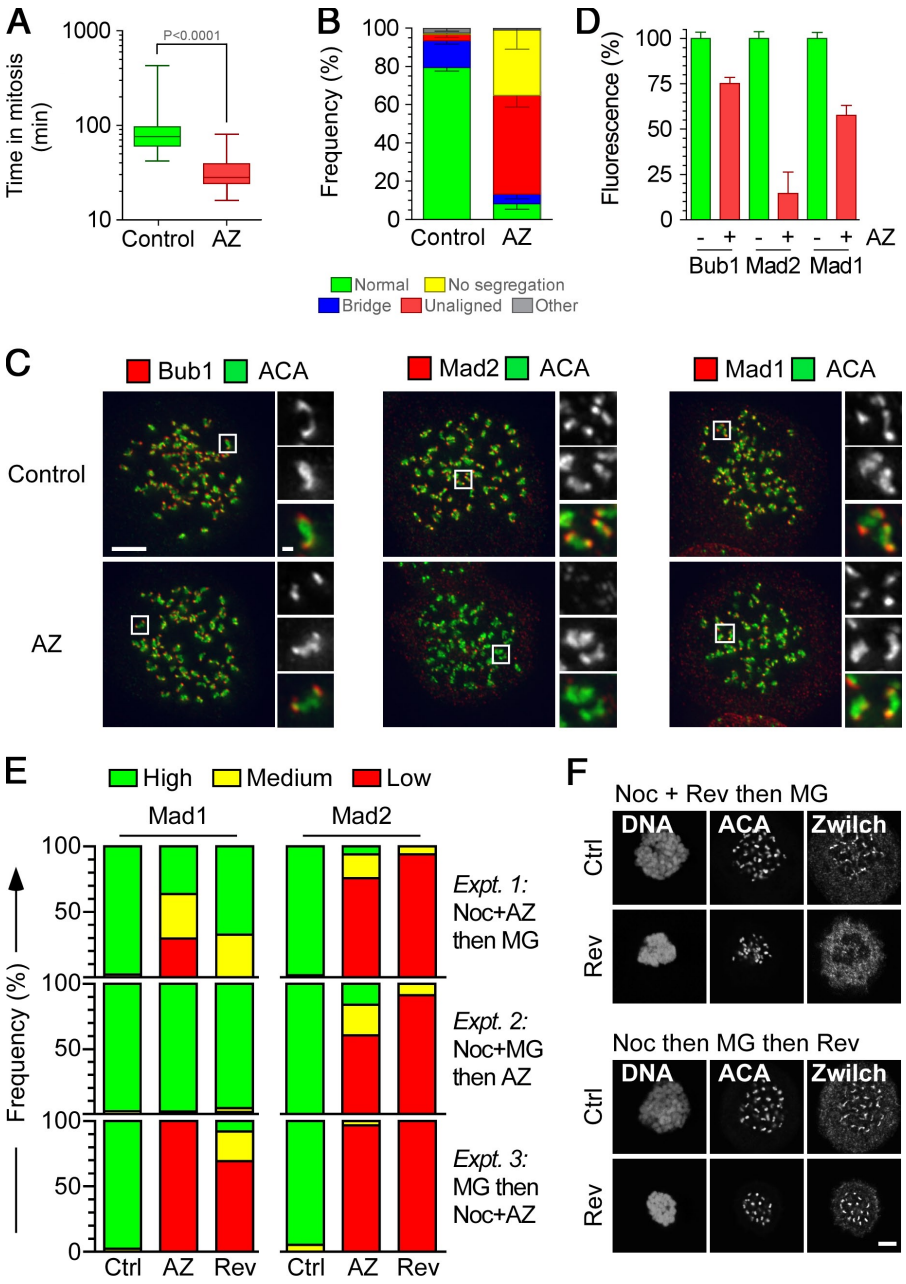

Figure 2. **AZ3146 compromises SAC function and inhibits Mad2 localization.** (A) Box and whisker plot of HeLa GFP-H2B cells treated with or without AZ3146 (AZ) and analyzed by time-lapse microscopy, showing the time from nuclear envelope breakdown to chromosome decondensation. Values were derived from ≥75 cells. (B) Bar graph quantifying mitotic phenotypes. Values were derived from ≥115 cells. (C) Images of HeLa cells treated with nocodazole and MG132 for 2 h with or without AZ3146, fixed, and stained to detect centromeres (ACA) and either Bub1, Mad1, or Mad2. Insets show higher magnification views of individual kinetochore pairs (boxed regions). (D) Bar graph quantifying pixel intensities at kinetochores normalized to ACA in mitotic HeLa cells treated with or without AZ3146. Values were derived from ≥228 kinetochores. (E) Bar graphs scoring kinetochore staining of Mad1/2 as high, medium, or low after exposure to nocodazole (Noc) or MG132 (MG) plus either AZ3146 or reversine (Rev). Data were derived from a two experiments in which at least 50 cells were counted per condition. (F) Images of HeLa cells stained to detect Zwilch and centromeres after exposure to nocodazole, reversine, and MG132 in the sequences indicated. AZ3146 was used at 2 µM and reversine at 500 nM. Ctrl, control. Error bars indicate SEM. Bars: (C and F) 5 µm; (C, insets) 0.5 µm.

AZ3146 overrides the spindle checkpoint

Cell cycle analysis showed that HeLa cells treated with nocodazole and 2 µM AZ3146 only delayed mitosis briefly and then rereplicated their genomes (Fig. S2, A–C), demonstrating that the drug overrides the SAC. AZ3146 also silenced an already established SAC signal; after release from a nocodazole block, AZ3146 dramatically accelerated mitotic exit (Fig. S2 D). This was blocked by MG132, a proteasome inhibitor (Fig. S2 E), ruling out direct inhibition of Cdk1 activity. Time-lapse analysis of HeLa cells expressing a GFP-tagged histone showed that during an otherwise unperturbed mitosis, AZ3146 reduced the time to complete mitosis from ∼90 min in controls to ∼32 min (Fig. 2 A). Strikingly, ∼90% of AZ3146-treated cells underwent abnormal mitoses; although ∼50% entered anaphase without aligning all of their chromosomes, ∼30% exited mitosis without undergoing obvious chromosome segregation (Fig. 2 B). Although AZ3146 had a dramatic effect on kinetochore localization of Mad2, reducing its levels to ∼15%, its effect on Mad1 was less pronounced, with levels remaining at ∼60% (Fig. 2, C and D). These data are entirely consistent with our prior observations, namely a dramatic inhibition of Mad2 and a partial effect on Mad1 (Tighe et al., 2008). Thus, taking together the enzyme data, the SAC override phenotype, and the effect on Mad1 and Mad2 localization, these data show that AZ3146 behaves as one would predict for an Mps1 inhibitor, strongly arguing that it is a useful tool for probing Mps1 function.

Mps1 plays two roles when recruiting Mad1 and Mad2 to kinetochores

We were puzzled why inhibiting Mps1 had a dramatic effect on kinetochore localization of Mad2 but only partially effected Mad1. Indeed, other studies suggest that Mps1 inhibition does

Published July 12, 2010

dramatically affect Mad1 (Jelluma et al., 2008b; Kwiatkowski et al., 2010; Sliedrecht et al., 2010); e.g., inhibition of Mps1 using another small molecule, reversine, blocked recruitment of Mad1 and its kinetochore receptor, the Rod–Zw10–Zwilch (RZZ) complex (Santaguida et al., 2010). We reasoned that these differences may be a result of when Mps1 was first inhibited either before or during mitosis. To test this, we designed three experiments, exposing cells to nocodazole, MG132, and AZ3146, but in different orders. After treatment, cells were fixed, stained, and the intensity of Mad1 at kinetochores was scored as high, medium, or low (Fig. S3 A).

First, we treated cells with nocodazole and AZ3146 for 2 h, adding MG132 for the last hour. Like our previous experiments, in this regimen, some cells should enter mitosis in the presence of AZ3146, whereas others would already be in mitosis. This yielded a mixed effect on Mad1: although some cells still had high levels of Mad1 at kinetochores, others had low levels (Fig. 2 E, Expt. 1). Thus, the aforementioned partial effect on Mad1 (Fig. 2 D) appears to arise from the fact that when we quantitate pixel intensities in a small population of cells, some have relatively normal levels of Mad1 at kinetochores, whereas in others, it is markedly reduced (Fig. S3 A). Next, we treated cells with nocodazole and MG132 for 2 h, adding AZ3146 for the last hour. Because MG132 blocks entry into and exit out of mitosis, in this regimen, all mitotic cells should have entered mitosis before AZ3146 exposure. Under these conditions, Mad1 was now largely unaffected (Fig. 2 E, Expt. 2). Finally, we treated cells with MG132 for 2 h, adding nocodazole and AZ3146 for the last hour. In this regimen, before AZ3146 treatment, all mitotic cells should have aligned chromosomes with kinetochores stripped of Mad1/2 (DeLuca et al., 2003). Therefore, adding nocodazole to destabilize microtubules should lead to rerecruitment of Mad1. Significantly, although Mad1 was present at kinetochores in controls, kinetochores in cells treated with nocodazole plus AZ3146 were devoid of Mad1 (Fig. 2 E, Expt. 3). Note that AZ3146 inhibited kinetochore localization of Mad2 regardless of the experimental regimen (Fig. 2 E).

The simplest explanation for these data is that Mps1 is involved in two distinct steps. First, it is required upon mitotic entry to get Mad1 to kinetochores (or, in the case of experiment 3, it is required in mitosis to rerecruit Mad1 when microtubules are removed from attached kinetochores). Although Mps1 activity is no longer needed to maintain Mad1 localization, it is continuously required during mitosis to promote Mad2 recruitment. Importantly, reversine yielded virtually identical phenotypes (Fig. 2 E). Furthermore, when cells were treated with reversine before mitotic entry, the RZZ component Zwilch was largely absent from kinetochores (Fig. 2 F). However, when cells accumulated in mitosis before exposure to reversine, Zwilch localization was normal.

Mps1 activity is required to recruit O-Mad2 to the Mad1–C-Mad2 core

The aforementioned data suggest that during mitosis, Mps1 activity is required continuously to recruit Mad2 to kinetochore-bound Mad1 (Fig. 2 E, Expt. 2). However, this notion contradicts data showing that the Mad1–C-Mad2 interaction is very stable (Howell et al., 2004; Shah et al., 2004; Vink et al., 2006). Because a key step in checkpoint activation is recruitment of O-Mad2 to kinetochore-bound Mad1–C-Mad2 (Musacchio and Salmon, 2007), we hypothesized that perhaps Mps1 activity is required to recruit O-Mad2 to Mad1–C-Mad2 complexes already at kinetochores. In that case, upon Mps1 inhibition, kinetochore-bound Mad2 should only fall to ∼50% (Fig. 3 A), yet AZ3146 abolishes Mad2 localization (Fig. 2, C–E). Therefore, we speculated that the Mad2 antibody SM2.2 does not efficiently detect C-Mad2 at the kinetochore either because the antibody cannot bind C-Mad2 or because the relevant epitopes are masked.

To test this, we generated cells expressing Myc-tagged Mad2 (Fig. 3 B and Fig. S3 B), reasoning that anti-Myc antibodies might detect it regardless of conformation or cellular context. Interestingly, Mad1 and Mad2 localize to the nuclear envelope in interphase (Campbell et al., 2001; Shah et al., 2004), and although we could readily detect Mad2 there using anti-Myc antibodies, SM2.2 did not decorate the envelope (Fig. 3 C), suggesting that it does not recognize C-Mad2 when bound to Mad1. In mitosis, both anti-Myc antibodies and SM2.2 decorated kinetochores (Fig. 3 D). Significantly, although AZ3146 reduced SM2.2 signal to background levels, anti-Myc antibodies still gave obvious kinetochore staining (Fig. 3, D and E). Importantly, however, quantitation showed that anti-Myc staining was reduced to 45 ± 5% (Fig. 3 E), i.e., approaching the 50% value predicted by our hypothesis.

To test the hypothesis further, we analyzed two Mad2 mutants. Mad2ΔC cannot adopt the closed conformation (Mapelli et al., 2007) or bind Mad1 and, thus, can only bind kinetochores via dimerizing with endogenous C-Mad2 (Fig. 3 A). Mad2RQ can bind Mad1 but cannot dimerize (Mapelli et al., 2007) and, thus, can only target kinetochores by binding Mad1 (Fig. 3 A). If Mps1 is required to recruit O-Mad2 to the core, upon exposure to AZ3146, Mad2ΔC should be absent from kinetochores, whereas Mad2RQ should be unaffected (Fig. 3 A). We generated stable cell lines expressing Myc-Mad2ΔC and Myc-Mad2RQ (Fig. 3 B and Fig. S3 B). Although both mutants localized to kinetochores in mitosis (Fig. 3 D), Myc-Mad2ΔC did not bind the nuclear envelope (Fig. S3 C). However, consistent with our hypothesis in response to AZ3146, Mad2ΔC was no longer abundant at kinetochores, whereas Mad2RQ appeared unaffected (Fig. 3 D). Indeed, quantitation showed that Myc-Mad2ΔC was reduced to a background level, whereas Myc-Mad2RQ remained at ∼90% (Fig. 3 E). Thus, these observations strongly support the notion that during mitosis, Mps1 kinase activity is required to recruit O-Mad2 to kinetochore-bound Mad1–C-Mad2.

Mps1 is required for chromosome alignment

To confirm and further probe the role of Mps1 in chromosome alignment (Maure et al., 2007; Jelluma et al., 2008b), we analyzed the effect of AZ3146 after a monastrol washout (Mayer et al., 1999; Kapoor et al., 2006). Note that cells were also treated with MG132 to prevent mitotic exit caused by SAC override. Under these conditions, AZ3146 inhibited chromosome alignment

Published July 12, 2010

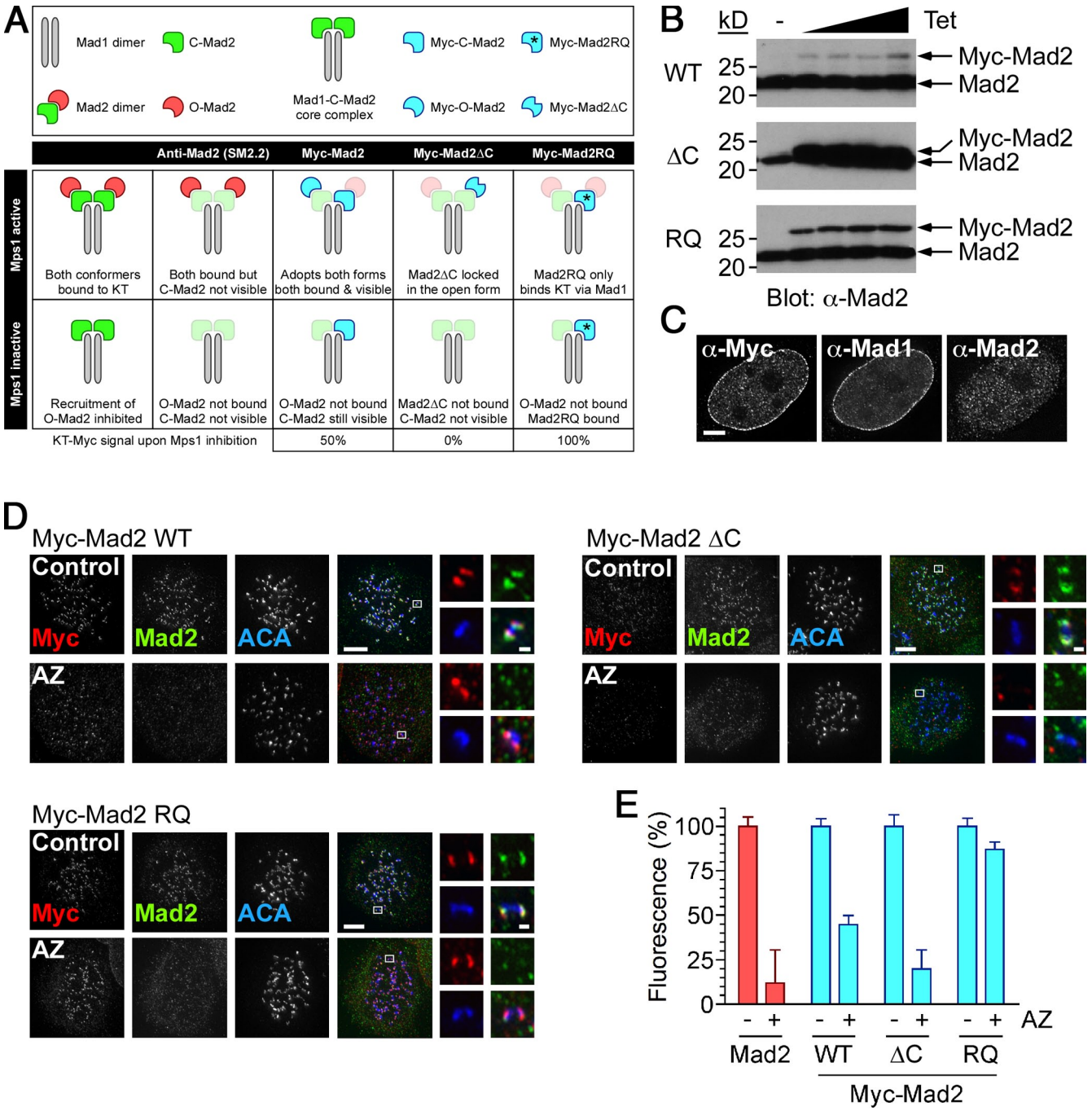

Figure 3. **AZ3146 inhibits kinetochore recruitment of O-Mad2.** (A) A scheme is shown predicting the behavior of endogenous Mad2 and Myc-tagged mutants in cells after inhibition of Mps1 activity. (B) Immunoblots of Tet-induced HeLa lines probed to detect Mad2. (C) Images of an interphase HeLa cell expressing Myc-Mad2 wild type stained to detect Mad1, Mad2 using SM2.2, and an anti-Myc antibody. (D) Images of nocodazole-treated cells stained to detect the Myc tag (red), Mad2 (green), and centromeres (ACA; blue) after a 2-h exposure to 2 µM AZ3146 (AZ) and MG132. Insets show higher magnification views of individual kinetochore pairs (boxed regions). (E) Bar graph quantitating either Mad2 (red) or Myc tag (blue) pixel intensities at kinetochores normalized to ACA. WT, wild type; RQ, Mad2RQ. Values indicate SEM derived from ≥245 kinetochores. Bars: (C and D) 5 µm; (C, insets) 0.5 µm.

in >85% of cells (Fig. 4, A and B), yielding either a mild phenotype with few unaligned chromosomes or a severe phenotype with most chromosomes near the poles (Fig. 4 A). Time-lapse microscopy showed that AZ3146-treated cells typically aligned all but a few chromosomes (Fig. 4 C, 96 min). However, sometime later, sister chromatids appeared to separate followed by rather chaotic attempts to realign (Fig. 4 C, 184 min; and Fig. S2 F). Thus, the mild phenotype appears to reflect Mps1's role in efficient chromosome alignment, whereas the severe phenotype, at least in some cells, may be a consequence of the prolonged mitotic arrest.

Mps1 activity is required for centromere protein E (CENP-E) localization

In light of Mps1 regulating aurora B via borealin phosphorylation (Jelluma et al., 2008b), we were surprised that the alignment

Published July 12, 2010

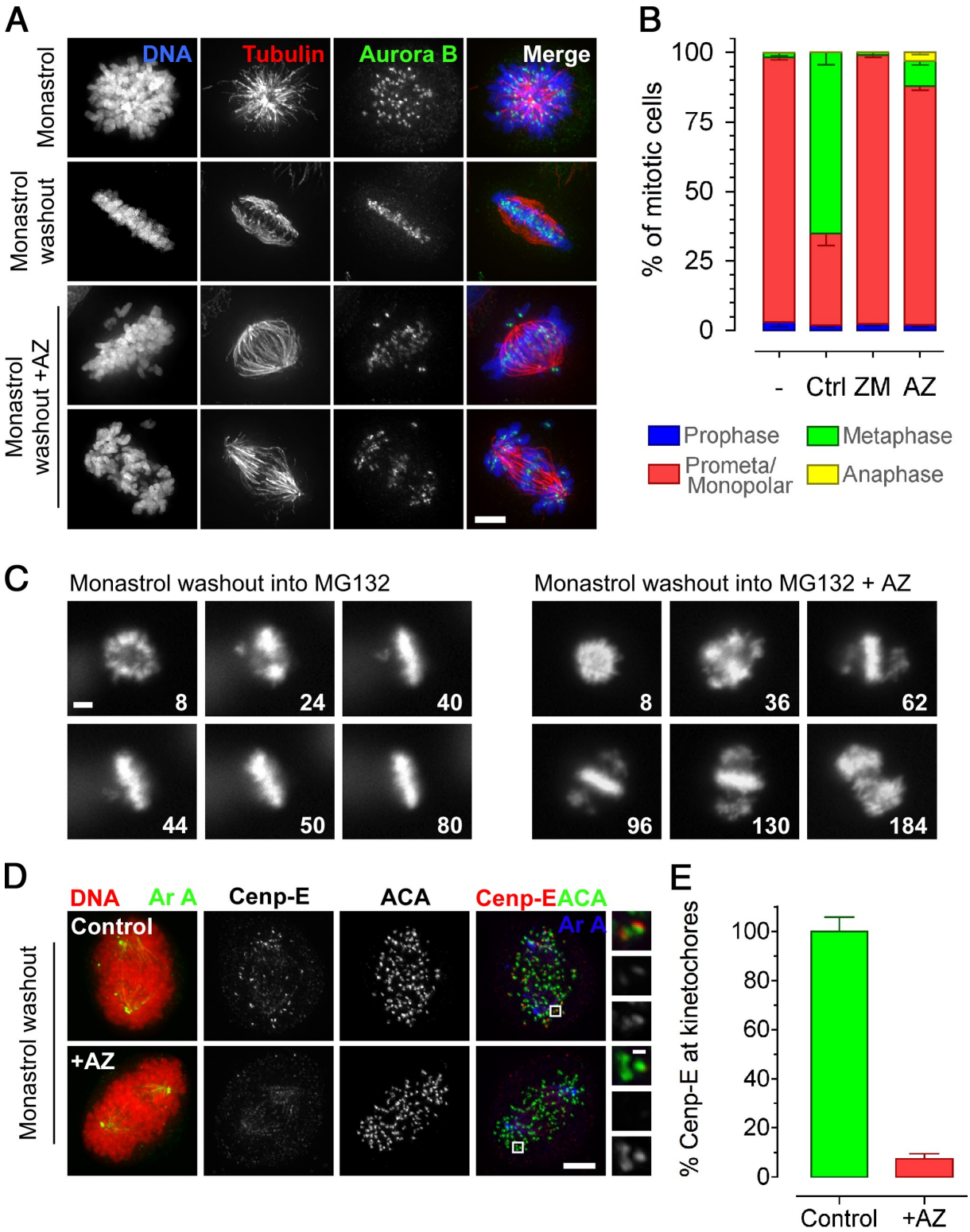

Figure 4. **AZ3146 inhibits chromosome alignment.** (A) Images of HeLa cells stained to detect the chromosomes (blue), tubulin (red), and aurora B (green) after monastrol washout into 2 µM AZ3146 (AZ) and MG132 for 90 min. (B) Bar graph quantitating the mitotic phenotypes observed after monastrol washout into AZ3146 or ZM447439 (ZM). Values were derived from ≥115 cells in three independent experiments. Ctrl, control. (C) Time-lapse sequences of GFP-H2B HeLa cells after monastrol washout into AZ3146 and MG132. Numbers represent minutes after monastrol washout. (D) Images of HeLa cells stained to detect the chromosomes (red), aurora A (green/blue), CENP-E (red), and centromeres (ACA; green) after monastrol washout into AZ3146 and MG132 for 60 min. Insets show higher magnification views of individual kinetochore pairs (boxed regions). (E) Bar graph quantitating CENP-E staining normalized to ACA at polar kinetochores in AZ3146-treated cells. The mean control value is normalized to 100%. At least 300 polar kinetochores were analyzed in ≥23 cells. Error bars indicate SEM. Bars: (A, C, and D) 5 µm; (D, insets) 0.5 µm.

Published July 12, 2010

defect was not typical of that observed after aurora B inhibition (Ditchfield et al., 2003). Indeed, AZ3146 had no obvious effect on several bona fide aurora B substrates (Fig. S1, D–F). Therefore, we turned our attention to other factors to explain the chromosome alignment defect. The phenotype observed in AZ3146-treated cells is quite exquisite; most chromosomes align, K-fibers are evident (Fig. 4 A), and only a few chromosomes remain near the spindle poles (Fig. 4, A–C). This reminded us of the phenotype typical of CENP-E inhibition (Wood et al., 1997; Weaver et al., 2003; Kapoor et al., 2006). Strikingly, 1 h after monastrol washout, the level of CENP-E at kinetochores was reduced to ∼10% (Fig. 4, D and E). Consistent with this being an on-target effect of AZ3146, when Mps1-RNAi cells were reconstituted with the $Mps1^{M602A}$ allele, 1NM-PP1 inhibited kinetochore localization of CENP-E (Fig. S3 D). Thus, CENP-E appears to be an important downstream effector of Mps1 kinase activity. Note that this is entirely consistent with a previous study analyzing *Xenopus laevis* egg extracts (Abrieu et al., 2001).

Inhibition of Mps1 increases its abundance at kinetochores

These data indicate that Mps1 contributes to mitotic fidelity by promoting kinetochore recruitment of O-Mad2 and Cenp-E. Although detailing the exact molecular mechanisms will require further experimentation, one observation may prove informative. In the presence of AZ3146, Mps1 staining at kinetochores increased by about sixfold (Fig. 5, A and B). This is not simply caused by increasing epitope accessibility, as direct fluorescence from a GFP-Mps1 fusion was also more evident at kinetochores in AZ3146-treated cells (Fig. 5 E).

To confirm that this reflected an on-target effect of AZ3146, we compared kinetochore localization of wild-type and kinase-dead GFP-Mps1 fusions after repression of the endogenous kinase by RNAi (Tighe et al., 2008). Strikingly, the kinase-dead mutant was about eightfold more abundant at kinetochores compared with wild-type (Fig. 5, C and D), supporting the notion that inhibiting Mps1's activity does indeed increase its levels at kinetochores. Because FRAP experiments have shown that GFP-Mps1 has a relatively short residency time at kinetochores (Howell et al., 2004), one explanation is that inhibiting Mps1 activity reduces its turnover at kinetochores.

Mps1 dimerizes and transphosphorylates

Importantly, the GFP-Mps1 kinase-dead fusion only increased at kinetochores when we repressed the endogenous kinase (Fig. 5 C). Therefore, we wondered whether Mps1 functions as a dimer that requires transphosphorylation to be released from the kinetochore. Interestingly, Mps1 transphosphorylation has been demonstrated in vitro, but there is no evidence to support dimerization in cells (Kang et al., 2007). Therefore, we transiently transfected GFP-tagged Mps1 into cells stably expressing Myc-tagged Mps1. Myc-tagged proteins were immunoprecipitated and blotted to detect GFP. When we immunoprecipitated Myc-Mps1, GFP-Mps1 was readily detectable (Fig. 5 F and Fig. S3 E), which is consistent with dimerization. Interestingly, when either fusion was catalytically active, a portion of the Myc-tagged protein was phosphorylated (Fig. 5 F). In contrast, when both fusions were catalytically inactive, the Myc-Mps1 band shift was absent (Fig. 5 F, lane 4). Together, these observations support the notion that Mps1 does dimerize and transphosphorylate in mitotic cells. Whether this regulates its localization requires further investigation.

Coupling SAC signaling with chromosome congression

Our observations suggest a two-step role for Mps1. Around the onset of mitosis, Mps1 activity is required to first recruit the Mad1–C-Mad2 core to kinetochores, possibly indirectly by promoting RZZ recruitment. During mitosis, Mps1 activity is continuously required to recruit O-Mad2 to the Mad1–C-Mad2 core. Although Mps1 may achieve this directly, e.g., by phosphorylating the core or O-Mad2, this seems unlikely because the Mad2 template mechanism can be recapitulated in vitro without Mps1 activity (Vink et al., 2006). Therefore, perhaps Mps1 kinase activity counters a cellular inhibitor not present in these in vitro assays. Interestingly, $p31^{comet}$ may act as an inhibitory "cap" on the Mad1–C-Mad2 core (Musacchio and Salmon, 2007). Thus, an attractive hypothesis is that Mps1 phosphorylates and inactivates $p31^{comet}$, removing the inhibitory cap to allow recruitment of O-Mad2 and thereby kick starting the Mad2 template reaction. However, we presently have no evidence linking Mps1 and $p31^{comet}$. As Mps1 levels at kinetochores increase when its activity is blocked, perhaps Mps1 is itself an inhibitory cap that must be released for checkpoint signaling. Having first recruited the Mad1–C-Mad2 core, perhaps Mps1 transphosphorylation promotes an autorelease mechanism that allows recruitment of O-Mad2, kick starting the Mad2 template mechanism.

We confirm a role for Mps1 activity in chromosome alignment. Although we observe no obvious effect on aurora B function, Mps1 activity is clearly required for CENP-E recruitment after monastrol washout. Interestingly, however, Mps1-RNAi did not prevent CENP-E recruitment (Jelluma et al., 2008b; Tighe et al., 2008). Because inactive Mps1 accumulates at kinetochores, perhaps Mps1 and CENP-E occupy mutually exclusive binding sites. In this scenario, Mps1 autorelease would normally expose the CENP-E–binding site. However, when its catalytic activity is inhibited, Mps1 blocks CENP-E recruitment by remaining bound to the kinetochore. In contrast, when the entire Mps1 protein is depleted by RNAi, the CENP-E–binding site is vacant, allowing its recruitment. Consistent with this notion, the levels of kinetochore-bound CENP-E have been observed to increase after Mps1 depletion (Jelluma et al., 2008b). Although speculative, these ideas warrant further exploration and should provide interesting insights into how Mps1 coordinates spindle checkpoint signaling and chromosome congression.

Materials and methods

Inhibitor screen

N-terminal GST-tagged full-length human Mps1 kinase (GenBank accession no. NM_003318) was expressed in insect cells and purified via the GST epitope tag. A 12 µl mixture of recombinant enzyme, an FITC-labeled peptide substrate (FITC-DHTGFLTEYVATR-$CONH_2$), 12 µM ATP, and a buffer solution (50 mM Hepes, pH 7.5, 0.015% vol/vol Brij-35, 1 mM DTT, and 10 mM $MgCl_2$) were incubated with test compounds at room temperature for 25 min. Test compounds were prepared and further diluted in DMSO and placed into 384-well low volume white polystyrene plates (Greiner) using an acoustic liquid handler (Echo; Labcyte, Inc.). Reactions were stopped by the

Published July 12, 2010

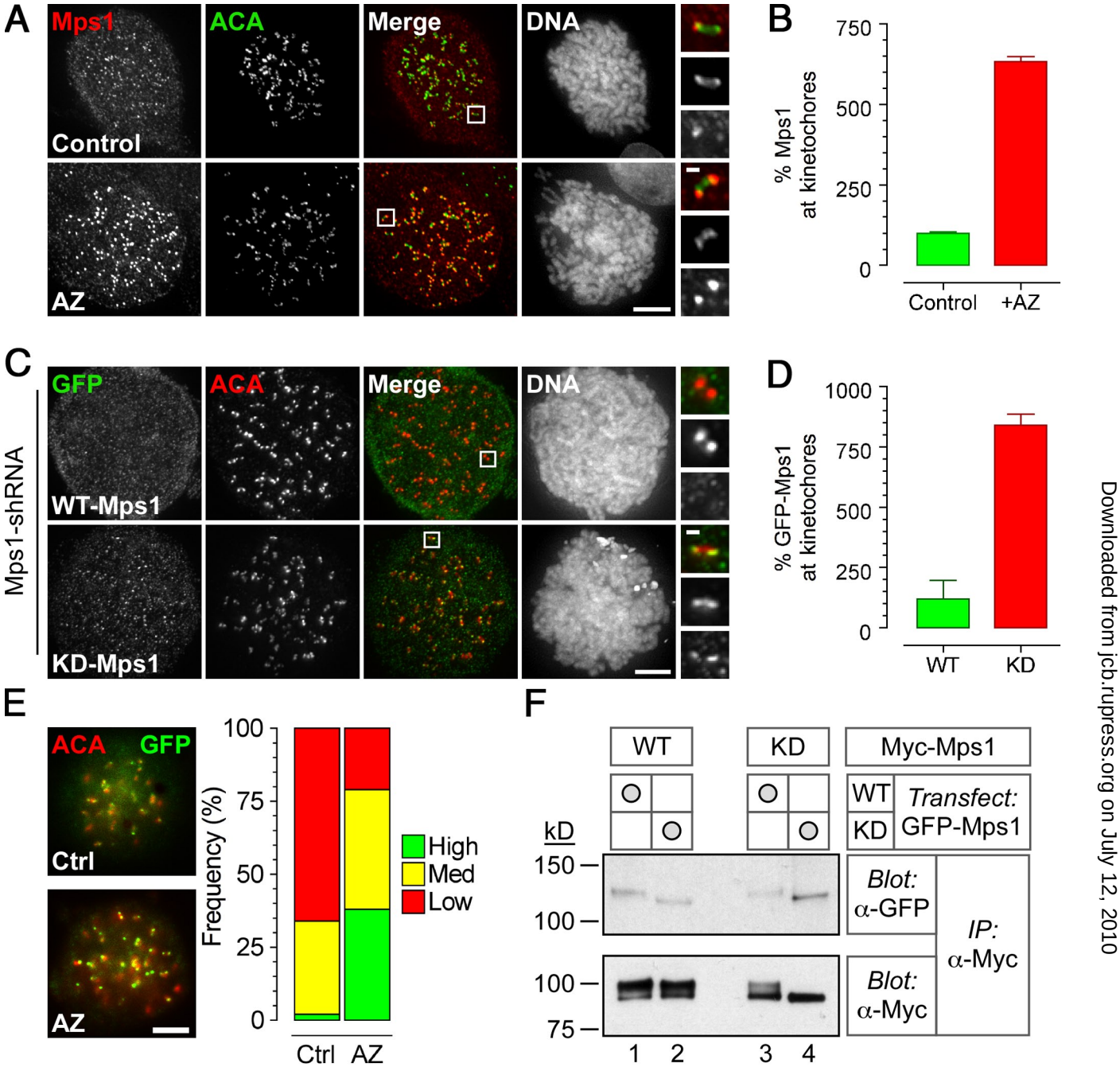

Figure 5. **AZ3146 enhances kinetochore localization of Mps1.** (A) Images of HeLa stained to detect Mps1 (red), centromeres (ACA; green), and the chromosomes after treatment with nocodazole and MG132 for 2 h ± 2 µM AZ3146 (AZ). (B) Bar graph quantitating Mps1 at kinetochores normalized to ACA. Values were derived from ≥345 kinetochores in ≥18 cells with the mean in control cells normalized to 100%. (C) Images of HeLa cells expressing GFP-Mps1, either wild type (WT) or kinase dead (KD), stained to detect GFP-Mps1 (green), centromeres (ACA; red), and chromosomes. Note that endogenous Mps1 was first repressed by RNAi. Before fixation, cells were treated with nocodazole and MG132 for 2 h with or without AZ3146. (D) Bar graph quantitating GFP pixel intensities at kinetochores normalized to ACA. Values were derived from ≥240 kinetochores in ≥17 cells with the mean in controls cells normalized to 100%. (E) Images of HeLa cells expressing GFP-Mps1 treated with or without AZ3146 and a bar graph scoring direct GFP fluorescence from kinetochores as high, medium, or low are shown. Data are representative of two independent experiments in which ≥50 cells were counted. Ctrl, control. (F) Immunoblots of anti-Myc immune complexes isolated from HEK293 cells stably expressing Myc-tagged Mps1 transgenes and transiently transfected with vectors encoding GFP-tagged Mps1 transgenes, either wild type or kinase dead. Membranes were blotted as indicated. IP, immunoprecipitation. (A and C) Insets show higher magnification views of individual kinetochore pairs (boxed regions). Error bars indicate SEM. Bars: (A, C, and E) 5 µm; (A and C, insets) 0.5 µm.

addition of 40 mM, 0.1% coating reagent (Caliper Life Sciences), 100 mM Hepes, pH 7.5, 0.015% vol/vol Brij-35, and 5% DMSO. Inhibitors of Mps1 activity were identified using a microfluidic chip and laser-induced fluorescence (LabChip LC3000; Caliper Life Sciences) to measure the conversion of the fluorescent-labeled peptide to a phosphorylated product.

In vitro kinase assays

His-tagged human $Mps1^{Cat}$ encoding amino acids 510–857 was generated as described previously (Chu et al., 2008). For kinase assays, 500 ng was added to buffer (25 mM Tris-HCl, pH 7.4, 100 mM NaCl, 50 µg/ml BSA, 0.1 mM EGTA, 0.1% β-mercaptoethanol, 10 mM $MgCl_2$, and 0.5 µg/ml

Published July 12, 2010

myelin basic protein), AZ3146, and 100 µM γ-[^{32}P]ATP (2 µCi/assay). Reactions were incubated at 30°C for 20 min, spotted onto P81 paper, washed in 0.5% phosphoric acid, and immersed in acetone. Phosphate incorporation was determined by scintillation counting. For immunoprecipitation kinase assays, HeLa cells were treated with nocodazole for 14 h, mitotic cells isolated, washed in PBS, and lysed for 30 min in 50 mM Tris-HCl, pH 7.4, 100 mM NaCl, 0.5% NP-40, 5 mM EDTA, 5 mM EGTA, 40 mM β-glycerophosphate, 0.2 mM PMSF, 1 mM DTT, 1 mM sodium orthovanadate, 20 mM sodium fluoride, 1 µM okadaic acid (EMD), and complete EDTA-free protease inhibitor cocktail (Roche). Full-length Mps1 was immunoprecipitated as described previously (Holland et al., 2007). Purified complexes were washed with lysis buffer containing 100 mM NaCl and assayed as described for the recombinant protein. To quantify ^{32}P incorporation, reactions were stopped with SDS sample buffer and separated by SDS-PAGE followed by phosphorimaging. The plate (Fujifilm) was analyzed using a phosphorimager (FLA-3000; Fujifilm) using AIDA software (Raytest Isotopenmessgerate GmbH). To assess the specificity of AZ3146, a single-point screen was carried using kinase profiling service (SelectScreen; Invitrogen). 50 kinases were selected and assayed with 1 µM AZ3146.

Cell lines and drugs

Parental HeLa cells, HeLa cells expressing GFP-tagged histone H2B, and Flp-in T-REx HeLa cells were used (Taylor and McKeon, 1997; Morrow et al., 2005; Tighe et al., 2008) and cultured as described previously (Taylor et al., 2001). Flp-in T-REx HEK293 cells were used as described previously (Tighe et al., 2004). A human Mad2 cDNA (Johnson et al., 2004) was cloned into pcDNA5/FRT/TO and mutagenized (QuickChange; Agilent Technologies) to create Mad2ΔC (Mad2 lacking amino acids 196–205) and Mad2 R133E, Q134A (Table S1). The resulting vectors were cotransfected into Flp-in T-REx HeLa cells with the Flp recombinase–encoding plasmid pOG44 (Tighe et al., 2004). Hygromycin-resistant colonies were pooled, expanded, and transgene expression was induced with 500 ng/ml tetracycline (Sigma-Aldrich). Nocodazole, taxol, monastrol, and MG132 (Sigma-Aldrich) were used at a final concentration of 0.2 µg/ml, 10 µM, 100 µM, and 20 µM, respectively. ZM447439 (Tocris) was used at 2 µM. The Mps1 inhibitor AZ3146 was used at a final concentration of 2 µM unless otherwise stated.

Cell biology and RNAi

DNA content, mitotic index measurement, and synchronization of HeLa cells at G1/S using a double-thymidine block were performed as described previously (Taylor and McKeon, 1997). In brief, cells were fixed in 70% ethanol, stained with MPM-2 antibodies (Millipore) followed by a FITC-conjugated donkey anti–mouse antibody (Jackson ImmunoResearch Laboratories, Inc.), and stained with propidium iodide. Flow cytometric analysis was performed using a Cyan (Dako). For inhibitor washout experiments, cells grown on coverslips were treated with monastrol for 4 h. The cells were washed twice with media and once with media containing AZ3146 and MG132. 2 h later, the cells were processed for immunofluorescence. For analysis by time-lapse microscopy, HeLa cells stably expressing GFP–histone H2B were cultured on 30-mm glass-bottomed dishes (MatTek Co) and treated with monastrol for 2 h. The cells were washed before being imaged as described previously (Morrow et al., 2005). Repression of endogenous Mps1 was performed as described previously (Tighe et al., 2008). In brief, cells were seeded into a 24-well plate and transfected using Lipofectamine Plus (Invitrogen) with an Mps1 shRNA plasmid. The DNA–lipid complexes were added to the cells, and 24 h later, the cells were replated onto coverslips or 6-well plates and analyzed 24 h later. To analyze the effect of reversine on Zwilch localization, two regimens were used. To ensure that cells were in mitosis before addition of reversine, HeLa cells were first treated with 3.3 µM nocodazole for 12 h, and 10 µM MG132 was added for 30 min followed by 0.5 µM reversine for 1.5 h. To allow cells to enter mitosis in the presence of reversine, cells were first synchronized at G1/S using a double-thymidine arrest. 5 h after release, the cells were treated with 3.3 µM nocodazole and 0.5 µM reversine for 2 h followed by 10 µM MG132 for 1.5 h.

Antibody techniques and Phos tag gels

Immunoprecipitations, immunoblotting, and immunofluorescence were performed as described previously (Tighe et al., 2004; Morrow et al., 2005; Tighe et al., 2008) using the antibodies described in Table S2. In brief, cells were harvested and lysed on ice for 30 min. Lysates were cleared by centrifugation, precleared with protein G–Sepharose, and incubated for 2 h with antibody-coupled beads. After washing in lysis buffer, isolated proteins were resolved by SDS-PAGE, transferred onto a PVDF membrane (Millipore), blocked in 5% milk, and primary antibodies were added overnight. After washing and incubation with appropriate secondary antibodies, proteins were visualized using chemiluminescence (SuperSignal; Thermo Fisher Scientific) and imaged on film (Biomax MR; Kodak). For immunofluorescence, cells grown on coverslips were fixed in 1% formaldehyde, quenched in glycine, pH 8.5, permeabilized using PBS plus 0.1% Triton X-100 (PBST), and incubated with primary antibodies. After washes in PBST and incubation with appropriate secondary antibodies, cells were counterstained with 1 µg/ml Hoechst 33358 in PBST and mounting in 90% glycerol and 20 mM Tris-HCl, pH 8.0. To visualize microtubules, cells were preextracted in 100 mM Pipes, 1 mM $MgCl_2$, 0.1 mM $CaCl_2$, and 0.1% Triton X-100 for 90 s before fixation in 4% formaldehyde in the same buffer for 10 min. To stain for CENP-E, cells were preextracted with a buffer containing 20 mM Tris-HCl, pH 7.4, 150 mM NaCl, 0.1% BSA, and 0.2% Triton X-100 for 2 min before fixation with 4% formaldehyde in PBS (Chan et al., 2000). Phos tag (Wako Chemicals USA, Inc.) was used according to the manufacturer's instructions. In brief, 25 µM Phos tag and 50 µM $MnCl_2$ were added to standard SDS-PAGE gels containing 6% acrylamide and visualized by immunoblotting.

Image acquisition and processing

Immunofluorescence images were acquired at room temperature on a restoration microscope (Delta Vision RT; Applied Precision) using a 100× 1.40 NA Plan Apo objective and a filter set (Sedat Quad; Chroma Technology Corp.). The images were collected at room temperature using a charge-coupled device camera (CoolSNAP HQ; Photometrics) with a z-optical spacing of 0.2 µm. Raw images were deconvolved using the SoftWorx software (Applied Precision), and maximum intensity projections of these deconvolved images are described in Results and discussion. Time-lapse microscopy was performed on a manual microscope (Axiovert 200; Carl Zeiss, Inc.) equipped with an automated stage (PZ-2000; Applied Biosystems) and an environmental control chamber (Solent Scientific), which maintained the cells at 37°C in a humidified stream of 5% CO_2. Imaging was performed using either a 32× 0.40 NA long-distance A-Plan or a 40× 0.75 NA Neo Fluor objective. Shutters, filter wheels, and point visiting were driven by MetaMorph software (Universal Imaging). Images were taken using a camera (CoolSNAP HQ; Photometrics), and individual tagged image file format files were imported into PhotoShop (Adobe) for printing or into QuickTime (Apple) for videos.

Online supplemental material

Fig. S1 shows that AZ3146 does not inhibit Cdk1 or aurora B. Fig. S2 shows that AZ3146 overrides the spindle checkpoint. Fig. S3 shows that Mps1 activity is required for kinetochore localization of CENP-E. Table S1 lists the PCR primers used in this study. Table S2 lists the antibodies used in this study. Online supplemental material is available at http://www.jcb.org/cgi/content/full/jcb.201002133/DC1.

We are grateful to Bill Earnshaw, Don Cleveland, and Keith Gull for reagents and to members of the Taylor laboratory for comments on the manuscript.

L. Hewitt is supported by a studentship from the Biotechnology and Biological Sciences Research Council and the University of Manchester Alumni Funds. A. Tighe is funded by Cancer Research UK, S. Santaguida is supported by a fellowship of the Italian Foundation for Cancer Research, S. Green and C.D. Jones are employees of AstraZeneca UK Ltd, and S.S. Taylor is supported by a Senior Fellowship from Cancer Research UK.

Submitted: 24 February 2010
Accepted: 5 June 2010

References

Abrieu, A., L. Magnaghi-Jaulin, J.A. Kahana, M. Peter, A. Castro, S. Vigneron, T. Lorca, D.W. Cleveland, and J.C. Labbé. 2001. Mps1 is a kinetochore-associated kinase essential for the vertebrate mitotic checkpoint. *Cell.* 106:83–93. doi:10.1016/S0092-8674(01)00410-X

Campbell, M.S., G.K. Chan, and T.J. Yen. 2001. Mitotic checkpoint proteins HsMAD1 and HsMAD2 are associated with nuclear pore complexes in interphase. *J. Cell Sci.* 114:953–963.

Chan, G.K., S.A. Jablonski, D.A. Starr, M.L. Goldberg, and T.J. Yen. 2000. Human Zw10 and ROD are mitotic checkpoint proteins that bind to kinetochores. *Nat. Cell Biol.* 2:944–947. doi:10.1038/35046598

Chu, M.L., L.M. Chavas, K.T. Douglas, P.A. Eyers, and L. Tabernero. 2008. Crystal structure of the catalytic domain of the mitotic checkpoint kinase Mps1 in complex with SP600125. *J. Biol. Chem.* 283:21495–21500. doi:10.1074/jbc.M803026200

Chung, E., and R.H. Chen. 2002. Spindle checkpoint requires Mad1-bound and Mad1-free Mad2. *Mol. Biol. Cell.* 13:1501–1511. doi:10.1091/mbc.02-01-0003

DeLuca, J.G., B.J. Howell, J.C. Canman, J.M. Hickey, G. Fang, and E.D. Salmon. 2003. Nuf2 and Hec1 are required for retention of the checkpoint proteins Mad1 and Mad2 to kinetochores. *Curr. Biol.* 13:2103–2109. doi:10.1016/j.cub.2003.10.056

Ditchfield, C., V.L. Johnson, A. Tighe, R. Ellston, C. Haworth, T. Johnson, A. Mortlock, N. Keen, and S.S. Taylor. 2003. Aurora B couples chromosome alignment with anaphase by targeting BubR1, Mad2, and Cenp-E to kinetochores. *J. Cell Biol.* 161:267–280. doi:10.1083/jcb.200208091

Holland, A.J., F. Böttger, O. Stemmann, and S.S. Taylor. 2007. Protein phosphatase 2A and separase form a complex regulated by separase autocleavage. *J. Biol. Chem.* 282:24623–24632. doi:10.1074/jbc.M702545200

Howell, B.J., B. Moree, E.M. Farrar, S. Stewart, G. Fang, and E.D. Salmon. 2004. Spindle checkpoint protein dynamics at kinetochores in living cells. *Curr. Biol.* 14:953–964. doi:10.1016/j.cub.2004.05.053

Jelluma, N., A.B. Brenkman, I. McLeod, J.R. Yates III, D.W. Cleveland, R.H. Medema, and G.J. Kops. 2008a. Chromosomal instability by inefficient Mps1 auto-activation due to a weakened mitotic checkpoint and lagging chromosomes. *PLoS One.* 3:e2415. doi:10.1371/journal.pone.0002415

Jelluma, N., A.B. Brenkman, N.J. van den Broek, C.W. Cruijsen, M.H. van Osch, S.M. Lens, R.H. Medema, and G.J. Kops. 2008b. Mps1 phosphorylates Borealin to control Aurora B activity and chromosome alignment. *Cell.* 132:233–246. doi:10.1016/j.cell.2007.11.046

Johnson, V.L., M.I. Scott, S.V. Holt, D. Hussein, and S.S. Taylor. 2004. Bub1 is required for kinetochore localization of BubR1, Cenp-E, Cenp-F and Mad2, and chromosome congression. *J. Cell Sci.* 117:1577–1589. doi:10.1242/jcs.01006

Kang, J., Y. Chen, Y. Zhao, and H. Yu. 2007. Autophosphorylation-dependent activation of human Mps1 is required for the spindle checkpoint. *Proc. Natl. Acad. Sci. USA.* 104:20232–20237. doi:10.1073/pnas.0710519105

Kapoor, T.M., M.A. Lampson, P. Hergert, L. Cameron, D. Cimini, E.D. Salmon, B.F. McEwen, and A. Khodjakov. 2006. Chromosomes can congress to the metaphase plate before biorientation. *Science.* 311:388–391. doi:10.1126/science.1122142

Kinoshita, E., E. Kinoshita-Kikuta, K. Takiyama, and T. Koike. 2006. Phosphate-binding tag, a new tool to visualize phosphorylated proteins. *Mol. Cell. Proteomics.* 5:749–757.

Kwiatkowski, N., N. Jelluma, P. Filippakopoulos, M. Soundararajan, M.S. Manak, M. Kwon, H.G. Choi, T. Sim, Q.L. Deveraux, S. Rottmann, et al. 2010. Small-molecule kinase inhibitors provide insight into Mps1 cell cycle function. *Nat. Chem. Biol.* 6:359–368. doi:10.1038/nchembio.345

Liu, S.T., G.K. Chan, J.C. Hittle, G. Fujii, E. Lees, and T.J. Yen. 2003. Human MPS1 kinase is required for mitotic arrest induced by the loss of CENP-E from kinetochores. *Mol. Biol. Cell.* 14:1638–1651. doi:10.1091/mbc.02-05-0074

Mapelli, M., L. Massimiliano, S. Santaguida, and A. Musacchio. 2007. The Mad2 conformational dimer: structure and implications for the spindle assembly checkpoint. *Cell.* 131:730–743. doi:10.1016/j.cell.2007.08.049

Martin-Lluesma, S., V.M. Stucke, and E.A. Nigg. 2002. Role of Hec1 in spindle checkpoint signaling and kinetochore recruitment of Mad1/Mad2. *Science.* 297:2267–2270. doi:10.1126/science.1075596

Maure, J.F., E. Kitamura, and T.U. Tanaka. 2007. Mps1 kinase promotes sister-kinetochore bi-orientation by a tension-dependent mechanism. *Curr. Biol.* 17:2175–2182. doi:10.1016/j.cub.2007.11.032

Mayer, T.U., T.M. Kapoor, S.J. Haggarty, R.W. King, S.L. Schreiber, and T.J. Mitchison. 1999. Small molecule inhibitor of mitotic spindle bipolarity identified in a phenotype-based screen. *Science.* 286:971–974. doi:10.1126/science.286.5441.971

Morrow, C.J., A. Tighe, V.L. Johnson, M.I. Scott, C. Ditchfield, and S.S. Taylor. 2005. Bub1 and aurora B cooperate to maintain BubR1-mediated inhibition of APC/CCdc20. *J. Cell Sci.* 118:3639–3652. doi:10.1242/jcs.02487

Musacchio, A., and E.D. Salmon. 2007. The spindle-assembly checkpoint in space and time. *Nat. Rev. Mol. Cell Biol.* 8:379–393. doi:10.1038/nrm2163

Santaguida, S., A. Tighe, A.M. D'Alise, S.S. Taylor, and A. Musacchio. 2010. Dissecting the role of MPS1 in chromosome biorientation and the spindle checkpoint through the small molecule inhibitor reversine. *J. Cell Biol.* 190:73–87.

Shah, J.V., E. Botvinick, Z. Bonday, F. Furnari, M. Berns, and D.W. Cleveland. 2004. Dynamics of centromere and kinetochore proteins; implications for checkpoint signaling and silencing. *Curr. Biol.* 14:942–952.

Sliedrecht, T., C. Zhang, K.M. Shokat, and G.J. Kops. 2010. Chemical genetic inhibition of Mps1 in stable human cell lines reveals novel aspects of Mps1 function in mitosis. *PLoS One.* 5:e10251. doi:10.1371/journal.pone.0010251

Taylor, S.S., and F. McKeon. 1997. Kinetochore localization of murine Bub1 is required for normal mitotic timing and checkpoint response to spindle damage. *Cell.* 89:727–735. doi:10.1016/S0092-8674(00)80255-X

Taylor, S.S., D. Hussein, Y. Wang, S. Elderkin, and C.J. Morrow. 2001. Kinetochore localisation and phosphorylation of the mitotic checkpoint components Bub1 and BubR1 are differentially regulated by spindle events in human cells. *J. Cell Sci.* 114:4385–4395.

Tighe, A., V.L. Johnson, and S.S. Taylor. 2004. Truncating APC mutations have dominant effects on proliferation, spindle checkpoint control, survival and chromosome stability. *J. Cell Sci.* 117:6339–6353. doi:10.1242/jcs.01556

Tighe, A., O. Staples, and S. Taylor. 2008. Mps1 kinase activity restrains anaphase during an unperturbed mitosis and targets Mad2 to kinetochores. *J. Cell Biol.* 181:893–901. doi:10.1083/jcb.200712028

Vink, M., M. Simonetta, P. Transidico, K. Ferrari, M. Mapelli, A. De Antoni, L. Massimiliano, A. Ciliberto, M. Faretta, E.D. Salmon, and A. Musacchio. 2006. In vitro FRAP identifies the minimal requirements for Mad2 kinetochore dynamics. *Curr. Biol.* 16:755–766. doi:10.1016/j.cub.2006.03.057

Weaver, B.A., Z.Q. Bonday, F.R. Putkey, G.J. Kops, A.D. Silk, and D.W. Cleveland. 2003. Centromere-associated protein-E is essential for the mammalian mitotic checkpoint to prevent aneuploidy due to single chromosome loss. *J. Cell Biol.* 162:551–563. doi:10.1083/jcb.200303167

Weiss, E., and M. Winey. 1996. The *Saccharomyces cerevisiae* spindle pole body duplication gene MPS1 is part of a mitotic checkpoint. *J. Cell Biol.* 132:111–123. doi:10.1083/jcb.132.1.111

Wood, K.W., R. Sakowicz, L.S. Goldstein, and D.W. Cleveland. 1997. CENP-E is a plus end-directed kinetochore motor required for metaphase chromosome alignment. *Cell.* 91:357–366. doi:10.1016/S0092-8674(00)80419-5

Published July 12, 2010

Hewitt et al., http://www.jcb.org/cgi/content/full/jcb.201002133/DC1

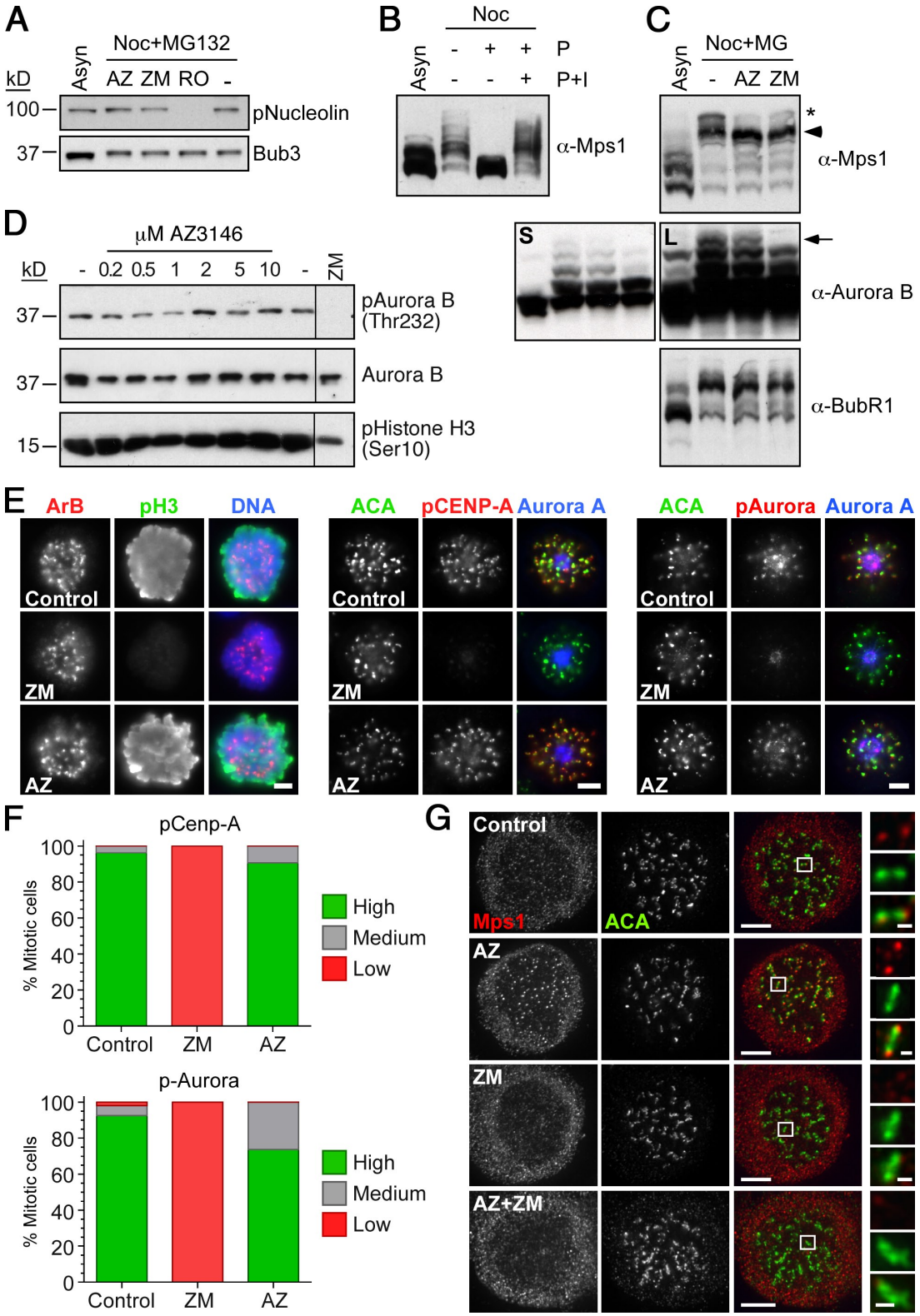

Published July 12, 2010

Figure S1. **AZ3146 does not inhibit Cdk1 or aurora B.** (A) Immunoblot of mitotic-arrested HeLa cells treated for 2 h with MG132 and either AZ3146 (AZ; Mps1 inhibitor), ZM447439 (ZM; aurora B inhibitor; Ditchfield et al., 2003), or RO-31-8220 (RO; Cdk1 inhibitor; Tighe et al., 2007) and blotted with an antibody to detect phosphonucleolin. Bub3 is used as a loading control. AZ3146 does not inhibit phosphorylation of nucleolin, suggesting that it does not target Cdk1. (B) Phos tag immunoblot of cell extracts isolated from interphase cells or nocodazole (Noc)-arrested cells treated with λ-phosphatase (P) ± 10 mM sodium orthovanadate (P + I), demonstrating that the super-shifted species are Mps1 phospho forms. (C) Phos tag immunoblot of extracts isolated from interphase cells or nocodazole-arrested cells treated with MG132 (MG) and either AZ3146 or ZM447439 for 2 h. When isolated from mitotic cells, Mps1 appeared as a major band (arrowhead) and a minor slower-migrating band (asterisk). The super-shifted isoform of Mps1 (asterisk) is reduced upon treatment with either AZ3146 or ZM447439. The faint super-shifted aurora B isoform (arrow) is absent in the presence of ZM447439. Short and long exposures of the aurora B blot are shown. Collectively, these data are consistent with aurora B being upstream of Mps1. The super-shifted forms of BubR1 are not affected by either drug. (D) Immunoblots of nocodazole-arrested HeLa cells treated with MG132 and increasing concentrations of AZ3146 for 2 h, then blotted to detect aurora B, aurora B when phosphorylated on threonine 232 in the T loop, and pHistone $H3^{Ser10}$. Note that although ZM447439 inhibits phosphorylation of aurora B and histone H3, AZ3146 does not. Black lines indicate that intervening lanes have been spliced out. (E) Immunofluorescence images of cells treated with ZM447439 or AZ3146 for 2 h and stained to detect aurora B, pHistone $H3^{Ser10}$, and DNA (left); pCENP-A^{Ser7}, ACA, and aurora A (middle); and pAurora A/B, ACA, and aurora A (right). The cells were also treated with nocodazole (left) or monastrol (middle and right) and MG132. Note that ZM447439 inhibits phosphorylation of histone $H3^{Ser10}$ and CENP-A^{Ser7} as well as the centromere signal revealed by the pan pAurora antibody. In contrast, AZ3146 inhibits none of these markers of aurora B activity. (F) Bar graphs scoring pCENP-A^{Ser7} and centromeric pAurora staining as either high, medium, or low in cells treated with spindle toxins and MG132 plus either AZ3146 or ZM447439 (as in E), confirming that although ZM447439 inhibits CENP-A^{Ser7} and aurora B phosphorylation, AZ3146 does not. Data are representative of two independent experiments in which ≥50 cells were counted per condition. (G) Projections of deconvolved image stacks showing HeLa cells treated with nocodazole and MG132 plus AZ3146 and/or ZM447439 and stained to detect Mps1 (red) and centromeres (ACA; green). Insets show magnified views of kinetochore pairs (boxed regions). Consistent with data in Fig. 5, kinetochore localization of Mps1 is more apparent in AZ3146-treated cells. However, this is reversed in cells treated with ZM447439, suggesting that kinetochore localization of Mps1 requires aurora B activity. AZ3146 was used at 2 µM in all experiments except that shown in D. Bars: (E and G) 5 µm; (G, insets) 0.5 µm.

Published July 12, 2010

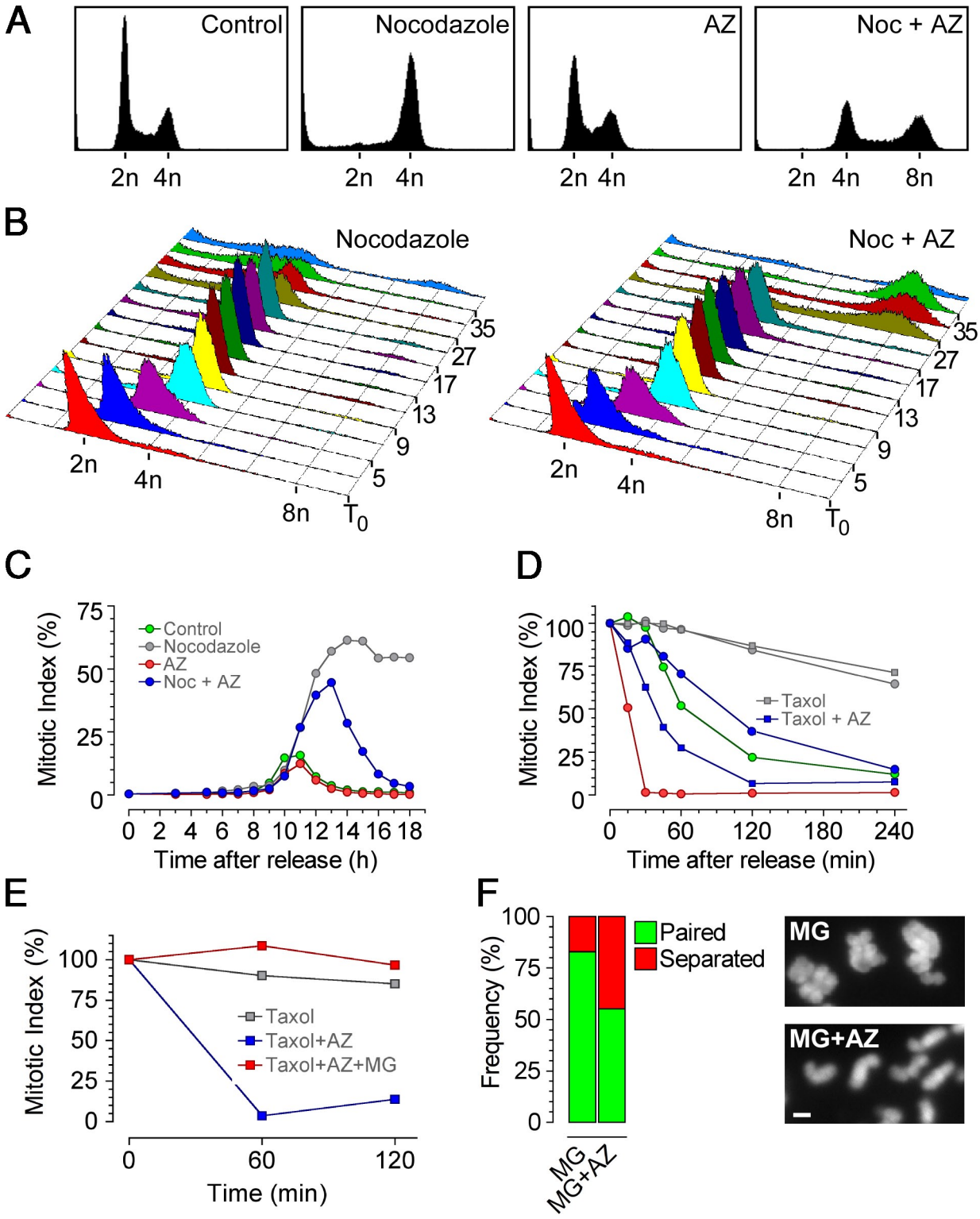

Figure S2. **AZ3146 overrides the spindle checkpoint.** (A) DNA content histograms of HeLa cells treated with either nocodazole (Noc), AZ3146 (AZ), or nocodazole plus AZ3146 for 24 h. (B) DNA content histograms of HeLa cells synchronized at G1/S using a double-thymidine block and released into nocodazole or nocodazole plus AZ3146. (C) Line graph showing mitotic index determined by MPM-2 staining of drug-treated HeLa cells after release from a G1/S block. (D) Line graph showing mitotic index determined by MPM-2 staining of drug-treated HeLa cells after release from a nocodazole block. Symbols in D are the same as those in C. (E) Line graph showing mitotic index determined by MPM-2 staining of nocodazole-blocked HeLa cells released into taxol or taxol plus AZ3146 ± MG132. (F) Bar graph quantitating cells with separated sister chromatids after release from a 2-h monastrol block into MG132 ± AZ3146 (MG + AZ) for 3 h. Images show examples of paired (MG) and separated chromatids (MG + AZ). AZ3146 was used at 2 µM in all cases. Bar, 1 µm.

Published July 12, 2010

Figure S3. **Mps1 activity is required for kinetochore localization of CENP-E.** (A) Images of HeLa cells treated simultaneously with nocodazole, MG132, and AZ3146 and stained to detect Mad1 and ACA. Mad1 levels are scored as low and high in cells 1 and 2, respectively. In this protocol, although some cells will already be in mitosis when exposed to the AZ3146, others will enter mitosis in the presence of the Mps1 inhibitor. (B) Immunoblot of HeLa cells expressing Myc-tagged Mad2 proteins blotted with antibodies to detect the Myc tag. WT, wild type; RQ, Mad2RQ; ΔC, Mad2ΔC. (C) Immunofluorescence images of interphase HeLa cells expressing Myc-tagged Mad2ΔC and Mad2RQ proteins stained with antibodies to the Myc tag. (D) HeLa cells harboring an RNAi-resistant and tetracycline-inducible Myc-tagged Mps1^{M602A} transgene were transfected with an shRNA designed to repress endogenous Mps1 (Tighe et al., 2008). Tetracycline was used to induce Mps1^{M602A}, thus restoring Mps1 function (Tighe et al., 2008). The cells were treated with monastrol for 2 h to inhibit bipolar spindle assembly. After monastrol washout, the ATP analogue 1NM-PP1 was added for 1 h to inhibit the enzymatic activity of Mps1^{M602A}. The cells were fixed and stained to detect CENP-E (red), centromeres (ACA; green), and DNA. Insets show magnified views of individual kinetochore pairs (boxed regions). In controls, i.e., cells retaining endogenous Mps1 activity, CENP-E is readily apparent at kinetochores. In contrast, in cells in which Mps1 activity is inhibited, kinetochore localization of CENP-E is severely affected; note that although background spindle staining is apparent, kinetochores are not. (E) Immunoblots of anti-Myc immune complexes isolated from HEK293 cells stably expressing Myc-tagged Mps1 transgenes and transiently transfected with vectors encoding GFP-tagged Mps1 transgenes, either wild-type or a kinase-dead mutant. Membranes were blotted as indicated.

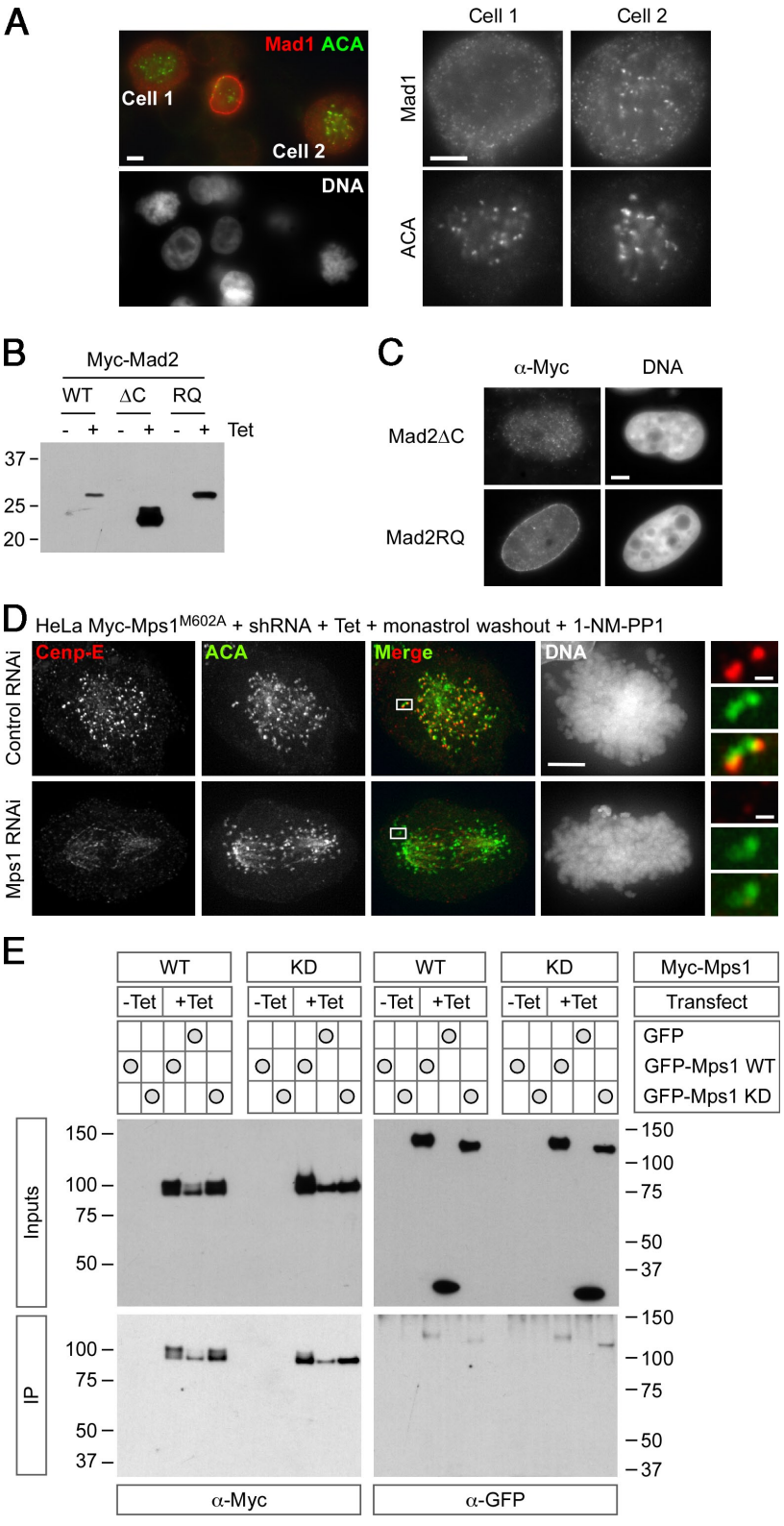

Published July 12, 2010

Table S1. **PCR primers used in this study**

Oligo	Sequence	Purpose
1	5′-CACGGATCCGCGCTGCAGCTCTCCCGG-3′	Forward primer for amplification of Mad2
2	5′-CACGCGGCCGCTCAGCTATTTACTTTGTGGATTGTAG-3′	Reverse primer for Mad2ΔC (196–205)
3	5′-GAAATCCGTTCAGTGATCGAAGCGATCACAGCTACGGTGAC-3′	Forward mutagenic primer for Mad2 R133E, Q134A
4	5′-GTCACCGTAGCTGTGATCGCTTCGATCACTGAACGGATTTC-3′	Reverse mutagenic primer for Mad2 R133E, Q134A

Table S2. **Antibodies used in this study**

Antibody	Description	Dilution	Source
SAA.1	Sheep anti–aurora A	1:5,000	Girdler et al., 2006
SAB.1	Sheep anti–aurora B	1:1,000	Girdler et al., 2006
SB1.3	Sheep anti-Bub1	1:1,000	Taylor et al., 2001
SB3.2	Sheep anti-Bub3	1:500	Gurden, 2010
SMP1.1	Sheep anti-Mps1	1:1,000	Tighe et al., 2008
ACA	Human anticentromere	1:500	B. Earnshaw[a]
9B10	Mouse anti-Mad1	1:500	Abcam
SM2.2	Sheep anti-Mad2	1:500	Johnson et al., 2004
4A6	Mouse anti-Myc	1:5,000	Millipore
CENP-E	Rabbit anti–CENP-E	1:2,000	D. Cleveland[b]
GFP	Rabbit anti-GFP	1:5,000	Abcam
TAT1	Mouse antitubulin	1:100	K. Gull[c]
pAurora	Rabbit anti–pAurora A (Thr288)/ B (Thr232)/C (Thr198)	1:2,000	Cell Signaling Technology
CENP-A	Rabbit anti–CENP-A	1:200	Millipore
Phospho–CENP-A	Rabbit anti–phospho (Ser7) CENP-A	1:1,000	Millipore
PH3	Rabbit anti–phospho (Ser10) histone H3	1:500 (WB, 1:10,000)	Millipore
MPM-2	Mouse anti–MPM-2	1:2,000	Millipore
TG3	Mouse anti-phosphonucleolin	1:25	P. Davies[d]
Cy2-, Cy3-, and Cy5-anti–sheep/mouse/rabbit/human	Conjugated secondaries	1:500	Jackson ImmunoResearch Laboratories, Inc.
HRP anti–sheep/mouse/rabbit	Conjugated secondaries	1:2,000	Invitrogen
FITC-anti–mouse	Conjugated secondary	1:1,000	Jackson ImmunoResearch Laboratories, Inc.

WB, western blot.

[a]University of Edinburgh, Edinburgh, Scotland, UK.

[b]University of California, San Diego, La Jolla, CA.

[c]Oxford University, Oxford, England, UK.

[d]Albert Einstein College of Medicine, Yeshiva University, New York, NY.

Published July 12, 2010

References

Ditchfield, C., V.L. Johnson, A. Tighe, R. Ellston, C. Haworth, T. Johnson, A. Mortlock, N. Keen, and S.S. Taylor. 2003. Aurora B couples chromosome alignment with anaphase by targeting BubR1, Mad2, and Cenp-E to kinetochores. *J. Cell Biol.* 161:267–280. doi:10.1083/jcb.200208091

Girdler, F., K.E. Gascoigne, P.A. Eyers, S. Hartmuth, C. Crafter, K.M. Foote, N.J. Keen, and S.S. Taylor. 2006. Validating Aurora B as an anti-cancer drug target. *J. Cell Sci.* 119:3664–3675. doi:10.1242/jcs.03145

Gurden, M.D., A.J. Holland, W. van Zon, A. Tighe, M.A. Vergnolle, D.A. Andres, H.P. Spielmann, M. Malumbres, R.M. Wolthuis, D.W. Cleveland, and S.S. Taylor. 2010. Cdc20 is required for the post-anaphase, KEN-dependent degradation of centromere protein F. *J. Cell Sci.* 123:321–330. doi:10.1242/jcs.062075

Tighe, A., A. Ray-Sinha, O.D. Staples, and S.S. Taylor. 2007. GSK-3 inhibitors induce chromosome instability. *BMC Cell Biol.* 8:34. doi:10.1186/1471-2121-8-34

Tighe, A., O. Staples, and S. Taylor. 2008. Mps1 kinase activity restrains anaphase during an unperturbed mitosis and targets Mad2 to kinetochores. *J. Cell Biol.* 181:893–901. doi:10.1083/jcb.200712028